RUHR-UNIVERSITÄT BOCHUM

RUB

An investigation of material microstructures via relaxation of non-convex potentials

Muhammad Sabeel Khan

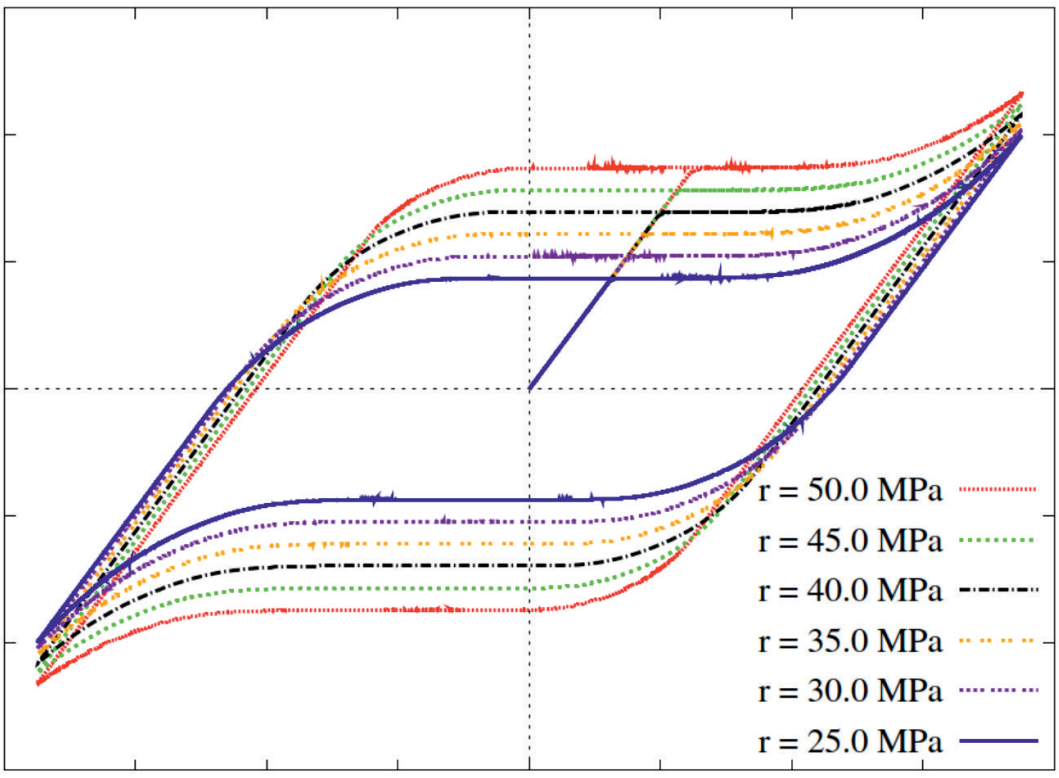

An Investigation of Material Microstructures via Relaxation of Non-convex Potentials

Dissertation

Zur
Erlangung des Grades
Dr.-Ing.

der
Fakultät für Maschinenbau
der Ruhr-Universität Bochum

von

Muhammad Sabeel Khan
aus Mansehra, Pakistan

Bochum 2013

Dissertation eingereicht am: 06.05.2013
Tag der mündlichen Prüfung: 13.06.2013

1. Gutachter: Prof. Dr. rer. nat. Klaus Hackl
2. Gutachter: Prof. Dr.-Ing. habil. Christian Miehe
Vorsitzender: Prof. Dr.-Ing. Franz Peters

Recite in the name of your Lord who created, created man from a clinging substance. Recite, and your Lord is the most Generous, Who taught by the pen; taught man that which he knew not.

(Al-Quran, Chapter 96, Verses 1-5)

The first revelation to the Prophet Muhammad (peace be upon him)

Herausgeber:

Institut für Mechanik
— Schriftenreihe —
Ruhr-Universität Bochum
D-44780 Bochum

Printed in Germany

Dedicated to my parents
and my wife Bushra Sabeel

Summary

This thesis presents an investigation of two complementary cases of material microstructures: formation of rotational microstructures in granular media, and the detwinning of martensitic microstructure. In both the cases a small-deformation framework is used for the analysis throughout this work. Due to their different modeling aspects as well as their applications are concerned, this work is divided into two main parts.

Granular materials tend to exhibit distinct patterns under deformation consisting of counter-rotating particles. *In the first part*, we are going to model this phenomenon on a continuum level by employing the calculus of variations, specifically the concept of energy relaxation. Our approach is based on the material model of a so-called Cosserat continuum. The fact that the macroscopic shear is influenced by micro-rotational deformations of the particles enables us to propose an interaction energy potential contributing to the material strain energy. The energy of the material is now enriched by adding this interaction potential. As a result the total energy becomes non-quasiconvex, thus giving rise to the development of microstructures occurring both in the displacement and micro-rotation field.

It turns out to be possible to derive an exact quasiconvex envelope of the potential by employing the direct methods in the calculus of variations. It is worth mentioning that there are no further assumptions necessary here. Moreover the computed relaxed energy yields all the possible displacement and micro-rotational field fluctuations as minimizers. We show that the material behaviour can be divided into three different regimes. Two of the material phases are exhibiting microstructures in rotational and translational motion of the particles, respectively, and the third one is corresponding to the case where there is no internal structure of the deformation field. Following the principle of minimum of potential energy the elastic response of granular materials is modeled within the framework of Cosserat elasticity, and by following the principle of minimum of dissipation potential the rate-dependent inelastic behavior of granular materials is modeled within the framework of Cosserat viscoplasticity. The properties of the proposed model are demonstrated by carrying out numerical computations. Simulations are presented on the determination of possible formation of microstructural zones in a granular medium.

In the second part, we model the phenomenon of detwinning of martensitic microstructure in phase transforming inelastic crystalline materials. The material can undergo a phase transition between two martensitic variants, associated with these phases is a two-well energy potential for the characterization of material response and the description of its equilibrium configuration. Relaxation techniques are employed to compute an analytical expression for the partially relaxed energy corresponding to the two-well non-convex energy potential. To quantify for the inelastic response a rate-independent dissipation function is introduced. The modeling approach is based on the energy principles where an incremental variational formulation of the proposed model is presented for the simulation and investigation of detwinning microstructure. Numerical computations are performed using finite element method to demonstrate on the distribution of detwinning microstructure in a single crystal.

Kurzfassung

Die vorliegende Arbeit beschäftigt sich mit der Erforschung von zwei Komplementärfällen der Material-Mikrostrukturen, nämlich die Ausbildung der Drehmikrostrukturen von granularen Medien, und die Entzwillingung der martensitischen Mikrostruktur. Bei unserer Analyse sind beide Fälle im Rahmen der infinitesimalen Verzerrungen berücksichtigt worden. Mit Rücksicht auf die unterschiedlichen Modellierungsaspekte, und auch auf die verschieden Anwendungen ist diese Arbeit in zwei Hauptteile aufgeteilt.

Granulare Medien neigen dazu, unter dem Einfluss der Verformung, unterschiedliche Muster von gegendrehenden Partikeln darzulegen. *Im ersten Teil* dieser Arbeit wird ein kontinuumsmechanisches Model von diesem Phänomen unter Einsatz der Methoden von Variationsrechnung, beziehungsweise der Energierelaxierung entwickelt. Unsere Methode basiert auf der sogenannten Cosserat-Kontinuumstheorie. Da die makroskopische Scherdehnung von mikroskopischen Drehverformungen beeinflusst ist, schlagen wir ein Wechselwirkungspotential vor, welches wiederum zur Dehnungsenergie beiträgt. Die Energiefunktion wird durch Einsetzen der Wechselwirkungsenergie erweitert. Hierdurch wird die Gesamtenergie nicht-konvex, was wiederum zu Mikrostrukturausbildung führt, die sich in Form von mikroskopischen Verschiebungen und Drehungen zeigt.

Es zeigte sich, dass die direkten Methoden der Variationsrechnung uns ermöglichen, eine konvexe Hülle des Potentials exakt herzuleiten, ohne zusätzliche Annahmen zu treffen. Hinzu kommt, dass alle möglichen Mikro-Fluktuationen des Verschiebungs- und Drehungsfelds als Minimierer der relaxierten Energie geliefert werden. Wir zeigen, dass das Materialverhalten in drei verschiedene Bereiche aufgeteilt werden kann. Zwei davon weisen Verschiebungs- und Drehmikrostrukturen auf, und das dritte entspricht dem Verschiebungsfeld, welches keine innere Struktur besitzt. Das elastische Verhalten des granularen Materials wird mit Hilfe des Prinzips vom Minimum der Potentialenergie im Rahmen der Cosserat Kontinuumstheorie modelliert, und das ratenabhängige inelastische Verhalten durch das Prinzip vom Minimum des Dissipationspotentials im Rahmen der Cosserat-Viskoplastizität. Danach werden die Eigenschaften des entwickelten Modells durch numerische Beispiele demonstriert, welche mit der Bestimmung der möglichen Mikrostrukturgebiete im granularen Medium zu tun haben.

Im zweiten Teil dieser Arbeit wird ein Modell für Entzwillingung der martensitischen Mikrostruktur in inelastischen, kristallinen Materialien entwickelt. Das Material kann eine Phasentransformation zwischen zwei Martensitvarianten erfahren, die zwei Gleichgewichtszustände von der Zwei-Quellen Energie potentielle charakterisieren. Relaxierungsmethoden werden verwendet, um einen analytischen Ausdruck der teil-relaxierten Energie zu berechnen, der dem nicht-konvexen Potential zugehört. Eine raten-unabhängige Dissipationsfunktion wird vorgestellt, um die inelastische Reaktion zu erklären. Die Methode basiert auf dem Energieprinzip, und auch auf der inkrementellen Variationsformulierung des Modells. Dadurch wird die Entzwillingung der Mikrostruktur untersucht. Finite Elemente Berechnungen werden durchgeführt, um die Verteilung der Entzwillingung von Mikrostruktur in einem Monokristall herauszufinden.

Acknowledgements

I would like to acknowledge all people who helped and cooperated with me, in one or the other way, during my research stay at the chair of Mechanics – Materials theory at Ruhr-Universität Bochum.

Foremost, I would like to express sincere gratitude to my advisor Prof. Dr. rer. nat. Klaus Hackl for providing me the opportunity to work in his research group. His immense knowledge of the field and indespensible research skills were always a great source of motivation for me. I would like to express my deepest appreciation for his kind supervision, illuminating discussions, patience and support during my research period at the institute. His valuable suggestions, focused guidence and encouragement helped me in completing this thesis. I could not have imagined having a better advisor for my PhD study.

I also would like to thank my co-supervisor Prof. Dr.-Ing. habil. Christian Miehe for valuable comments and acting as a second referee for my dissertation. I would like to extend my thanks to all my friends and colleagues at the chair of Mechanics – Materials theory. In particular, I would like to express my sincere appreciation to Dr. Hoppe for providing me technical support during my research stay. I would like to offer my special thank to Dr. Trinh for the useful discussions we had and for her insightful comments and suggestions in improving the first draft of this dissertation. Also, I would like to thank Dr. Makowski for the early discussions on the topic. I would like to say thank to my friends Mehdi and Christoph for their help in translating my dissertation summary in German language.

I would like to acknowledge the financial support by Higher Education Commission (HEC) of Pakistan and also would like to thank Deutscher Akademischer Austauschdienst (DAAD) for supporting my research stay in Germany.

I would to thank my parents for the love and affection they have showered upon me throughout my life. Last, but not least, I would like to thank my wife Bushra Sabeel for her patience, love and encouragement that enabled me to complete this thesis. Also, I would extend my thanks to my son Muhammad Ahmed Sabeel who waited for me and missed my love during the days when I was busy in writing this dissertation.

Contents

Nomenclature

The notations and symbols mentioned in each chapter has the same purpose of use in other chapters unless it is specified.

Notations & Symbols in Chapter 1 and 2

I	integral functional
$\boldsymbol{\xi}$	deformation field
Ψ	non-quasiconvex energy potential
Ψ^{rel}	relaxed energy potential
$\boldsymbol{u}$	displacement field vector
$\boldsymbol{\varphi}$	microrotation field vector
Ω	volume possessed by the material body
$W^{1,p}$	space of p-integrable functions .OR. Sobolev space
u_l	sequence of displacement field variables
inf	infimum
lim	limiting value
W	energy density
$\mathbb{R}$	set of real numbers
$\bigcup$	union symbol
∞	infinity symbol
$\mathbb{R}^n$	set of n-tuple real numbers
∇	gradient or divergence operator
$\in$	belongs to
vol(-)	volume of (-)
$\partial\Omega$	surface of the volume Ω
W^c	convex energy potential
W^{pc}	polyconvex energy potential
W^{qc}	quasiconvex energy potential
W^{rc}	rank-one convex energy potential
$\otimes$	tensor product
W^{rel}	relaxed energy potential

Notations & symbols in Chapter 3

$\mathbb{C}$	fourth order constitutive tensor of elastic constants
$\overline{\mathbb{C}}$	fourth order constitutive tensor of elastic constants
$\boldsymbol{S}$	second order tensor
$\boldsymbol{e}_i$	unit vector in i^{th} coordinate direction
α	a material parameter
β	a material parameter related to the particle size

$\boldsymbol{\varepsilon}$	second order strain tensor
$\mathrm{tr}(\cdot)$	trace of $(\cdot)$
$\boldsymbol{\sigma}$	force-stress tensor
$\boldsymbol{\mu}$	couple-stress tensor
$\boldsymbol{\mathcal{E}}$	third order permutation tensor
$\mathcal{I}$	interaction energy potential
$\boldsymbol{\varepsilon}$	second order strain tensor
$\boldsymbol{\kappa}$	curvature strain tensor
$\boldsymbol{e}$	Cosserat strain tensor
$\mathrm{dev}(\cdot)$	deviatoric part of $(\cdot)$
$\arg$	argument
$\mathrm{W}^{\mathrm{enh}}$	enhanced energy function
ℓ	potential of external forces and couples
λ	Lame's constant
μ	shear modulus of elasticity
μ_c	Cosserat shear modulus of elasticity
$\overline{\mu}$	bending modulus
$\overline{\mu}_c$	coupled shear modulus or bending modulus
$\overline{\lambda}$	Cosserat material dilatancy parameter
∂	partial derivative
$\min$	minimum
W^{rel}	relaxed energy
W_1^{rel}	relaxed energy corresponding to material regime 1
W_2^{rel}	relaxed energy corresponding to material regime 2
W_3^{rel}	relaxed energy corresponding to material regime 3
$\mathrm{sym}(\cdot)$	symmetric part of the tensor $(\cdot)$
$\mathrm{asy}(\cdot)$	anti-symmetric part of the tensor $(\cdot)$
$\dot{(\cdot)}$	total time derivative of $(\cdot)$
Δ	dissipation potential
Δ_1	dissipation potential related to material regime 1
Δ_2	dissipation potential related to material regime 2
Δ_3	dissipation potential related to material regime 3
Ψ	Helmholtz free energy
G	Gibbs free energy
$\frac{d}{dt}$	time derivative
$\mathcal{D}$	total dissipation functional
ℓ_{ext}	potential of external forces and couples
$\boldsymbol{\omega}$	Cosserat rotation tensor
$\boldsymbol{\vartheta}$	angular velocity

Notations & symbols in Chapter 4

δ	a small variation operator
Γ	boundary surface
$\boldsymbol{I}$	second order unit matrix

$\mathcal{I}$	fourth order unit matrix
$\overline{\mathcal{I}}$	fourth order unit matrix
$(\cdot)^n$	previous time step
$(\cdot)^{n+1}$	current time step
Δt	time step
Γ_u	boundary with prescribed displacements
Γ_φ	boundary with prescribed microrotations
$J^{-1}_{\mathrm{n+1}}$	Jacobian inverse at $(n+1)^{th}$ load step
$\left(J^{i}_{\mathrm{n+1}}\right)^{-1}$	Jacobian inverse at $(n+1)^{th}$ load step
ϵ	assumed tolerance
R^e_{lin}	matrix of residual equations corresponding to balance of linear momentum
R^e_{ang}	matrix of residual equations corresponding to balance of angular momentum
$\mathcal{A}$	assembly operator

Notations & symbols in Chapter 6

Ψ^{rel}	relaxed energy
Ψ^{con}	condensed energy
θ	volume fraction of martensite
$\boldsymbol{\varepsilon}_{\mathrm{T}}$	transformation strain
sign	signum function
inf	infimum

1. Introduction

1.1. Motivation

It is always of interest to know the general analytical solution of the following non-quasiconvex energy minimization problem

$$\inf_{\boldsymbol{\xi}} \left\{ I(\boldsymbol{\xi}) = \int_{\Omega} \underbrace{\Psi(\nabla \boldsymbol{\xi})}_{non-quasiconvex} dV - \ell(\boldsymbol{\xi}) \; ; \boldsymbol{\xi} \in W^{1,p\in(1,\infty)}(\Omega, \mathbb{R}^n) \right\}. \tag{1.1}$$

The minimizers of such non-quasiconvex energy minimization problem do not exist in general, which is highly due to fine scale oscillations of the gradients of infimizing deformations. Physically, the socillatory behavior of these infimizing deformations can be seen as a distortions of finite element meshes [GM11, MLG04]. Thus leading to the development of microstructures in the materials. Formation of such microstructures can be seen as extended microstructures [Bag41, GN04] which is distributed through the material domain or the localized microstructures as seen in [BH01, dB91, M9b, TW93, TS98]. One possible way to solve the non-quasiconvex energy minimization problem (1.1) is to apply the direct numerical schemes as suggested by [AP01, Bar01, CCO08, CP97, CR97, Chi99, CC92, CKL91, DW00, Ped96, Rou96], hence leading to the mesh dependent minimizers which are of no practical interest in general. Moreover, minimization using direct numerical procedures do not guarantee the attainment of these minimizers. To avoid such problems, different methodologies have been suggested in literature. One possibility is to use regularization technique which is based on the gradient-type enhancement of the original non-convex energy function in (1.1). Regularization method has its own limitations as far as the physical properties of the unrelaxed problems are concerned. Contrary to this is the method of relaxation which is more effective and natural way to treat the non-quasiconvex energy minimization problem. There are two ways to relax the original non-quasiconvex energy minimization problem (1.1). Either to enlarge the space of admissible deformations $\left(W^{1,p\in(1,\infty)}(\Omega, \mathbb{R}^n)\right)$ to the space of parametrized measures [Ped97, You37], or, to replace the original non-quasiconvex energy $\Psi(\nabla \boldsymbol{\xi})$ with its relaxed energy envelope $\Psi^{rel}(\nabla \boldsymbol{\xi})$. A detailed discussion on the methods of relaxation is presented in Chapter 2. If possible to compute the exact relaxed envelope of the corresponding non-quasiconvex energy in the energy minimization problem (1.1) one do not only guarantee general solutions of the associated energy minimization problem but also can predict on the formation of both the extended and localized microstructures in the materials. In this study, we investigated two complementary cases of material microstructures where it is possible to construct the exact relaxed energies of corresponding non-quasiconvex energy function. By doing so we do not only ensure the existence of the minimizers to the arising non-quasiconvex energy minimization problems but also guarantee the mesh objectivity of these minimizers. Moreover, we are able to characterize both the extended and localized microstructures within the materials.

Figure 1.1.: Granular patterns: sand ripples (in first column), sand ridges (in second column). Copyrights of Martyn L Gorman, "www.abdn.ac.uk/talpa/Sand/Welcome.html". These photographs are used with permission.

1.2. Rotational microstructures in granular materials

In nature granular materials are found to exhibit distinct patterns under deformation such as sand dunes [Bag41, NO93], granular ripples [BMD87, NO93, San09, TZ05] (see Figure 1.1) and shear bands [BH99, dB91, dBS91, HB03, M9*b*, MV87, Tej97, TB96] etc. Formation of these granular patterns is highly governed by the interaction among the counter-rotating granular particles. These counter-rotating granular particles play a very crucial role in the development of material microstructures [Bar94, TPM05, TW05]. Formation of such microstructures is thus called rotational microstructures in granular materials. To observe the formation of these microstructural patterns thus requires an extensive study on the intriguing phenomenon of counter-rotations of particles at the micro-scale. Because of intricate nature of particle rotations and complex behavior of the granular materials under deformation it is therefore difficult to understand the intergranular cohesive interactions of these particles completely. In literature almost no comprehensive study appears that completely discuss the intergranular interactions and arising phenomenon in detail which can truly justify the naturally observed microstructural patterns in the granular materials. Although some researchers have realized the significance of interparticle contacts and the rotational phenomenon of granular particles in modeling the granular structures. For a comprehensive review few of them are mentioned here. In developing a micro-mechanical model for granular material behavior Suiker et al. [SdBC01a] formulated a constitutive theory featuring the microstructural effects governed by the particle displacements and rotations. One of the possible application of this theory is emphasized in [SdBC01b]. Tordesillas and Walsh [AT02] discusses the intergranular interactions and incorporate the rolling resistance and contact anisotropy in the micropolar model for granular materials where they devised a homogenization scheme to capture the material microstructures. Also an elastic and elastoplastic analysis of granular material microstructures has been presented by them [TW05] where again a homogenization procedure on particle scale is developed using a micropolar continuum model. Walsh et al. [WTP07] use a micromechanical approach in modeling the mechanical behavior of granular materials where the micro-scale behavior of interparticle contacts are linked to the macroscopic free energy density of the granular material. They computed the free energy by averaging it at each interparticle contact which assumed to behave as a spring-slider system. Based on their micromechanical model [CM91] in a Cosserat continuum Chang and Ma [CM92] studied particle rotations in a granulate medium

to derive elastic material constants using interparticle stiffness. Within the framework of Cosserat elasticity [Eri68, Min64, Now70] they use rotation and stretch springs for transmitting contact moments and forces at the interconnected granulates. Pasternak and Mühlhaus [PM01] also consider the particle rotations at the interparticle contact and model particulate medium based on the idea where particles are connected through translational and rotational springs. Among the other works are [AMVH$^+$06, PV11] and also see references therein. From these studies it is easier to realize that the phenomenon of particle rotations in granular structures is essentially important to study in modeling the granular structures. No unified theory appeared in literature that appropriately consider and discuss the particle rotations in a granular assemblage, thus demonstrating on the intricate nature of particle interactions. All the previous studies that appeared in literature for modeling the mechanical behavior of granular materials with consideration of particle rotations at the micro-scale are based on the micromechanical approach. Moreover, the established theories are no doubt able to model the material microstructures to some extent, but are not able to distinguish among the microstructural and non-microstructural regimes in a deforming granular material. Based on a continuum approach we present a material model taking into account the counter rotation of the particles leading to the development of microstructural regimes in a deforming granular structure.

In the first part of the thesis we are going to model the phenomenon of particle rotations in a granular assemblage. For this purpose we discuss the intergranular kinematics and propose an interaction energy potential. This interaction energy potential takes the effect of counter-rotations of the granular particles at the continuum scale. Thereby introducing two new material parameters related to the interparticle friction and the length scale of the granular material. This length scale parameter for example can be considered as a particle size of a granular medium likewise we consider the grain size in a polycrystalline material and a fiber length in fibrous material. Granular materials shows important length scale effects as experimentally seen by Anderson et al. [ACL94], Anderson and Lakes [AL94], Buechner and Lakes [BL03] and Lakes [Lak86]. For the modeling of such materials who exhibit length scale effects the classical/Boltzmann continuum theories are not sufficient [AS06], since the constitutive equations in these theories are independent of length scale parameters. The continuum theories that incorporate the length scale effects are the generalized/higher order continuum theories [Eri02, Mau92, FS06, KE71, KE76, Min64, Now69, Now68, Now70, SE64, Ste94, Sto69, Sto72] whose constitutive relations are embedded with the length scale parameters. Thus generalized continuum theories are requisite to best capture the real deformation mechanism of granular materials and are capable to describe their mechanical behavior. These theories of microstructured media are well developed by Eringen [Eri02, Eri68, ES64], Forest [FS06], Mindlin [Min64], Toupin [Tou62, Tou64], Truesdel and Toupin [TT60], Vardoulakis and Sulem [VS95] and are used extensively in modeling the mechanical behavior of granular materials where many interesting phenomenon are predicted during the deformation of these materials. Cosserat continuum theory [CC09, Sch67, Var09] is a special case of generalized continuum theory which has been proved successful and attained maximum attention of many researchers [AAE10, CM91, dB91, DSW93, PV11, PM01, MNR99, M9b, M6, Tej97] in modeling the behavior of granular materials with microstructures. It has been used to analyze the granular material microstructures using different constitutive settings. An elastoplastic Cosserat constitutive theory has been applied by de Borst [dB91], de Borst and Sluys [dBS91], Dietsche et al. [DSW93], Ehlers and Volks [EV97], Mühlhaus [M9b] and Mühlhaus and Vardoulakis [MV87] for the observation of microstructures of localized deformations in a granular material. Bauer and Huang [BH99], Huang and Bauer [HB03], Tejchman [Tej97], Tejchman and Bauer[TB96] have used hypoplastic constitutive framework of Cosserat con-

tinuum in the observation of localized deformations in granular materials. An updated review on the application of Cosserat continuum theory in the analyiss of localized deformations in geomaterials can be found in the book by Vardoulakis and Sulem [VS95]. It has been adopted to model the granular material microstructures by Chambon et al. [CCM01] where they emphasized on its applications in particular towards the modeling of geomaterials behavior. In a Cosserat continuum theory each material point has an independent micro-rotational motion in addition to its translational motion.

We use Cosserat theory for the continuum description of the granular material in our work. The resulting interaction energy potential from the consideration of intergranular interactions and their counter rotations is embedded with the Helmholtz free energy of the Cosserat continuum. Thereby providing an energy potential on the macroscale taking into consideration the counter rotations at the micro-scale for the modeling of granular materials. The total energy potential at the continuum scale thus becomes nonconvex and the associated energy minimization problem leads to many local minimizers. In the solution of arising nonconvex variational problem thus needs the implication of relaxation methods. For this purpose to assure the existence of unique minimizer of the related energy minimization problem an exact relaxed potential is derived by employing the direct methods in the calculus of variations [Dac89]. Thereby guaranteeing the solution to the resulting nonconvex variational problem and transforming it into a quasiconvex variational problem. It is important to note that the resulting solution from the developed quasiconvex variational problem would be the same as if possible could be achieved from the nonconvex variational problem. In deriving the exact relaxed energy we come up with a three regime granular material where two of the material regimes/phases are with microstructure in independent micro-rotational motions and the translational motions of the continuum particles and the third one is corresponding to the regime where there is no internal structure in the material. This is in accordance with the well known fact that the microstructures in the granular materials occurs at high translational and rotational deformations [AVA06]. Hence depending upon the translational and micro-rotational motions of the granular particles we are able to classify the granular material microstructures into two categories, a microstructure due to translational motions and a microstructure due to micro-rotational motions of the granular particles. Thus we develope a granular material model at continuum scale that is able to characterize the development of microstructural and non-microstructural phases in a granular medium. Furthermore, it enables one to differentiate the regimes of the material that are related to the energy dissipation, material flow, and material failure.

1.3. Detwinning of martensitic microstructures

Detwinning is a well recognized mechanism of inelastic deformations which has been observed experimentally in a number of crystalline materials. For an example, see Figure 1.2 which demonstrate on its formation in a mixture of Copper and Silicon alloy, Figure 1.3 and 1.4 for its formation in nanocrystalline copper material. For more experimental results see [HZWL08] and references there in. For the most recent and a detailed overview on the experimental observation of detwinning in different crystalline solids, their mechanism and the factors affecting the formation of detwinning, theoretical approaches to simulate the experimental observed detwinning microstructures using mathematical models, the reader is referred to the work of Zhu et al. [ZLW12] and references cited in.

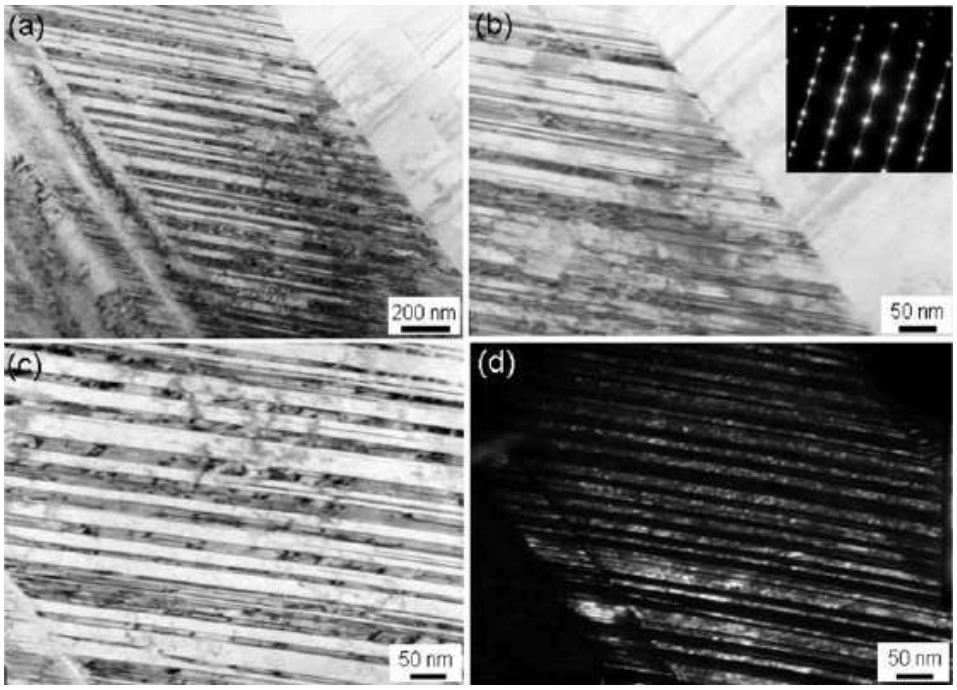

Figure 1.2.: Transmission electron microscopy (TEM) micrographs (a) of deformation twins formed in a Cu-3% Si alloy, (b) a magnified image at the boundary of the band (c) high magnified image in the inner part and (d) corresponding dark-field image. Reprinted from [HZWL08] with permission of Zhang, Z. F.

In the second part of the thesis, we model the phenomenon of detwinning in phase transforming inelastic solids. Our modeling approach is based on the energy formulation where the deformation behavior of inelastic materials is described by the specification of two energy potentials. Such an approach to model different material behaviors has been considered in the work of Bartels et al. [BCC+06, BCHH04], Carstensen et al. [CHM02], Conti et al. [CDK09, CHO07], Conti and Ortiz [CO05], Conti and Theil [CT05], Gürses and Miehe [GM11], Hackl [Hac97], Hackl and Fischer [HF08], Hackl and Hoppe [HH01], Hackl et al. [HHK12], Miehe and Lambrecht [ML03], Miehe et al. [LMD03, MLG04], Mielke [Mie04], Mielke and Roubíček [MR06], Ortiz and Repetto [OR99]. The two energy potentials comprises of elastic free energy potential of the material and the dissipation potential. Consideration of two martensitic variants and the corresponding energies leads to work with a non-convex energy potential. A partially (in the sense that it is not minimized with respect to the internal variables which in our case are the volume fractions of each martensitic variant) relaxed energy is computed which is further used along with the dissipation potential in a two field minimization problem. A time incremental formulation of this minimization problem as suggested by Carstensen et al. [CHM02], Hackl et al. [HHK12] is introduced where the original minimization problem is splitted into a two step algorithm. In the first step, the displacement field is obtained via a pure elastic problem and afterwards in the second step an update for the volume fraction of each of the martensitic variant is computed via the minimum-principle of dissipation potential (see Hackl and Fischer [HF08]) as its stationarity conditions while working within the framework of rate-independent inelasticity.

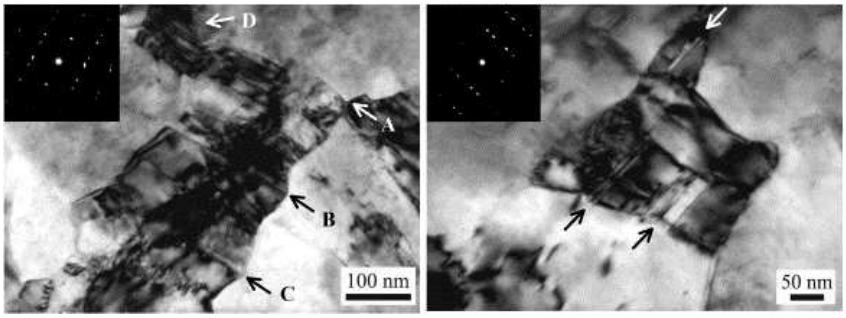

Figure 1.3.: Deformation twins in an ultrafine grain and a nanocrystallite of UFG-Cu. Reprinted from [HWW+06] with permission.

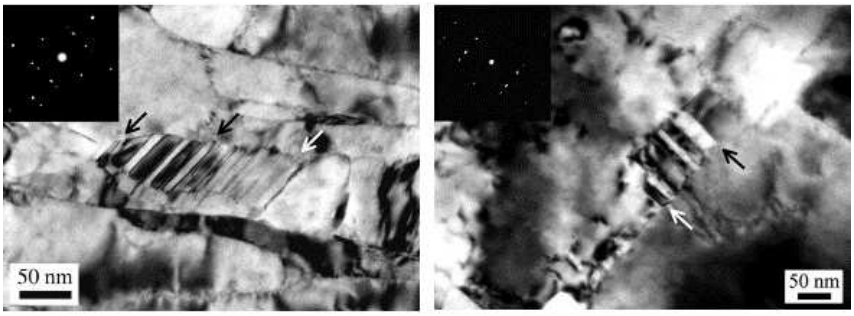

Figure 1.4.: Deformation twins in NC-Cu where the arrows indicates the elongated nanocrystallites. Reprinted from [HWW+06] with permission.

1.4. Structure of the thesis

This thesis is organized as follows. Following the motivation and introduction from Chapter 1, theory of relaxation is presentedin in Chapter 2. Special emphasis has been placed on its possible applications in solid mechanics and state of the art in modeling the material microstructures. Generalized variational principle, different notions of convexity, both the analytical and numerical theories and methods for computing relaxed potentials of the associated non-quasiconvex potentials are discussed.

In Chapter 3, following an introduction to continuum theories, specifically, the generalized continuum theories for modeling the granular materials with microstructures, a continuum model for granular materials within the framework of Cosserat continuum is developed. Relaxation methods have been employed to construct an analytical expression for the quasiconvex envelope of the non-quasiconvex energy potential resulted from the consideration of intergranular interactions. Numerical computations have been performed to obtain results demonstrating on different properties of the computed relaxed potential. Finally, a Cosserat-viscoplastic approach based on the principle of minimum of dissipation potential is considered for modeling the rate-dependent response of granular materials.

In Chapter 4, variational formulation of the proposed models and related numerical procedures based on the finite element method for their implementation on computer are addressed. In Chapter 5, numerical results obtained from both the Cosserat-elastic and Cosserat-viscoplastic models are presented and discussed in different cases. Numerical simulations

are shown to demonstrate on the possible distribution of granular material microstructures in these cases.

In Chapter 6, a simple model for modeling the detwinning phenomenon of martensitic microstructure in phase transforming inelastic solids is outlined. A rate-independent response of the material is considered. Variational formulation based on the principle of minimum of potential energy and the principle of minimum of dissipation potential is presented. The model is implemented using finite element method and the numerical results shown in Chapter 7 for the case of a single crystal NiTi alloy exhibits on the distribution of detwinned martensitic variants in a two-dimensional settings.

Finally, the conclusions are drawn in Chapter 8. Many possible directions to be investigated and open issues to be addressed in future have been outlined in this Chapter.

2. Relaxation of non-convex potentials and the material microstructure

2.1. Introduction

The experimental evidence on the exhibition of microstructure in many advance materials in material science, structural mechanics and especially in geomaterials is now an open secret [Bag41, BJ92, AT09, Lak83, Lak86, Lak95, OKNN82]. In formulating a mathematical model for the description of mechanical behavior of these materials with microstructures often leads to work with non-quasiconvex energy potentials [BJ87, Bha03, BCC$^+$06, BCHH04, CCO08, CHM02, CP97, CDK09, CHO07, CO05]. For instance, in modeling the mechanical response of the granular materials exhibiting internal structures, in the first part of this thesis, new finding and measures are presented which lead to deal with the non-convex variational problems within the framework of Cosserat continuum theory. The consideration of counter rotating particles in a granular material leads us to an innovative idea which allows us to propose some new measures for the characterization of the underlying microstructure within a granular material. The major finding is an interaction energy potential taking into account the intergranular interaction of the particles in a Cosserat continuum. This newly defined interaction energy potential is added to the existing free energy potential in a Cosserat continuum. As a consequence we have to work with a non-convex energy potential. In the second part of this thesis, we address the phenomenon of deformation twinning (also called mechanical twinning in literature) microstructures by modeling the phase transforming inelastic materials. The approach is based on the energy principles which requires the specification of two energy potentials called the free energy of the material and the dissipation potential. The free energy of the inelastic material (already assumed to have twinned microstructure) has a two well structure in this case. As a result we had to work with a non-convex energy potential in the related minimization problem. Associated to these non-convex energy potentials are the non-convex variational problems whose study is thus significant.

Relaxation methods have been employed to treat these nonconvex variational problems in particular in this thesis and in general for the analysis of materials with microstructures [BJ87, BCHH04, Dac89, HH01, Koh91, LMD03]. Here in this chapter, the reader is introduced to the theory and methods of relaxation of non-convex potentials for the analysis of materials with microstructures. The chapter is organized as follows. In Section 2.2 some notions of convexity are introduced briefly in connection to the generalized variational principle of continuum mechanics. Section 2.3 emphasize on the connection of material microstructure to the non-quasiconvexity of its associated energy potential. Finally, the use of relaxation theory for the characterization of material microstructure is presented in Section 2.4.

2.2. Generalized variational principle and different notions of convexity

This Section is devoted to present some mathematical concepts and definitions that are connected to the following integral functional

$$I(\mathbf{u}) \;=\; \int_{\Omega} W(\nabla \mathbf{u})\, dV - \ell(\mathbf{u}) \tag{2.1}$$

when it is considered with its associated minimization problem

$$\inf_{\mathbf{u}} \left\{ I(\mathbf{u}) \;:\; \mathbf{u} = \mathbf{u}_{\circ} \text{ on } \partial\Omega \text{ and } \mathbf{u} \in W^{1,p}(\Omega, \mathbb{R}^n) \right\} \tag{2.2}$$

where W is the stored energy function of the corresponding material, $\ell(\mathbf{u})$ is the potential of external forces and $W^{1,p}(\Omega, \mathbb{R}^n)$ is the space of all admissible deformations (Sobolev space), here $p \in (1, \infty)$ is associated with the growth of the energy function. Study of these kind of minimization problems in the field of continuum mechanics have been proved successful in modeling many engineering material behaviors [CCO08, CHM02, CT05, CHO07, CDK09, CO05, Dac89, Dac82, Dac01, DeS04, DD02, Dol99, DR95, DW00, GM11, HH01, JK89, KS82, M9, Mie04, ML03, MLG04, LMD03, MR06, OR99, SBH03]. The question arises that under which conditions or constraints on the energy function W the above variational problem admits minimizers. This query leads to search those properties and conditions on the energy function W that assures the solution to these variational problems. A well established fact (the consequence of Generalized Weierstraß Theorem) that the above minimization problem admits minimizers is that the integral functional $I(\mathbf{u})$ in (2.1) must be weakly sequentially lower semi-continuous (wslsc). Weakly sequentially lower semicontinuity of the functionals of type $I(\mathbf{u})$ has already been delineated in the work of Acerbi et al. [AF84], Dacorogna [Dac89], [Dac82] and Zeidler [Zei90]. It is defined as

Definition 1. *(**Weakly sequentially lower semicontinuity of I(u)**). Let $I(\mathbf{u})$ be an integral functional defined as in equation (2.2) and u_l be any sequence in $W^{1,p}$, then $I(\mathbf{u})$ is said to be weakly sequentially lower semicontinuous if*

$$\textit{for every } u_l \rightharpoonup u \in W^{1,p} \;\Rightarrow\; \liminf_{l\to\infty} I(u_l) \geq I(u),$$

here $\rightharpoonup$ means weak convergence in $W^{1,p}$

In one dimensional case where u is a scalar variable the restriction on the energy functional W for $I(u)$ to be weakly sequentially lower semi-continuous is the convexity of W. A convex function in a scalar variable is defined as follows

Definition 2. *(**convex function**). A real-valued function $W : \mathbb{R}^n \to \mathbb{R} \cup \{+\infty\}$ is said to be convex if it satisfies the condition*

$$W(\lambda\varepsilon_1 + (1-\lambda)\varepsilon_2) \leq \lambda W(\varepsilon_1) + (1-\lambda) W(\varepsilon_2), \quad \forall\, \varepsilon_1, \varepsilon_2 \in \mathbb{R}^n \quad \textit{and} \quad \lambda \in [0,1]\,.$$

In general, the energy function W is not a scalar-valued function, instead it is a vector-valued function. In case of vector-valued function $I(u)$ is weakly sequentially lower semi-continuous if the following properties for W holds

- W be continuous

- W satisfy the growth condition: for any $A \in \mathbb{R}$, $\mathbf{u} \in \mathbb{R}^n$ $W(\nabla \mathbf{u}) \leq A(1 + \|\nabla \mathbf{u}\|^p)$, where $n < p < \infty$

- W satisfy the coercivity condition: there exist some scalars B, $C \in \mathbb{R}$, with $C > 0$ such that $W(\nabla \mathbf{u}) \geq B + C(\|\nabla \mathbf{u}\|^p)$, where $n < p < \infty$

- W should be quasiconvex

Before the work of Morrey in 1952, it was established that the sufficient condition for the integral functional $I(\mathbf{u})$ to be weakly sequentially lower semi-continuous is the quasiconvexity along with the properties mentioned above. In his paper [Mor52] he gave the definition of quasiconvexity (see Definition 2.2) and right afterwards (in Theorem 2.1) the proof that quasiconvexity of energy function W is necessary for the lower semicontinuity of the integral functional $I(\mathbf{u})$. Hence after his work one can conclude mathematically that under the continuity, growth and coercivity conditions for W the integral functional $I(\mathbf{u})$ is weakly sequentially lower semicontinuous if and only if W is quasiconvex and this implies

$$\text{W is quasicovex } \Leftrightarrow I(\mathbf{u}) \text{ is weakly sequentially lower semicontinuous.}$$

Thus notion of quasiconvexity appears to be a natural restriction on the energy function W for the weakly sequentially lower semi-continuity of integral functional $I(\mathbf{u})$. The quasiconvexity of energy function W is the fundamental property that ensures the existence of minimizers in the energy minimization problem (2.2), and thus implies the ellipticity of the Euler equations ($I^{'}(\mathbf{u}) = 0$) for the integral functional $I(\mathbf{u})$. For existence theorems in elasticity for example see the work of Ball [Bal76], Ciarlet [Cia88] and Dacorogna [Dac89]. Here we state the definition of quasiconvexity as introduced by Morrey in [Mor52].

Definition 3. *(***quasiconvex function***). A vector-valued function $W : \mathbb{R}^{n\times n} \to \mathbb{R}$ is said to be quasiconvex if for any open domain (a unit ball is sufficient) $D \subset \mathbb{R}^n$ it satisfies*

$$W(\boldsymbol{\varepsilon}) \leq \frac{1}{vol(D)} \int_D W(\boldsymbol{\varepsilon} + \nabla \tilde{\boldsymbol{\varepsilon}})\, dV\,, \quad \forall\, \tilde{\boldsymbol{\varepsilon}} \in W^{1,\infty} \quad \textit{such that} \quad \tilde{\boldsymbol{\varepsilon}} = \mathbf{0} \quad \textit{on} \quad \partial D.$$

The notion of quasiconvexity [Mor52] is by definition a nonlocal criteria, which makes it difficult to check or even to contradict for most of the energy functionals. For this reason many other notions of convexity are introduced which are more easier to check or even to contradict in comparison to quasiconvexity criteria. Among these are the polyconvexity and the rank-one convexity, for detailed discussion on the topic see for example [Dac89]. The relation among the different notions of convexity is easy to remember in a (C-P-Q-R) relation as

$$Convexity \Rightarrow Polyconvexity \Rightarrow Quasiconvexity \Rightarrow Rank - one\ convexity.$$

Here it is important to note that the converse is not true in general (vectorial case) i.e.

$$Convexity \nLeftarrow Polyconvexity \nLeftarrow Quasiconvexity \nLeftarrow Rank - one\ convexity,$$

however, for the scalar case all the above notions of convexity coinsides. Among them the rank-one convexity is easiest to check which is defined as

Definition 4. *(***rank-one convex function***). A vector-valued function $W : \mathbb{R}^{n\times n} \to \mathbb{R}$ is said to be rank-once convex if the function $f : \mathbb{R} \to \mathbb{R}$ defined by*

$$f(t) = W\left(\mathbf{A} + t\left(\mathbf{a} \otimes \mathbf{b}\right)\right)$$

is convex in $t \in \mathbb{R}$ *such that rank*$(\mathbf{a} \otimes \mathbf{b}) \leq 1$*, where* $\mathbf{A} \in \mathbb{R}^{n\times n}$ *and* $\mathbf{a}, \mathbf{b} \in \mathbb{R}^n$.

The convex, polyconvex, quasiconvex and rank-one convex envelops of the energy function W are defined as their pointwise supremum, which are bounded above by their respective non-convex energy function W. The definitions of these envelopes reads

Definition 5. *(***convex, polyconvex, quasiconvex and rank-one convex envelopes***). Let* $W : \mathbb{R}^{n\times n} \to \mathbb{R}$ *be a convex, polyconvex, quasiconvex or rank-one convex function, then for every deformation gradient* $\boldsymbol{\varepsilon} \in \mathbb{R}^{n\times n}$

$$\begin{aligned}
W^c &= \sup\left\{cf(\boldsymbol{\varepsilon}) : W \geq cf(\boldsymbol{\varepsilon})\ \forall\ \textit{convex functions cf}\right\},\\
W^{pc} &= \sup\left\{pf(\boldsymbol{\varepsilon}) : W \geq pf(\boldsymbol{\varepsilon})\ \forall\ \textit{polyconvex functions pf}\right\},\\
W^{qc} &= \sup\left\{qf(\boldsymbol{\varepsilon}) : W \geq qf(\boldsymbol{\varepsilon})\ \forall\ \textit{quasiconvex functions qf}\right\},\\
W^{rc} &= \sup\left\{rf(\boldsymbol{\varepsilon}) : W \geq rf(\boldsymbol{\varepsilon})\ \forall\ \textit{rank-one convex functions rf}\right\}.
\end{aligned}$$

For completeness of a brief review on different notions of convexity we conclude with a result due to Sverak [Sev92] that if an energy function is rank-one convex it does not means that it is also quasiconvex.

2.3. Non-quasiconvex potentials and the material microstructures

Development of microstructures in a wide range of materials are predicted experimentally [BJ92, Bha03, BJS97]. If possible, the mathematical description of these material microstructures is very crucial since it provides with the mathematical tools for the numerical simulations of these materials, with which one can observe and analyze the material macroscopic behavior without expending high experimental cost. Mathematical models have been proposed to predict the microstructural behavior of many advanced materials. For example, for the materials related to the phenomenon of shape memory and ferroelasticity the models first introduced by Ball and James [BJ87] and afterwards developed by [ACB04, Bal88, BJ92, Bha01, BJS97, GP98b, GP98a, GHH07, GMH02, HH08, JK89, Koh91]. Such models determining martensitic microstructures are also formulated by Bhatacharya [Bha03] where multi-well energy potentials are characterizing the solid-solid phase transitions where in the transition zone one can observe fine scale oscillations in the infimizing sequences and thus the occurrence of microstructure. In modeling the strain softening materials Gürses and Miehe demonstrate on the formation of microstructures due to the emergence of non-convex energy minimization problem. The mathematical modeling of materials exhibiting microstructure leads in a natural way to deal with nonconvex energy potentials. The development of the associated nonconvex energy minimization problems leads to the understanding that the formation of these microstructures is essentially due to the fine-scale oscillations of the gradient of corresponding infimizing deformation sequences. These fine scale oscillations of the gradients of infimizing deformation sequences are directly connected to the non-existence of solutions of the corresponding energy minimization problems.

In continuum mechanics there are increasing number of problems where the energy function in the associated minimization problem fails to fulfill the condition of quasiconvexity. This non-quasiconvexity of the energy density can be due to many reasons, e.g., in the case of strain-softening plasticity models it can be due to non-monotonic constitutive function [GM11], in single slip plasticity models it can be due to the single slip constraint on the deformation of crystal [CO05], [CT05]. This renders the variational problems non-quasiconvex and thus lacks the minimizers. In simple words, the solution to the these problems does not exists which is another indication of the ill-posedness of the mathematical model. The general theory is that the minimization problem (2.2) predicts a microstructure in the material if the related energy function W is non-quasiconvex in the associated integral functional $I(\mathbf{u})$. This occurrence of material microstructure is due to non-existence of the minimizers of the integral functional $I(\mathbf{u})$ and the fine scale oscillations of gradients of the related infimizing sequences (∇u_h). Mathematical modeling of a finite-strain elastoplastic material addressed with associated energy minimization methods often leads to work with nonconvex potentials. Carstensen et al. in [CHM02] have shown that modeling of finite-strain elastoplasticity even with a single slip system and von Mises plasticity using non-quasiconvex energy functionals leads to the non-attainment of energy minimizers of the associated minimization problem, and hence the formation of microstructures within a material.

There are three main issues that are connected to the convexification of a material energy. These issues comprises of mesh dependency of solutions, existence of unique minimizers of corresponding minimization problem and stability conditions of the relevant mechanical problem. Material stability is directly influenced by the convexity of its energy functional. The convexification of the energy functional not only helps to predict on the formation and distribution of material microstructure but it also substantially reduce the mesh dependence of the solution of its corresponding variational problem in consideration. Analysis of a material behavior with finite elements using non-quasiconvex energy minimization method results in strong mesh dependent solutions. The issue of non-existence of unique minimizers of the corresponding energy minimization problem is raised due to lack of quasiconvexity of its related energy functional. In such a situation when the free energy of the material in consideration is not quasiconvex the material forms different patterns of microstructures (see Ball and James [BJ87, BJ92]). Numerical solutions of the non-quasiconvex minimization problem using finite element method leads to mesh dependent results and also the oscillations in the gradients of the minimizing deformations is observed. Moreover, Bartels and Prohl in [BP04] observed that the minimizing deformations sequence generates a complicated branching structure which is difficult to solve numerically. For these reasons, it is better not to use direct numerical simulations of non-quasiconvex minimization problems rather the non-quasiconvex minimization problems can be replaced by the relaxed one to void these complications and difficulties.

One possible recipe to avoid such oscillations of the infimizing sequences is to introduce regularization in the original energy minimization problem. For instance, the nonconvex energy function $W(\nabla \mathbf{u})$ in (2.1) can be replaced by $W(\nabla \mathbf{u}) + \epsilon \left\|\nabla \mathbf{u}\right\|^2$ for a small $\epsilon > 0$. But these methods do not work in all situations and have their limitations, and therefore are not suitable in general situations. The alternative to this is the method of relaxation where the original nonconvex energy minimization problem is replaced with its quasiconvexfied energy minimization problem and thus guaranteeing the existence of solutions. Of course, the direct numerical minimization of the non-quasiconvex variational problems is possible in some cases [AP01, Bar01, CCO08, CP97, Chi99, CC92, CKL91, DW00, Ped96, Rou96]. A detailed discussion on the relaxation techniques and methods is provided in the subsequent

Sections.

2.4. Relaxation of variational problems in continuum mechanics

In the mathematical modeling of solid materials behavior many cases arises where the free energy of the material comes out to be non-quasiconvex. Hence relaxation methods need to be employed in such situations. Some examples are pointed out by Raoult in [Rao10], among them are the modeling in nonlinear elasticity using Saint Venant-Kirchhoff energy density (which fails to be quasiconvex in three dimension, see for instance [Rao86]), In deriving slender structure models and in deriving a continuum model of a given discrete atom lattice behaving similar macroscopically. Other cases are mentioned in [SBH03, CO05, CT05, CDK09, CO05, DD02, HH01, MLG04, KS86a, KS86b, KV87, Wil81]. In this Section, we study relaxation theory and the use of relaxed potentials for the macroscopic analysis of materials exhibiting microstructures. For the analysis of the macroscopic response of a material the use of relaxed energies in continuum mechanics has proven successful. The relaxed energy which is in mathematical terms often named as quasiconvex envelope of the microscopic energy function, has been found useful for the macroscopic analysis of materials having internal structures. The influence of internal structure of a material on its macroscopic behavior is often efficiently analyzed by the use of relaxed potentials corresponding to its minimization problem.

Minimization using relaxed variational problems has its own advantages over the unrelaxed variational problems. One prominent advantange is the integration of all possible preffered oscillations of infimizing sequences into the relaxed problem, which appear beneficial in finding the minimizers. The relaxed potential has a smaller value than the unrelaxed potential for any selected mesh size. Among many possible local minima the characterization of global minima is more easily distinguishable, since the relaxed minimization problems have less possible local minima than the unrelaxed minimization problems. The existence of a minimizer is ensured in the relaxed energy minimization problem. And if the corresponding energy function is convex in vectorial case then this minimizer is unique. The minimizer of a relaxed variational problem is the same as that of non-quasiconvex (unrelaxed) variatioal problem (if it exists in case of unrelaxed problem, which might be the case). This is because the new relaxed problem naturally inherit the minimizers of the original non-quasiconvex energy function in a natural way by the implication of mathematical relaxation. Another possible and the most important advantage of using relaxed variational minimization problems is the mesh independency of its minimizers. The minimizer which is the weak limiting value of its infimizing sequence is therefore mesh independent. Where in the minimization problems using unrelaxed potentials this is not the case in general, if the minimizer exists these are very critical with the selection of mesh size. This means that the solutions to unrelaxed variational minimization problems are highly mesh dependent and therefore not reliable in practical situations. Thus relaxed variational minimization problems are more effective and reliable for the macro-mechanical analysis of the corresponding materials.

Relaxation theory has its applications in many advanced engineering problems. For the macro-mechanical analysis of inelastic materials exhibiting microstructures relaxation methods have been successfully applied see for instance the work of Conti et al. [CHO07, CO05, CT05], DeSimone et al. [DeS04, DD02], Hackl et al. [HH01], Miehe et al. [GM11, MLG04]. For instance its application to the structural design optimization is highlighted

in the technical literature of Kohn et al. [KS86a, KS86b, KS83]. Another possible area of application could be the homogenization of inelastic solids, see for detailed discussion e.g. the work of Miehe et al. [MSL02], Murat et al. [MT85] and Kohn et al. [KS82]. Kohn et al. [KS86b] and Willis [Wil81] have thrown some light for its useful application for the macro-mechanical analysis of composite solids. An interrelation between the relaxation theory for design optimization, homogenization of elastic solids and composite materials has been summarized and presented in a series of three papers [KS86a, KS86b] by Kohn and Strang, thus drawing attention to its application in these areas. Kohn and Vogelius in [KV87] applied relaxation theory for the inverse analysis problem of Impedance Computed Tomography. Another possible application could be the modeling of strain softening material behavior where the instabilities leads to deal with non-quasiconvex energy minimization problems. In this regard see for example the work of Gürses et al. [GM11] and Lambrecht et al. [LMD03] where they address the instabilities in strain softening material using relaxed incremental variational problem. Further it can be applied to damage mechanics, e.g., see the work of Francfort and Marigo [FM93] who uses energy relaxation for the modeling of stable damage evolution in a brittle material. Other related work demonstrating on the possible application of relaxation theory in damage mechanics can be seen in the work of Baldassari et al. [SBH03], Francfort et al. [FG06], Gürses et al. [GM11], Lambrecht et al. [LGM] and Mielke et al. [MR06]. The relaxed analysis on the formation of shear bands in strain-softening elasto-plastic solids is treated by Miehe et al. [ML03]. Their approach to the localization phenomenon using relaxation theory is demonstrating on its use in the strain softening inelastic materials. Its application to the modeling of dislocation dynamics in single crystals can be found in the work of Conti et al. [CO05]. Further applications towards the modeling of finite strain elastoplasticity using single crystal plasticity are emphasized by Carstensen et al. [CCO08]. Other related literature can be found in [CDK09]. Relaxation theory has been applied prosperously in the modeling of martensitic microstructures. For the analysis of microstructure in martensitic crystals using relaxation theory see for example the work of Ball and James [BJ87, BJ92], Bartels et al. [BCC$^+$06], Carstensen et al. [CP97], Gobbert and Prohl [GP98b, GP98a], Govindjee et al. [GHH07, GMH02], Hackl and Heinen [HH08] and Kohn [Koh91]. Other than its mechanical applications a vast range of engineering problems are addressed by the relaxation theory. Its use in finding the solutions to many non-convex problems in optimization theory is promising. There is no intention to provide with a complete list of applications of relaxation theory, although only few of them are mentioned here. Its applications in optimal control theory, in non-cooperative games, in designing algorithms for modern machine learning, in combinatorial optimization and intriguing use in optimal problems for communication systems is remarkable.

2.4.1. Relaxation of non-convex potentials - Theory and Methods

In mathematical terms the process of relaxation means replacing the ill-posed problem with a well posed one. Here by well posedness of the problem means its solution exists and is guaranteed. Specifically, two approaches are used so far for dealing with ill posed problems to make them well posed. The general concept is either to replace the original nonconvex function W in the minimization problem (2.2) with at least its quasiconvex envelope or to enlarge the space of admissible deformations with the space of parameterized measures.

The technical literature on the subject shows that the idea of replacing the original nonconvex potential W in the minimization problem (2.2) goes back to L.C. Young. In 1937 he [You37]

suggested to use a lower-quasiconvex envelope QW of the original nonconvex energy function W. This reformulates the original problem into a relaxed problem without changing its essential characteristics (about these essential characteristics we would talk about later in our discussion). The relaxed version of the problem in (2.2) is thus stated as

$$\inf_{\mathbf{u}} \left\{ \int_{\Omega} W^{rel}(\nabla \mathbf{u})\, dV - \ell(\mathbf{u}) \,:\, \mathbf{u} = \mathbf{u}_{\circ} \text{ on } \partial\Omega \text{ and } \mathbf{u} \in W^{1,p}(\Omega, \mathbb{R}^n) \right\} \tag{2.3}$$

where $W^{rel}(\nabla \mathbf{u})$ is the quasiconvex envelope of W. The second technique suggested by him for the formulation of minimization problem without taking care about the lower semi-continuity of the integral functional $(I(\mathbf{u}))$ is to replace the space of admissible functions (Sobolev space) by the space of parameterized measures, in this way one can enlarge the space of a priori solutions, but this is not a good idea in many situations since it can change the problem into a completely new problem which may be of no interest anymore as far as its physical applications are concerned. His first suggestion of replacing the original nonconvex energy function with its corresponding quasiconvex envelope was appealing and therefore adopted to many applications later e.g., see in the work of Bartels et al. [BCC$^+$06], Carstensen et al. [CCO08, CHM02], Conti. et al. [CDK09, CHO07, CO05, CT05], DeSimone et al. [DeS04, DD02], Hackl et al. [HH01], Kohn et al. [Koh91, KS86a, KS86b, KS82, KS83, KV87], Lambrecht et al. [LGM , LMD03], Miehe et al. [ML03, MLG04, MSL02] and Müller [M9]. Nevertheless the idea of enlarging the space of admissible deformations has its own significance in many engineering problems. The effort in this direction can be seen in the literature of Carstensen et al. [CP97, CR97, CR00]. Energy relaxation techniques allows us to find an approximate solution of the original non-convex problem which lacks the unique solution.

The effect of relaxation on the physical behavior of the material is realized by its macro-mechanical features. Relaxation extract all possible information of material microstructure pertinent to its macro-mechanical behavior. After reformulating the original non-quasiconvex energy minimization problem to a relaxed one, the new problem is now more effective, efficient and well defined for practical applications.

Analytical computation of the relaxed energy

The computation of exact analytical formulae for the relaxed (quasiconvex) energy W^{qc} functions corresponding to non-quasiconvex variational minimization problems in continuum mechanics is not an easy task. The difficulty arises due to the non-local definition (3) of the quasiconvex energy function. Moreover, for a space dimension n= 2 (or 3) in (3) the energy density is defined on a four (or nine)-dimensional matrix spaces, which can be reduced using invariance property under rotations.

The exact analytical results for the relaxed energy are known only for few variational problems in the literature so far. For example the work of DeSimone and Dolzmann [DD02] where they give an exact envelope of the relaxed energy potential for the free energy of the nematic elastomers undergoing a transition from isotropic to nematic-phase. Dret and Raoult in [DR95] compute an exact quasiconvex envelope for the Saint Venant-Kirchhoff strored energy function expressed in terms of singular values. The resulting quasiconvex envelope is

not only rank-one convex and polyconvex but also convex. Some analytical examples of quasiconvex envelopes are also mentioned by Raoult in [Rao10] for different models in nonlinear elasticity. Kohn and Strang [KS86a, KS86b] gave an exact formula (see Theorem 1.1 in [KS86a]) for the relaxed energy for a variational problem which has its emergence from the shape optimization problems for electrical conduction. Another exact relaxed result is mentioned by Conti and Theil in [CT05] where they give two results (Theorem 3.1 (quasiconvex envelope for two dimensional case), and Theorem 3.2 (the coinciding rank-one and polyconvex envelopes for the general three dimensional case)) for the incremental nonconvex variational problem for rate-independent single active slip elastoplastic materials. Conti and Ortiz [CO05] determine an exact analytical expression for the relaxed energy in single crystal plasticity with a nonconvex constraint on the deformation of the crystal that all the material points must deform in a single slip direction. The macroscopic study of effective behavior leads them to predict different possible regimes that shows different type of dislocation microstructure in a sigle crystal. They extended their analytical expression in [CHO07] to the case of crystal plasticity with arbitrary hardening features. Kohn and Vogelius study the inverse problem of applied potential tomography (also called electrical impedance tomography) and come up with an analytical formula [KV87] for the relaxed energy by using the results from homogenization. In a similar manner but this time with the use of Fourier analysis Kohn presents in Theorem 3.1 of [Koh91] an exact analytical expression for a two well energy function with application to solid-solid phase transitions.

Exact relaxed energies not only ease the search for the minimizing deformations of the corresponding minimization problem but also reduce the computational cost (which is needed when one compute the quasiconvex envelope numerically) and work load in finding these energy minimizing deformations. The micro-mechanical features of the material from its microstructure are carried safely and predicted certainly at the macroscopic computational scale. Use of exact relaxed energies for the modeling of complex microstructural material enables us to formulate more accurate constitutive relations for the macro-mechanical analysis of these materials. But the fact is that not in every needed physical situation we have exact analytical formula for the related non-quasiconvex free energy of the material. For an example among many other energy densities let us consider the Ericksen-James energy density, which has its applications in the modeling of smart materials. Ericksen-James energy density fails to be quasiconvex (see for reference [GP98b] and [Rao10]) and there is no analytical expression present in three dimension till to date. Another important energy density is the energy function of Saint Venant-Kirchhoff materials which also fails to be quasiconvex in three dimension [Rao86].

Relaxed problems for which there is a possibility of deriving an analytical expression for the free energy of the material are free of fine oscillations of the minimizing deformations unless there is an error in the numerical computations. For the problems where the analytical expression for the relaxed energy is not easy to derive one opt the numerical procedures for the computation of its relaxed envelopes. There are many situations where these numerical computed relaxed energies suited to the desired mechanical response of the material in examination. By computing the relaxed energy numerically we are computing the weak lower semi continuous envelope of the original energy integral functional. These numerical approximations of the weakly lower semi continuous envelopes of the energy functional $I(\mathbf{u})$ are worked out by Brighi et al. [BC94] and Carstensen et al. [CP97] where even in very special cases the level of difficulty in finding these envelopes is prominant. Other numerical procedures have been therefore intorduced to find the relaxed energy envelopes of the corresponding non-quasiconvex energy functions [CR97, CR00]. These procedure

[AP01, Bar01, CCO08, Chi99, CC92, CKL91, Dol99, DW00, Rou96] are efficient enough to approximate the quasiconvex envelope W^{qc} which is the largest convex envelope below W.

Polyconvex and rank-one convex envelopes which give upper and lower bounds to the quasiconvex envelope are also useful for the characterization of quasiconvex envelopes. Numerical procedures for the polyconvexification and rank-one convexification are suggested e.g. in the work of Bartels et al. [BCC$^+$06]. Numerical approximation of rank-one convex function for the incremental stress potential has been employed in the energy minimization problems for the macro-mechanical analysis of strain softening inelastic solids by Miehe et al. [ML03]. Dolzmann et al. have presented numerical algorithms for the computation of rank-one convex envelopes in [Dol99, DW00]. Another numerical iterative procedure is presented by Wang et al. in [WL07] for the computation of rank-one convex envelopes.

Numerical approximation via generalized solutions (young measures)

The highly oscillatory behavior of the gradients of infimizing deformations sequence of the non-quasiconvex variational problems in continuum mechanics lacks classical solutions and therefore develop the interest in finding the generalized solutions to these non-quasiconvex variational problems. Lack of weakly lower semicontinuity of the integral functional $I(\mathbf{u})$ is kept responsible for the non-convergence of the sequence of infimizing deformations (u_l) in a minimization problem. This non-convergence of (u_l) is due to the oscillations of the gradients of these infimizing deformations at finer and finer scale. These oscillatory behavior of the infimizing deformations can be captured by a mathematical tool called Young measures. For the existence of Young measures and its mathematical definition see [BCC$^+$06, M9]. The formation of internal structure in a material is strongly connected to the oscillatory behavior of the gradient of the sequence of infimizing deformations (∇u_l) in a related minimization problem. The Young meansures associated with these sequences (∇u_l) are called gradient Young measures. The problem is reformulated into a quasiconvex minimization problem where the physical structure of the original non-quasiconvex energy function in not changed but theoretically it is replaced by its approximated quasiconvex energy function using young measures. The idea, first discussed by Young [You37] and afterwards refined by others [Bal88, BJ87, JK89, KP94], is to enlarge the space of admissible deformations that account for the energy minimization. For this purpose numerical procedures and techniques are proposed. The methodology of constructing a relaxed energy minimization problem by using Young measures is discussed e.g. in [CR97, CR00, NW92a, NW92b, Ped97, Ped95, Ped96, Rou94, Rou96, Rou97]. A numerical scheme for the microstructure in a nonconvex vectorial variational problem is discussed in [AP01] using Young measure approximations.

2.4.2. Direct numerical minimization

Non-quasiconvex energy functionals are minimized directly by the application of finite element discretization for both the related non-quasiconvex energy density and the material domain. By doing so one preserve the physical relevance of the energy function, i.e. the physical importance is not removed from the energy minimization problem. Although by using these numerical methods it is difficult to reach the desired minimum energy state, since

the numerical procedure may stop at a local minimum energy state. But for some application (e.g. in hysterises phenomenon the metastable states may be desired) it is equally advantageous. This non-attainment of the global energy minimizer is due to the non-quasiconvex nature of the energy density.

Finite element method has been applied to obtain the energy minimizers directly solving the non-quasiconvex energy minimization problems [GP98b]. Using direct numerical simulation for solving the non-quasiconvex energy minimization problem leads to mesh dependent results. This means that on a coarse mesh the solution of the non-quasiconvex energy minimization problem strongly differs from that on a finer mesh. Although Gobbert and Prohl [GP98b] have shown that the choice of discontinuous finite elements rather than classical finite elements can take to mesh independent solutions. For a detailed discussion on the subject we refer to the following articles [Col90], [GP98a], [LL96], [LL98], [Lus96a], [Lus96b] for reading. A numerical strategy based on finite element analysis is outlined by Carstensen et al. in [CP97] for the solution of two-well problem with application to solid-solid phase transformations. Other numerical treatment of non-quasiconvex variational problems with potential wells are discussed by Chipot et al. in [Chi99, CC92, CL95]. Also the work of Collins et al. [CKL91, CLR93] give an insight that how these numerical approximations can be used for the approximation of relaxed variational problems with application to phase transforming solids. Roubíček [Rou96] has treated the non-quasiconvex variational problems in a two way approach, first he get a relaxation by gradient Young measures and then apply the direct numerical minimization using finite element strategy.

We close this discussion on relaxation theory and methods with the conclusion that here in this dissertation we provide an exact analytical expression for the quasiconvex envelope of the nonconvex free energy density which arise during our study of intergranular interactions of the continuum particles in a granular medium. Moreover an analytical expression for the free energy of a two phase material which undergoes a phase transition form martensites to detwinned martensites.

Part I.

Variational modeling of granular materials using exact relaxed potential

3. Modeling of a granular medium with microstructures

Due to a large number of industrial applications and their use in everyday life granular materials have been studied extensively throughout the past years. A numerous investigations have been performed in order to model the different mathematical and mechanical aspects of these materials [AVA06, KAV06, AS06, Bar94, CM92, EV97, EGGS00, God86, HC07, HNB02, MNR99, M9*b*, MV87, MGC12, OK98, PV11, PM01, dPIA02, SZY06], [SdBC01a, SdBC01b, Tej97, TN06, Tp01, TS98, TS99, AT02, TW05, TWG04, Var09, WT06, WTP07]. Our focus is to consider the counter-rotations of granular particles at the microscale and to develop a mechanical model that can predict on the formation of distinct deformation patterns (for an overview on the experimental observations of such patterns the reader is referred to the book by Aranson and Tsimring [AT09]) which are related to the microstructures in the granular materials. The mechanical behavior of granular materials have been simulated and investigated mainly by two distinct approaches where discrete and continuum description of the granular particles are considered. In developing a mathematical model for their deformation behavior we focus our attention to the continuum description of granular particles. Consideration of continuum description of granular particles in modeling the granular materials with microstructures have been proved successful, a survey on which is presented in the next section.

3.1. Continuum theories for the modeling of granular materials

Continuum theories for the simulation of granular materials have been employed since 1776 when the first yield criterion for the granular materials was stated by Coulomb [Cou76]. Here, in this section, we review continuum theories more specifically the generalized continuum theories for the modeling of granular materials with microstructures. Among the generalized continuum theories the emphasis would be particularly on the Cosserat continuum theory, which would be further used for the development of material model for the granular media with microstructures.

Continuum theories are divided into two main branches consisting of nonlocal and local continuum theories. Nonlocal continuum theories based on the concept of nonlocal actions which means that at a particular material point the mechanical behavior of a material under deformation is influenced or depends upon the state of all other material points in the domain. A published treatise on nonlocal theories is present in the literature due to Eringen [Eri02]. Nonlocal action principle in the continuum is a generalization of the local action principle. Local action principle states that the deformation behavior of a material at a particular point can be completely determined by the variables defined at that point only. Local continuum theories are further divided into two main categories in one of which lies is the classical continuum theory and in the other lies are the non-classical continuum theories. Classical continuum theory is the usual Boltzman continuum in which each material point of the continuum body has three degrees of freedom which are related to the displacements

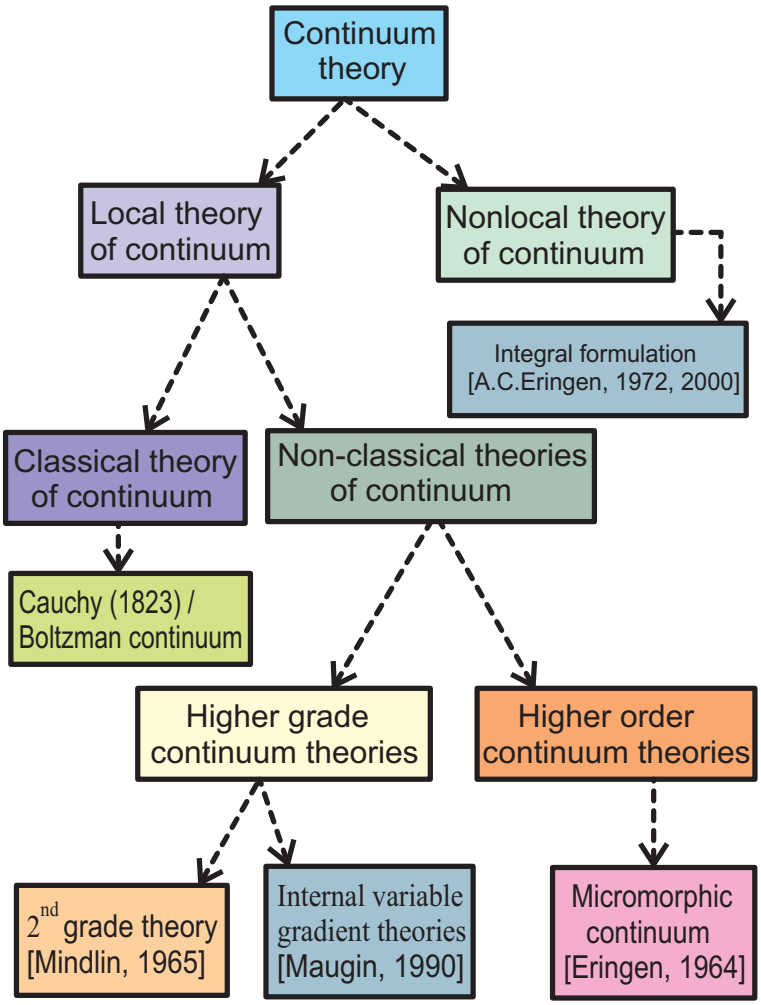

Figure 3.1.: A tree diagram of different continuum theories.

of that particular point. Non-classical continuum theories are endowed with additional degrees of freedom. Generalized continuum theories are the non-classical continuum theories which can further be categorized into two subgroups. In one of which lies is the higher-grade continua, and in the other, higher-order continua is placed. In the higher-grade continuum theory (e.g. the second-grade theory of Mindlin [Min64] and Maugin [Mau92]) either the higher-order derivatives of the displacement field or the gradient of the internal field variables are involved. In higher-order continuum theories additional (to classical Cauchy continuum theory) degrees of freedom are incorporated. A tree categorizing the continuum theories is given in the Figure 3.1.

Higher-order continuum theories are well suited for the modeling of granular materials with microstructures due to the integration of additional degrees of freedom. Since these additional degrees of freedom becomes an important mean of information regarding the microstructural changes which are further inter-related to the overall macroscopic changes with suitable deformation measures. Higher order continuum theories are further categorized into three microcontinuum field theories which were sorted out by Eringen [Eri02] using the concept of directors initially introduced by Ericksen and Truesdell [ET58] in 1958. These directors are being attached to each microcontinuum point. According to them each continuum point is endowed with nine additional degrees of freedom. Thus the state of the elastic material body at any particular time is depending upon a total of twelve degrees of freedom.

Three of them are the usual displacement degrees of freedom of Cauchy continuum and the nine additional degrees of freedom arising from the micro-deformation of the continuum points (also called deformable directors) which are related to the material microstructures. In Cosserat continuum these directors are assumed to be rigid. Thus generalizing the concept of Cosserat continuum they therefore introduced a new theory in which they considered the three additional micro-stretches of each rigid director of Cosserat continuum and named the theory as microstretch theory of continuum, which was further generalized to the theory of micromorphic continuum in which each rigid director of Cosserat continuum is assumed to be deformable. In microcontinuum theories of Eringen [Eri02, Eri68], the second order deformation tensor is related to macroscopic deformation and the third order deformation tensor is related to the microdeformation of the continuum points. Both these second and third order tensors can be decomposed into dilation, rotation and strain tensors (see Figure 3.2), with a unique description for the second order decomposition and a non-unique description for the third order tensor. For instance, if we consider that the second order deformation tensor is denoted by $\mathbf{S}$ and the third order deformation tensor by $\mathbb{T}$ then the decomposition into the dilation, rotation and shear part is described mathematically as

$$\mathbf{S} = \underbrace{\frac{1}{d}\,\mathrm{tr}\,\mathbf{S}\,\mathbf{I}}_{\text{Dilational part}} + \underbrace{\mathbf{S}_A}_{\text{Rotational part}} + \underbrace{\mathrm{dev}\,\mathbf{S}_S}_{\text{Shearing part}}, \tag{3.1}$$

and

$$\mathbb{T} = \underbrace{\mathbf{t}\otimes\mathbf{I}}_{\text{Dilational part}} + \underbrace{\mathbb{T}_A}_{\text{Rotational part}} + \underbrace{\mathrm{dev}\,\mathbb{T}_S}_{\text{Shearing part}}, \tag{3.2}$$

where d is the dimension of the problem under consideration, $\mathrm{dev}(\cdot) = (\cdot) - \frac{1}{d}\,\mathrm{tr}(\cdot)\mathbf{I}$, $\mathbf{I}$ is the second order identity tensor, the subscript S and A stands for symmetric and asymmetric part and the vector $\mathbf{t}$ has the following form

$$t_i = \frac{1}{d}T_{ikk} \quad \text{where} \quad \mathbb{T} = T_{ijk}\mathbf{e}_i \otimes \mathbf{e}_j \otimes \mathbf{e}_k. \tag{3.3}$$

The non-unique decomposition of the third order tensor into dilation, rotation and shear part can be realized after observing equation (3.3) where the indices (j, k) have been fixed for the decomposition of $\mathbb{T}$. The other two possibilities could be with the fixed (i, j) or (i, k).
This decomposition of the second and third order tensors of microcontinuum field theories and the probability of possibly existing deformation modes in a granular material as indicated in the Figure 3.2, allows Forest and Sievert [FS06] to further classify these theories. This classification of the microcontinuum field theories is shown in the Figure 3.3 where they can be sorted out according to the number of degrees of freedom incorporated with.

For the complete description of kinematic and constitutive relations see for instance the work of Eringen [Eri02] and Forest and Sievert [FS06]. Also, a very good survey on the consequences of these constitutive equations of the generalized continuum is provided in the work of Lakes [Lak95]. Here the purpose of this study is not to give a detailed description of the constitutive relations in each of the case but to understand their development on the basis of the idea of deformation tensor decomposition, in order to complete the discussion on the higher order continuum theories for the modeling of granular materials behavior. Furthermore, the aim of this section is to provide an overview of the higher order theories which are capable of modeling the granular material with microstructures.

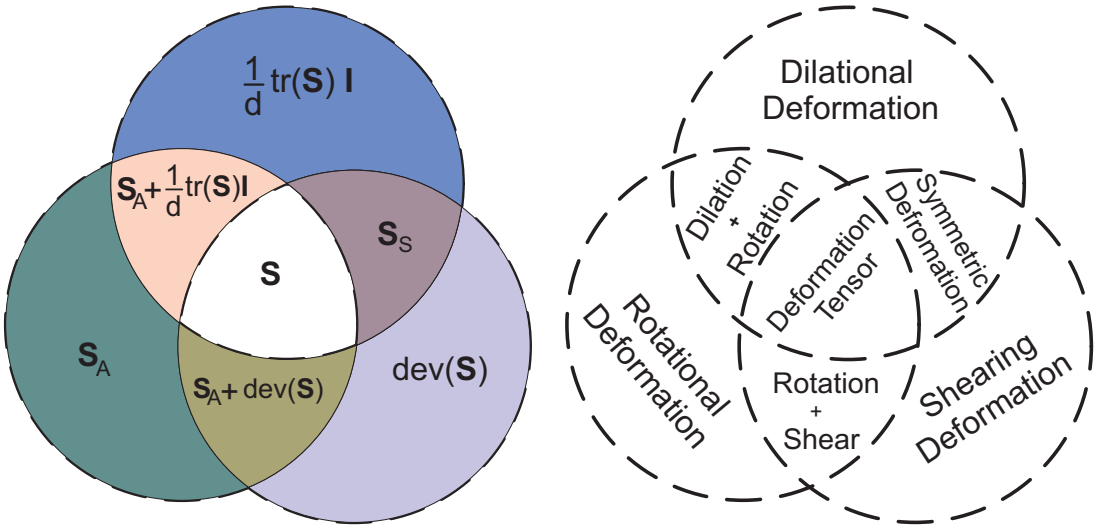

Figure 3.2.: In left: Deformation tensor **S** is decomposed into different parts. In right: The possible deformation mechanisms as a result of decomposition of the deformation tensor.

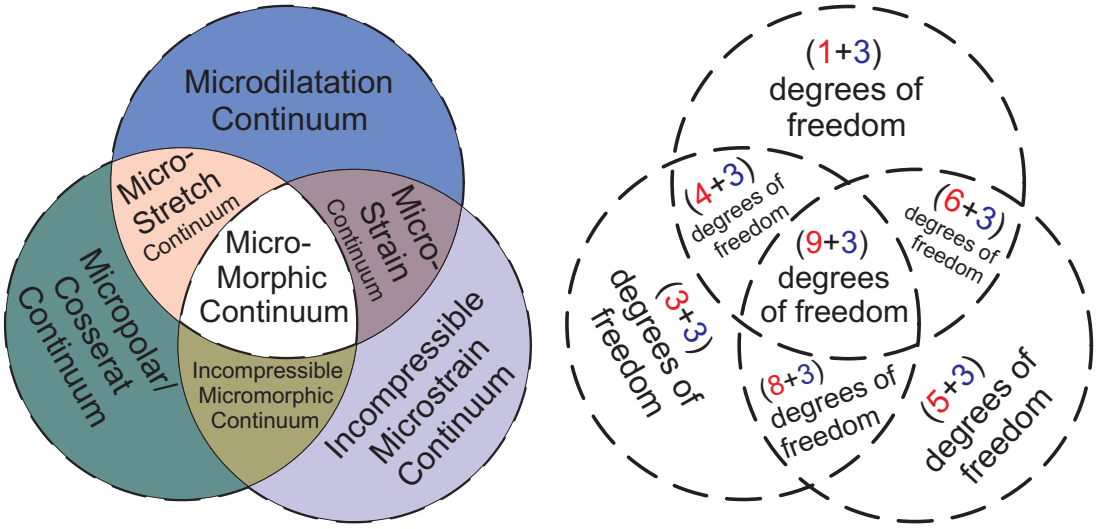

Figure 3.3.: In left: Seven-subclasses of higher order continua. In right: Degrees of freedom associated to each sub-class, the blue colored digit is the number related to the three displacement degrees of freedom of Cauchy continuum whereas each red color digit is related to the micro-deformational degrees of freedom of corresponding higher order continuum.

Granular materials often exhibit soft zones under deformation. These soft zones are also called shear bands [BH99, EV97, GN04, ML03, M9*b*, MV87, OK98, TB96, TPG04] and are precursors to the material failure in general. The reasons of their development in granular material can be traced to the phenomenon of particle rotations. These particle rotations cannot be well understand by the classical continuum models. And at the onset of these softening zones in the material classical continuum models fails to describe the material behavior anymore. Thus the initial or boundary value problem described by the classical continuum approach becomes ill-posed due to the fine oscillations of the gradient of minimizing deformations. Moreover in such situations modeling with classical continuum approach leads to mesh dependent solution to these initial or boundary value problems. A remedy to such problematic situation is to introduce the regularization techniques to the classical continuum model, or to use higher order gradient theories [CCM01, Mau92, SdBC01a], or introduce length scale effects to the constitutive relations [AS06, TWG04], or to use coupled stress theory [Now68, Now70, Tou62, Tou64] which take contribution from particle rotations. Among the theories which aptly incorporate the length scale effects is the Cosserat continuum theory. Moreover Cosserat continuum takes into account the particle rotation in an independent way. It introduces independent rotational degrees of freedom with the translational degrees of freedom of the classical continuum. And therefore considered to be suitable to describe the behavior of granular materials.

The main objective of this study is to reconsider the rotational phenomenon of granular material and propse some new measures that help in predicting the microstructural features of the material.

3.2. Intergranular kinematics and the interaction energy potential

Particle rotations in a granular assemblage is an intriguing and experimentally well recognized [OK98, OKNN82, SZY06] phenomenon that contribute in the development of material microstructures [Bar94, SdBC01a, TPM05, TW05]. Although the rotations of particles at the microscale in a granular medium has been considered in the work of Alonso-Marroqun et al. [AMVH^{+}06], Chang and Hicher [CH05], Chang and Ma [CM92], Hicher and Chang [HC07], Papanicolopulos and Veveakis [PV11], Suiker et al. [SdBC01a, SdBC01b], Tordesillas et al. [TPM05], Tordesillas and Walsh [TW05] and Vardoulakis [VS95] , but the essence of these particle rotations especially their interactions in observing the formation of distinct deformation patterns in a granulate medium is not well understood. It is therefore our aim to reconsider the intergranular kinematics of the counter-rotating particles at the microscale in a granular assemblage. In this section, we try to develop an interaction energy potential in a granulate medium which arises as a consequence of counter-rotations of its particles. In the next sections, we will describe the different features of this interaction energy potential and will demonstrate on its contribution in observing different microstructural regimes in a granular medium.

We propose some new measures for the characterization of microstructural phases in Cosserat continuum after taking into consideration the kinematics of the particles of a granular structure at the continuum scale. Due to numerous applications of the granular materials and the exhibition of distinct deformation patterns it got to our attention to consider the inter granular cohesive interactions of their discrete particles. The key issue while discussing the intergranular kinematics of granular material at the continuum scale is to establish a relation

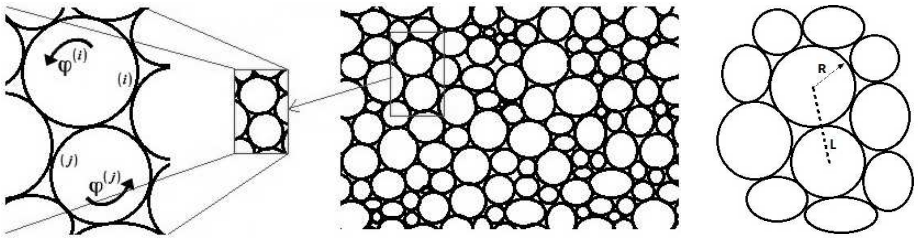

Figure 3.4.: A schematic representation of a granular structure with counter rotating particles.

between the microscopic response of the material due to particle interactions and its macroscopic behavior. The particles in the granular assembly at the microscale are discrete in nature. Therefore to understand the effect of their interaction on the physical properties and the overall response of the material at the continuum scale has been a long discussion in the field of micromechanics of granular materials. These particle interactions leads to two important modes of deformations in the granular assembly called sliding and rolling of particles in contact which play crucial role in the dissipation of the material energy [AMVH$^+$06, PV11] at the continuum scale.

In our study we develop an interaction energy potential that takes into account the intergranular kinematics at the continnuum scale and define two new material parameters as a suitable measure for the observation of microstructural phases of the material. For this purpose consider the granular material where two neighboring grains/particles are in contact with each other as shown in Figure 3.4. The two particles have sliding and rolling effects which contribute to the material energy, therefore it is necessary to take into account this micro-rotational and translational interacting motions of these particles at the continuum scale.

Intergranular kinematics is governed by independent translational and rotational motions of the granules at the microscale. Consider now that at the continuum scale the translational motion of the two interacting particles is represented by the displacement vector field $u_i\,\mathbf{e}_i$ and the rotational motion of the interacting granular particles is represented by a field vector analogous to the micro-rotational vector field $\varphi_i\,\mathbf{e}_i$ of the Cosserat continuum. The strain measures are then associated with the deformation of these interacting particles. Corresponding to displacement vector field and the microrotational vector field are the associated deformation tensor fields $u_{j,i}\,\mathbf{e}_i\otimes\mathbf{e}_j$ and $\varphi_{j,i}\,\mathbf{e}_i\otimes\mathbf{e}_j$ respectively. The symmetric part of $u_{j,i}\,\mathbf{e}_i\otimes\mathbf{e}_j$ is the classical strain tensor $\varepsilon_{ij}\,\mathbf{e}_i\otimes\mathbf{e}_j$. A deep insight into the rotating phenomenon of the interacting grains/particles clears that the macroscopic shear $\left(\varepsilon_{ij}-\dfrac{1}{d}\varepsilon_{kk}\,\delta_{ij}\right)\mathbf{e}_i\otimes\mathbf{e}_j$ influence the microrotational deformation $\varphi_{j,i}\,\mathbf{e}_i\otimes\mathbf{e}_j$ of the granular particles. This leads us to suggest a proportionality relation between the gradient of the microrotational vector field and the macroscopic shear strain which in mathematical terms is given by

$$\sqrt{\sum_{i,j=1}^{d}\left(\varphi_{j,i}\right)^2}\propto\sqrt{\sum_{i,j=1}^{d}\left(\varepsilon_{ij}-\frac{1}{d}\varepsilon_{kk}\,\delta_{ij}\right)^2} \tag{3.4}$$

where d is the dimension of the space under consideration. This proportionality relation is solved with the introduction of the length scale parameter β with the dimension of the inverse

of a length. Thus we can write

$$\sqrt{\sum_{i,j=1}^{d} (\varphi_{j,i})^2} = \beta \sqrt{\sum_{i,j=1}^{d} \left(\varepsilon_{ij} - \frac{1}{d} \varepsilon_{kk}\, \delta_{ij} \right)^2} \tag{3.5}$$

This brief but comprehensive discussion on itergranular kinematics enables to propose an interaction energy potential that will contribute to the material strain energy functional. This interaction energy potential is stated as

$$\mathcal{I} = \alpha \left(\sum_{i,j=1}^{d} (\varphi_{j,i})^2 - \beta^2 \sum_{i,j=1}^{d} \left(\varepsilon_{ij} - \frac{1}{d} \varepsilon_{kk}\, \delta_{ij} \right)^2 \right)^2 \tag{3.6}$$

or, in tensor notation

$$\mathcal{I} \;=\; \alpha \left(\left\| \nabla \boldsymbol{\varphi} \right\|^2 - \beta^2 \left\| \operatorname{dev} \operatorname{sym} \nabla \mathbf{u} \right\|^2 \right)^2 \tag{3.7}$$

where α and β are non-negative material constants, α is the interaction modulus having information regarding frictional effect in the interacting particles and β is related to the particle size having information regarding intrinsic length scale in Cosserat continuum. The proposed interaction energy potential not only bridges the gap between microstructural properties and the macroscopic behavior of the material but also enables us to characterize the different microstructural phases in the granular material.

3.3. Cosserat continuum theory

The origin or the main idea of the Cosserat continuum theory should be credited to a German physist Woldemar Voigt who in 1887 published the article [Voi87] which possibly lead to the development of this theory. In a detailed description, it was first discussed in 1909 by the French brothers, Eugèn Cosserat and François Cosserat, in the monograph [CC09] written originally in French which was afterwards translated into English by D. H. Delphenich in 2007. A first review of the book [CC09] was published in 1913 by Wilson in his article [Wil13]. The importance of the theory was not recognized for many years due to its unexplored applications, non availability of additionally introduced material parameters (for example in case of linear isotropic elastic material other than the two Lame's parameters it has four additional material parameters) and unsettled description of the constitutive relations (since the Cosserat brothers did not established the constitutive equations of the Cosserat continuum theory when it was first presented in [CC09]). The theory enjoyed its renaissance with the work of Günther [G8] in 1958. In the 1960's Eringen [Eri68], Eringen and Suhubi [ES64], Grioli [Gri60], Mindlin [Min64], Nowacki [Now69, Now68, Now70], Palmov [Pal64], Schaefer [Sch62, Sch67], Suhubi and Eringen [SE64], Toupin [Tou62, Tou64], Truesdell and Toupin [TT60] have published their work on Cosserat continuum in which they further developed the theory in different directions and provide a more reliable and sophisticated constitutive description of the Cosserat continuum. The theory got the attention of many researchers in the sixties of the last century which can be realized from the work of Stojanović [Sto69] where four hundred references are presented. At the same time the theory was generalized to the framework of finite deformations by Aero and Kuvshinskii [AK60], Grioli [Gri60], Kafadar and Eringen [KE71, KE76], Reissner [Rei73, Rei87], Stojanović [Sto72], Toupin [Tou62] and Truesdell and Toupin [TT60].

Later, with the deeper understanding on the advanced engineering materials and their mechanical behavior the necessity of working in the framework of Cosserat continuum theory was realized to address different engineering problems. The theory was completely developed in 1960s, since than it has been used in modeling the mechanical behavior of a large number of materials. For example in modeling the behavior of granular medium [AVA06, KAV06, Bar94, CM91, CM92, EV98, HB03, M9b, MV87, PV11, PM01, SZY06, Sch62], [Sch67, SdBC01a, SdBC01b, SD02, Tej97, TB96, Tp01, TN06, TPM05, TS98, TS99, AT02, TW05, TWG04, WT06, WTP07, ZJM06], in foams [AL94], in failure analysis [Bar94], [Eri68], [PV11], in plate and shells [AAE10], in observations of localized zones [AVA06, KAV06, BH01, dB91, dBS91, DSW93, EV97, GN04, HB03, HNB02, M9b, MV87, Tej97], [TB96, Tp01, TN06, TPG04, TW05, WADS95], in porous media [EV98] (and references there in), in rods and shells [ET58] (and references there in), in sands [GN04] (and references there in), in bones [PL86] (and references there in), in rocks [SD02] (and references cited in), in wave propagation through infinite medium [SdBC01b] (and references cited in) and in modeling the thermomechanical behavior of materials [Now69, Now68, TW05]. A more detailed review of the Cosserat continuum theory can be found in the paper [AAE10] by Altenbach et al. where they present a detailed bibliography (consisting of 333 references) on the many possible applications of the Cosserat continuum theory.

The exhibition of deformation behavior pertinent to the theory of Cosserat continuum has also been noticed by experimental investigations. Park and Lakes observed the microstructural effects in the deformation behavior of the human compact bone in torsion while performing an experiment [PL86]. According to them the redistribution of the strain measured in wet bone was almost similar as calculated with the Cosserat elasticity theory. The experimental work of Lake [Lak86, Lak95], Tejchman and Gudehus [TG93] and the reference cited in there also demonstrate on the possible applications of the Cosserat continuum theory.

The Cosserat continuum theory adequately describes the microstructural behavior of granular materials due to the consideration of additional and independent rotational degrees of freedom. Here we present a brief review on the applications of Cosserat continuum with special emphasis on the use of Cosserat continuum in different aspects for the observation of deformation mechanisms of granular materials with microstructures.

Various approaches have been adopted to model the granular materials with microstructure using Cosserat continuum theory. For instance, Tordesillas and Walsh [AT02] use micromechanical approach in modeling the mechanical behavior of granular materials. They incorporated rolling resistance and contact anisotropy in a Cosserat continuum model and devised a homogenization procedure to capture the localized patterns related to the granular material microstructures. Modeling the localized behavior of granular material has been considered a major application of Cosserat theory. Tordesillas and Walsh and Tordesillas et al. [TPG04, AT02, TW05] use a micromechanical approach for modeling the localization behavior of granular materials with microstructures. Based on a micromechanical theory of Cosserat continua Chang and Ma [CM91] model the deformation behavior of granular materials using a constitutive relations accounting for the particle interactions. Within the framework of small strain theory a constitutive description based on second-grade micropolar continua is developed by Suiker et al. [SdBC01a] incorporating the microstructural effects due to particle kinematics, which can be reduced to the Cosserat continuum theory for modeling the granular materials behavior. Using a Cosserat continuum theory a micromechanical approach in modeling the dense granular materials is also presented by Zhang et al. [ZJM06]. A multiscale analysis using non-local constitutive setting has been carried out by

Tordesillas et al. [TWG04] in modeling the granular material microstructures. A numerous of different constitutive models have been proposed for the analysis of localized deformation bands developed in granular materials that are the precursors to the material failure. A polar hypoplastic constitutive settings of Cosserat continuum have been used by Bauer and Huang [BH01], Huang et al. [HNB02], Tejchman and Bauer [TB96] and Tejchman and Poland [Tp01] to calculate the shear zone patterns in granular medium. A finite element analysis of localized bands based on anisotropic micropolar hypoplastic model is performed by Tejchman and Niemunis [TN06]. Using hypoplastic constitutive laws in the framework of Cosserat continuum Gudehus and Nübel [GN04] present a comparison of experimentally and numerically observed localized deformation patterns in granular material. An elastoplastic constitutive theory of Cosserat continuum is used by Ehlers and Volk [EV97] for modeling the strain softening patterns in the granular materials. In the framework of large deformations and rotations Steinmann [Ste94] give an elastoplastic Constitutive model to investigate the phenomenon of localized bands in granular materials. Willam et al. [WADS95] use plasticity theory of Cosserat continuum to capture the localization behavior of granular material leading to the development of microstructures. Alsaleh et al. [AVA06] developed a Cosserat continuum model by incorporating micro-rotations, couple stresses in the Lade's model for modeling the localized deformations in granular materials. They present [KAV06] its numerical implementation to simulate the sand and glass beads samples and predict the shear bands. A homogenization technique based on differential expansion in the framework of Cosserat continuum has been considered and generalized by Pasternak and Mühlhaus [PM01] for the granular materials with microstructures. They developed a Cosserat continuum model based on the idea where each granular particles are connected through translational and rotational springs. According to them the micro-rotational degrees of freedom of Cosserat continuum are natural outcome from the consideration of a discrete system of granular particles with interparticle contact forces and moments using mathematical homogenization procedure.

Although the Cosserat continuum has proved to be an appropriate theory for the modeling of granular materials with microstructures, it also has been used in modeling the mechanical behavior of many other engineering materials. There is a growing interest in its applications in crystal plasticity, for instance, see the work of Steinmann [Ste94] and references in [DFC98, FS06]. Here the Cosserat continuum theory is used for modeling the mechanical behavior of a granular medium considering the microstructural effects at the continuum scale.

3.3.1. Kinematics of the Cosserat continuum

The material point of a Cosserat continuum has six degrees of freedom. Three of them are the translational motions represented by the displacement vector field $\mathbf{u}$ and three are the micromotions represented by the microrotational vector field $\boldsymbol{\varphi}$. The micromotions of the continuum points are independent of its translational motions. Associated with the displacement and microrotational vector fields are the Cosserat strain tensor $\boldsymbol{e}$ and the curvature strain tensor $\boldsymbol{\kappa}$, respectively. These strain tensors are defined as

$$\boldsymbol{e} \;=\; \nabla\mathbf{u} - \operatorname{asy}\boldsymbol{\varphi}, \qquad \text{in index notation: } e_{ij} = u_{j,i} - \mathcal{E}_{ijk}\,\varphi_k, \tag{3.8}$$

$$\boldsymbol{\kappa} \;=\; \nabla\boldsymbol{\varphi}, \qquad \text{in index notation: } \kappa_{ij} = \varphi_{j,i} \tag{3.9}$$

where in (3.8) $\operatorname{asy}\boldsymbol{\varphi}$ is the second order microrotational deformation tensor

$$\operatorname{asy}\boldsymbol{\varphi} = \boldsymbol{\mathcal{E}}\cdot\boldsymbol{\varphi}, \tag{3.10}$$

and $\boldsymbol{\mathcal{E}} = \mathcal{E}_{ijk}\,\mathbf{e}_i \otimes \mathbf{e}_j \otimes \mathbf{e}_k$ is the third order permutation tensor, where $\mathcal{E}_{ijk} = 1,\ -1$ or 0 if respectively (ijk) is an even permutation, an odd permutation or either of the index is repeated. Since the deformation of a Cosserat material depends on the particle rotations therefore being a measure of deformation the Cosserat strain tensor $\boldsymbol{e}$ depends upon the microrotations of the continuum particles and hence is inter-related to the curvature strain tensor $\boldsymbol{\kappa}$. The interesting point to note in these kinematic relations is that the two field variable displacement and microrotation of two different structures are unified in a compatible way. This compatible description not only preserves the independence of the two field variables but also provide a connection of the field variables at two different structures (micro and macro structure) of the material. For the formalism of these deformation measures which connect the microstructural degrees of freedom to the macrostructural degrees of freedom in Cosserat continuum in an independent manner the reader is referred to Section 3 of [BS89] and also [CC09].

The macrorotational deformation in a Cosserat continuum is influenced by the microrotational deformation of the continuum particles and therefore an appropriate relative measure for the macro-rotational deformation is defined as

$$\boldsymbol{\omega} \;=\; \operatorname{asy} \nabla \mathbf{u} - \operatorname{asy} \boldsymbol{\varphi}, \qquad \text{in index notation: } \omega_{ij} = \frac{1}{2}\left(u_{j,i} - u_{i,j}\right) - \mathcal{E}_{ijk}\,\varphi_k. \tag{3.11}$$

3.3.2. Balance laws in a Cosserat continuum

The balance of mass and balance of linear momentum in a Cosserat continuum are identical to that in Boltzmann continuum except with the understanding that here the force-stress tensor is not symmetric. Due to this non-symmetricity of the force-stress tensor an additional balance equation called the balance of angular momentum need to be satisfied by a continuum body to be in equilibrium. This balance equation takes into consideration the independent micro-rotations of the Cosserat medium and the associated couples in the form of couple-stress tensor. To be precise, the law of balance of mass, mechanical energy and entropy are not presented here, for the description of these laws the reader is referred to the book by Vardoulakis [Var09]. The mathematical description of balance of linear and angular momentum is given below

Balance of linear momentum

The balance of linear momentum also called translational momentum states that the material rate of change of total linear momentum of a body $\mathcal{B}$ at a given time instant 't' is equals to the total force acting on that body. Let $\mathcal{L}$ be the total linear momentum at time instant 't' then

$$\mathcal{L} \;=\; \int_V \boldsymbol{p}\, dV \;=\; \int_V \rho \boldsymbol{v}\, dV \tag{3.12}$$

where ρ is the mass density of $\mathcal{B}$ and $\boldsymbol{v}$ is the velocity. Further, let $\mathcal{F}$ be the total force acting on this body then

$$\mathcal{F} \;=\; \int_V \boldsymbol{b}\, dV + \int \boldsymbol{t}\, dS \tag{3.13}$$

where $\boldsymbol{b}$ is the body force and $\boldsymbol{t}$ is the traction force acting on that body. Now, according to the balance of linear momentum

$$\frac{D\mathcal{L}}{Dt} = \mathcal{F}. \tag{3.14}$$

Using equation (3.12) and the definition of $\mathcal{F}$ one can write

$$\int_V \rho \frac{D\boldsymbol{v}}{Dt}\, dV = \int_V \boldsymbol{b}\, dV + \int_{\partial V} \boldsymbol{\sigma}\cdot\boldsymbol{n}\, dS, \tag{3.15}$$

where $\boldsymbol{\sigma}$ is the force-stress tensor acting at the surface ∂V of the body with volume V. After the application of the divergence theorem on the second term on the right hand side of equation (3.15) one can write

$$\int_V \rho\, \ddot{\mathbf{u}}\, dV = \int_V \boldsymbol{b}\, dV + \int_V \nabla\cdot\boldsymbol{\sigma}\, dV. \tag{3.16}$$

Since this formula is true for each subdomain of the volume V of the continuum body therefore one can write the local form of the balance of linear momentum as

$$\rho\, \ddot{\mathbf{u}} - \boldsymbol{b} - \nabla\cdot\boldsymbol{\sigma} = \mathbf{0}, \qquad \text{in index notation: } \rho\, \ddot{u}_i - b_i - \sigma_{ji,j} = 0. \tag{3.17}$$

Balance of angular momentum

The balance of angular momentum in a body $\mathcal{B}$ at a given time t states that the material rate of change of the total angular momentum equals to the total angular momentum due to the body force, traction force and traction moment acting on that body. In a mathematical expression one can write

$$\frac{D\mathcal{J}}{Dt} = \mathcal{M}, \tag{3.18}$$

where $\mathcal{J}$ is the total angular momentum (see Figure 3.5) expressed as

$$\mathcal{J} = \int_V (\mathcal{J}_o + \mathcal{J}_s)\, dV = \int_V (\boldsymbol{x}\times\boldsymbol{p} + I\boldsymbol{\vartheta})\, dV, \tag{3.19}$$

and $\mathcal{M}$ is the total angular momentum due to body force, traction force and traction moment, which is given by

$$\mathcal{M} = \int_V \boldsymbol{x}\times\boldsymbol{b}\, dV + \int_{\partial V} (\boldsymbol{x}\times\boldsymbol{t}_f + \boldsymbol{t}_m)\, dS. \tag{3.20}$$

In (3.19) $\boldsymbol{x}$ is the position vector, $\boldsymbol{p}$ is the linear momentum, I is the moment of inertia of the spinning particle and $\boldsymbol{\vartheta}$ is the angular velocity of this particle. From (3.19) Left hand side of (3.18) is obtained as

$$\frac{D\mathcal{J}}{Dt} = \frac{D}{Dt}\int_V (\boldsymbol{x}\times\boldsymbol{p} + I\,\boldsymbol{\vartheta})\, dV \tag{3.21}$$

which implies

$$\frac{D\mathcal{J}}{Dt} = \int_V \left(\boldsymbol{x}\times\frac{D\boldsymbol{p}}{Dt} + I\,\frac{D\boldsymbol{\vartheta}}{Dt}\right) dV \tag{3.22}$$

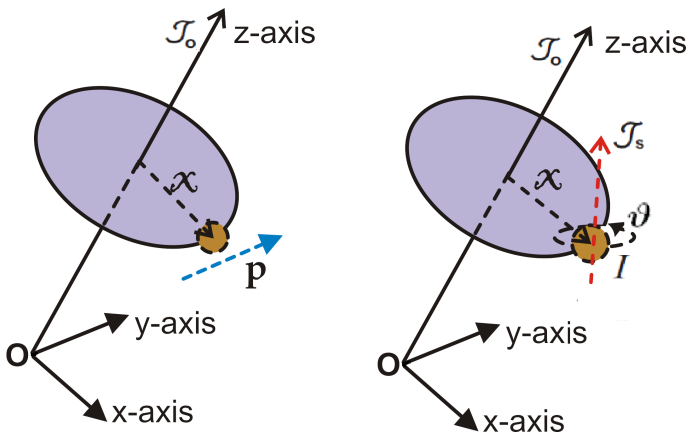

Figure 3.5.: $\mathcal{J}_o$ is the angular momentum due to orbital position $\mathcal{J}_s$ is the angular momentum due to orbital spin.

Now due to the inconvenience of dealing the cross product of vectors with tensors we first derive equations for the balance of angular momentum using index notation and then state the resulting expression in tensorial form. In index notation (3.22) becomes

$$\frac{D\mathcal{J}_i}{Dt} = \int_V \mathcal{E}_{ijk} x_j \left(\frac{D\boldsymbol{p}_k}{Dt}\right) + I\,\frac{D\boldsymbol{\vartheta}_i}{Dt}\,dV \tag{3.23}$$

Using the property of cross product one can write the middle term in (3.20) as

$$\int_{\partial V} \boldsymbol{x}\times\boldsymbol{t}_f\,dS = \int_{\partial V} \mathcal{E}_{ijk} x_j t_{f_k}\,dS \qquad ;\text{Einstein summation convention is assumed} \tag{3.24}$$

now since the cauchy stress theorem suggests that $(t_f)_k = \sigma_{lk} n_l$ therefore (3.24) becomes

$$\int_{\partial V} \boldsymbol{x}\times\boldsymbol{t}_f\,dS = \int_{\partial V} \mathcal{E}_{ijk} x_j \sigma_{lk} n_l\,dS \tag{3.25}$$

After applying divergence theorem we get

$$\int_{\partial V} \boldsymbol{x}\times\boldsymbol{t}_f\,dS = \int_V \mathcal{E}_{ijk}\partial_l\left(x_j\sigma_{lk}\right)\,dV \tag{3.26}$$

$$\int_{\partial V} \boldsymbol{x}\times\boldsymbol{t}_f\,dS = \int_V \mathcal{E}_{ijk}\,\sigma_{jk} + x_j\sigma_{lk,l}\,\,dV \tag{3.27}$$

Also the traction moment using cauchy theorem can be written as

$$(t_m)_i = \mu_{ki} n_k \tag{3.28}$$

Thus (3.20) becomes

$$\mathcal{M} = \int_V \mathcal{E}_{ijk} x_j b_k + \mathcal{E}_{ijk}\sigma_{jk} + \mathcal{E}_{ijk} x_j \sigma_{lk,l} + \mu_{ki,k}\,\,dV \tag{3.29}$$

Using (3.18) implies

$$\int_V \mathcal{E}_{ijk} x_j b_k + \mathcal{E}_{ijk}\sigma_{jk} + \mathcal{E}_{ijk} x_j \sigma_{lk,l} + \mu_{ki,k}\,\,dV = \int_V \mathcal{E}_{ijk} x_j \left(\frac{Dp_k}{Dt}\right) + I\,\frac{D\vartheta_i}{Dt} \tag{3.30}$$

or

$$\int_V \mathcal{E}_{ijk} x_j \, \sigma_{lk,l} + b_k - \frac{Dp_k}{Dt} + \int_V \mu_{ki,k} + \mathcal{E}_{ijk}\sigma_{jk} \, dV \; = \; \int_V I \, \frac{D\vartheta_i}{Dt} \, dV \tag{3.31}$$

The first term on the left hand side of (3.31) is zero due to the balance of linear momentum, therefore we arrive at

$$\int_V \mu_{ki,k} + \mathcal{E}_{ijk}\sigma_{jk} \, dV \; = \; \int_V I \, \frac{D\vartheta_i}{Dt} \, dV \tag{3.32}$$

which is the balance equations for the angular momentum where the term on the right hand side is the contribution of the particle spinning around its own axis. Local form of (3.32) is

$$\mu_{ki,k} + \mathcal{E}_{ijk}\sigma_{jk} \; = \; I \, \frac{D\vartheta_i}{Dt} \tag{3.33}$$

If we assume zero angular velocity then (3.33) becomes

$$\mu_{ki,k} + \mathcal{E}_{ijk}\sigma_{jk} \; = \; \mathbf{0} \tag{3.34}$$

thus we conclude the balance of angular momentum in tensor notation by

$$\nabla \cdot \boldsymbol{\mu} + \boldsymbol{\mathcal{E}} : \boldsymbol{\sigma} \; = \; \mathbf{0}. \tag{3.35}$$

3.4. Development of a continuum model for granular materials

Continuum modeling of granular materials with microstructures taking into account the effects of both the translational and micro-rotational motions of the granular particles at the microscale has been discussed in the work of Suiker et al. [SdBC01a, SdBC01b], Chang and Hicher [CH05], Chang and Ma [CM91, CM92], Hicher and Chang [HC07]. But all these models are based on the micromechanical approach where a two scale (micro and macro) scale computations are required in order to analyze the averaged behavior of the granular material in deformation.

We develop a continuum scale model for granular materials with microstructure taking into account the microstructural interaction of the granular particles at the microscale. Our approach is based on the energy relaxation methods [Dac89] where we introduce an interaction energy potential induced by the counter-rotations of the granular particles together with the Cosserat energy in the case of isotropic elastic solid. A two field energy minimization problem is afterwards formulated to analyze the mechanical behavior of granular structures.

3.4.1. An elastic Cosserat material model

The most prominent feature of the Cosserat theory is the consideration of the couple stresses in the elastic continuum. In fact Cosserat brothers were not only the first to introduce the idea of couple stresses in an elastic continuum of a three dimensional body but the origin of the idea traced back to the work of Voigt [Voi87] on the theory of shells. This promising idea probably adopted by the Cosserat brothers which leads them to develop a theory of an

elastic continuum with additional degrees of freedom whose constitutive relations incorporate the couple stresses. After a systematic treatment they acquired the balance of forces and moments in the following form

$$\nabla \cdot \boldsymbol{\sigma} + \mathbf{b} = \mathbf{0} \tag{3.36}$$

$$\nabla \cdot \boldsymbol{\mu} + \text{asy}\, \boldsymbol{\sigma} + \mathbf{m} = \mathbf{0} \tag{3.37}$$

where $\mathbf{b}$ and $\mathbf{m}$ are the body force and moment respectively. Conjugate to the non-symmetric force-stress tensor $\boldsymbol{\sigma}$ and the couple-stress tensor $\boldsymbol{\mu}$ are the Cosserat strain tensor $\boldsymbol{e}$ and curvature strain tensor $\boldsymbol{\kappa}$ which can be decomposed into a recoverable elastic part and a non-recoverable inelastic part as follows

$$\boldsymbol{e} = \boldsymbol{e}_{el} + \boldsymbol{e}_{pl}, \qquad \boldsymbol{\kappa} = \boldsymbol{\kappa}_{el} + \boldsymbol{\kappa}_{pl}. \tag{3.38}$$

The force-stress tensor $\boldsymbol{\sigma}$ and the couple-stress tensor $\boldsymbol{\mu}$ can be determined from the Clausius-Duhem inequality. This approach has been followed in deriving the constitutive response of materials working within the framework of thermodynamics. The Clausius-Duhem inequality in the absence of thermal effects can be written as

$$D = -\dot{W} + p_i \geq 0. \tag{3.39}$$

The left hand side of inequality (3.39) is the intrinsic dissipation potential of the material under consideration, where W is the free energy of the material and p_i is the power of internal forces and is given by

$$p_i = \boldsymbol{\sigma} : \dot{\boldsymbol{e}} + \boldsymbol{\mu} : \dot{\boldsymbol{\kappa}}. \tag{3.40}$$

Hence, 3.39 becomes

$$D = -\dot{W} + \boldsymbol{\sigma} : \dot{\boldsymbol{e}} + \boldsymbol{\mu} : \dot{\boldsymbol{\kappa}} \geq 0. \tag{3.41}$$

Since, the free energy potential W is purely depending upon the elastic part of the Cosserat strain tensor, the curvature strain tensor and (or) the hardening (denoted here by 'h', either latent or kinematic) variable, such that

$$W = W\left(\boldsymbol{e}_{el}, \boldsymbol{\kappa}_{el}, h\right). \tag{3.42}$$

Which implies

$$\dot{W} = \frac{\partial W}{\partial \boldsymbol{e}_{el}} : \dot{\boldsymbol{e}}_{el} + \frac{\partial W}{\partial \boldsymbol{\kappa}_{el}} : \dot{\boldsymbol{\kappa}}_{el} + \frac{\partial W}{\partial h} \cdot \dot{h} \tag{3.43}$$

Consider the decomposition of deformation measures from equation (3.38) with the assumption that there is no hardening effect then the Clausius-Duhem inequality (3.39) implies

$$\left(\boldsymbol{\sigma} - \frac{\partial W}{\partial \boldsymbol{e}_{el}}\right) : \dot{\boldsymbol{e}}_{el} + \left(\boldsymbol{\mu} - \frac{\partial W}{\partial \boldsymbol{\kappa}_{el}}\right) : \dot{\boldsymbol{\kappa}}_{el} + \boldsymbol{\sigma} : \dot{\boldsymbol{e}_{pl}} + \boldsymbol{\mu} : \dot{\boldsymbol{\kappa}}_{pl} = 0 \tag{3.44}$$

which results in the following relations to describe the constitutive response of the granular material

$$\boldsymbol{\sigma} = \frac{\partial W}{\partial \boldsymbol{e}}, \qquad \boldsymbol{\mu} = \frac{\partial W}{\partial \boldsymbol{\kappa}}. \tag{3.45}$$

The energy potential W does not only depends on the gradients of the macro and micro-motions of the continuum particles but also on a macrodeformation tensor which relates the

macro and micro-motions of the continuum particles. Precisely, this means, that the energy density is a function of two independent field variables (the displacement and micro-rotation) which has contribution form a relative rotation tensor associating the macrodeformation with the microdeformation of the continuum particles. In the framework of generalized elasticity it can be expressed in the following form

$$W\left(\nabla\mathbf{u},\nabla\boldsymbol{\varphi}\right)=\frac{1}{2}\boldsymbol{e}\left(\mathbf{u},\boldsymbol{\varphi}\right):\mathbb{C}:\boldsymbol{e}\left(\mathbf{u},\boldsymbol{\varphi}\right)\;+\;\frac{1}{2}\boldsymbol{\kappa}\left(\boldsymbol{\varphi}\right):\overline{\mathbb{C}}:\boldsymbol{\kappa}\left(\boldsymbol{\varphi}\right) \tag{3.46}$$

where $\mathbf{u}$ is the displacement vector field, $\boldsymbol{\varphi}$ is the micro-rotation vector field, $\mathbb{C}$ and $\overline{\mathbb{C}}$ are the fourth order constitutive tensors of elastic constants. The displacement and micro-rotation vector fields are to be determined from the energy minimization problem which reads
Find $\{\mathbf{u},\boldsymbol{\varphi}\}$ such that

$$\{\mathbf{u},\boldsymbol{\varphi}\}\;=\;\arg\left\{\min_{\mathbf{u},\boldsymbol{\varphi}}\left\{\int_{\Omega}W\left(\nabla\mathbf{u},\nabla\boldsymbol{\varphi}\right)\;dV-\ell\left(\mathbf{u},\boldsymbol{\varphi}\right)\right\}\right\} \tag{3.47}$$

along with certain prescribed boundary conditions of the type $\mathbf{u}|_{\partial\Omega_u}=u_\circ$ and $\boldsymbol{\varphi}|_{\partial\Omega_\varphi}=\varphi_\circ$, whereas $\ell\left(\mathbf{u},\boldsymbol{\varphi}\right)$ is the potential of external foreces and couples

$$\ell\left(\mathbf{u},\boldsymbol{\varphi}\right)\;=\;\int_{\Omega}\left(\mathbf{b}\cdot\mathbf{u}+\mathbf{m}\cdot\boldsymbol{\varphi}\right)\;dV+\int_{\partial\Omega_u}\mathbf{t}_{_u}\cdot\mathbf{u}\;dS+\int_{\partial\Omega_\varphi}\mathbf{t}_{_\varphi}\cdot\boldsymbol{\varphi}\;dS \tag{3.48}$$

where $\mathbf{t}_{_u}$ is the traction force and $\mathbf{t}_{_\varphi}$ is the traction moment. The fourth order constitutive tensors $\mathbb{C}$ and $\overline{\mathbb{C}}$ can be determined by

$$\mathbb{C}=\frac{\partial^2 W\left(\nabla\mathbf{u},\nabla\boldsymbol{\varphi}\right)}{\partial\nabla\mathbf{u}\otimes\partial\nabla\mathbf{u}},\quad\text{and}\quad\overline{\mathbb{C}}=\frac{\partial^2 W\left(\nabla\mathbf{u},\nabla\boldsymbol{\varphi}\right)}{\partial\nabla\boldsymbol{\varphi}\otimes\partial\nabla\boldsymbol{\varphi}}. \tag{3.49}$$

Consideration of intergranular kinematics leads us to introduce an interaction energy potential as discussed in Section 3.2. This interaction energy potential is now integrated with the free energy (3.46) of the Cosserat continuum. This enables us to define a new enhanced energy potential for the granular materials in a Cosserat medium which is given by

$$W^{enh}\left(\nabla\mathbf{u},\nabla\boldsymbol{\varphi}\right)=\underbrace{W\left(\nabla\mathbf{u},\nabla\boldsymbol{\varphi}\right)}_{\text{Cosserat energy function}}\;+\;\underbrace{\alpha\left(\left\|\boldsymbol{\kappa}\right\|^2-\beta^2\left\|\operatorname{dev}\operatorname{sym}\nabla\mathbf{u}\right\|^2\right)^2}_{\text{Interaction energy potential}}. \tag{3.50}$$

The minimization problem (3.47) thus now becomes
Find $\{\mathbf{u},\boldsymbol{\varphi}\}$ such that

$$\{\mathbf{u},\boldsymbol{\varphi}\}\;=\;\arg\left\{\min_{\mathbf{u},\boldsymbol{\varphi}}\left\{\int_{\Omega}W^{\text{enh}}\left(\nabla\mathbf{u},\nabla\boldsymbol{\varphi}\right)\;dV-\ell\left(\mathbf{u},\boldsymbol{\varphi}\right)\right\}\right\} \tag{3.51}$$

The strain energy function (3.46) was quadratic in both the gradient of the displacement field $\nabla\mathbf{u}$ and the gradient of the microrotation vector field $\nabla\boldsymbol{\varphi}$ therefore the constitutive tensors for elastic constants were independent of the deformation field variables. After the integration of interaction energy potential with the Cosserat strain energy function (3.46) the fourth order constitutive tensors become dependent of the deformation fields which implies material nonlinearity. This integration of the interaction energy potential with the quadratic Cosserat strain energy function (3.46) it is now possible to observe the nonlinear behavior of the granular materials. The fourth order constitutive tensors thus now becomes

$$\mathbb{C}\left(\nabla\mathbf{u},\nabla\boldsymbol{\varphi}\right)=\frac{\partial^2 W\left(\nabla\mathbf{u},\nabla\boldsymbol{\varphi}\right)}{\partial\left(\nabla\mathbf{u}\right)_{ij}\;\partial\left(\nabla\mathbf{u}\right)_{kl}}\;\mathbf{e}_i\otimes\mathbf{e}_j\otimes\mathbf{e}_k\otimes\mathbf{e}_l, \tag{3.52}$$

and

$$\overline{\mathbb{C}}\left(\nabla\mathbf{u},\nabla\boldsymbol{\varphi}\right)=\frac{\partial^2 W\left(\nabla\mathbf{u},\nabla\boldsymbol{\varphi}\right)}{\partial\left(\nabla\boldsymbol{\varphi}\right)_{ij}\,\partial\left(\nabla\boldsymbol{\varphi}\right)_{kl}}\,\mathbf{e}_i\otimes\mathbf{e}_j\otimes\mathbf{e}_k\otimes\mathbf{e}_l. \tag{3.53}$$

In an isotropic Cosserat medium the enhanced energy potential (3.50) takes the form

$$\begin{aligned}W^{\mathrm{enh}}\left(\nabla\mathbf{u},\nabla\boldsymbol{\varphi}\right) \;=\; & \frac{\lambda}{2}\Big(\operatorname{tr}\left(\nabla\mathbf{u}-\boldsymbol{\mathcal{E}}\cdot\boldsymbol{\varphi}\right)\Big)^2+\mu\left\|\operatorname{sym}\nabla\mathbf{u}\right\|^2+\mu_c\left\|\operatorname{asy}\nabla\mathbf{u}-\boldsymbol{\mathcal{E}}\cdot\boldsymbol{\varphi}\right\|^2\\ & +\frac{\overline{\lambda}}{2}\left(\operatorname{tr}\nabla\boldsymbol{\varphi}\right)^2+\overline{\mu}\left\|\operatorname{sym}\nabla\boldsymbol{\varphi}\right\|^2+\overline{\mu}_c\left\|\operatorname{asy}\nabla\boldsymbol{\varphi}\right\|^2+\alpha\Big(\left\|\operatorname{sym}\nabla\boldsymbol{\varphi}\right\|^2\\ & +\left\|\operatorname{asy}\nabla\boldsymbol{\varphi}\right\|^2-\beta^2\left\|\operatorname{dev}\operatorname{sym}\nabla\mathbf{u}\right\|^2\Big)^2\end{aligned} \tag{3.54}$$

where $\boldsymbol{\varepsilon}$ is the Cauchy strain tensor whose deviatoric part is computed as $\operatorname{dev}(*)=(*)-\frac{1}{d}\operatorname{tr}(*)\,\mathbf{I}$; d being the dimension of the Cosserat problem under consideration and $\mathbf{I}$ is the second order unity tensor, $\operatorname{sym}(*)$ is the symmetric part of the second order tensor $(*)$, $\operatorname{asy}(*)$ is the anti-symmetric part of $(*)$, $\|(*)\|$ is the euclidean norm of the tensor $(*)$ which is defined as $\|(*)\|=\sum_{i,j}(*)_{ij}^2$, and $\left\{\lambda,\mu,\mu_c,\bar{\lambda},\bar{\mu},\bar{\mu}_c\right\}$ are the Cosserat material constants whose physical description along with their units are given in Table 3.1. It is extremely difficult to attach any specific physical meaning to the four Cosserat material parameters μ_c, $\bar{\lambda}$, $\bar{\mu}$ and $\bar{\mu}_c$, without understanding their effect upon the mechanical behavior of a material structure under deformation. A very few number of both the mathematical and experimental procedures have been proposed in the literature for the determination of these elastic Cosserat constants. For instance, Lakes [Lak83] suggests a torsion test of rods with different radii for the determination of all the six Cosserat constants. Forest et al. [DFC98] figured out the values of the elastic Cosserat material constants for the case of beam network. For composite materials the values of these elastic constants can be traced in the work of Besdo and Dorau [BD88] and also in Mühlhaus [M6], whereas for cellular materials in the work of Adachi and Yomita [Var96]. For porous elastic material Lakes [Lak86] determined the six Cosserat constants while determining the dependence of torsional and bending rigidity upon the diameter of a rod shaped foam specimen. The method of size effects [Lak95] is also proved by Lakes to be successful in determination of Cosserat elastic constants. A comprehensive review on the experimental results for the Cosserat elastic constants is made by Lakes in [Lak95], where he presents the calculated values of these constants for twelve different materials.

The energy potential (3.54) is clearly nonconvex, and therefore when it enters in the minimization problem (3.51) will lead to the possible displacement and microrotation field fluctuations at the fine scale and thus leading to internal structure of the material. Moreover, the existence of the unique minimizing deformations are not guaranteed and it fails to be elliptic in nature. Since the loss of convexity is related to the loss of ellipticity of the derived governing field equations from the variational problem, resulting in an ill-posed boundary value problem. Thus to avoid these problems and to resolve the internal structure of the material it is therefore necessary to compute a quasiconvex (relaxed) energy potential W^{rel}. The relaxed potential when enters in the minimization problem (3.51) now assures the ellipticity of the resulting boundary value problem, since it satisfy the Legendre-Hadamard condition (for definition see the book by Dacorogna [Dac89] and also the paper by Ball [Bal76]). The study by Morrey [Mor52], Dacorogna [Dac89, Dac82, Dac01] gives sufficient justification

Material parameter	**Meaning**	**Units**
λ	Classical material dilatancy parameter: A constant of proportionality between the Cosserat stress tensor $\boldsymbol{\sigma}$ and the dilatant part of the Cosserat deformation strain tensor $\mathbf{e}$.	MPa
μ	Classical elastic shear modulus: A constant of proportionality between the symmetric part of the Cosserat stress tensor $\boldsymbol{\sigma}$ and the Cosserat deformation strain tensor $\mathbf{e}$.	MPa
μ_c	Cosserat shear modulus: A constant of proportionality between the asymmetric part of the Cosserat stress tensor $\boldsymbol{\sigma}$ and the Cosserat deformation strain tensor $\mathbf{e}$.	MPa
$\bar{\lambda}$	Cosserat material dilatancy parameter: A constant of proportionality between the Cosserat coupled stress tensor $\boldsymbol{\mu}$ and the dilatant part of the rotational deformation strain tensor $\boldsymbol{\kappa}$.	N
$\bar{\mu}$	Coupled shear modulus or bending modulus: A constant of proportionality between the symmetric part of the curvature strain tensor $\boldsymbol{\kappa}$ and the coupled stress tensor $\boldsymbol{\mu}$.	N
$\bar{\mu}_c$	Coupled shear modulus or bending modulus: A constant of proportionality between the asymmetric part of the curvature strain tensor $\boldsymbol{\kappa}$ and the coupled stress tensor $\boldsymbol{\mu}$.	N
α	A non-negative material parameter: Interaction modulus.	$N.mm^2$
β	A material parameter related to the particle/grain size.	$\frac{1}{mm}$

Table 3.1.: Material parameters and their physical meanings

for the relation of Legendre-Hadamard (ellipticity) condition with the constitutive description of a mechanical problem. A strictly satisfying Legendre-Hadamard inequality condition is sufficient for the existence of solution of a displacement boundary value problem (Necessary and sufficient conditions for strong ellipticity can be found in the work of Dacorogna [Dac01]). In case of non-linear elasticity it has been studied by Hughes et al. (1977), Kato (1977), Wheeler (1977) and Potier and Ferry (1982) (These references are found in the book by Phillipe G. Ciarlet [Cia88]).

The energy function (3.46) is quasiconvex therefore the solution to the minimization problem (3.47) is guaranteed due to the existence theorems by Neff [Nef06]. The question on the existence of the minimizers arises when the energy function W fails to be quasiconvex. This is the case with the energy function W^{enh} in the energy minimization problem (3.51). W^{enh} in (3.54) fails to be convex (see definition 2 in Chapter 2) as seen in Figure 3.8, which further implies that it is not quasiconvex. The non-quasiconvexity of the enhanced energy function thus indicates that there is some microstructures in the material corresponding to the energy minimization problem (3.51). As discussed in Chapter 2, the energy relaxation methods needs to be employed in order to extract this microstructural information. For this purpose, in the next Section we compute an analytical expression for the relaxed (quasiconvex) envelope of the non-convex energy potential in (3.54).

3.4.2. Development of material microstructures

The development of material microstructure is evident when the non-quasiconvex potentials are used in the energy minimization problem (3.51) for the modeling of material behavior. Here the energy potential (3.54) is clearly nonconvex. This nonconvexity arises due to the integration of the nonconvex interaction energy potential in the existing convex energy of the Cosserat material. Since this nonconvexity is due to the interaction energy potential term which takes the effect of both the displacement and micro-rotation fields, therefore the material microstructure is possible in both the displacements and micro-rotations of the material particles.

3.4.3. Computation of relaxed energy envelope

In this Section, we compute the exact relaxed energy envelope of the nonconvex enhanced energy function (3.54). Direct methods in the calculus of variations [Dac89] are employed in order to compute this quasiconvex envelope, which afterwards would be used in the energy minimization problem for finding the state solution. Let us start from the original energy (3.54) which can be rewritten in the following form

$$\begin{aligned} W^{enh}\left(\nabla\mathbf{u},\nabla\boldsymbol{\varphi}\right) \;=\; & \left(\frac{\lambda}{2}+\frac{\mu}{d}\right)\Big(\operatorname{tr}\operatorname{sym}\nabla\mathbf{u}\Big)^{2} \;+\; \mu\left\|\operatorname{dev}\operatorname{sym}\nabla\mathbf{u}\right\|^{2} \;+\; \mu_{c}\left\|\operatorname{asy}\nabla\mathbf{u}-\boldsymbol{\mathcal{E}}\cdot\boldsymbol{\varphi}\right\|^{2} \\ & +\frac{\overline{\lambda}}{2}\left(\operatorname{tr}\nabla\boldsymbol{\varphi}\right)^{2} \;+\; \overline{\mu}\left\|\operatorname{sym}\nabla\boldsymbol{\varphi}\right\|^{2} \;+\; \overline{\mu}_{c}\left\|\operatorname{asy}\nabla\boldsymbol{\varphi}\right\|^{2} \;+\; \alpha\Big(\left\|\operatorname{sym}\nabla\boldsymbol{\varphi}\right\|^{2} \\ & +\left\|\operatorname{asy}\nabla\boldsymbol{\varphi}\right\|^{2} \;-\; \beta^{2}\left\|\operatorname{dev}\operatorname{sym}\nabla\mathbf{u}\right\|^{2}\Big)^{2} \end{aligned} \tag{3.55}$$

where d is the dimension of the Cosserat problem under consideration. The quasiconvex envelope which here termed as the relaxed energy W^{rel} is thus computed as

$$W^{rel} = \left(\frac{\lambda}{2}+\frac{\mu}{d}\right)\left(\text{tr sym } \nabla\mathbf{u}\right)^2 + \mu_c \left\|\text{asy } \nabla\mathbf{u} - \boldsymbol{\mathcal{E}}\cdot\boldsymbol{\varphi}\right\|^2 + \frac{\overline{\lambda}}{2}\left(\text{tr } \nabla\boldsymbol{\varphi}\right)^2 + g\left(\left\|\text{sym } \nabla\boldsymbol{\varphi}\right\|^2, \left\|\text{asy } \nabla\boldsymbol{\varphi}\right\|^2, \left\|\text{dev sym}\,\nabla\mathbf{u}\right\|^2\right), \tag{3.56}$$

where g is a convex multivalued scalar function. Following the arguments in [Rao86] we can find the scalar function g by the minimization problem

$$g = \min_{\substack{a,b,c;\, c\geq\left\|\text{dev sym}\,\nabla\mathbf{u}\right\|^2,\\ a\geq\left\|\text{sym } \nabla\boldsymbol{\varphi}\right\|^2, b\geq\left\|\text{asy } \nabla\boldsymbol{\varphi}\right\|^2}} \left\{\bar{\mu}\, a + \bar{\mu}_c\, b + \mu\, c + \alpha\left(a + b - \beta^2\, c\right)^2\right\}. \tag{3.57}$$

This is a three field minimization problem which can further be reduced into the following two field minimization problem in the variables s and c as follows

$$g = h\left(\left\|\text{sym } \nabla\boldsymbol{\varphi}\right\|^2, \left\|\text{asy } \nabla\boldsymbol{\varphi}\right\|^2\right) + \min_{\substack{c,s;\, c\geq\left\|\text{dev sym}\,\nabla\mathbf{u}\right\|^2\\ s\geq\left\|\text{sym } \nabla\boldsymbol{\varphi}\right\|^2+\left\|\text{asy } \nabla\boldsymbol{\varphi}\right\|^2}} \left\{\mu_\circ\, s + \mu\, c + \alpha\left(s - \beta^2\, c\right)^2\right\}, \tag{3.58}$$

where the material parameter $\mu_\circ$ is to be determined by

$$\mu_\circ = \min\left\{\overline{\mu}, \overline{\mu}_c\right\} \tag{3.59}$$

and h is a non-negative function explicitly given by

$$h\left(\left\|\text{sym } \nabla\boldsymbol{\varphi}\right\|^2, \left\|\text{asy } \nabla\boldsymbol{\varphi}\right\|^2\right) = \begin{cases} \left(\overline{\mu} - \overline{\mu}_c\right)\left\|\text{sym } \nabla\boldsymbol{\varphi}\right\|^2 & \text{if } \overline{\mu} \geq \overline{\mu}_c \\ \left(\overline{\mu}_c - \overline{\mu}\right)\left\|\text{asy } \nabla\boldsymbol{\varphi}\right\|^2 & \text{otherwise} \end{cases}. \tag{3.60}$$

Above, in both the cases h vanishes for the same choice of $\bar{\mu}$ and $\bar{\mu}_c$.

Stationarity conditions

The stationarity conditions to the minimization problem in (3.58) are as follows

$$(1).\quad \text{for}\quad s = \left\|\text{sym } \nabla\boldsymbol{\varphi}\right\|^2 + \left\|\text{asy } \nabla\boldsymbol{\varphi}\right\|^2 \text{ and } \quad c \geq \left\|\text{dev sym}\,\nabla\mathbf{u}\right\|^2 \quad : \quad \frac{\partial g}{\partial c} = 0, \quad \frac{\partial g}{\partial s} \geq 0, \tag{3.61}$$

$$(2).\quad \text{for}\quad s = \left\|\text{sym } \nabla\boldsymbol{\varphi}\right\|^2 + \left\|\text{asy } \nabla\boldsymbol{\varphi}\right\|^2 \text{ and } \quad c = \left\|\text{dev sym}\,\nabla\mathbf{u}\right\|^2 \quad : \quad \frac{\partial g}{\partial c} \geq 0, \quad \frac{\partial g}{\partial s} \geq 0, \tag{3.62}$$

$$(3).\quad \text{for}\quad c = \left\|\text{dev sym}\,\nabla\mathbf{u}\right\|^2 \text{ and } \quad s \geq \left\|\text{sym } \nabla\boldsymbol{\varphi}\right\|^2 + \left\|\text{asy } \nabla\boldsymbol{\varphi}\right\|^2 \quad : \quad \frac{\partial g}{\partial s} = 0, \quad \frac{\partial g}{\partial c} \geq 0. \tag{3.63}$$

On the basis of these three stationarity conditions the material energy can be characterized into the following three phases

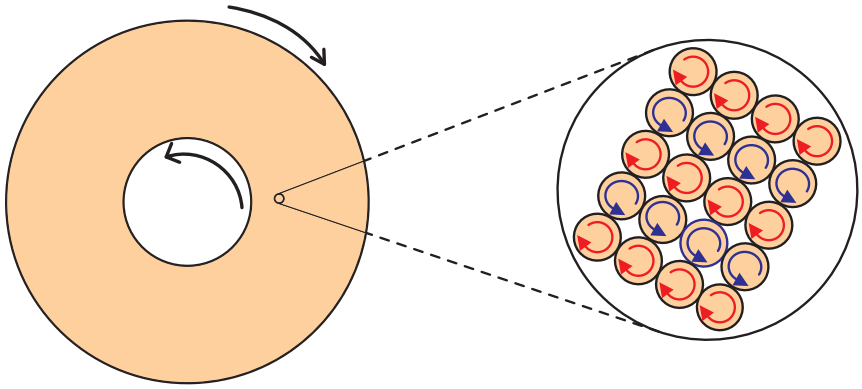

Figure 3.6.: A Couette shear cell where the two arrows indicates the shearing direction. In inset the microstructure patterns due to microrotational motions of the particles is shown.

Material phase with microstructure in microrotational motions (micromotions) (Phase 1)

This phase is corresponding to the material regime where there are microstructures due to the micromotions (which are in fact the rotational degrees of freedom assembled in the microrotational vector field $\boldsymbol{\varphi}$) of the continuum particles. A schematic representation of such microstructure is given in Figure 3.6. The enhanced energy potential (3.55) is nonconvex in this microstructural phase. It is observed that whenever the norm of the curvature strain tensor is dominating over the norm of the macroscopic shear strain tensor for some specific choice of the material parameters μ, α and β, the material experiences a microstructure in micromotions. This microstructural material phase is characterized by the following inequality relation

$$\|\nabla\boldsymbol{\varphi}\|^2 \geq \beta^2 \|\text{dev sym}\,\nabla\mathbf{u}\|^2 + \frac{\mu}{2\alpha\beta^2}. \tag{3.64}$$

It is important to note the effect of shear modulus μ, internal length scale (e.g., the diameter of particles) β and the coherency interaction modulus or frictional modulus α in conjunction with the curvature and macroscopic shear strains which plays very crucial role in the observation of this internal structural phase of the material.

Using the first stationarity condition (3.61) the minimizers of the problem in 3.58 are obtained as

$$s = \|\text{sym}\,\nabla\boldsymbol{\varphi}\|^2 + \|\text{asy}\,\nabla\boldsymbol{\varphi}\|^2, \qquad c = \frac{1}{\beta^2}\left(\|\text{sym}\,\nabla\boldsymbol{\varphi}\|^2 + \|\text{asy}\,\nabla\boldsymbol{\varphi}\|^2\right) - \frac{\mu}{2\alpha\beta^4}. \tag{3.65}$$

Thus, the scalar convex function g is given by

$$g = \begin{cases} \left(\overline{\mu} - \overline{\mu}_c + \mu_\circ + \frac{\mu}{\beta^2}\right)\|\text{sym}\,\nabla\boldsymbol{\varphi}\|^2 + \left(\mu_\circ + \frac{\mu}{\beta^2}\right)\|\text{asy}\,\nabla\boldsymbol{\varphi}\|^2 - \frac{\mu^2}{4\alpha\beta^4} & \text{if} \quad \overline{\mu} \geq \overline{\mu}_c \\ \left(\mu_\circ + \frac{\mu}{\beta^2}\right)\|\text{sym}\,\nabla\boldsymbol{\varphi}\|^2 + \left(\overline{\mu}_c - \overline{\mu} + \mu_\circ + \frac{\mu}{\beta^2}\right)\|\text{asy}\,\nabla\boldsymbol{\varphi}\|^2 - \frac{\mu^2}{4\alpha\beta^4} & \text{if} \quad \overline{\mu} < \overline{\mu}_c \end{cases} \tag{3.66}$$

The relaxed energy of the material in this phase is obtained as

$$W_1^{rel} = \begin{cases} \left\{ \begin{array}{l} \left(\frac{\lambda}{2}+\frac{\mu}{d}\right)\left(\text{tr sym } \nabla\mathbf{u}\right)^2 + \mu_c \left\|\text{asy } \nabla\mathbf{u} - \boldsymbol{\mathcal{E}}\cdot\boldsymbol{\varphi}\right\|^2 - \frac{\mu^2}{4\alpha\beta^4} \\ +\frac{\bar{\lambda}}{2}(\text{tr } \nabla\boldsymbol{\varphi})^2 + (\bar{\mu}-\bar{\mu}_c)\left\|\text{sym } \nabla\boldsymbol{\varphi}\right\|^2 + \left(\mu_\circ + \frac{\mu}{\beta^2}\right)\left\|\nabla\boldsymbol{\varphi}\right\|^2 \end{array} \right. & \text{if} \quad \bar{\mu} \geq \bar{\mu}_c, \\ \left\{ \begin{array}{l} \left(\frac{\lambda}{2}+\frac{\mu}{d}\right)\left(\text{tr sym } \nabla\mathbf{u}\right)^2 + \mu_c \left\|\text{asy } \nabla\mathbf{u} - \boldsymbol{\mathcal{E}}\cdot\boldsymbol{\varphi}\right\|^2 - \frac{\mu^2}{4\alpha\beta^4} \\ +\frac{\bar{\lambda}}{2}(\text{tr } \nabla\boldsymbol{\varphi})^2 - (\bar{\mu}-\bar{\mu}_c)\left\|\text{asy } \nabla\boldsymbol{\varphi}\right\|^2 + \left(\mu_\circ + \frac{\mu}{\beta^2}\right)\left\|\nabla\boldsymbol{\varphi}\right\|^2 \end{array} \right. & \text{if} \quad \bar{\mu} < \bar{\mu}_c \end{cases} \tag{3.67}$$

Material phase with no microstructure (Phase 2)

This phase is connected to the material regime where there is no internal structure in the material. The second stationarity condition (3.62) clearly shows that the minimizers of the functional in (3.58) are itself $\left\|\text{sym } \nabla\boldsymbol{\varphi}\right\|^2 + \left\|\text{asy } \nabla\boldsymbol{\varphi}\right\|^2$ and $\left\|\text{dev sym}\,\nabla\mathbf{u}\right\|^2$ respectively. This is another indication that the original energy potential in (3.55) is convex in this material phase. The criteria for the recognition of this material phase is given by the following inequality relation

$$\beta^2\left\|\text{dev sym}\,\nabla\mathbf{u}\right\|^2 - \frac{\mu_\circ}{2\alpha} \leq \left\|\nabla\boldsymbol{\varphi}\right\|^2 \leq \beta^2\left\|\text{dev sym}\,\nabla\mathbf{u}\right\|^2 + \frac{\mu}{2\alpha\beta^2}. \tag{3.68}$$

The function g in this phase is given by

$$\begin{aligned} g \;=\; \overline{\mu}\left\|\text{sym } \nabla\boldsymbol{\varphi}\right\|^2 \;+\; \overline{\mu}_c\left\|\text{asy } \nabla\boldsymbol{\varphi}\right\|^2 \;+\; \mu\left\|\text{dev sym}\,\nabla\mathbf{u}\right\|^2 \;+\; \alpha\Big(\left\|\text{sym } \nabla\boldsymbol{\varphi}\right\|^2 \\ +\; \left\|\text{asy } \nabla\boldsymbol{\varphi}\right\|^2 \;-\; \beta^2\left\|\text{dev sym}\,\nabla\mathbf{u}\right\|^2\Big)^2. \end{aligned} \tag{3.69}$$

The relaxed energy potential in this phase is thus the original energy potential (3.55) itself and we write

$$\begin{aligned} W_2^{rel} \;=\; \left(\frac{\lambda}{2}+\frac{\mu}{d}\right)\Big(\text{tr sym}\,\nabla\mathbf{u}\Big)^2 \;+\; \mu\left\|\text{dev sym}\,\nabla\mathbf{u}\right\|^2 \;+\; \mu_c\left\|\text{asy}\,\nabla\mathbf{u} - \boldsymbol{\mathcal{E}}\cdot\boldsymbol{\varphi}\right\|^2 \\ +\; \frac{\overline{\lambda}}{2}\Big(\text{tr } \nabla\boldsymbol{\varphi}\Big)^2 \;+\; \overline{\mu}\left\|\text{sym } \nabla\boldsymbol{\varphi}\right\|^2 \;+\; \overline{\mu}_c\left\|\text{asy } \nabla\boldsymbol{\varphi}\right\|^2 \;+\; \alpha\Big(\left\|\text{sym } \nabla\boldsymbol{\varphi}\right\|^2 \\ +\; \left\|\text{asy } \nabla\boldsymbol{\varphi}\right\|^2 - \beta^2\left\|\text{dev sym}\,\nabla\mathbf{u}\right\|^2\Big)^2 \end{aligned} \tag{3.70}$$

Material phase with microstructure in translational motions (Phase 3)

This phase is related to the material regime where there is a microstructure in translational motions (which are in fact the displacement degrees of freedom of the continuum particles and are assembled in the displacement vector field $\mathbf{u}$) of the continuum particles. A

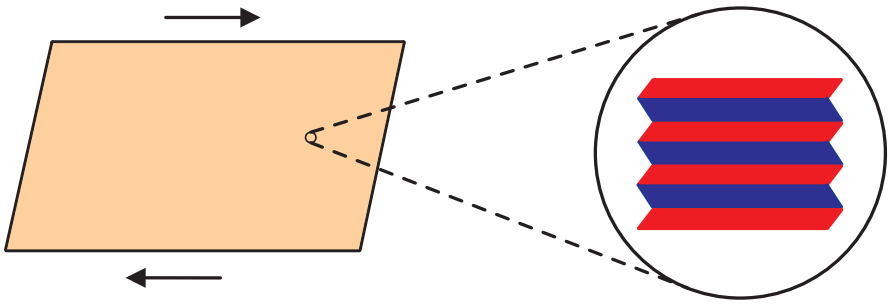

Figure 3.7.: A rectangular specimen under shear with two arrow head pointing towards the shearing direction. In inset the microstructure patterns formed due to the translational motions of the continuum particles is shown.

schematic representation of such microstructure formation is shown in Figure 3.7. The enhanced energy potential (3.55) thus becomes nonconvex in this phase. Using the third stationarity condition (3.63) it is observed that the norm of the macroscopic shear strain tensor is dominating over the norm of the rotational strain tensor. The material is said to be in this phase whenever the following criteria is satisfied

$$\beta^2 \left\|\text{dev sym}\,\nabla \mathbf{u}\right\|^2 - \frac{\mu_\circ}{2\alpha} \geq \left\|\nabla \boldsymbol{\varphi}\right\|^2. \tag{3.71}$$

It is important to note the effect the coherency/frictional modulus α and the Cosserat material modulus $\mu_\circ$ in the characterization of this microstructural phase. The minimizers of the functional in (3.58) are obtained after solving the third stationarity condition (3.63) which are given as

$$c \;=\; \left\|\text{dev sym}\,\nabla \mathbf{u}\right\|^2 \qquad \text{and} \qquad s \;=\; \beta^2 \left\|\text{dev sym}\,\nabla \mathbf{u}\right\|^2 - \frac{\mu_\circ}{2\alpha}. \tag{3.72}$$

Thus minimum potential g in (3.58) takes the following form

$$g \;=\; \begin{cases} (\bar{\mu} - \bar{\mu}_c) \left\|\text{sym}\;\nabla \boldsymbol{\varphi}\right\|^2 + \left(\mu_\circ \beta^2 + \mu\right) \left\|\text{dev sym}\,\nabla \mathbf{u}\right\|^2 - \dfrac{\mu_\circ^{\,2}}{4\alpha} & \text{if} \quad \bar{\mu} \geq \bar{\mu}_c \\[2ex] (\bar{\mu}_c - \bar{\mu}) \left\|\text{asy}\;\nabla \boldsymbol{\varphi}\right\|^2 + \left(\mu_\circ \beta^2 + \mu\right) \left\|\text{dev sym}\,\nabla \mathbf{u}\right\|^2 - \dfrac{\mu_\circ^{\,2}}{4\alpha} & \text{if} \quad \bar{\mu} < \bar{\mu}_c \end{cases} \tag{3.73}$$

Hence the relaxed energy potential in this phase is obtained as

$$W_3^{rel} \;=\; \begin{cases} \left\{ \begin{array}{l} \left(\dfrac{\lambda}{2} + \dfrac{\mu}{d}\right) \left(\text{tr sym}\;\nabla \mathbf{u}\right)^2 + \mu_c \left\|\text{asy}\;\nabla \mathbf{u} - \boldsymbol{\mathcal{E}} \cdot \boldsymbol{\varphi}\right\|^2 + \dfrac{\bar{\lambda}}{2} (\text{tr}\;\nabla \boldsymbol{\varphi})^2 \\ \quad + (\bar{\mu} - \bar{\mu}_c) \left\|\text{sym}\;\nabla \boldsymbol{\varphi}\right\|^2 + \left(\mu_\circ \beta^2 + \mu\right) \left\|\text{dev sym}\;\nabla \mathbf{u}\right\|^2 - \dfrac{{\mu_\circ}^2}{4\alpha} \end{array} \right. & \text{if} \quad \bar{\mu} \geq \bar{\mu}_c \\[4ex] \left\{ \begin{array}{l} \left(\dfrac{\lambda}{2} + \dfrac{\mu}{d}\right) \left(\text{tr sym}\;\nabla \mathbf{u}\right)^2 + \mu_c \left\|\text{asy}\;\nabla \mathbf{u} - \boldsymbol{\mathcal{E}} \cdot \boldsymbol{\varphi}\right\|^2 + \dfrac{\bar{\lambda}}{2} (\text{tr}\;\nabla \boldsymbol{\varphi})^2 \\ \quad - (\bar{\mu} - \bar{\mu}_c) \left\|\text{asy}\;\nabla \boldsymbol{\varphi}\right\|^2 + \left(\mu_\circ \beta^2 + \mu\right) \left\|\text{dev sym}\;\nabla \mathbf{u}\right\|^2 - \dfrac{{\mu_\circ}^2}{4\alpha} \end{array} \right. & \text{if} \quad \bar{\mu} < \bar{\mu}_c \end{cases} \tag{3.74}$$

Relaxed energy

The total relaxed energy thus comprises all the three energies in each of the phase and it acquires finally the following form

$$W^{rel} = \begin{cases} W_1^{rel} & \text{if} \quad \|\nabla\boldsymbol{\varphi}\|^2 \geq \beta^2 \|\text{dev sym } \nabla\mathbf{u}\|^2 + \dfrac{\mu}{2\alpha\beta^2} \\ W_2^{rel} & \text{if} \quad -\dfrac{\mu_\circ}{2\alpha} \leq \|\nabla\boldsymbol{\varphi}\|^2 - \beta^2 \|\text{dev sym } \nabla\mathbf{u}\|^2 \leq \dfrac{\mu}{2\alpha\beta^2} \\ W_3^{rel} & \text{if} \quad \|\nabla\boldsymbol{\varphi}\|^2 \leq \beta^2 \|\text{dev sym } \nabla\mathbf{u}\|^2 - \dfrac{\mu_\circ}{2\alpha} \end{cases} \tag{3.75}$$

where W_1^{rel}, W_2^{rel} and W_3^{rel} are given as in (3.67), (3.70) and (3.74), respectively.

Nonlinear constitutive relations in a Cosserat medium

The proposed granular material model is completed with the formulation of constitutive relations between stress and strain tensors in a Cosserat medium. The constitutive structure of the proposed theory thus comprises of three phases (as discussed in section 3.4.2) where in each phase the force-stress are explicitly related to the Cosserat strain tensors according to the following formulae

$$\boldsymbol{\sigma} = \begin{cases} \dfrac{\partial W_1^{rel}}{\partial \nabla\mathbf{u}} & \text{if} \quad \|\nabla\boldsymbol{\varphi}\|^2 \geq \beta^2 \|\text{dev sym } \nabla\mathbf{u}\|^2 + \dfrac{\mu}{2\alpha\beta^2} \\ \dfrac{\partial W_2^{rel}}{\partial \nabla\mathbf{u}} & \text{if} \quad -\dfrac{\mu_\circ}{2\alpha} \leq \|\nabla\boldsymbol{\varphi}\|^2 - \beta^2 \|\text{dev sym } \nabla\mathbf{u}\|^2 \leq \dfrac{\mu}{2\alpha\beta^2} \\ \dfrac{\partial W_3^{rel}}{\partial \nabla\mathbf{u}} & \text{if} \quad \|\nabla\boldsymbol{\varphi}\|^2 \leq \beta^2 \|\text{dev sym } \nabla\mathbf{u}\|^2 - \dfrac{\mu_\circ}{2\alpha} \end{cases} \tag{3.76}$$

where $\dfrac{\partial W_1^{rel}}{\partial \nabla\mathbf{u}}$, $\dfrac{\partial W_2^{rel}}{\partial \nabla\mathbf{u}}$ and $\dfrac{\partial W_3^{rel}}{\partial \nabla\mathbf{u}}$ are given respectively as

$$\frac{\partial W_1^{rel}}{\partial \nabla\mathbf{u}} = 2\left(\frac{\lambda}{2} + \frac{\mu}{d}\right)\big(\text{tr sym } \nabla\mathbf{u}\big)\,\mathbf{I} + 2\mu_c\,\big(\text{asy } \nabla\mathbf{u} - \boldsymbol{\mathcal{E}}\cdot\boldsymbol{\varphi}\big), \tag{3.77}$$

$$\begin{aligned} \frac{\partial W_2^{rel}}{\partial \nabla\mathbf{u}} = {} & \lambda\,\big(\text{tr sym } \nabla\mathbf{u}\big)\,\mathbf{I} + 2\mu\,\big(\text{sym } \nabla\mathbf{u}\big) + 2\mu_c\,\big(\text{asy } \nabla\mathbf{u} - \boldsymbol{\mathcal{E}}\cdot\boldsymbol{\varphi}\big) \\ & - 4\alpha\beta^2\left(\|\nabla\boldsymbol{\varphi}\|^2 - \beta^2\|\text{dev sym } \nabla\mathbf{u}\|^2\right)\big(\text{dev sym } \nabla\mathbf{u}\big), \end{aligned} \tag{3.78}$$

and

$$\frac{\partial W_3^{rel}}{\partial \nabla\mathbf{u}} = \lambda\big(\text{tr sym } \nabla\mathbf{u}\big)\mathbf{I} + 2\mu\big(\text{sym}\,\nabla\mathbf{u}\big) + 2\mu_\circ\beta^2\big(\text{dev sym } \nabla\mathbf{u}\big) + 2\mu_c\big(\text{asy } \nabla\mathbf{u} - \boldsymbol{\mathcal{E}}\cdot\boldsymbol{\varphi}\big). \tag{3.79}$$

The couple-stress tensor is related to the curvature strain tensors by the following formulae

$$\boldsymbol{\mu} = \begin{cases} \dfrac{\partial W_1^{rel}}{\partial \nabla \boldsymbol{\varphi}} & \text{if} \quad \|\nabla \boldsymbol{\varphi}\|^2 \geq \beta^2 \|\text{dev sym } \nabla \mathbf{u}\|^2 + \dfrac{\mu}{2\alpha\beta^2} \\ \dfrac{\partial W_2^{rel}}{\partial \nabla \boldsymbol{\varphi}} & \text{if} \quad -\dfrac{\mu_\circ}{2\alpha} \leq \|\nabla \boldsymbol{\varphi}\|^2 - \beta^2 \|\text{dev sym } \nabla \mathbf{u}\|^2 \leq \dfrac{\mu}{2\alpha\beta^2} \\ \dfrac{\partial W_3^{rel}}{\partial \nabla \boldsymbol{\varphi}} & \text{if} \quad \|\nabla \boldsymbol{\varphi}\|^2 \leq \beta^2 \|\text{dev sym } \nabla \mathbf{u}\|^2 - \dfrac{\mu_\circ}{2\alpha} \end{cases} \tag{3.80}$$

where $\dfrac{\partial W_1^{rel}}{\partial \nabla \boldsymbol{\varphi}}$, $\dfrac{\partial W_2^{rel}}{\partial \nabla \boldsymbol{\varphi}}$ and $\dfrac{\partial W_3^{rel}}{\partial \nabla \boldsymbol{\varphi}}$ are given respectively as

$$\frac{\partial W_1^{rel}}{\partial \nabla \boldsymbol{\varphi}} = \begin{cases} \bar{\lambda} \left(\text{tr } \nabla \boldsymbol{\varphi} \right) \mathbf{I} + 2 \left(\bar{\mu} - \bar{\mu}_c \right) \left(\text{sym } \nabla \boldsymbol{\varphi} \right) + 2 \left(\mu_\circ + \dfrac{\mu}{\beta^2} \right) \nabla \boldsymbol{\varphi} & \text{if} \quad \bar{\mu} \geq \bar{\mu}_c, \\ \bar{\lambda} \left(\text{tr } \nabla \boldsymbol{\varphi} \right) \mathbf{I} - 2 \left(\bar{\mu} - \bar{\mu}_c \right) \left(\text{asy } \nabla \boldsymbol{\varphi} \right) + 2 \left(\mu_\circ + \dfrac{\mu}{\beta^2} \right) \nabla \boldsymbol{\varphi} & \text{if} \quad \bar{\mu} < \bar{\mu}_c. \end{cases} \tag{3.81}$$

$$\frac{\partial W_2^{rel}}{\partial \nabla \boldsymbol{\varphi}} = \bar{\lambda} \left(\text{tr } \nabla \boldsymbol{\varphi} \right) \mathbf{I} + 2\bar{\mu} \left(\text{sym } \nabla \boldsymbol{\varphi} \right) + 2\bar{\mu_c} \left(\text{asy } \nabla \boldsymbol{\varphi} \right) + 4\alpha \Big(\|\text{sym } \nabla \boldsymbol{\varphi}\|^2 + \|\text{asy } \nabla \boldsymbol{\varphi}\|^2 - \beta^2 \|\text{dev sym } \nabla \mathbf{u}\|^2 \Big) \nabla \boldsymbol{\varphi} \tag{3.82}$$

and

$$\frac{\partial W_3^{rel}}{\partial \nabla \boldsymbol{\varphi}} = \begin{cases} \bar{\lambda} \left(\text{tr } \nabla \boldsymbol{\varphi} \right) \mathbf{I} + 2(\bar{\mu} - \bar{\mu}_c) \left(\text{sym } \nabla \boldsymbol{\varphi} \right) & \text{if} \quad \bar{\mu} \geq \bar{\mu}_c, \\ \bar{\lambda} \left(\text{tr } \nabla \boldsymbol{\varphi} \right) \mathbf{I} - 2(\bar{\mu} - \bar{\mu}_c) \left(\text{asy } \nabla \boldsymbol{\varphi} \right) & \text{if} \quad \bar{\mu} < \bar{\mu}_c. \end{cases} \tag{3.83}$$

3.5. One-dimensional numerical results

Based on the proposed formulation, numerical examples of a simple shear and a tension-compression tests are briefly presented in this section. The mechanical response of the material is analyzed along some chosen macroscopic strain paths. Development of microstructure is observed during both the tension-compression and shear tests, which is characterized by the activation of different material phases as discussed in the Section 3.4.2.

3.5.1. A simple shear test

In this example we study the proposed model in a plain strain simple shear test. The macroscopic strain paths are taken to be

$$\boldsymbol{\varepsilon} = \begin{bmatrix} 0 & \frac{\gamma}{2} & 0 \\ \frac{\gamma}{2} & 0 & 0 \\ 0 & 0 & 0 \end{bmatrix}, \quad \boldsymbol{e} = \begin{bmatrix} 0 & -\varphi_3 & 0 \\ \gamma + \varphi_3 & 0 & 0 \\ 0 & 0 & 0 \end{bmatrix}, \quad \boldsymbol{\omega}_e = \begin{bmatrix} 0 & -c & 0 \\ c & 0 & 0 \\ 0 & 0 & 0 \end{bmatrix}, \tag{3.84}$$

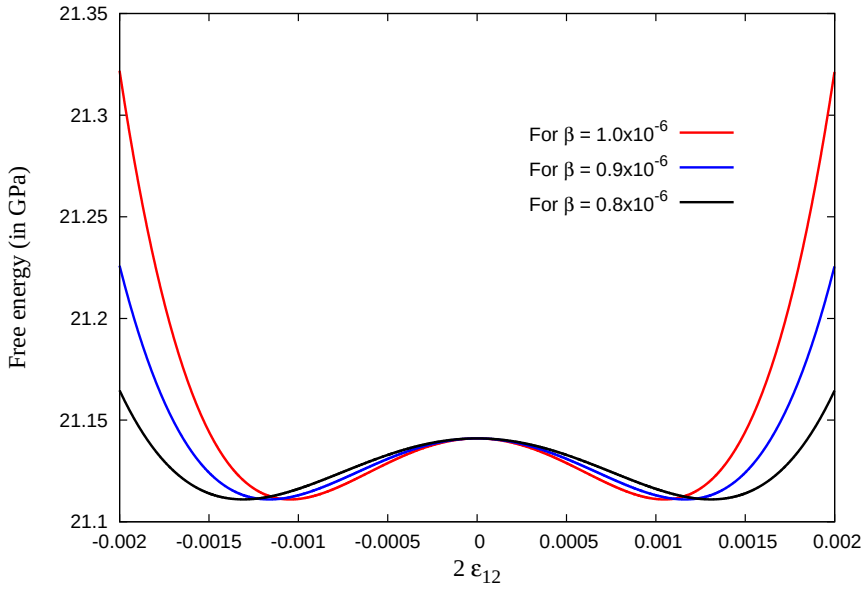

Figure 3.8.: Unrelaxed energy (3.55) curves for $\alpha = \beta = 100$, $\mu_c = 200.0$ and $\phi_3 = \dfrac{\pi}{6}$, in a simple shear test.

where $c = \dfrac{\gamma}{2} + \varphi_3$. We assume that the rotational degree of freedom, φ_3 is linearly depending on both of the coordinates X_1 and X_2 of the coordinate system and we write

$$\varphi_3 = b(X_1 + X_2) \tag{3.85}$$

where $b = \dfrac{\pi}{6}$ is some assumed curvature. In our analysis we calculate φ_3 for all those material points which lies on the line $X_1 + X_2 = 1$.

The nonconvexity of the energy potential in (3.55) is clearly seen in Figure 3.8 along the above mentioned strain paths in a simple shear test for varying values of the material parameter β. The material parameters utilized in the calculations are given in Table 3.2. The Figure

Table 3.2.: Material parameters for the analytical computations in a simple shear test.

E	ν	μ_c	α	β	$\overline{\mu}$	$\overline{\lambda}$	$\overline{\mu}_c$
(GPa)	-	(GPa)	(kN.mm^2)	(mm^{-1})	(kN)	(kN)	(kN)
2.0×10^2	0.3	2.0×10^{-4}	1.0×10^{-1}	-	7.69×10^1	1.154×10^2	8.0×10^{-2}

3.9 presents the relaxed and unrelaxed energy curves for $\beta = 1.0 \times 10^{-6}$, $\beta = 0.9 \times 10^{-6}$ and $\beta = 0.8 \times 10^{-6}$ from top to bottom whereas the Figure 3.10 describes the behavior of relaxed and unrelaxed stress and strain curves for the above mentioned values of β, where it is observed that the non-monotone stress-strain curve is replaced by its energetically equivalent Maxwell line corresponding to a uniform vanishing stress. We observe that the material experiences a change in the phase with the occurrence of microstructure. Initially the material is in a phase with microstructure in micromotions then changing its phase to a regime where there is no microstructure in the material and after increasing the strain it transforms to the third phase where there is a microstructure in translational motions. Thus all the three phases, one with no microstructure, and the two with microstructure in micromotions

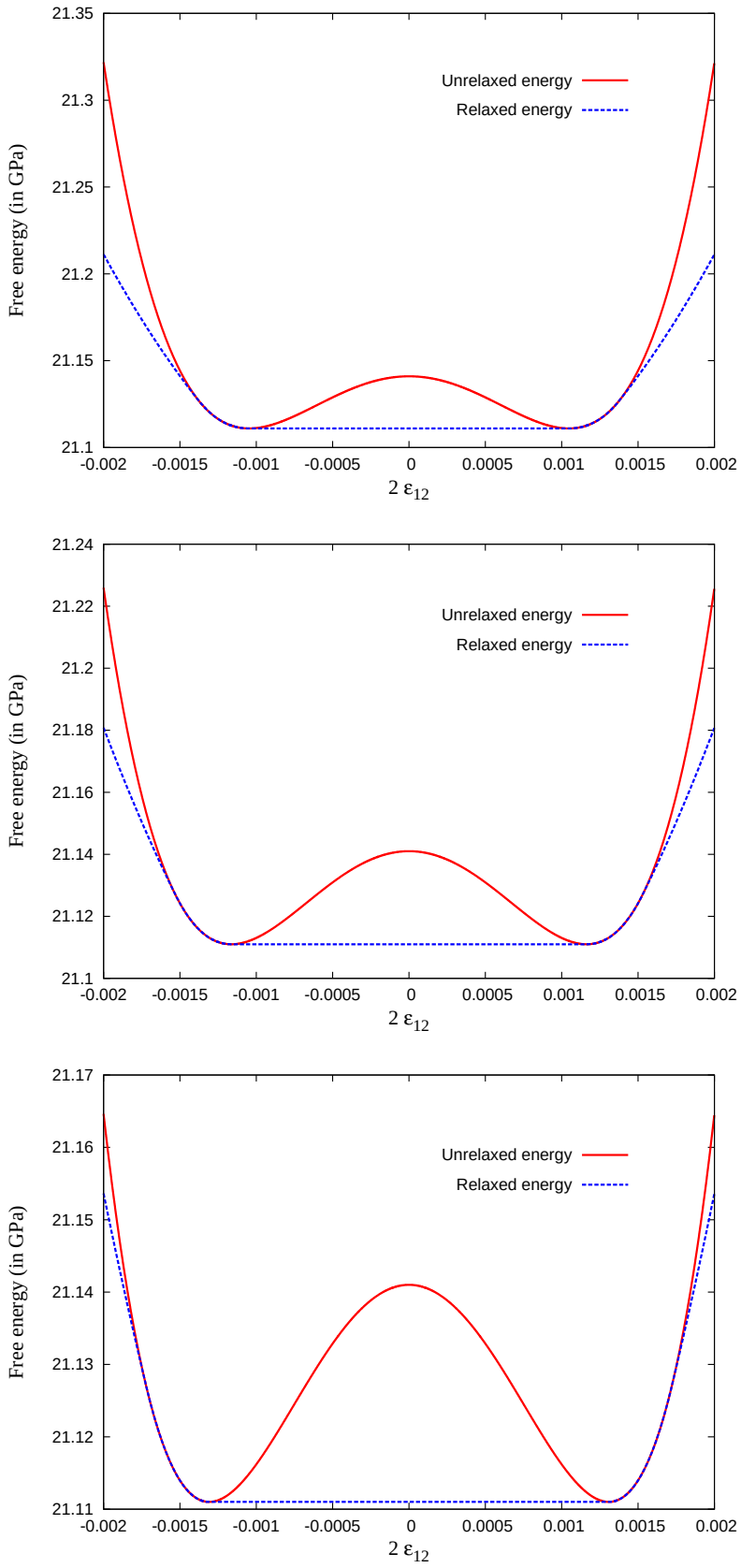

Figure 3.9.: Unrelaxed and relaxed energy curves for different values of the material parameter β in a simple shear test.

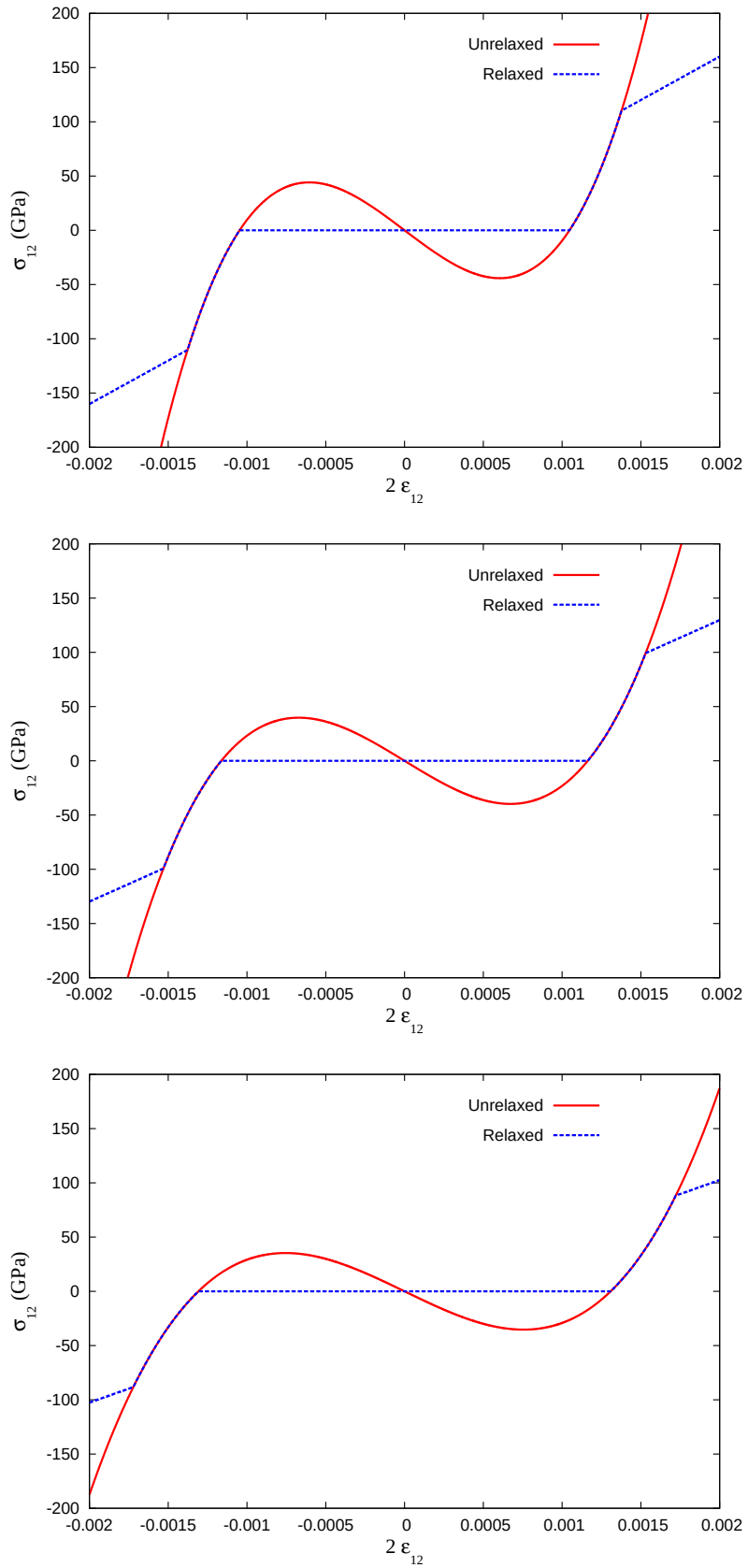

Figure 3.10.: Unrelaxed and relaxed stress-strain curves for different values of the material parameter β in a simple shear test.

and translational motions can be seen during this test. The influence of material parameter β is observed, where we see that for small values of β the material microstructure in micromotions is more pronounced as in comparison to large values of β where the material microstructure in translational motions is more noticeable. This shows that for larger particle size the material microstructure due to micromotion is certain whereas for small particle size the material microstructure in translational motions is pronounced.

3.5.2. A tension-compression test

In this example the material behavior in a plain strain tension-compression test is investigated using our proposed model. The macroscopic strain tensors for this analysis take the form

$$\boldsymbol{\varepsilon} = \begin{bmatrix} \delta & 0 & 0 \\ 0 & 0 & 0 \\ 0 & 0 & 0 \end{bmatrix}, \quad \boldsymbol{e} = \begin{bmatrix} \delta & -\varphi_3 & 0 \\ \varphi_3 & 0 & 0 \\ 0 & 0 & 0 \end{bmatrix}, \quad \boldsymbol{\omega}_e = \begin{bmatrix} 0 & -\varphi_3 & 0 \\ \varphi_3 & 0 & 0 \\ 0 & 0 & 0 \end{bmatrix}. \tag{3.86}$$

The micro-rotational degree of freedom, φ_3 at each material point is calculated according to (3.85). In our analysis the assumed value for φ_3 is $\frac{\pi}{3}$. For both the above tests $\boldsymbol{\kappa}$ has the form

$$\boldsymbol{\kappa} = \begin{bmatrix} 0 & 0 & b \\ 0 & 0 & b \\ 0 & 0 & 0 \end{bmatrix}. \tag{3.87}$$

The material parameters are chosen as in Table 3.3.

Table 3.3.: Material parameters for the analytical computations in a tension-compression test.

E	ν	μ_c	α	β	$\overline{\mu}$	$\overline{\lambda}$	$\overline{\mu}_c$
(MPa)	-	(MPa)	(N.mm^2)	(mm^{-1})	(N)	(N)	(N)
2.0×10^2	0.3	1.0×10^{-2}	1.0×10^{-1}	1.2×10^2	7.69×10^1	1.154×10^2	1.0×10^1

Figure 3.11 presents the stress-strain curve in tension test where it is observed that the microstructure develops in both the translational and microrotational motions. The magnified picture shows that the material has microstructure in micromotions initially. The material exhibits multiphase stress strain behavior in tension test. Figure 3.12 describes the stress-strain curve in compression test. The activation of the phase with translational microstructure is clearly seen in Large picture whereas the observation of microstructure in micromotion is clear in the magnified picture within it. A change of phase is seen in the stress-strain graph. In Figure 3.13 the two curves from tension and compression tests are combined to illustrate the complete picture during loading (tension), unloading and then in reverse loading (compression) test. All the three phases are observed during tension-compression test. Finally, in Figure 3.14 the relaxed and unrelaxed energy curve in the tension-compression test is shown, where the nonconvexity of the energy potential 3.55 in magnified picture is due to the presence of microstructure in micromotion of the continuum particles. It is seen that the slope

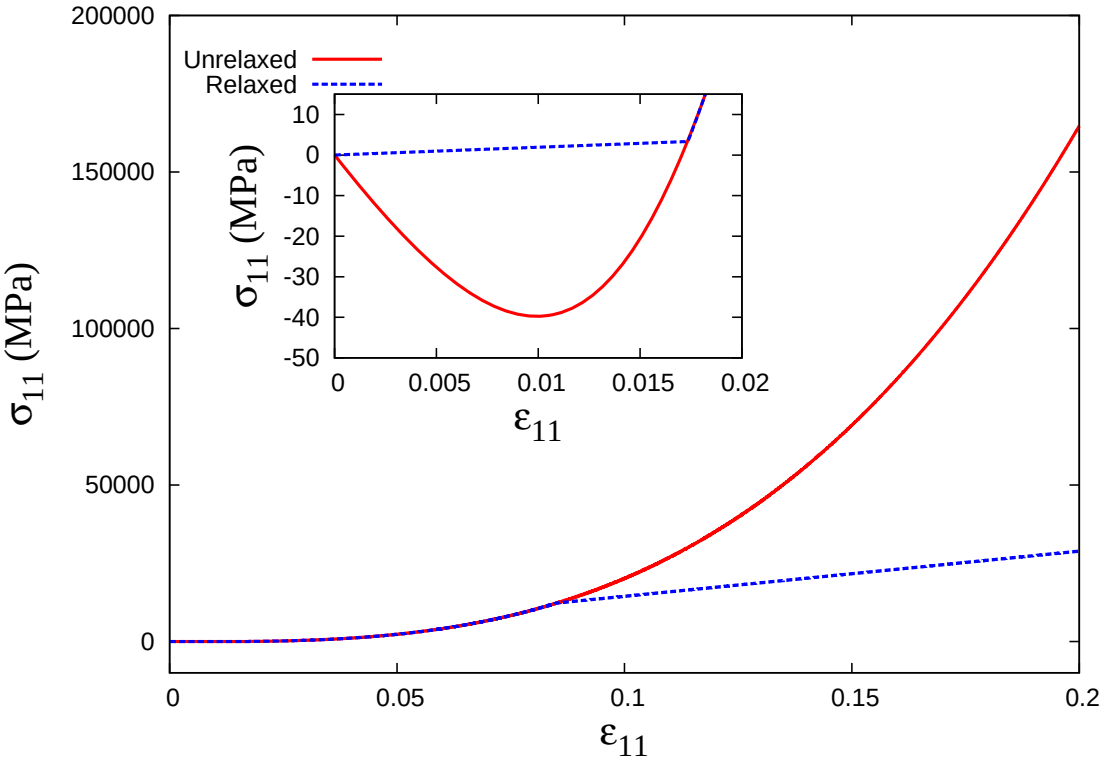

Figure 3.11.: Relaxed and unrelaxed stress-strain curves in tension test.

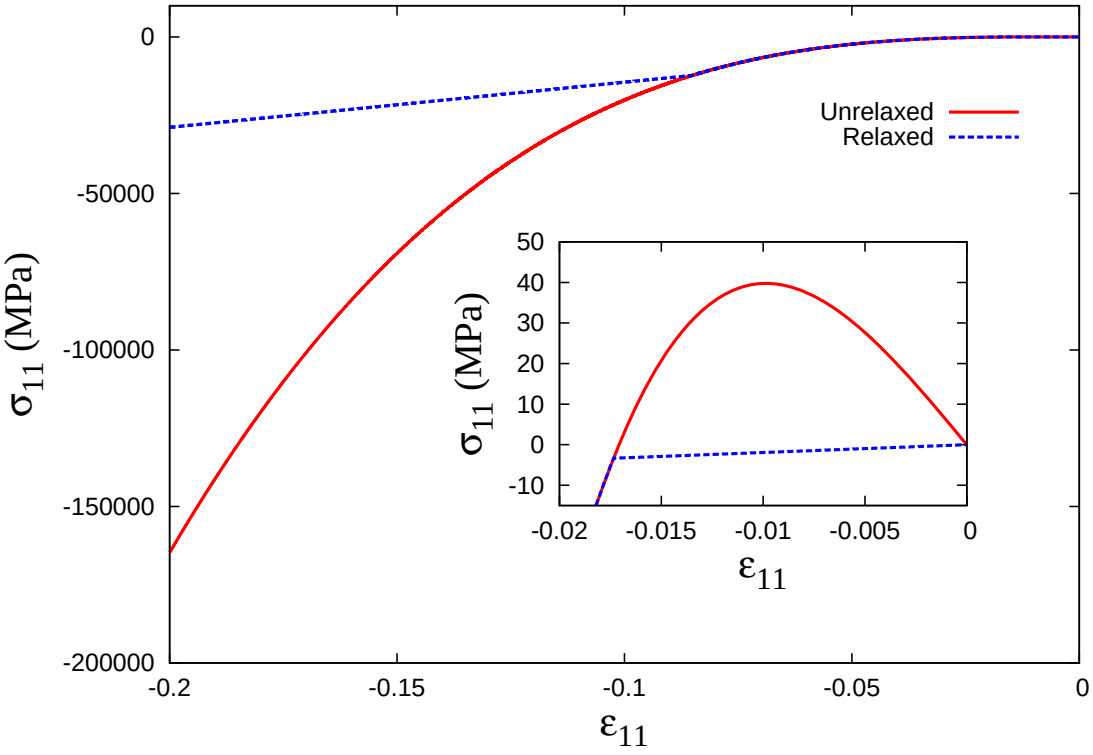

Figure 3.12.: Relaxed and unrelaxed stress-strain curves in compression test.

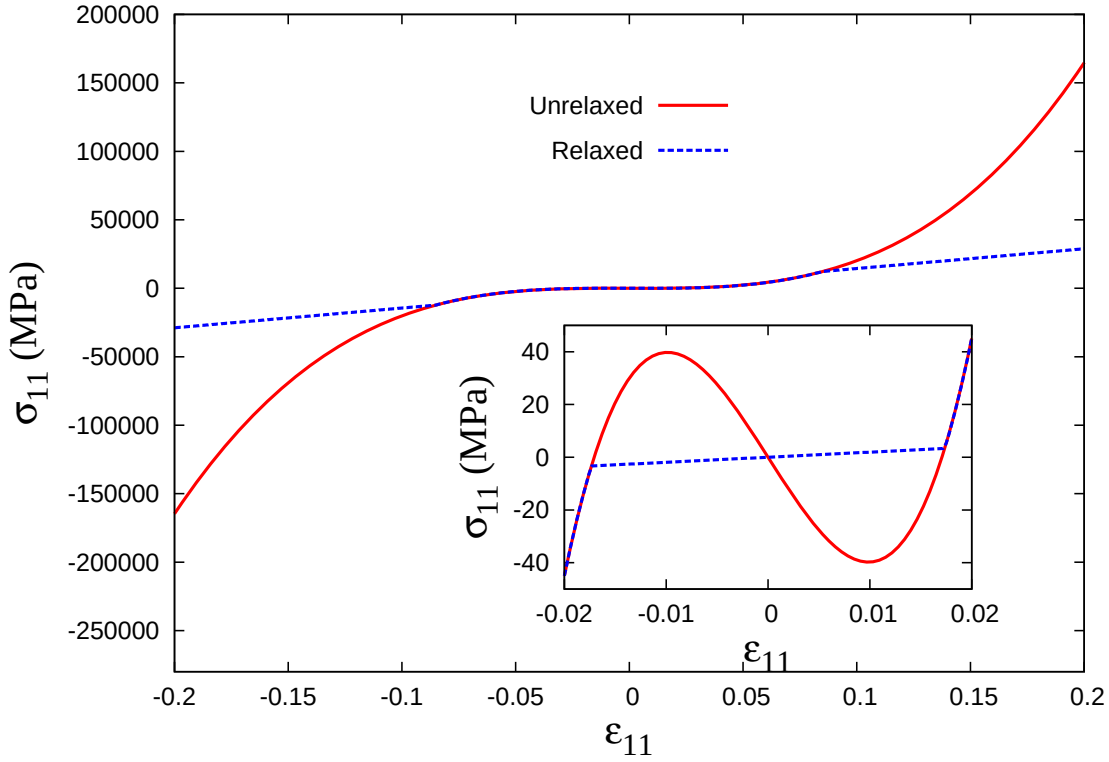

Figure 3.13.: Relaxed and unrelaxed stress-strain curves in tension-compression test.

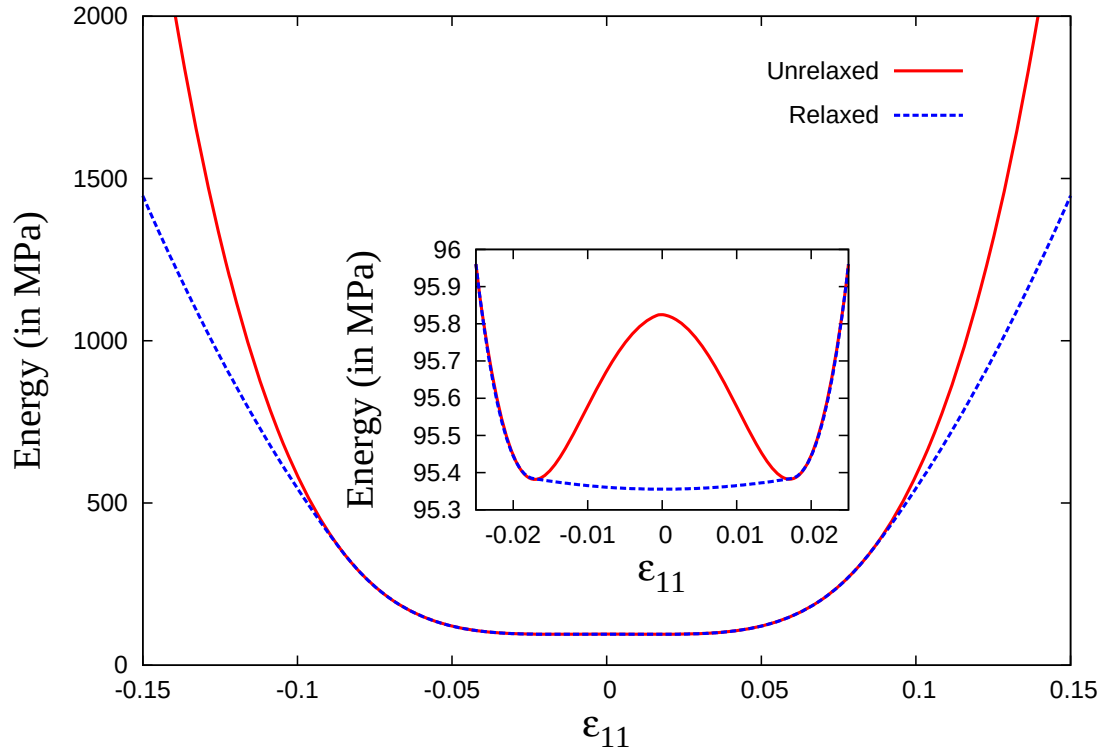

Figure 3.14.: Relaxed and unrelaxed energy curves in tension-compression test.

of the convex envelope in the globally nonconvex range of the unrelaxed energy potential is not constant contrary to the case of shear test. As a consequence the stress is monotonically increasing in the transformation phase where the material is experiencing microstructure in micromotions, again contrary to the case of shear test where a Maxwell line was seen for the stress-strain relation in the regime of microstructure in micromotions.

3.6. Modeling of rate-dependent inelastic material behavior

Granular materials often exhibit dissipative behavior in nature. For example in the modeling of granular materials consisting of sand particles a dissipative nature has been observed by []. Goddard also demonstrates on the dissipative behavior of granular materials in [God86] where a constitutive theory for such materials is discussed in the framework of visco-plasticity. Moreover, experimental studies by Lade [Lad94], Mitchell and Solymar [MS84], Murayama et al. [sKMS84] and di Prisco and Imposimato [dPI96] reveals on the time dependency and viscoplastic nature of granular materials behavior.

Due to this characteristic of the granular materials the elastic effects in modeling the mechanical response of these materials can be neglected for simplicity. The continuum models based on purely plastic strain and with the assumption that the elastic part of the strain is negligible are oriented to show rate-dependent response. Such models for the analysis of granular material behaviors are discussed very rarely in literature in the framework of Cosserat continuum. However, in general, abundant studies appears in literature that demonstrate on the use of viscplastic approach in modeling many mechanical materials behavior. A general theory accounting for microstructural effects based on small deformation viscoplastic approach using energy principles has been developed by Gurtin [Gur03]. Here within the framework of Cosserat continuum a review over the modeling of granular materials behavior using visco-inelastic approaches is presented. Rate-dependent constitutive model for the analysis of localized deformation behavior of granular materials has been developed by Mühlhaus and Aifantis [MA91]. A large number of problems have been discussed with the framework of Cosserat plasticity, for example, shear bands thickness in a granular medium are analyzed by Mühlhaus and Vardoulakis [MV87] and Mohan et al. [MNR99], limit load problems are discussed by Mühlhaus [M$9a$], study on sands and shear bands patterning in a granular medium was carried out by Tejchman and Wu [TW93, TW94, TW12], a comparison between experimental and numerical observations of vibrations and shocks in emptying a silo was made by Tejchman and Gudehus [TG93]. Many interesting features of the granular flows can be observed using the rigid-plastic or viscoplastic based Cosserat models as discussed by Mohan et al. [MNR99] and Elaskar et al. [EGGS00], the later is based on the non-associated viscoplasticity approach. Zienkiewicz et al. [ZHL75] also established an associated as well as a non-associated viscoplasticity approach to model the mechanical behavior of granular materials. A good review on the use of Cosserat continuum within the framework of plasticity is made in a book by Vardoulakis and Sulem [VS95], with the emphasis on localized deformation behavior of geomaterials. An already developed visco-plastic constitutive model can be modified [dPIA02] using two distinct non-local and gradient approaches for modeling the granular materials behavior.

3.6.1. A rate-dependent inelastic Cosserat material model

For modeling the inelastic response of the granular materials our approach is confined to the case of rigid-plasticity. Based on the Cosserat continuum [CC09, Sch67] theory the granular materials are modeled within the framework of rate-dependent viscoplasticity. Inelastic material response of such materials can be completely describable with the specification, if possible, of the two potentials, the stored free energy potential and the dissipation potential. Modeling of the inelastic material behaviors with the mathematical theories based on variational principles using these potentials have been studied and developed in the work of Baldassari and Hackl [SBH03], Carstensen et al. [CHM02], Conti and Ortiz [CO05], Conti and Theil [CT05], Conti et al. [CDK09, CHO07], Hackl [Hac97], Hackl and Fischer [HF08], Hackl and Hoppe [HH01], Hackl et al. [HHK12], Mielke [Mie04]. Consider that the Gibbs energy of the granular materials in consideration is characterized by

$$G = \int_{\Omega} \Psi\left(\mathbf{u}, \boldsymbol{\varphi}\right) \, dV - \ell_{\text{ext}}\left(\mathbf{u}, \boldsymbol{\varphi}\right), \tag{3.88}$$

where $\mathbf{u}$ is the displacement field, $\boldsymbol{\varphi}$ is the microrotation field in context of generalized continuum theories [CC09, Eri02, KE76, Min64, Now70, Sch67, Tou62, Tou64, TT60], Ψ is the stored energy density of the material and ℓ_{ext} is the potential of external forces acting on the granular body Ω. Working within the framework of infinitely small strain theory the total Cosserat strain tensor and the curvature strain tensor can be decomposed in an additive manner into the following two parts

$$\boldsymbol{e} = \boldsymbol{e}_{el} + \boldsymbol{e}_{in}, \qquad \boldsymbol{\kappa} = \boldsymbol{\kappa}_{el} + \boldsymbol{\kappa}_{in}. \tag{3.89}$$

In modeling the mechanical response of granular materials with above mentioned assumptions it is thus required to consider negligibly small elastic strains or no recoverable strains at all. Precisely, this means that the elastic parts of the total strains are zero, i.e.

$$\boldsymbol{e}_{el} = \mathbf{0}, \qquad \boldsymbol{\kappa}_{el} = \mathbf{0}. \tag{3.90}$$

Since the stored energy density function Ψ purely depends on the elastic deformation tensors of the medium, therefore, in the case where there are no elastic deformations it becomes zero. Hence in a regime of purely inelastic deformations the relation for the Gibbs energy in (3.88) reduces to

$$\Psi = 0 \quad \Rightarrow \quad G = -\ell_{\text{ext}}\left(\mathbf{u}, \boldsymbol{\varphi}\right). \tag{3.91}$$

As a result the total strain tensors are now purely depending upon the inelastic (non-recoverable) part of the strain tensors. This allows one to write both the Cosserat strain and the curvature strain tensors as

$$\boldsymbol{e} = \boldsymbol{e}_{in}, \qquad \boldsymbol{\kappa} = \boldsymbol{\kappa}_{in}. \tag{3.92}$$

The evolution of these inelastic strains can be determined completely from a variational principle using a specified dissipation potential Δ. This variational principle is called minimum principle for the dissipation potential which has already been used in different settings by Hackl and Fischer [HF08], Halphen and Nguyen [HN75], Maier [Mai69], Martin and Ponter [MP66], Maugin [Mau92] and in context of evolution of inelastic microstructures by Carstensen et al. [CHM02], Hackl [Hac97] and Ortiz and Repetto [OR99]. In this

context, here we search for all those admissible inelastic variables $\boldsymbol{e}_{in}$ and $\boldsymbol{\kappa}_{in}$ that minimize $\left\{\dfrac{d}{dt}G + D\right\}$, or equivalently, one can write $\min\limits_{\dot{\mathbf{u}},\dot{\boldsymbol{\varphi}}}\left\{\dfrac{d}{dt}G + D\right\}$, where $\dot{\mathbf{u}}$ is the time derivative of the displacement field (velocity vector field), $\dot{\boldsymbol{\varphi}}$ is the time derivative of micro-rotation field (gyration vector field) and D is the dissipation function and is determined by

$$D = \int_{\Omega} \Delta \, dV. \tag{3.93}$$

In a more detailed description this principle reduces to the following energy minimization problem, that reads

$$\{\dot{\mathbf{u}}, \dot{\boldsymbol{\varphi}}\} = \arg\left\{\min_{\dot{\mathbf{u}},\dot{\boldsymbol{\varphi}}}\left\{\int_{\Omega} \Delta\left(\dot{\mathbf{e}}_{\mathrm{in}}, \dot{\boldsymbol{\kappa}}_{\mathrm{in}}\right) - \dot{\ell}_{\mathrm{ext}}\left(\dot{\mathbf{u}}, \dot{\boldsymbol{\varphi}}\right)\right\}\right\}, \tag{3.94}$$

where the inelastic Cosserat strain tensor $\dot{\mathbf{e}}_{\mathrm{in}}$ and the curvature strain tensor $\dot{\boldsymbol{\kappa}}_{\mathrm{in}}$ are defined according to

$$\dot{\mathbf{e}}_{\mathrm{in}} = \nabla\dot{\mathbf{u}} - \operatorname{asy}\dot{\boldsymbol{\varphi}}, \qquad \dot{\boldsymbol{\kappa}}_{\mathrm{in}} = \nabla\dot{\boldsymbol{\varphi}}. \tag{3.95}$$

In equation 3.93 the nonlinear dissipation potential Δ is expressed as

$$\Delta = \left\{\begin{array}{c} \left(\dfrac{\lambda}{2} + \dfrac{\mu}{d}\right)\left(\operatorname{tr}\,\dot{\boldsymbol{\varepsilon}}\right)^2 + \mu\left\|\operatorname{dev}\,\dot{\boldsymbol{\varepsilon}}\right\|^2 + \mu_c\left\|\dot{\boldsymbol{\omega}}\right\|^2 + \dfrac{\bar{\lambda}}{2}\left(\operatorname{tr}\,\dot{\boldsymbol{\kappa}}\right)^2 + \bar{\mu}\left\|\operatorname{sym}\,\dot{\boldsymbol{\kappa}}\right\|^2 \\ + \bar{\mu}_c\left\|\operatorname{asy}\,\dot{\boldsymbol{\kappa}}\right\|^2 + \alpha\left(\left\|\operatorname{sym}\,\dot{\boldsymbol{\kappa}}\right\|^2 + \left\|\operatorname{asy}\,\dot{\boldsymbol{\kappa}}\right\|^2 - \beta^2\left\|\operatorname{dev}\,\dot{\boldsymbol{\varepsilon}}\right\|^2\right)^2 \end{array}\right. \tag{3.96}$$

The above dissipation potential is clearly nonconvex, and therefore when it enters in the minimization problem (3.94) will lead to the possible velocity field fluctuations at the fine scale and thus leading to internal structure of the material. Moreover, the existence of the unique minimizing velocities are not guaranteed. Furthermore, the nonconvex dissipation functional associated to the variational problem (3.94) illustrates on the loss of ellipticity of the resulting governing velocity field equations. Hence, it is therefore required to compute a quasiconvex dissipation function Δ^{rel} for the nonconvex dissipation potential in 3.96 which satisfies the ellipticity condition (Legendre Hadamard condition) [BJ87] and guarantee on the existence of the minimizing deformations.

3.6.2. Computation of a relaxed potential for the dissipation

Due to nonconvexity of the dissipation potential a relaxed function is derived in this Section. The procedure of computing this relaxed potential is the same as adopted for the computation of the exact relaxed energy in Section 3.4.3. The resulting quasiconvex dissipation potential comprises of three different material regimes. Each of the material regime is characterized according to the following conditions

$$\text{if} \quad \left\|\dot{\boldsymbol{\kappa}}\right\|^2 \geq \beta^2\left\|\operatorname{dev}\,\dot{\boldsymbol{\varepsilon}}\right\|^2 + \frac{\mu}{2\alpha\beta^2} \quad \text{then the material is in regime 1,} \tag{3.97}$$

$$\text{if} \quad \beta^2\left\|\operatorname{dev}\,\dot{\boldsymbol{\varepsilon}}\right\|^2 - \frac{\mu_\circ}{2\alpha} \leq \left\|\dot{\boldsymbol{\kappa}}\right\|^2 \leq \beta^2\left\|\operatorname{dev}\,\dot{\boldsymbol{\varepsilon}}\right\|^2 + \frac{\mu}{2\alpha\beta^2} \quad \text{then the material is in regime 2,} \tag{3.98}$$

$$\text{if} \quad \|\dot{\boldsymbol{\kappa}}\|^2 \leq \beta^2 \|\operatorname{dev} \dot{\boldsymbol{\varepsilon}}\|^2 - \frac{\mu_\circ}{2\alpha} \quad \text{then the material is in regime 3.} \tag{3.99}$$

In each regime the dissipation potential depends upon the rate of the strain tensors $\mathbf{e}$ and $\boldsymbol{\kappa}$. We consider the rigid plastic deformation case where the elastic part of the strain tensors are assumed to be zero and the total strain is equivalent the inelastic part of the strain tensors, which is purely associated with the plastic deformation of the granular materials. The dissipation potential in this case is expressed as

$$\Delta = \Delta\left(\dot{\mathbf{e}}_{\text{in}}, \dot{\boldsymbol{\kappa}}_{\text{in}}\right). \tag{3.100}$$

The dissipation potential $\Delta\left(\dot{\mathbf{e}}_{\text{in}}, \dot{\boldsymbol{\kappa}}_{\text{in}}\right)$ is comprising of three phases where in each of the material phase the dissipation potential is characterizes according to

$$\Delta = \begin{cases} \Delta_1 & \text{if} \quad \|\dot{\boldsymbol{\kappa}}\|^2 \geq \beta^2 \|\operatorname{dev} \dot{\boldsymbol{\varepsilon}}\|^2 + \dfrac{\mu}{2\alpha\beta^2} \\ \Delta_2 & \text{if} \quad \beta^2 \|\operatorname{dev} \dot{\boldsymbol{\varepsilon}}\|^2 - \dfrac{\mu_\circ}{2\alpha} \leq \|\dot{\boldsymbol{\kappa}}\|^2 \leq \beta^2 \|\operatorname{dev} \dot{\boldsymbol{\varepsilon}}\|^2 + \dfrac{\mu}{2\alpha\beta^2} \\ \Delta_3 & \text{if} \quad \|\dot{\boldsymbol{\kappa}}\|^2 \leq \beta^2 \|\operatorname{dev} \dot{\boldsymbol{\varepsilon}}\|^2 - \dfrac{\mu_\circ}{2\alpha} \end{cases} \tag{3.101}$$

where Δ_1 is the dissipation potential in the regime of microstructure in micromotions of the particles expressed as

$$\Delta_1 = \begin{cases} \left(\dfrac{\lambda}{2} + \dfrac{\mu}{d}\right)(\operatorname{tr} \dot{\boldsymbol{\varepsilon}})^2 + \mu_c \|\dot{\boldsymbol{\omega}}\|^2 + \dfrac{\bar{\lambda}}{2}(\operatorname{tr} \dot{\boldsymbol{\kappa}})^2 + \\ (\bar{\mu} - \bar{\mu}_c) \|\operatorname{sym} \dot{\boldsymbol{\kappa}}\|^2 + \left(\mu_\circ + \dfrac{\mu}{\beta^2}\right) \|\dot{\kappa}\|^2 - \dfrac{\mu^2}{4\alpha\beta^4} & \text{if} \quad \bar{\mu} \geq \bar{\mu}_c, \\ \left(\dfrac{\lambda}{2} + \dfrac{\mu}{d}\right)(\operatorname{tr} \dot{\boldsymbol{\varepsilon}})^2 + \mu_c \|\dot{\boldsymbol{\omega}}\|^2 + \dfrac{\bar{\lambda}}{2}(\operatorname{tr} \dot{\boldsymbol{\kappa}})^2 - \\ (\bar{\mu} - \bar{\mu}_c) \|\operatorname{asy} \dot{\boldsymbol{\kappa}}\|^2 + \left(\mu_\circ + \dfrac{\mu}{\beta^2}\right) \|\dot{\boldsymbol{\kappa}}\|^2 - \dfrac{\mu^2}{4\alpha\beta^4} & \text{if} \quad \bar{\mu} < \bar{\mu}_c \end{cases} \tag{3.102}$$

Δ_2 is the dissipation potential in the regime where there is no internal structure microstructure of the material and is given by

$$\Delta_2 = \begin{cases} \left(\dfrac{\lambda}{2} + \dfrac{\mu}{d}\right)(\operatorname{tr} \dot{\boldsymbol{\varepsilon}})^2 + \mu \|\operatorname{dev} \dot{\boldsymbol{\varepsilon}}\|^2 + \mu_c \|\dot{\boldsymbol{\omega}}\|^2 + \dfrac{\bar{\lambda}}{2}(\operatorname{tr} \dot{\boldsymbol{\kappa}})^2 + \bar{\mu} \|\operatorname{sym} \dot{\boldsymbol{\kappa}}\|^2 \\ \quad + \bar{\mu}_c \|\operatorname{asy} \dot{\boldsymbol{\kappa}}\|^2 + \alpha\left(\|\operatorname{sym} \dot{\boldsymbol{\kappa}}\|^2 + \|\operatorname{asy} \dot{\boldsymbol{\kappa}}\|^2 - \beta^2 \|\operatorname{dev} \dot{\boldsymbol{\varepsilon}}\|^2\right)^2 \end{cases} \tag{3.103}$$

Δ_3 is the dissipation potential in the regime where there is a microstructure in the material due translational motions of the continuum particles and is given by

$$\Delta_3 = \begin{cases} \left(\dfrac{\lambda}{2} + \dfrac{\mu}{d}\right)(\operatorname{tr} \dot{\boldsymbol{\varepsilon}})^2 + \mu_c \|\dot{\boldsymbol{\omega}}\|^2 + \dfrac{\bar{\lambda}}{2}(\operatorname{tr} \dot{\boldsymbol{\kappa}})^2 + \\ (\bar{\mu} - \bar{\mu}_c) \|\operatorname{sym} \dot{\boldsymbol{\kappa}}\|^2 + \left(\mu_\circ \beta^2 + \mu\right) \|\operatorname{dev} \dot{\boldsymbol{\varepsilon}}\|^2 - \dfrac{\mu_\circ^2}{4\alpha} & \text{if} \quad \bar{\mu} \geq \bar{\mu}_c \\ \left(\dfrac{\lambda}{2} + \dfrac{\mu}{d}\right)(\operatorname{tr} \dot{\boldsymbol{\varepsilon}})^2 + \mu_c \|\dot{\boldsymbol{\omega}}\|^2 + \dfrac{\bar{\lambda}}{2}(\operatorname{tr} \dot{\boldsymbol{\kappa}})^2 - \\ (\bar{\mu} - \bar{\mu}_c) \|\operatorname{asy} \dot{\boldsymbol{\kappa}}\|^2 + \left(\mu_\circ \beta^2 + \mu\right) \|\operatorname{dev} \dot{\boldsymbol{\varepsilon}}\|^2 - \dfrac{\mu_\circ^2}{4\alpha} & \text{if} \quad \bar{\mu} < \bar{\mu}_c \end{cases} \tag{3.104}$$

3.6.3. Rate-dependent constitutive equations

Following the arguments given by Hackl and Fischer in [HF08] the relations for the generalized thermodynamical forces can be derived from the stationarity conditions of the minimum principle for dissipation potential [HF08]. This could be achieved directly as the derivative of the dissipation potential with respect to the admissible inelastic variables (also called thermodynamic fluxes) which results in the following thermodynamic forces

$$\mathfrak{g} = \frac{\partial \Delta}{\partial \boldsymbol{e}_{in}}, \qquad \mathfrak{q} = \frac{\partial \Delta}{\partial \boldsymbol{\kappa}_{in}}, \tag{3.105}$$

where $\mathfrak{g}$ is the Cosserat generalized force tensor and $\mathfrak{q}$ is the generalized couple tensor, being conjugate to the inelastic Cosserat strain tensor and curvature strain tensor respectively. The rate-dependent constitutive response of the material is thus comprises of three phase response which would be determined from the following relation

$$\mathfrak{g} = \begin{cases} \mathfrak{g}_1 & \text{if} \quad \|\dot{\boldsymbol{\kappa}}\|^2 \geq \beta^2 \|\operatorname{dev} \dot{\boldsymbol{\varepsilon}}\|^2 + \dfrac{\mu}{2\alpha\beta^2} \\ \mathfrak{g}_2 & \text{if} \quad \beta^2 \|\operatorname{dev} \dot{\boldsymbol{\varepsilon}}\|^2 - \dfrac{\mu_\circ}{2\alpha} \leq \|\dot{\boldsymbol{\kappa}}\|^2 \leq \beta^2 \|\operatorname{dev} \dot{\boldsymbol{\varepsilon}}\|^2 + \dfrac{\mu}{2\alpha\beta^2} \\ \mathfrak{g}_3 & \text{if} \quad \|\dot{\boldsymbol{\kappa}}\|^2 \leq \beta^2 \|\operatorname{dev} \dot{\boldsymbol{\varepsilon}}\|^2 - \dfrac{\mu_\circ}{2\alpha} \end{cases} \tag{3.106}$$

where $\mathfrak{g}_1$ is the generalized force tensor in a material phase where there is a microstructure in micromotions of the continuum particles, $\mathfrak{g}_2$ is the generalized force tensor in the material phase where there is no internal structure in the material and $\mathfrak{g}_3$ is the generalized force tensor in the material phase where there is a microstructure in translational motions of the continuum particles and are given respectively as

$$\mathfrak{g}_1 = 2\left(\frac{\lambda}{2} + \frac{\mu}{d}\right) \operatorname{tr} \dot{\boldsymbol{\varepsilon}}\, \mathbf{I} + 2\mu_c\, \dot{\boldsymbol{\omega}}_e, \tag{3.107}$$

$$\mathfrak{g}_2 = \lambda \operatorname{tr} \dot{\boldsymbol{\varepsilon}}\, \mathbf{I} + 2\mu\, \dot{\boldsymbol{\varepsilon}} + 2\mu_c\, \dot{\boldsymbol{\omega}}_e - 4\alpha\beta^2 \left(\|\dot{\boldsymbol{\kappa}}\|^2 - \beta^2 \|\operatorname{dev} \dot{\boldsymbol{\varepsilon}}\|^2 \right) \operatorname{dev} \dot{\boldsymbol{\varepsilon}} \tag{3.108}$$

and

$$\mathfrak{g}_3 = \lambda \operatorname{tr} \dot{\boldsymbol{\varepsilon}}\, \mathbf{I} + 2\mu\, \dot{\boldsymbol{\varepsilon}} + 2\mu_\circ \beta^2 \operatorname{dev} \dot{\boldsymbol{\varepsilon}} + 2\mu_c\, \dot{\boldsymbol{\omega}}_e. \tag{3.109}$$

The generalized couple tensor is to be determined from the following formula

$$\mathfrak{q} = \begin{cases} \mathfrak{q}_1 & \text{if} \quad \|\dot{\boldsymbol{\kappa}}\|^2 \geq \beta^2 \|\operatorname{dev} \dot{\boldsymbol{\varepsilon}}\|^2 + \dfrac{\mu}{2\alpha\beta^2} \\ \mathfrak{q}_2 & \text{if} \quad \beta^2 \|\operatorname{dev} \dot{\boldsymbol{\varepsilon}}\|^2 - \dfrac{\mu_\circ}{2\alpha} \leq \|\dot{\boldsymbol{\kappa}}\|^2 \leq \beta^2 \|\operatorname{dev} \dot{\boldsymbol{\varepsilon}}\|^2 + \dfrac{\mu}{2\alpha\beta^2} \\ \mathfrak{q}_3 & \text{if} \quad \|\dot{\boldsymbol{\kappa}}\|^2 \leq \beta^2 \|\operatorname{dev} \dot{\boldsymbol{\varepsilon}}\|^2 - \dfrac{\mu_\circ}{2\alpha} \end{cases} \tag{3.110}$$

where $\mathfrak{q}_1$ is the generalized couple tensor in a material phase where there is a microstructure in micromotions of the continuum particles, $\mathfrak{q}_2$ is the generalized couple tensor in the material phase where there is no internal structure in the material and $\mathfrak{q}_3$ is the generalized couple

tensor in the material phase where there is a microstructure in translational motions of the continuum particles and are given respectively as

$$\mathbf{q}_1 = \begin{cases} \bar{\lambda}\ \mathrm{tr}\,\dot{\boldsymbol{\kappa}}\,\mathbf{I} + 2\,(\bar{\mu} - \bar{\mu}_c)\ \mathrm{sym}\,\dot{\boldsymbol{\kappa}} + 2\left(\mu_\circ + \dfrac{\mu}{\beta^2}\right)\dot{\boldsymbol{\kappa}} & \text{if} \quad \bar{\mu} \geq \bar{\mu}_c, \\ \bar{\lambda}\ \mathrm{tr}\,\dot{\boldsymbol{\kappa}}\,\mathbf{I} - 2\,(\bar{\mu} - \bar{\mu}_c)\ \mathrm{asy}\,\dot{\boldsymbol{\kappa}} + 2\left(\mu_\circ + \dfrac{\mu}{\beta^2}\right)\dot{\boldsymbol{\kappa}} & \text{if} \quad \bar{\mu} < \bar{\mu}_c, \end{cases} \tag{3.111}$$

$$\mathbf{q}_2 = \bar{\lambda}\ \mathrm{tr}\,\dot{\boldsymbol{\kappa}}\,\mathbf{I} + 2\bar{\mu}\,\mathrm{sym}\,\dot{\boldsymbol{\kappa}} + 2\bar{\mu_c}\ \mathrm{asy}\ \dot{\boldsymbol{\kappa}} + 4\alpha\left(\|\dot{\boldsymbol{\kappa}}\|^2 - \beta^2\,\|\mathrm{dev}\,\dot{\boldsymbol{\varepsilon}}\|^2\right)\dot{\boldsymbol{\kappa}}, \tag{3.112}$$

and

$$\mathbf{q}_3 = \begin{cases} \bar{\lambda}\ \mathrm{tr}\,\dot{\boldsymbol{\kappa}}\,\mathbf{I} + 2\,(\bar{\mu} - \bar{\mu}_c)\ \mathrm{sym}\,\dot{\boldsymbol{\kappa}} & \text{if} \quad \bar{\mu} \geq \bar{\mu}_c, \\ \bar{\lambda}\ \mathrm{tr}\,\dot{\boldsymbol{\kappa}}\,\mathbf{I} - 2\,(\bar{\mu} - \bar{\mu}_c)\ \mathrm{asy}\,\dot{\boldsymbol{\kappa}} & \text{if} \quad \bar{\mu} < \bar{\mu}_c. \end{cases} \tag{3.113}$$

4. Variational formulation and finite element implementation

4.1. A two-field variational formulation

A two-field variational formulation of the Cosserat material model is presented. In a Cosserat elastic continuum the equilibrium of forces and couples acting on a body in the absence of angular velocity is expressed as

$$\nabla \cdot \boldsymbol{\sigma} + \mathbf{b} = \mathbf{0}, \tag{4.1}$$

$$\nabla \cdot \boldsymbol{\mu} + \boldsymbol{\sigma} : \boldsymbol{\mathcal{E}} + \mathbf{m} = \mathbf{0}, \tag{4.2}$$

where $\boldsymbol{\mathcal{E}}$ is the third order permutation tensor, $\mathbf{b}$ is the body force and $\mathbf{m}$ is the body moment, subjected to certain Drichlet boundary conditions of the type $\boldsymbol{\sigma} \cdot \mathbf{n}_{\mathrm{u}} = \mathbf{t}_{\mathrm{u}}$ and $\boldsymbol{\mu} \cdot \mathbf{n}_{\varphi} = \mathbf{t}_{\varphi}$. The Cosserat force-stress tensor $\boldsymbol{\sigma}$ and couple stress tensor $\boldsymbol{\mu}$ are computed as the derivatives of the strain energy function with respect to the Cosserat strain tensor $\mathbf{e}$ and curvature strain tensor $\boldsymbol{\kappa}$, respectively

$$\boldsymbol{\sigma} = \frac{\partial W^{rel}}{\partial \boldsymbol{e}}, \qquad \boldsymbol{\mu} = \frac{\partial W^{rel}}{\partial \boldsymbol{\kappa}}. \tag{4.3}$$

To derive weak balance equations or the variational formulation of (4.1) let us choose an arbitrary displacement field variation as $\delta\mathbf{u}$. Further let $\mathbf{t}_u = \boldsymbol{\sigma} \cdot \mathbf{n}_u$ be the applied traction on the surface Γ_u of the continuum body $\mathcal{B}$ having a volume Ω, with $\mathbf{n}_u$ being the normal unit vector to Γ_u. The variational formulation of (4.1) is obtained by multiplying equation (4.1) with the chosen arbitrary displacement variation $\delta\mathbf{u}$ and applying integrating to the resultant equation as

$$\int_{\Omega} (\nabla \cdot \boldsymbol{\sigma} + \mathbf{b}) \cdot \delta\mathbf{u} \, d\Omega \; = \; \int_{\Omega} \mathbf{0} \cdot \delta\mathbf{u} \, d\Omega. \tag{4.4}$$

Integrating equation (4.4) by parts implies

$$\int_{\Omega} \Big(\nabla \cdot (\boldsymbol{\sigma} \cdot \delta\mathbf{u}) \; - \; \boldsymbol{\sigma} : (\nabla \otimes \delta\mathbf{u}) \Big) \, d\Omega + \int_{\Omega} \mathbf{b} \cdot \delta\mathbf{u} \, d\Omega \; = \; \mathbf{0}. \tag{4.5}$$

Applying divergence theorem to first term in equation (4.5) one obtain

$$\int_{\Gamma_u} \Big(\underbrace{\boldsymbol{\sigma} \cdot \mathbf{n}_u}_{\mathbf{t}_{\mathrm{u}}} \Big) \cdot \delta\mathbf{u} \, d\Gamma_u - \int_{\Omega} \boldsymbol{\sigma} : (\nabla \otimes \delta\mathbf{u}) \; d\Omega + \int_{\Omega} \mathbf{b} \cdot \delta\mathbf{u} \, d\Omega \; = \; \mathbf{0} \tag{4.6}$$

$$\Rightarrow \qquad \int_{\Omega} \boldsymbol{\sigma} : (\nabla \otimes \delta\mathbf{u}) \; d\Omega \; = \; \int_{\Omega} \mathbf{b} \cdot \delta\mathbf{u} \, d\Omega + \int_{\Gamma_u} \mathbf{t}_{\mathrm{u}} \cdot \delta\mathbf{u} \, d\Gamma_u \tag{4.7}$$

Equation (4.7) is the resulting variational form of the balance of linear momentum. Consider now the second equation (4.2), the weak form is obtained by multiplying it with the arbitrary function $\delta\boldsymbol{\varphi}$ and integrating the resultant equation over the domain Ω as

$$\int_{\Omega} (\nabla \cdot \boldsymbol{\mu} + \boldsymbol{\mathcal{E}} : \boldsymbol{\sigma} + \mathbf{m}) \cdot \delta\boldsymbol{\phi} \, d\Omega \; = \; \int_{\Omega} \mathbf{0} \cdot \delta\boldsymbol{\varphi} \, d\Omega \tag{4.8}$$

since

$$\nabla \cdot (\boldsymbol{\mu} \cdot \delta\boldsymbol{\phi}) \; = \; (\nabla \cdot \boldsymbol{\mu}) \cdot \delta\boldsymbol{\phi} + \boldsymbol{\mu} : (\nabla \otimes \delta\boldsymbol{\phi}) \, . \tag{4.9}$$

By using the property $\boldsymbol{\mathcal{E}} : \boldsymbol{\sigma} \; = \; \boldsymbol{\sigma} : \boldsymbol{\mathcal{E}}$ and (4.9) equation (4.8) can be rewritten in the form

$$\int_{\Omega} \Big(\nabla \cdot (\boldsymbol{\mu} \cdot \delta\boldsymbol{\phi}) - \boldsymbol{\mu} : (\nabla \otimes \delta\boldsymbol{\phi}) + (\boldsymbol{\sigma} : \boldsymbol{\mathcal{E}}) \cdot \delta\boldsymbol{\phi} + \mathbf{m} \cdot \delta\boldsymbol{\phi} \Big) \, d\Omega \; = \; \mathbf{0} \tag{4.10}$$

$$\Rightarrow \quad \int_{\Gamma_\varphi} \Big(\underbrace{\boldsymbol{\mu} \cdot \mathbf{n}_\varphi}_{\mathbf{t}_\varphi} \Big) \cdot \delta\boldsymbol{\phi} d\Gamma_\varphi - \int_{\Omega} \boldsymbol{\mu} : (\nabla \otimes \delta\boldsymbol{\phi}) \, d\Omega + \int_{\Omega} (\boldsymbol{\sigma} : \boldsymbol{\mathcal{E}}) \cdot \delta\boldsymbol{\phi} d\Omega + \int_{\Omega} \mathbf{m} \cdot \delta\boldsymbol{\phi} d\Omega = \mathbf{0} \tag{4.11}$$

$$\Rightarrow \quad \int_{\Omega} \boldsymbol{\mu} : (\nabla \otimes \delta\boldsymbol{\phi}) \, d\Omega - \int_{\Omega} (\boldsymbol{\sigma} : \boldsymbol{\mathcal{E}}) \cdot \delta\boldsymbol{\phi} d\Omega \; = \; \int_{\Omega} \mathbf{m} \cdot \delta\boldsymbol{\phi} d\Omega + \int_{\Gamma_\varphi} \mathbf{t}_\varphi \cdot \delta\boldsymbol{\phi} d\Gamma_\varphi \tag{4.12}$$

The final set of variational equations for (4.1) and (4.2) that must be satisfied for the equilibrium configuration of a body by its each material point in a Cosserat continuum in an integrated sense are respectively

$$\int_{\Omega} \boldsymbol{\sigma} : (\nabla \otimes \delta\mathbf{u}) \; d\Omega \; = \; \int_{\Omega} \mathbf{b} \cdot \delta\mathbf{u} \, d\Omega + \int_{\Gamma_u} \mathbf{t}_u \cdot \delta\mathbf{u} \, d\Gamma_u, \tag{4.13}$$

and

$$\int_{\Omega} \Big(\boldsymbol{\mu} : (\nabla \otimes \delta\boldsymbol{\phi}) - (\boldsymbol{\sigma} : \boldsymbol{\mathcal{E}}) \cdot \delta\boldsymbol{\phi} \Big) \, d\Omega \; = \; \int_{\Omega} \mathbf{m} \cdot \delta\boldsymbol{\phi} \, d\Omega + \int_{\Gamma_\varphi} \mathbf{t}_\varphi \cdot \delta\boldsymbol{\phi} \, d\Gamma_\varphi. \tag{4.14}$$

4.2. Numerical implementation procedure using Finite element method

To solve the system of linear and angular momentum weak-balance equations (4.13) and (4.14) the finite element method is employed. Finite element method has been proved efficient and successful in solving the system of both the linear and nonlinear equations which arose in the modeling of many materials behaviors in general [AAE10, GP98b, GP98a, GM11, LGM , LMD03, LL96, ML03, MLG04, Rou94, ZT00] and in particular, the Cosserat materials behavior [KAV06, AS06, dB91, dBS91, HB03, HNB02, SD02, TG93, TN06, VS95, WT06].

The numerical implementation procedure is presented in the absence of the body force $\mathbf{b}$ and body couple $\mathbf{m}$. The material body or the domain Ω is discretized into finite elements in such a way that

$$\Omega = \bigcup_{e=1}^{n_e} \Omega_e, \tag{4.15}$$

where Ω_e is the domain of a descretized element 'e' in the entire material body. Each element is further consists of nodal points or coordinates on which the shape functions are defined to interpolate the nodal field variables, which are in fact none other than the degrees of freedom of a material point. In the case of first grade theory of a Cosserat continuum there are only two field variables called the displacement and microrotation which together contains a total of nine degrees of freedom at a single material point. These displacement and microrotation vector field variables are approximated at the elemental level using matrices of shape functions $\mathbf{N_u}$ and $\mathbf{N}_\varphi$ respectively as

$$\mathbf{u}^e = \mathbf{N_u}\hat{\mathbf{u}}^e \qquad \text{and} \qquad \boldsymbol{\varphi}^e = \mathbf{N}_\varphi\hat{\boldsymbol{\varphi}}^e \tag{4.16}$$

where the matrices of shape functions are expressed as

$$\mathbf{N_u} = \begin{bmatrix} N^1 & 0 & 0 & N^2 & 0 & 0 & \cdots & N^{NN} & 0 & 0 \\ 0 & N^1 & 0 & 0 & N^2 & 0 & \cdots & 0 & N^{NN} & 0 \\ 0 & 0 & N^1 & 0 & 0 & N^2 & \cdots & 0 & 0 & N^{NN} \end{bmatrix}, \tag{4.17}$$

$$\mathbf{N}_\varphi = \begin{bmatrix} N^1 & 0 & 0 & N^2 & 0 & 0 & \cdots & N^{NN} & 0 & 0 \\ 0 & N^1 & 0 & 0 & N^2 & 0 & \cdots & 0 & N^{NN} & 0 \\ 0 & 0 & N^1 & 0 & 0 & N^2 & \cdots & 0 & 0 & N^{NN} \end{bmatrix}, \tag{4.18}$$

and the vector of nodal degrees of freedoms are calculated as

$$\hat{\mathbf{u}}^e = \left[u_1^1, u_2^1, u_3^1, u_1^2, u_2^2, u_3^2, u_1^3, u_2^3, u_3^3, ..., u_1^{NN}, u_2^{NN}, u_3^{NN}\right], \tag{4.19}$$

$$\hat{\boldsymbol{\varphi}}^e = \left[\varphi_1^1, \varphi_2^1, \varphi_3^1, \varphi_1^2, \varphi_2^2, \varphi_3^2, \varphi_1^3, \varphi_2^3, \varphi_3^3, ..., \varphi_1^{NN}, \varphi_2^{NN}, \varphi_3^{NN}\right] \tag{4.20}$$

with 'NN' being the total number of nodes per element. Two types of elements as shown in Figure 4.1 are used for the calculations, where the shape functions at each of the node in a

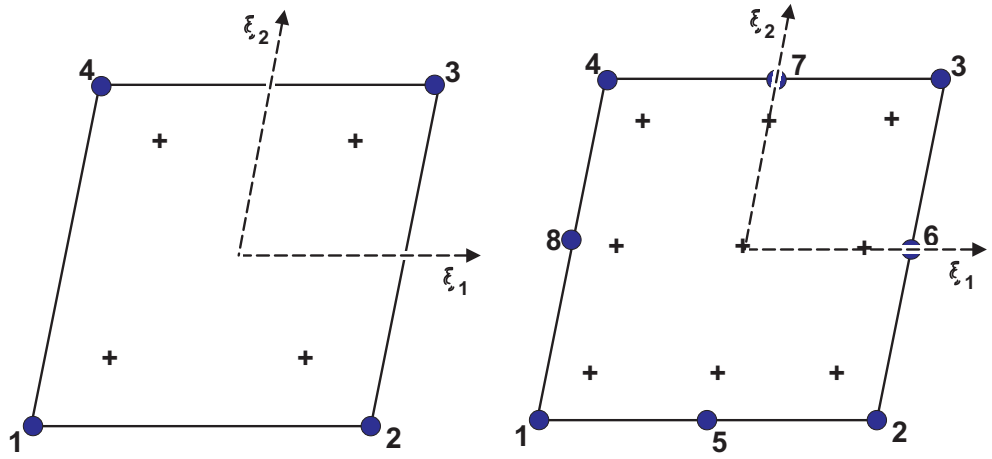

Figure 4.1.: Four-node linear element (first column) and eight-node bi-quadratic element (second column). The plus (+) symbol indicates the Guass integration point location and the number of Guass points used.

four-node element are computed as

$$N^1 = \frac{1}{4}(1-\xi_1)(1-\xi_2), \quad N^2 = \frac{1}{4}(1+\xi_1)(1-\xi_2),$$

$$N^3 = \frac{1}{4}(1+\xi_1)(1+\xi_2), \quad N^4 = \frac{1}{4}(1-\xi_1)(1+\xi_2),$$

and in an eight-node element as the following bi-quadratic functions

$$N^1 = -\frac{1}{4}(1-\xi_1)(1-\xi_2)(1+\xi_1+\xi_2), \quad N^2 = -\frac{1}{4}(1+\xi_1)(1-\xi_2)(1-\xi_1+\xi_2),$$

$$N^3 = -\frac{1}{4}(1+\xi_1)(1+\xi_2)(1-\xi_1-\xi_2), \quad N^4 = -\frac{1}{4}(1-\xi_1)(1+\xi_2)(1+\xi_1-\xi_2),$$

$$N^5 = \frac{1}{2}\left(1-\xi_1^2\right)(1-\xi_2), \quad N^6 = \frac{1}{2}\left(1-\xi_2^2\right)(1+\xi_1),$$

$$N^7 = \frac{1}{2}\left(1-\xi_1^2\right)(1+\xi_2), \quad N^8 = \frac{1}{2}\left(1-\xi_2^2\right)(1-\xi_1).$$

Associated to these displacement and microrotation vector field variables are the strain measures called the Cosserat strain tensor $\boldsymbol{e}$ and the curvature strain tensor $\boldsymbol{\kappa}$. In vector notation these tensors can be expressed as

$$\boldsymbol{e}^e = \left[e_{11}, e_{22}, e_{33}, e_{12}, e_{21}, e_{13}, e_{31}, e_{23}, e_{32}\right]^T, \tag{4.21}$$

$$\boldsymbol{\kappa}^e = \left[\kappa_{11}, \kappa_{22}, \kappa_{33}, \kappa_{12}, \kappa_{21}, \kappa_{13}, \kappa_{31}, \kappa_{23}, \kappa_{32}\right]^T, \tag{4.22}$$

and are computed using the relations

$$\boldsymbol{e}^e = \mathbf{D_u}\mathbf{N_u}\hat{\mathbf{u}}^e - \mathbf{H}\hat{\boldsymbol{\varphi}}^e \qquad \text{and} \qquad \boldsymbol{\kappa}^e = \mathbf{D}_\varphi\mathbf{N}_\varphi\hat{\boldsymbol{\varphi}}^e, \tag{4.23}$$

where the differential operator matrices $\mathbf{D_u}$, $\mathbf{D}_\varphi$ and the transformation matrix $\mathbf{H}$ are given by

$$\mathbf{D_u} = \mathbf{D}_\varphi = \begin{bmatrix} \frac{\partial}{\partial X_1} & 0 & 0 & 0 & \frac{\partial}{\partial X_2} & 0 & \frac{\partial}{\partial X_3} & 0 & 0 \\ 0 & \frac{\partial}{\partial X_2} & 0 & \frac{\partial}{\partial X_1} & 0 & 0 & 0 & 0 & \frac{\partial}{\partial X_3} \\ 0 & 0 & \frac{\partial}{\partial X_3} & 0 & 0 & \frac{\partial}{\partial X_1} & 0 & \frac{\partial}{\partial X_2} & 0 \end{bmatrix}^T$$

and

$$\mathbf{H} = \begin{bmatrix} 0 & 0 & 0 & 0 & 0 & 0 & \cdots & 0 & 0 & 0 \\ 0 & 0 & 0 & 0 & 0 & 0 & \cdots & 0 & 0 & 0 \\ 0 & 0 & 0 & 0 & 0 & 0 & \cdots & 0 & 0 & 0 \\ 0 & 0 & N^1 & 0 & 0 & N^2 & \cdots & 0 & 0 & N^{NN} \\ 0 & 0 & -N^1 & 0 & 0 & -N^2 & \cdots & 0 & 0 & -N^{NN} \\ 0 & -N^1 & 0 & 0 & -N^2 & 0 & \cdots & 0 & -N^{NN} & 0 \\ 0 & N^1 & 0 & 0 & N^2 & 0 & \cdots & 0 & N^{NN} & 0 \\ N^1 & 0 & 0 & N^2 & 0 & 0 & \cdots & N^{NN} & 0 & 0 \\ -N^1 & 0 & 0 & -N^2 & 0 & 0 & \cdots & -N^{NN} & 0 & 0 \end{bmatrix}.$$

Conjugate to the Cosserat strain tensor $\boldsymbol{e}$ and the curvature strain tensor $\boldsymbol{\kappa}$ are the Cosserat force-stress tensor $\boldsymbol{\sigma}$ and the coupled stress tensor $\boldsymbol{\mu}$ respectively. Expressing them in vector notation one can compute them for each element as

$$\boldsymbol{\sigma}^e = \left[\sigma_{11}, \sigma_{22}, \sigma_{33}, \sigma_{12}, \sigma_{21}, \sigma_{13}, \sigma_{31}, \sigma_{23}, \sigma_{32}\right]^T, \tag{4.24}$$

$$\boldsymbol{\mu}^e = \left[\mu_{11}, \mu_{22}, \mu_{33}, \mu_{12}, \mu_{21}, \mu_{13}, \mu_{31}, \mu_{23}, \mu_{32}\right]^T. \tag{4.25}$$

Hence, using these representations of field vectors and tensor in matrix notation one can rewrite the weak-balance equations (4.13) and (4.14) as

$$\int_{\Omega} \delta\hat{\mathbf{u}}^{e,T}\Big(\mathbf{B}_{\mathbf{u}}^{T}\,\boldsymbol{\sigma}^{e}\Big)\,d\Omega - \int_{\partial\Omega_{\mathrm{u}}} \delta\hat{\mathbf{u}}^{e,T}\Big(\mathbf{N}_{\mathbf{u}}^{T}\,\mathbf{t}_{\mathbf{u}}^{e}\Big)\,d\Gamma_{u} \;=\; 0, \tag{4.26}$$

$$\int_{\Omega} \delta\hat{\varphi}^{e,T}\Big(-\mathbf{H}^{T}\boldsymbol{\sigma}^{e} + \mathbf{B}_{\boldsymbol{\varphi}}^{T}\,\boldsymbol{\mu}^{e}\Big)\,d\Omega - \int_{\partial\Omega_{\varphi}} \delta\hat{\varphi}^{e,T}\Big(\mathbf{N}_{\boldsymbol{\varphi}}^{T}\,\mathbf{t}_{\boldsymbol{\varphi}}^{e}\Big)\,d\Gamma_{\varphi} \;=\; 0. \tag{4.27}$$

By using principle of variational calculus with knowing the fact that $\delta\hat{\mathbf{u}}^{e,T}$ and $\delta\hat{\varphi}^{e,T}$ are arbitrarily chosen vectors one arrives at the following set of residual equations

$$\mathfrak{R}_{\text{lin}}^{e} = \int_{\Omega} \mathbf{B}_{\mathbf{u}}^{T}\,\boldsymbol{\sigma}^{e}\,d\Omega - \int_{\partial\Omega_{\mathrm{u}}} \mathbf{N}_{\mathbf{u}}^{T}\,\mathbf{t}_{\mathbf{u}}^{e}\,d\Gamma_{u} \;=\; 0, \tag{4.28}$$

$$\mathfrak{R}_{\text{ang}}^{e} = \int_{\Omega} \Big(-\mathbf{H}^{T}\boldsymbol{\sigma}^{e} + \mathbf{B}_{\boldsymbol{\varphi}}^{T}\,\boldsymbol{\mu}^{e}\Big)\,d\Omega - \int_{\partial\Omega_{\varphi}} \mathbf{N}_{\boldsymbol{\varphi}}^{T}\,\mathbf{t}_{\boldsymbol{\varphi}}^{e}\,d\Gamma_{\varphi} \;=\; 0. \tag{4.29}$$

Thus the solution variables at the elemental level are obtained by solving these two equations. The procedure is to compute the stiffness matrix for each element *e* by taking the derivatives of these differential equations $\mathfrak{R}_{\text{lin}}$ and $\mathfrak{R}_{\text{ang}}$ with respect to the element nodal vectors $\hat{\mathbf{u}}^{e}$ and $\hat{\boldsymbol{\varphi}}^{e}$ and arranging them in the matrix form as

$$\mathbf{S}^{e} = \begin{bmatrix} \dfrac{\partial\mathfrak{R}_{\text{lin}}^{e}}{\partial\hat{\mathbf{u}}^{e}} & \dfrac{\partial\mathfrak{R}_{\text{lin}}^{e}}{\partial\hat{\boldsymbol{\varphi}}^{e}} \\[2ex] \dfrac{\partial\mathfrak{R}_{\text{ang}}^{e}}{\partial\hat{\mathbf{u}}^{e}} & \dfrac{\partial\mathfrak{R}_{\text{ang}}^{e}}{\partial\hat{\boldsymbol{\varphi}}^{e}} \end{bmatrix} = \begin{bmatrix} K_{\mathbf{uu}}^{e} & K_{\mathbf{u}\boldsymbol{\varphi}}^{e} \\[2ex] K_{\boldsymbol{\varphi}\mathbf{u}}^{e} & K_{\boldsymbol{\varphi}\boldsymbol{\varphi}}^{e} \end{bmatrix} \tag{4.30}$$

where the matrices $K_{\mathbf{uu}}^{e}$, $K_{\mathbf{u}\boldsymbol{\varphi}}^{e}$, $K_{\boldsymbol{\varphi}\mathbf{u}}^{e}$ and $K_{\boldsymbol{\varphi}\boldsymbol{\varphi}}^{e}$ are calculated according to the following relations

$$K_{\mathbf{uu}}^{e} \;=\; \int_{\Omega} \mathbf{B}_{\mathbf{u}}^{T}\mathbf{K}_{\boldsymbol{ee}}\mathbf{B}_{\mathbf{u}}\,d\Omega, \tag{4.31}$$

$$K_{\mathbf{u}\boldsymbol{\varphi}}^{e} \;=\; \int_{\Omega} \Big(-2\mu_{c}\,\mathbf{B}_{\mathbf{u}}^{T}\mathbf{H} + \mathbf{B}_{\mathbf{u}}^{T}\mathbf{K}_{\boldsymbol{e\kappa}}\mathbf{B}_{\boldsymbol{\varphi}}\Big)\,d\Omega, \tag{4.32}$$

$$K_{\boldsymbol{\varphi}\mathbf{u}}^{e} = \int_{\Omega} \Big(-\mathbf{H}^{T}\mathbf{K}_{\boldsymbol{ee}}\mathbf{B}_{\mathbf{u}} + \mathbf{B}_{\boldsymbol{\varphi}}^{T}\mathbf{K}_{\boldsymbol{\kappa e}}\mathbf{B}_{\mathbf{u}}\Big)\,d\Omega, \tag{4.33}$$

$$K_{\boldsymbol{\varphi}\boldsymbol{\varphi}}^{e} = \int_{\Omega} \Big(2\mu_{c}\,\mathbf{H}^{T}\mathbf{H} - \mathbf{H}^{T}\mathbf{K}_{\boldsymbol{e\kappa}}\mathbf{B}_{\boldsymbol{\varphi}} + \mathbf{B}_{\boldsymbol{\varphi}}^{T}\mathbf{K}_{\boldsymbol{\kappa\kappa}}\mathbf{B}_{\boldsymbol{\varphi}}\Big)\,d\Omega. \tag{4.34}$$

The matrices $\mathbf{K}_{\boldsymbol{ee}}$, $\mathbf{K}_{\boldsymbol{e\kappa}}$, $\mathbf{K}_{\boldsymbol{\kappa e}}$ and $\mathbf{K}_{\boldsymbol{\kappa\kappa}}$ are to be computed from the fourth order tensors $\mathbb{K}_{\boldsymbol{ee}}$, $\mathbb{K}_{\boldsymbol{e\kappa}}$, $\mathbb{K}_{\boldsymbol{\kappa e}}$ and $\mathbb{K}_{\boldsymbol{\kappa\kappa}}$ respectivly which are defined according to the formulae

$$\mathbb{K}_{\boldsymbol{ee}} = \frac{\partial^{2} W^{rel}}{\partial\nabla\mathbf{u}\otimes\partial\nabla\mathbf{u}}, \qquad \mathbb{K}_{\boldsymbol{e\kappa}} = \frac{\partial^{2} W^{rel}}{\partial\nabla\boldsymbol{\varphi}\otimes\partial\nabla\mathbf{u}}, \tag{4.35}$$

$$\mathbb{K}_{\boldsymbol{\kappa e}} = \frac{\partial^{2} W^{rel}}{\partial\nabla\mathbf{u}\otimes\partial\nabla\boldsymbol{\varphi}}, \qquad \mathbb{K}_{\boldsymbol{\kappa\kappa}} = \frac{\partial^{2} W^{rel}}{\partial\nabla\boldsymbol{\varphi}\otimes\partial\nabla\boldsymbol{\varphi}}. \tag{4.36}$$

The resulting expressions for these fourth order tensors in each of the material phase are given as

$$\mathbb{K}_{\boldsymbol{ee}} = \begin{cases} {}^1\mathbb{K}_{\boldsymbol{ee}} & \text{if} \quad \|\boldsymbol{\kappa}\|^2 \geq \beta^2 \|\operatorname{dev}\boldsymbol{\varepsilon}\|^2 + \dfrac{\mu}{2\alpha\beta^2} \\ {}^2\mathbb{K}_{\boldsymbol{ee}} & \text{if} \quad \beta^2 \|\operatorname{dev}\boldsymbol{\varepsilon}\|^2 - \dfrac{\mu_\circ}{2\alpha} \leq \|\boldsymbol{\kappa}\|^2 \leq \beta^2 \|\operatorname{dev}\boldsymbol{\varepsilon}\|^2 + \dfrac{\mu}{2\alpha\beta^2} \\ {}^3\mathbb{K}_{\boldsymbol{ee}} & \text{if} \quad \|\boldsymbol{\kappa}\|^2 \leq \beta^2 \|\operatorname{dev}\boldsymbol{\varepsilon}\|^2 - \dfrac{\mu_\circ}{2\alpha} \end{cases} \tag{4.37}$$

where

$${}^1\mathbb{K}_{\boldsymbol{ee}} = 2\left(\frac{\lambda}{2} + \frac{\mu}{d}\right)\mathbf{I}\otimes\mathbf{I} + \mu_c\mathbb{I} - \mu_c\bar{\mathbb{I}} \tag{4.38}$$

$$\begin{aligned} {}^2\mathbb{K}_{\boldsymbol{ee}} = {} & \left\{\lambda + 2\alpha\beta^2\left(\|\boldsymbol{\kappa}\|^2 - \beta^2\|\operatorname{dev}\boldsymbol{\varepsilon}\|^2\right)\right\}\mathbf{I}\otimes\mathbf{I} + \left\{\mu + \mu_c - 2\alpha\beta^2\left(\|\boldsymbol{\kappa}\|^2\right.\right. \\ & \left.\left. - \beta^2\|\operatorname{dev}\boldsymbol{\varepsilon}\|^2\right)\mathbb{I} + \left\{\mu - \mu_c - 2\alpha\beta^2\left(\|\boldsymbol{\kappa}\|^2 - \beta^2\|\operatorname{dev}\boldsymbol{\varepsilon}\|^2\right)\right\}\bar{\mathbb{I}}\right. \\ & + 8\alpha\beta^4\left(\operatorname{dev}\boldsymbol{\varepsilon}\otimes\operatorname{dev}\boldsymbol{\varepsilon}\right) \end{aligned} \tag{4.39}$$

$${}^3\mathbb{K}_{\boldsymbol{ee}} = (\lambda - \mu_\circ\beta^2)\mathbf{I}\otimes\mathbf{I} + (\mu_\circ\beta^2 + \mu + \mu_c)\mathbb{I} + (\mu_\circ\beta^2 + \mu - \mu_c)\bar{\mathbb{I}} \tag{4.40}$$

$$\mathbb{K}_{\boldsymbol{e\kappa}} = \begin{cases} -8\alpha\beta^2\left(\operatorname{dev}\boldsymbol{\varepsilon}\otimes\boldsymbol{\kappa}\right) & \text{if} \quad \beta^2\|\operatorname{dev}\boldsymbol{\varepsilon}\|^2 - \dfrac{\mu_\circ}{2\alpha} \leq \|\boldsymbol{\kappa}\|^2 \leq \beta^2\|\operatorname{dev}\boldsymbol{\varepsilon}\|^2 + \dfrac{\mu}{2\alpha\beta^2} \\ \mathbb{O} & \text{otherwise} \end{cases} \tag{4.41}$$

$$\mathbb{K}_{\boldsymbol{\kappa e}} = \begin{cases} -8\alpha\beta^2\left(\boldsymbol{\kappa}\otimes\operatorname{dev}\boldsymbol{\varepsilon}\right) & \text{if} \quad \beta^2\|\operatorname{dev}\boldsymbol{\varepsilon}\|^2 - \dfrac{\mu_\circ}{2\alpha} \leq \|\boldsymbol{\kappa}\|^2 \leq \beta^2\|\operatorname{dev}\boldsymbol{\varepsilon}\|^2 + \dfrac{\mu}{2\alpha\beta^2} \\ \mathbb{O} & \text{otherwise} \end{cases} \tag{4.42}$$

$$\mathbb{K}_{\boldsymbol{\kappa\kappa}} = \begin{cases} {}^1\mathbb{K}_{\boldsymbol{\kappa\kappa}} & \text{if} \quad \|\boldsymbol{\kappa}\|^2 \geq \beta^2\|\operatorname{dev}\boldsymbol{\varepsilon}\|^2 + \dfrac{\mu}{2\alpha\beta^2} \\ {}^2\mathbb{K}_{\boldsymbol{\kappa\kappa}} & \text{if} \quad \beta^2\|\operatorname{dev}\boldsymbol{\varepsilon}\|^2 - \dfrac{\mu_\circ}{2\alpha} \leq \|\boldsymbol{\kappa}\|^2 \leq \beta^2\|\operatorname{dev}\boldsymbol{\varepsilon}\|^2 + \dfrac{\mu}{2\alpha\beta^2} \\ {}^3\mathbb{K}_{\boldsymbol{\kappa\kappa}} & \text{if} \quad \|\boldsymbol{\kappa}\|^2 \leq \beta^2\|\operatorname{dev}\boldsymbol{\varepsilon}\|^2 - \dfrac{\mu_\circ}{2\alpha} \end{cases} \tag{4.43}$$

$${}^1\mathbb{K}_{\boldsymbol{\kappa\kappa}} = \bar{\lambda}(\mathbf{I}\otimes\mathbf{I}) + \left\{\bar{\mu} - \bar{\mu}_c + 2\left(\mu_o + \frac{\mu}{\beta^2}\right)\right\}\mathbb{I} + (\bar{\mu} - \bar{\mu}_c)\,\bar{\mathbb{I}} \tag{4.44}$$

$${}^2\mathbb{K}_{\boldsymbol{\kappa\kappa}} = \bar{\lambda}\,\mathbf{I}\otimes\mathbf{I} + \left\{\bar{\mu} + \bar{\mu}_c + 4\alpha\left(\|\boldsymbol{\kappa}\|^2 - \beta^2\|\operatorname{dev}\boldsymbol{\varepsilon}\|^2\right)\right\}\mathbb{I} + (\bar{\mu} - \bar{\mu}_c)\,\bar{\mathbb{I}} + 8\alpha\left(\boldsymbol{\kappa}\otimes\boldsymbol{\kappa}\right) \tag{4.45}$$

$${}^3\mathbb{K}_{\boldsymbol{\kappa\kappa}} = \bar{\lambda}(\mathbf{I}\otimes\mathbf{I}) + (\bar{\mu} - \bar{\mu}_c)\,\mathbb{I} + (\bar{\mu} - \bar{\mu}_c)\,\bar{\mathbb{I}} \tag{4.46}$$

where $\mathbb{O}$ is the fourth order zero tensor, $\mathbb{I}$, $\bar{\mathbb{I}}$ are the fourth order unit tensors and $\mathbf{I}$ is the second order identity tensor computed as

$$\mathbf{I} = \delta_{ij}\,\mathbf{e}_i\otimes\mathbf{e}_j, \quad \mathbb{I} = \delta_{ik}\delta_{jl}\,\mathbf{e}_i\otimes\mathbf{e}_j\otimes\mathbf{e}_k\otimes\mathbf{e}_l, \quad \bar{\mathbb{I}} = \delta_{il}\delta_{jk}\,\mathbf{e}_i\otimes\mathbf{e}_j\otimes\mathbf{e}_k\otimes\mathbf{e}_l. \tag{4.47}$$

The system of nonlinear equations to solve for each element is thus stated as

$$\begin{bmatrix} K^e_{\mathbf{uu}} & K^e_{\mathbf{u}\boldsymbol{\varphi}} \\ K^e_{\boldsymbol{\varphi}\mathbf{u}} & K^e_{\boldsymbol{\varphi}\boldsymbol{\varphi}} \end{bmatrix} \begin{bmatrix} \hat{\mathbf{u}}^e \\ \hat{\boldsymbol{\varphi}}^e \end{bmatrix} = \begin{bmatrix} \mathfrak{f}^e_u \\ \mathfrak{f}^e_\varphi \end{bmatrix} \tag{4.48}$$

where $\mathfrak{f}^e_u$ and $\mathfrak{f}^e_\varphi$ are respectively the vectors of external forces and couples acting on the body Ω and are given by

$$\mathfrak{f}^e_u = \int_{\partial\Omega_{\mathrm{u}}} [\mathbf{N}^T_{\mathbf{u}}\, \mathbf{t}^e_u]\, d\Gamma_u, \qquad \mathfrak{f}^e_\varphi = \int_{\partial\Omega_\varphi} [\mathbf{N}^T_{\boldsymbol{\varphi}}\, \mathbf{t}^e_\varphi]\, d\Gamma_\varphi \tag{4.49}$$

The global unknown vector for the displacement and micro-rotational degrees of freedoms are

$$\mathbf{U} = (\mathbf{u}, \boldsymbol{\varphi})^T, \qquad \text{here} \quad \mathbf{u} = \overset{n_e}{\underset{e=1}{\mathcal{A}}}\, \hat{\mathbf{u}}^e \quad \text{and} \quad \boldsymbol{\varphi} = \overset{n_e}{\underset{e=1}{\mathcal{A}}}\, \hat{\boldsymbol{\varphi}}^e \tag{4.50}$$

where $\overset{n_e}{\underset{e=1}{\mathcal{A}}}$ is the finite element assembly operator. The global system of nonlinear equations to solve thus can be written as

$$\begin{bmatrix} K_{\mathbf{uu}} & K_{\mathbf{u}\boldsymbol{\varphi}} \\ K_{\boldsymbol{\varphi}\mathbf{u}} & K_{\boldsymbol{\varphi}\boldsymbol{\varphi}} \end{bmatrix} \begin{bmatrix} \mathbf{u} \\ \boldsymbol{\varphi} \end{bmatrix} = \begin{bmatrix} \mathfrak{f}_u \\ \mathfrak{f}_\varphi \end{bmatrix} \tag{4.51}$$

where the global stiffness matrices

$$K_{\mathbf{uu}} = \overset{n_e}{\underset{e=1}{\mathcal{A}}}\, K^e_{\mathbf{uu}}, \quad K_{\mathbf{u}\boldsymbol{\varphi}} = \overset{n_e}{\underset{e=1}{\mathcal{A}}}\, K^e_{\mathbf{u}\boldsymbol{\varphi}}, \quad K_{\boldsymbol{\varphi}\mathbf{u}} = \overset{n_e}{\underset{e=1}{\mathcal{A}}}\, K^e_{\boldsymbol{\varphi}\mathbf{u}}, \quad K_{\boldsymbol{\varphi}\boldsymbol{\varphi}} = \overset{n_e}{\underset{e=1}{\mathcal{A}}}\, K^e_{\boldsymbol{\varphi}\boldsymbol{\varphi}} \tag{4.52}$$

and the global external force and moment vectors are respectively defined by

$$\mathfrak{f}_u = \overset{n_e}{\underset{e=1}{\mathcal{A}}}\, \mathfrak{f}^e_u, \qquad \text{and} \quad \mathfrak{f}_\varphi = \overset{n_e}{\underset{e=1}{\mathcal{A}}}\, \mathfrak{f}^e_\varphi. \tag{4.53}$$

4.2.1. Iterative solution procedure

The set of equations in (4.51) for which the stress tensors $\boldsymbol{\sigma}$ and $\boldsymbol{\mu}$ are computed from the strain energy function W^{rel} (given as in Chapter 3, Section 3.4.3) are highly nonlinear. For the solution of these nonlinear algebraic equations an iterative scheme is necessary to adopt. Therefore, for this purpose we choose Newton-Raphson iteration scheme (see [ZT00]) as an iterative solver of the set of these nonlinear algebraic equations (also called residual equations). Rewriting them in the form

$$\boldsymbol{\pi}_{lin}(\mathbf{u}, \boldsymbol{\varphi}) = \mathbf{0}, \tag{4.54}$$

$$\boldsymbol{\pi}_{ang}(\mathbf{u}, \boldsymbol{\varphi}) = \mathbf{0}. \tag{4.55}$$

The method adopts an incremental-iterative procedure in the calculation of the solution for which a quasi-time dependent loading is used. The loading is divided into a total number of time steps $(tnts)$. For each quasi-time increment

$$t_{n+1} = t_n + \Delta t_{n+1}, \quad n \in \{0, 1, 2, 3, ..., tnts\} \tag{4.56}$$

the set of residual equations (4.55) and (4.55) are solved with an iterative procedure assuming initially at the i^{th} iterate a zero known solution $\{\mathbf{u}^i, \boldsymbol{\varphi}^i\}$ (and in the case of already one iteration has been processed a converged solution from the previous $(i-1)^{th}$ iteration) by solving a linearized system of equations at the quasi-time step t_{n+1}

$$\begin{aligned}
\mathbf{0} &= \boldsymbol{\pi}^{i+1}_{lin,n+1}\left(\mathbf{u}^{i+1}, \boldsymbol{\varphi}^{i+1}\right) \\
&= \boldsymbol{\pi}^{i}_{lin,n+1}\left(\mathbf{u}^{i}_{n+1}, \boldsymbol{\varphi}^{i}_{n+1}\right) + \frac{\partial \boldsymbol{\pi}^{i}_{lin}}{\partial \mathbf{u}^{i+1}_{n+1}}_{\{\mathbf{u}^i_{n+1}, \boldsymbol{\varphi}^i_{n+1}\}} \Delta\mathbf{u}^i_n + \left.\frac{\partial \boldsymbol{\pi}^{i}_{lin}}{\partial \boldsymbol{\varphi}^{i+1}_{n+1}}\right|_{\{\mathbf{u}^i_{n+1}, \boldsymbol{\varphi}^i_{n+1}\}} \Delta\boldsymbol{\varphi}^i_n \\
&+ \frac{1}{2}\left\{ \left.\frac{\partial^2 \boldsymbol{\pi}^{i}_{lin}}{\partial \mathbf{u}^{i+1\,2}_{n+1}}\right|_{\{\mathbf{u}^i_{n+1}, \boldsymbol{\varphi}^i_{n+1}\}} (\Delta\mathbf{u}^i_n)^2 + \left.\frac{\partial^2 \boldsymbol{\pi}^{i}_{lin}}{\partial \boldsymbol{\varphi}^{i+1\,2}_{n+1}}\right|_{\{\mathbf{u}^i_{n+1}, \boldsymbol{\varphi}^i_{n+1}\}} (\Delta\boldsymbol{\varphi}^i_n)^2 \right\} \\
&+ \text{... (higher order terms)}
\end{aligned} \tag{4.57}$$

and

$$\begin{aligned}
\mathbf{0} &= \boldsymbol{\pi}^{i+1}_{ang,n+1}\left(\mathbf{u}^{i+1}, \boldsymbol{\varphi}^{i+1}\right) \\
&= \boldsymbol{\pi}^{i}_{ang,n+1}\left(\mathbf{u}^{i}_{n+1}, \boldsymbol{\varphi}^{i}_{n+1}\right) + \frac{\partial \boldsymbol{\pi}^{i}_{ang}}{\partial \mathbf{u}^{i+1}_{n+1}}_{\{\mathbf{u}^i_{n+1}, \boldsymbol{\varphi}^i_{n+1}\}} \Delta\mathbf{u}^i_n + \left.\frac{\partial \boldsymbol{\pi}^{i}_{ang}}{\partial \boldsymbol{\varphi}^{i+1}_{n+1}}\right|_{\{\mathbf{u}^i_{n+1}, \boldsymbol{\varphi}^i_{n+1}\}} \Delta\boldsymbol{\varphi}^i_n \\
&+ \frac{1}{2}\left\{ \left.\frac{\partial^2 \boldsymbol{\pi}^{i}_{ang}}{\partial \mathbf{u}^{i+1\,2}_{n+1}}\right|_{\{\mathbf{u}^i_{n+1}, \boldsymbol{\varphi}^i_{n+1}\}} (\Delta\mathbf{u}^i_n)^2 + \left.\frac{\partial^2 \boldsymbol{\pi}^{i}_{ang}}{\partial \boldsymbol{\varphi}^{i+1\,2}_{n+1}}\right|_{\{\mathbf{u}^i_{n+1}, \boldsymbol{\varphi}^i_{n+1}\}} (\Delta\boldsymbol{\varphi}^i_n)^2 \right\} \\
&+ \text{... (higher order terms)}
\end{aligned} \tag{4.58}$$

where $\Delta\mathbf{u}^i_n = \mathbf{u}^{i+1}_{n+1} - \mathbf{u}^i_{n+1}$ and $\Delta\boldsymbol{\varphi}^i_n = \boldsymbol{\varphi}^{i+1}_{n+1} - \boldsymbol{\varphi}^i_{n+1}$ are very small therefore higher order terms in the above approximations can be neglected. Now, the solution state variables $\left\{\mathbf{u}^{i+1}_{n+1}, \boldsymbol{\varphi}^{i+1}_{n+1}\right\}$ at the $(i+1)^{th}$ iteration is approximated by

$$\begin{cases}
\boldsymbol{\pi}^{i+1}_{lin\ n+1}\left(\mathbf{u}^{i+1}_{n+1}, \boldsymbol{\varphi}^{i+1}_{n+1}\right) = \mathbf{0} \\
\boldsymbol{\pi}^{i+1}_{ang\,n+1}\left(\mathbf{u}^{i+1}_{n+1}, \boldsymbol{\varphi}^{i+1}_{n+1}\right) = \mathbf{0}
\end{cases} \tag{4.59}$$

which implies

$$\begin{cases}
\left(\dfrac{\partial \boldsymbol{\pi}_{lin}}{\partial \mathbf{u}}\right)^i_{n+1} \Delta\mathbf{u}^i_n + \left(\dfrac{\partial \boldsymbol{\pi}_{lin}}{\partial \boldsymbol{\varphi}}\right)^i_{n+1} \Delta\boldsymbol{\varphi}^i_n = -\boldsymbol{\pi}^i_{lin,n+1}\left(\mathbf{u}^i_{n+1}, \boldsymbol{\varphi}^i_{n+1}\right) \\
\left(\dfrac{\partial \boldsymbol{\pi}_{ang}}{\partial \mathbf{u}}\right)^i_{n+1} \Delta\mathbf{u}^i_n + \left(\dfrac{\partial \boldsymbol{\pi}_{ang}}{\partial \boldsymbol{\varphi}}\right)^i_{n+1} \Delta\boldsymbol{\varphi}^i_n = -\boldsymbol{\pi}^i_{ang,n+1}\left(\mathbf{u}^i_{n+1}, \boldsymbol{\varphi}^i_{n+1}\right)
\end{cases} \tag{4.60}$$

In matrix notation we can write

$$\begin{bmatrix}
\dfrac{\partial \boldsymbol{\pi}_{lin}}{\partial \mathbf{u}} & \dfrac{\partial \boldsymbol{\pi}_{lin}}{\partial \boldsymbol{\varphi}} \\
\dfrac{\partial \boldsymbol{\pi}_{ang}}{\partial \mathbf{u}} & \dfrac{\partial \boldsymbol{\pi}_{ang}}{\partial \boldsymbol{\varphi}}
\end{bmatrix}^i_{n+1}
\begin{bmatrix} \Delta\mathbf{u}^i_n \\ \Delta\boldsymbol{\varphi}^i_n \end{bmatrix} = -\begin{bmatrix} \boldsymbol{\pi}^i_{lin}\left(\mathbf{u}^i, \boldsymbol{\varphi}^i\right) \\ \boldsymbol{\pi}^i_{ang}\left(\mathbf{u}^i, \boldsymbol{\varphi}^i\right) \end{bmatrix} \tag{4.61}$$

or in compact equation form as

$$J_{n+1}\left(\mathbf{U}^i\right) \Delta\mathbf{U}^i_n = -\mathbf{R}^i_{n+1}\left(\mathbf{U}^i\right) \tag{4.62}$$

Hence the solution at the $(i+1)^{th}$ state is obtained by the iterative formulae

$$\mathbf{U}_{n+1}^{i+1} \;=\; \mathbf{U}_{n+1}^{i} - \left(J_{n+1}^{i}\right)^{-1} \left(\mathbf{U}_{n+1}^{i}\right) \mathbf{R}_{n+1}^{i} \left(\mathbf{U}_{n+1}^{i}\right). \tag{4.63}$$

This iterative procedure is known as Newton-Raphson iteration method used for solving nonlinear set of equations. In context of finite element method the above procedure is summarized as

$$\hat{\mathbf{U}}_{n+1}^{i+1} \;=\; \hat{\mathbf{U}}_{n+1}^{i} - J_{n+1}^{-1} \left(\hat{\mathbf{U}}_{n+1}^{i}\right)\Big|_{\hat{\mathbf{U}}_{n+1}^{i}} \mathbf{R}^{i} \left(\mathbf{U}_{n+1}^{\hat{i}}\right). \tag{4.64}$$

where $\hat{\mathbf{U}} = (\hat{\mathbf{u}}, \hat{\boldsymbol{\varphi}})$ are the elemental nodal variables which with the use of appropriate interpolation transformations are transformed back to the elemental variables $\mathbf{u}$ and $\boldsymbol{\varphi}$. Since the solution is an approximation therefore some stopping criterion is necessary to state for the desired accuracy in the solution. After each $(i+1)^{th}$ iteration the algorithm stops if the norm of the residual at the current solution $\hat{\mathbf{U}}_{n+1}^{i+1}$ is less than some assumed tolerance ϵ, i.e.,

$$\left|\boldsymbol{\pi}_{lin}\left(\hat{\mathbf{U}}_{n+1}^{i+1}\right)\right| < \epsilon \qquad \text{and} \qquad \left|\boldsymbol{\pi}_{ang}\left(\hat{\mathbf{U}}_{n+1}^{i+1}\right)\right| < \epsilon. \tag{4.65}$$

4.2.2. Simplification of the model to two dimension

The model presented in the previous section is reduced to two dimension with the application of plain strain conditions. In this case there are three degrees of freedom at each node in an element, two of them are displacement component u_1 and u_2 and third is the micro rotation φ_3, i.e,

$$\mathbf{u}^{e} \;=\; (u_1, u_2, 0)^{T,e}, \qquad \varphi_3^{e} \;=\; (0, 0, \varphi_3)^{T,e} \tag{4.66}$$

whereas nodal variables takes the form

$$\hat{\mathbf{u}}^{e} \;=\; \left[u_{_1}^{1}, u_{_2}^{1}, u_{_1}^{2}, u_{_2}^{2}, u_{_1}^{3}, u_{_2}^{3}, ..., u_{_1}^{NN}, u_{_2}^{NN}\right]^{T}, \qquad \hat{\varphi}_3^{e} \;=\; \left[\varphi_{_3}^{1}, \varphi_{_3}^{2}, \varphi_{_3}^{3}, ..., \varphi_{_3}^{NN}\right]^{T} \tag{4.67}$$

elemental variables are calculated according to

$$\varphi_3^{e} \;=\; \mathbf{N}_{\varphi}\, \hat{\varphi}_{_3}{}^{e}, \qquad \mathbf{u}^{e} \;=\; \mathbf{N}_{\mathbf{u}}\, \hat{\mathbf{u}}^{e}, \qquad \boldsymbol{\varepsilon}^{e} \;=\; \mathbf{D}_{\varepsilon}\mathbf{N}_{\mathbf{u}}\, \hat{\mathbf{u}}^{e}, \qquad \boldsymbol{\kappa}^{e} \;=\; \mathbf{D}_{\varphi}\mathbf{N}_{\varphi}\, \hat{\varphi}_{_3}{}^{e}. \tag{4.68}$$

$$\mathbf{N}_{\varphi} \;=\; \left[N^{1}, N^{2}, ..., N^{NN}\right], \quad \mathbf{N}_{\mathbf{u}} \;=\; \begin{bmatrix} N^{1} & 0 & N^{2} & ... & N^{NN} & 0 \\ 0 & N^{1} & 0 & ... & 0 & N^{NN} \end{bmatrix} \tag{4.69}$$

and

$$\mathbf{D}_{\varepsilon} \;=\; \begin{bmatrix} \frac{\partial}{\partial X_1} & 0 \\ 0 & \frac{\partial}{\partial X_2} \\ \frac{1}{2}\frac{\partial}{\partial X_2} & \frac{1}{2}\frac{\partial}{\partial X_1} \\ \frac{1}{2}\frac{\partial}{\partial X_2} & \frac{1}{2}\frac{\partial}{\partial X_1} \end{bmatrix}, \quad \mathbf{D}_{\mathbf{u}} \;=\; \begin{bmatrix} \frac{\partial}{\partial X_1} & 0 \\ 0 & \frac{\partial}{\partial X_2} \\ 0 & \frac{\partial}{\partial X_1} \\ \frac{\partial}{\partial X_2} & 0 \end{bmatrix}, \quad \mathbf{D}_{\varphi} \;=\; \begin{bmatrix} \frac{\partial}{\partial X_1} \\ \frac{\partial}{\partial X_2} \end{bmatrix} \tag{4.70}$$

The reduced form of elemental strains and stress in vector notations are

$$\boldsymbol{e}^{e} = \left[e_{11}, e_{22}, e_{12}, e_{21}\right]^{T}, \qquad \boldsymbol{\kappa}^{e} = \left[\kappa_{13}, \kappa_{23}\right]^{T}, \tag{4.71}$$

$$\boldsymbol{\sigma}^e = [\sigma_{11}, \sigma_{22}, \sigma_{12}, \sigma_{21}]^T, \qquad \text{and} \qquad \boldsymbol{\mu}^e = [\mu_{13}, \mu_{23}]^T. \tag{4.72}$$

The element residual equations are taken as in (4.28) and (4.29) where

$$\mathbf{H} = \begin{bmatrix} \mathbf{0} & \mathbf{0} & \mathbf{N}_\varphi & -\mathbf{N}_\varphi \end{bmatrix}^T, \quad \mathbf{B_u} = \mathbf{D_u N_u}, \quad \mathbf{B}_\varphi = \mathbf{D}_\varphi \mathbf{N}_\varphi. \tag{4.73}$$

The element stiffness matrix is obtained by taking the partial derivatives of $\mathfrak{R}_{\text{lin}}$ and $\mathfrak{R}_{\text{ang}}$ with respect to the element nodal vectors $\hat{\mathbf{u}}$ and $\hat{\varphi}_3$ and by arranging them in the matrix form as in (4.30). The stiffness matrix calculations are explicitly given as follows

Matrices for the stiffness calculations in **phase1** are

$$\mathbb{K}_{\boldsymbol{ee}} = \begin{bmatrix} \lambda+\mu & \lambda+\mu & 0 & 0 \\ \lambda+\mu & \lambda+\mu & 0 & 0 \\ 0 & 0 & \mu_c & -\mu_c \\ 0 & 0 & -\mu_c & \mu_c \end{bmatrix} \tag{4.74}$$

$$\mathbb{K}_{\boldsymbol{\kappa\kappa}} = \begin{cases} \begin{bmatrix} \bar{\mu} - \bar{\mu}_c + 2(\mu_\circ + \frac{\mu}{\beta^2}) & 0 \\ 0 & \bar{\mu} - \bar{\mu}_c + 2(\mu_\circ + \frac{\mu}{\beta^2}) \end{bmatrix}, & \text{if } \bar{\mu} > \bar{\mu}_c \\ \begin{bmatrix} \bar{\mu}_c - \bar{\mu} + 2(\mu_\circ + \frac{\mu}{\beta^2}) & 0 \\ 0 & \bar{\mu}_c - \bar{\mu} + 2(\mu_\circ + \frac{\mu}{\beta^2}) \end{bmatrix}, & \text{if } \bar{\mu} \leq \bar{\mu}_c \end{cases} \tag{4.75}$$

Matrices in the stiffness calculations for **phase2** are

$$\mathbb{K}_{\boldsymbol{ee}} = \begin{bmatrix} \begin{cases} \lambda + 2\mu - 2\alpha\beta^2 m \\ +2\alpha\beta^4 (\varepsilon_{11} - \varepsilon_{22})^2 \end{cases} & \begin{cases} \lambda + 2\alpha\beta^2 m \\ -2\alpha\beta^4 (\varepsilon_{11} - \varepsilon_{22})^2 \end{cases} & \begin{cases} 4\alpha\beta^4 \varepsilon_{11}\varepsilon_{12} \\ -4\alpha\beta^4 \varepsilon_{22}\varepsilon_{12} \end{cases} & \begin{cases} 4\alpha\beta^4 \varepsilon_{11}\varepsilon_{21} \\ -4\alpha\beta^4 \varepsilon_{22}\varepsilon_{21} \end{cases} \\ \begin{cases} \lambda + 2\alpha\beta^2 m \\ -2\alpha\beta^4 (\varepsilon_{22} - \varepsilon_{11})^2 \end{cases} & \begin{cases} \lambda + 2\mu - 2\alpha\beta^2 m \\ +2\alpha\beta^4 (\varepsilon_{22} - \varepsilon_{11})^2 \end{cases} & \begin{cases} 4\alpha\beta^4 \varepsilon_{22}\varepsilon_{12} \\ -4\alpha\beta^4 \varepsilon_{11}\varepsilon_{12} \end{cases} & \begin{cases} 4\alpha\beta^4 \varepsilon_{22}\varepsilon_{21} \\ -4\alpha\beta^4 \varepsilon_{11}\varepsilon_{21} \end{cases} \\ \begin{cases} 4\alpha\beta^4 \varepsilon_{11}\varepsilon_{12} \\ -4\alpha\beta^4 \varepsilon_{22}\varepsilon_{12} \end{cases} & \begin{cases} 4\alpha\beta^4 \varepsilon_{22}\varepsilon_{12} \\ -4\alpha\beta^4 \varepsilon_{11}\varepsilon_{12} \end{cases} & \begin{cases} \mu + \mu_c - 2\alpha\beta^2 m \\ +8\alpha\beta^4 \varepsilon_{12}^2 \end{cases} & \begin{cases} \mu - \mu_c - 2\alpha\beta^2 m \\ +8\alpha\beta^4 \varepsilon_{12}\varepsilon_{21} \end{cases} \\ \begin{cases} 4\alpha\beta^4 \varepsilon_{11}\varepsilon 21 \\ -4\alpha\beta^4 \varepsilon_{22}\varepsilon_{21} \end{cases} & \begin{cases} 4\alpha\beta^4 \varepsilon_{22}\varepsilon 21 \\ -\varepsilon_{11}\varepsilon_{21} \end{cases} & \begin{cases} \mu - \mu_c - 2\alpha\beta^2 m \\ +8\alpha\beta^4 \varepsilon_{12}\varepsilon_{21} \end{cases} & \begin{cases} \mu + \mu_c - 2\alpha\beta^2 m \\ +8\alpha\beta^4 \varepsilon_{21}^2 \end{cases} \end{bmatrix} \tag{4.76}$$

$$\mathbb{K}_{\boldsymbol{\kappa\kappa}} = \begin{bmatrix} \bar{\mu} + \bar{\mu}_c + 4\alpha m + 8\alpha\kappa_{13}^2 & 8\alpha\kappa_{13}\kappa_{23} \\ 8\alpha\kappa_{23}\kappa_{13} & \bar{\mu} + \bar{\mu}_c + 4\alpha m + 8\alpha\kappa_{23}^2 \end{bmatrix} \tag{4.77}$$

where $m = \left(\|\boldsymbol{\kappa}\|^2 - \beta^2 \|\text{dev}\,\boldsymbol{\varepsilon}\|^2\right)$. Matrices in the stiffness calcualations of **phase3** are

$$\mathbb{K}_{\boldsymbol{ee}} = \begin{bmatrix} \lambda + 2\mu + \mu_\circ\beta^2 & \lambda - \mu_\circ\beta^2 & 0 & 0 \\ \lambda - \mu_\circ\beta^2 & \lambda + 2\mu + \mu_\circ\beta^2 & 0 & 0 \\ 0 & 0 & \mu + \mu_c + \mu_\circ\beta^2 & \mu - \mu_c + \mu_\circ\beta^2 \\ 0 & 0 & \mu - \mu_c + \mu_\circ\beta^2 & \mu + \mu_c + \mu_\circ\beta^2 \end{bmatrix} \tag{4.78}$$

$$\mathbb{K}_{\boldsymbol{\kappa}\boldsymbol{\kappa}} = \begin{cases} \begin{bmatrix} \bar{\mu} - \bar{\mu}_c & 0 \\ 0 & \bar{\mu} - \bar{\mu}_c \end{bmatrix}, & \text{if } \bar{\mu} > \bar{\mu}_c \\ \begin{bmatrix} \bar{\mu}_c - \bar{\mu} & 0 \\ 0 & \bar{\mu}_c - \bar{\mu} \end{bmatrix}, & \text{if } \bar{\mu} \leq \bar{\mu}_c \end{cases} \tag{4.79}$$

4.3. Numerical implementation of the rate-dependent inelastic Cosserat material model

Consider the two-field minimization problem, find $\{\dot{\mathbf{u}}, \dot{\boldsymbol{\varphi}}\}$ such that

$$\{\dot{\mathbf{u}}, \dot{\boldsymbol{\varphi}}\} = \arg\left\{ \min_{\dot{\mathbf{u}}, \dot{\boldsymbol{\varphi}}} \left\{ \int_\Omega \Delta\left(\dot{\mathbf{e}}_{\text{in}}, \dot{\boldsymbol{\kappa}}_{\text{in}}\right) - \dot{\ell}_{\text{ext}}\left(\dot{\mathbf{u}}, \dot{\boldsymbol{\varphi}}\right) \right\} \right\}, \tag{4.80}$$

where $\dot{\mathbf{u}}$ is the velocity vector field, $\dot{\boldsymbol{\varphi}}$ is the gyration vector field, $\dot{\mathbf{e}}_{\text{in}}$ and $\dot{\boldsymbol{\kappa}}_{\text{in}}$ are the time derivatives of the Cosserat strain tensors $\mathbf{e}$ and curvature strain tensor $\boldsymbol{\kappa}$ respectively.

The stationarity conditions to the above minimization problem are

$$\int_\Omega \frac{\partial \Delta}{\partial \dot{\mathbf{u}}}\, dV - \frac{\partial \dot{\ell}_{\text{ext}}}{\partial \dot{\mathbf{u}}} \ni \mathbf{0}, \quad \int_\Omega \frac{\partial \Delta}{\partial \dot{\boldsymbol{\varphi}}}\, dV - \frac{\partial \dot{\ell}_{\text{ext}}}{\partial \dot{\boldsymbol{\varphi}}} \ni \mathbf{0}. \tag{4.81}$$

With the dissipation potential Δ as formulated in previous chapter. Using this dissipation potential the evolution equations for the inelastic strains thus becomes

$$\int_\Omega \left(\mathbf{g}^{\text{n}+1} : \frac{\partial \nabla \dot{\mathbf{u}}}{\partial \dot{\mathbf{u}}} \right) dV - \frac{\partial \dot{\ell}_{\text{ext}}}{\partial \dot{\mathbf{u}}} \ni \mathbf{0}, \tag{4.82}$$

and

$$\int_\Omega \left(-2\mu_c \dot{\boldsymbol{\omega}} : \frac{\partial \left(\text{asy}\, \dot{\boldsymbol{\varphi}}\right)}{\partial \dot{\boldsymbol{\varphi}}} + \mathbf{q}^{\text{n}+1} : \frac{\partial \nabla \dot{\boldsymbol{\varphi}}}{\partial \dot{\boldsymbol{\varphi}}} \right) dV - \frac{\partial \dot{\ell}_{\text{ext}}}{\partial \dot{\boldsymbol{\varphi}}} \ni \mathbf{0}, \tag{4.83}$$

where $\dot{\mathbf{g}}$ and $\mathbf{q}$ are descretized according to the Backward Euler implicit scheme as $\mathbf{g}^{\text{n}+1} = \mathbf{g}^{\text{n}} + \Delta t \dot{\mathbf{g}}$ and $\mathbf{q}^{\text{n}+1} = \mathbf{q}^{\text{n}} + \Delta t \dot{\mathbf{q}}$. In the context of finite elements $\dot{\mathbf{u}}$ and $\dot{\boldsymbol{\varphi}}$ are approximated on the nodes of an element by their corresponding nodal shape functions N_{u} and N_φ respectively as

$$\dot{\mathbf{u}} = N_{\text{u}}\, \hat{\dot{\mathbf{u}}}, \quad \dot{\boldsymbol{\varphi}} = \mathbf{N}_\varphi\, \hat{\dot{\boldsymbol{\varphi}}}. \tag{4.84}$$

The potential of external forces is given by

$$\dot{\ell}_{\text{ext}} = \int_\Omega \left(\mathbf{b} \cdot \dot{\mathbf{u}} + \mathbf{m} \cdot \dot{\boldsymbol{\varphi}} \right) dV + \int_{\partial\Omega_{\text{u}}} \mathbf{t}_{\text{u}} \cdot \dot{\mathbf{u}}\, dS + \int_{\partial\Omega_\varphi} \mathbf{t}_\varphi \cdot \dot{\boldsymbol{\varphi}}\, dS, \tag{4.85}$$

where the term $\int_\Omega \left(\dot{\mathbf{b}} \cdot \mathbf{u} + \dot{\mathbf{m}} \cdot \boldsymbol{\varphi} \right) dV + \int_{\partial\Omega_{\text{u}}} \dot{\mathbf{t}}_{\text{u}} \cdot \mathbf{u}\, dS + \int_{\partial\Omega_\varphi} \dot{\mathbf{t}}_\varphi \cdot \boldsymbol{\varphi}\, dS$ is neglected since it do not enter the minimization problem (4.80). Using the interpolation functions for the field

variables at the element level we can write the equations (4.82) and (4.83) in the following form

$$\mathfrak{R}^e_{\text{lin}} = \int_\Omega \mathbf{B}_{\text{u}}^T\, \mathfrak{g}^{e,\text{n+1}}\, dV - \int_{\partial\Omega_{\text{u}}} \mathbf{N}_{\text{u}}^T\, \mathbf{t}_{\text{u}}^{e,\text{n+1}}\, dS_u \;=\; 0, \tag{4.86}$$

$$\mathfrak{R}^e_{\text{ang}} = \int_\Omega \Big(-2\,\mu_{\text{c}}\, \mathbf{H}^T \dot{\boldsymbol{\omega}}^{e,\text{n+1}} + \mathbf{B}_\varphi^T\, \mathbf{q}^{e,\text{n+1}} \Big)\, dV - \int_{\partial\Omega_\varphi} \mathbf{N}_\varphi^T\, \mathbf{t}_\varphi^{e,\text{n+1}}\, dS_\varphi \;=\; 0. \tag{4.87}$$

where S_{u} is the boundary with prescribed displacements, S_φ is the boundary with prescribed microrotations, $\mathbf{B_u}$, $\mathbf{H}$ and $\mathbf{B}_\varphi$ are computed according to the equation 4.73. To solve the residual equations (4.86) and (4.87) it is equivalent to solve the system of equations

$$\begin{bmatrix} \dfrac{\partial \mathfrak{R}^e_{lin}}{\partial \mathbf{u}^{e,i+1}_{\text{n+1}}} & \dfrac{\partial \mathfrak{R}^e_{lin}}{\partial \boldsymbol{\varphi}^{e,i+1}_{\text{n+1}}} \\[2ex] \dfrac{\partial \mathfrak{R}^e_{ang}}{\partial \mathbf{u}^{e,i+1}_{\text{n+1}}} & \dfrac{\partial \mathfrak{R}^e_{ang}}{\partial \boldsymbol{\varphi}^{e,i+1}_{\text{n+1}}} \end{bmatrix} \begin{bmatrix} \Delta \mathbf{u}^{e,i+1}_{\text{n+1}} \\[2ex] \Delta \boldsymbol{\varphi}^{e,i+1}_{\text{n+1}} \end{bmatrix} = - \begin{bmatrix} \mathfrak{R}^e_{lin}\left(\mathbf{u}^{e,i}_{\text{n+1}}, \boldsymbol{\varphi}^{e,i}_{\text{n+1}}\right) \\[2ex] \mathfrak{R}^e_{ang}\left(\mathbf{u}^{e,i}_{\text{n+1}}, \boldsymbol{\varphi}^{e,i}_{\text{n+1}}\right) \end{bmatrix} \tag{4.88}$$

where $\Delta \mathbf{u}^{e,i+1}_{\text{n+1}} = \mathbf{u}^{e,i+1}_{\text{n+1}} - \mathbf{u}^{e,i}_{\text{n+1}}$, $\quad \Delta \boldsymbol{\varphi}^{e,i+1}_{\text{n+1}} = \boldsymbol{\varphi}^{e,i+1}_{\text{n+1}} - \boldsymbol{\varphi}^{e,i}_{\text{n+1}}$ and the terms in the tangent matrix are given as

$$\frac{\partial \mathfrak{R}^e_{lin}}{\partial \mathbf{u}^{e,i+1}_{\text{n+1}}} = \int_\Omega \mathbf{B}_{\mathbf{u}}^T\, \frac{\partial \mathfrak{g}^e_{\text{n+1}}}{\partial \mathbf{u}^e_{\text{n+1}}}\, dV, \tag{4.89}$$

$$\frac{\partial \mathfrak{R}^e_{lin}}{\partial \boldsymbol{\varphi}^{e,i+1}_{\text{n+1}}} = \int_\Omega \mathbf{B}_{\mathbf{u}}^T\, \frac{\partial \mathfrak{g}^e_{\text{n+1}}}{\partial \boldsymbol{\varphi}^e_{\text{n+1}}}\, dV, \tag{4.90}$$

$$\frac{\partial \mathfrak{R}^e_{ang}}{\partial \mathbf{u}^{e,i+1}_{\text{n+1}}} = \int_\Omega \left(-\frac{2\mu_c}{\Delta t}\, \mathbf{H}^T\, \frac{\partial \boldsymbol{\omega}^e_{\text{n+1}}}{\partial \mathbf{u}^e_{\text{n+1}}} + \mathbf{B}_\varphi^T\, \frac{\partial \mathbf{q}^e_{\text{n+1}}}{\partial \mathbf{u}^e_{\text{n+1}}} \right) dV, \tag{4.91}$$

$$\frac{\partial \mathfrak{R}^e_{ang}}{\partial \boldsymbol{\varphi}^{e,i+1}_{\text{n+1}}} = \int_\Omega \left(-\frac{2\mu_c}{\Delta t}\mathbf{H}^T\, \frac{\partial \boldsymbol{\omega}^e_{\text{n+1}}}{\partial \boldsymbol{\varphi}^e_{\text{n+1}}} + \mathbf{B}_\varphi^T\, \frac{\partial \mathbf{q}^e_{\text{n+1}}}{\partial \boldsymbol{\varphi}^e_{\text{n+1}}} \right) dV. \tag{4.92}$$

The differential terms in the equations (4.89), (4.90), (4.91) and (4.92) are calculated according to the following relations in each of the material regimes

In the material regime with microstructure in micromotions:

$$\frac{\partial \mathfrak{g}^e_{\text{n+1}}}{\partial \mathbf{u}^e_{\text{n+1}}} \;=\; \frac{1}{\Delta t} \left\{ 2 \left(\frac{\lambda}{2} + \frac{\mu}{d} \right) \mathbf{I} \otimes \mathbf{I} + \mu_c \left(\mathbb{I} - \bar{\mathbb{I}} \right) \right\} \mathbf{B_u}, \tag{4.93}$$

where d is the dimension of the problem,

$$\frac{\partial \mathfrak{g}^e_{\text{n+1}}}{\partial \boldsymbol{\varphi}^e_{\text{n+1}}} \;=\; -\frac{2}{\Delta t}\, (\mu_c\, \mathbb{I})\, \mathbf{H}, \quad \frac{\partial \boldsymbol{\omega}^e_{\text{n+1}}}{\partial \boldsymbol{\varphi}^e_{\text{n+1}}} \;=\; -\mathbf{H}, \tag{4.94}$$

$$\frac{\partial \boldsymbol{\omega}^e_{\text{n+1}}}{\partial \mathbf{u}^e_{\text{n+1}}} \;=\; \frac{1}{2}\, \left(\mathbb{I} - \bar{\mathbb{I}} \right)\, \mathbf{B_u}, \quad \frac{\partial \mathbf{q}^e_{\text{n+1}}}{\partial \mathbf{u}^e_{\text{n+1}}} \;=\; \mathbb{O}, \tag{4.95}$$

$$\frac{\partial \mathbf{q}^e_{\text{n+1}}}{\partial \boldsymbol{\varphi}^e_{\text{n+1}}} = \frac{1}{\Delta t} \left\{ \bar{\lambda} (\mathbf{I} \otimes \mathbf{I}) + \left\{ \bar{\mu} - \bar{\mu}_c + 2 \left(\mu_o + \frac{\mu}{\beta^2} \right) \right\} \mathbb{I} - (\bar{\mu} - \bar{\mu}_c)\, \bar{\mathbb{I}} \right\} \mathbf{B}_\varphi, \quad \text{if} \quad \bar{\mu} > \bar{\mu}_c. \tag{4.96}$$

$$\frac{\partial \mathbf{q}^e_{\text{n+1}}}{\partial \boldsymbol{\varphi}^e_{\text{n+1}}} = \frac{1}{\Delta t} \left\{ \bar{\lambda} (\mathbf{I} \otimes \mathbf{I}) + \left\{ \bar{\mu}_c - \bar{\mu} + 2 \left(\mu_o + \frac{\mu}{\beta^2} \right) \right\} \mathbb{I} + (\bar{\mu} - \bar{\mu}_c)\, \bar{\mathbb{I}} \right\} \mathbf{B}_\varphi, \quad \text{if} \quad \bar{\mu} < \bar{\mu}_c.$$

(4.97)

In the material regime with no internal structure:

$$\frac{\partial \mathbf{g}^{e}_{n+1}}{\partial \mathbf{u}^{e}_{n+1}} = \frac{1}{\Delta t}\left\{ \begin{array}{l} \left(\lambda + 2\alpha\beta^{2} m\right)\, \mathbf{I}\otimes\mathbf{I} + \left(\mu + \mu_c - 2\alpha\beta^{2} m\right)\, \mathbb{I} \\ \\ + \left(\mu - \mu_c - 2\alpha\beta^{2} m\right)\, \bar{\mathbb{I}} + 8\alpha\beta^{4}\, \left(\operatorname{dev}\dot{\boldsymbol{\varepsilon}} \otimes \operatorname{dev}\dot{\boldsymbol{\varepsilon}}\right) \end{array} \right\} \mathbf{B}_{\mathbf{u}}, \tag{4.98}$$

where $m = \|\dot{\boldsymbol{\kappa}}\|^{2} - \beta^{2}\, \|\operatorname{dev}\dot{\boldsymbol{\varepsilon}}\|^{2}$,

$$\frac{\partial \mathbf{g}^{e}_{n+1}}{\partial \boldsymbol{\varphi}^{e}_{n+1}} = -\frac{2}{\Delta t}\Big(\left(\mu_c\, \mathbb{I}\right)\, \mathbf{H} + 4\alpha\beta^{2}\, \left(\operatorname{dev}\dot{\boldsymbol{\varepsilon}} \otimes \dot{\boldsymbol{\kappa}}\right)\Big)\mathbf{B}_{\varphi} \tag{4.99}$$

$$\frac{\partial \mathbf{q}^{e}_{n+1}}{\partial \mathbf{u}^{e}_{n+1}} = -\frac{8\alpha\beta^{2}}{\Delta t}\, \left(\dot{\boldsymbol{\kappa}} \otimes \operatorname{dev}\dot{\boldsymbol{\varepsilon}}\right) \mathbf{B}_{\mathbf{u}}, \tag{4.100}$$

$$\frac{\partial \mathbf{q}^{e}_{n+1}}{\partial \boldsymbol{\varphi}^{e}_{n+1}} = \frac{1}{\Delta t}\Big(\bar{\lambda}\, \mathbf{I}\otimes\mathbf{I} + \left(\bar{\mu} + \bar{\mu}_c + 4\alpha m\right)\, \mathbb{I} + \left(\bar{\mu} - \bar{\mu}_c\right)\, \bar{\mathbb{I}} + 8\alpha\, \left(\dot{\boldsymbol{\kappa}} \otimes \dot{\boldsymbol{\kappa}}\right)\Big)\mathbf{B}_{\varphi}. \tag{4.101}$$

In the material regime with microstructure in translational motions:

$$\frac{\partial \mathbf{g}^{e}_{n+1}}{\partial \mathbf{u}^{e}_{n+1}} = \frac{1}{\Delta t}\Big(\left(\lambda - \mu_{\circ}\beta^{2}\right)\mathbf{I}\otimes\mathbf{I} + \left(\mu_{\circ}\beta^{2} + \mu + \mu_c\right)\mathbb{I} + \left(\mu_{\circ}\beta^{2} + \mu - \mu_c\right)\bar{\mathbb{I}}\Big)\mathbf{B}_{\mathbf{u}}, \tag{4.102}$$

$$\frac{\partial \mathbf{g}^{e}_{n+1}}{\partial \boldsymbol{\varphi}^{e}_{n+1}} = -\frac{2}{\Delta t}\, \left(\mu_c\, \mathbb{I}\right)\, \mathbf{H}, \quad \frac{\partial \boldsymbol{\omega}^{e}_{n+1}}{\partial \boldsymbol{\varphi}^{e}_{n+1}} = -\mathbf{H}, \tag{4.103}$$

$$\frac{\partial \boldsymbol{\omega}^{e}_{n+1}}{\partial \mathbf{u}^{e}_{n+1}} = \frac{1}{2}\, \left(\mathbb{I} - \bar{\mathbb{I}}\right)\, \mathbf{B}_{\mathbf{u}}, \quad \frac{\partial \mathbf{q}^{e}_{n+1}}{\partial \mathbf{u}^{e}_{n+1}} = \mathbb{O}, \tag{4.104}$$

$$\frac{\partial \mathbf{q}^{e}_{n+1}}{\partial \boldsymbol{\varphi}^{e}_{n+1}} = \frac{1}{\Delta t}\Big(\bar{\lambda}\, \left(\mathbf{I}\otimes\mathbf{I}\right) + \left(\bar{\mu} - \bar{\mu}_c\right)\, \left(\mathbb{I} + \bar{\mathbb{I}}\right)\Big)\mathbf{B}_{\varphi}. \quad \text{if} \quad \bar{\mu} > \bar{\mu}_c \tag{4.105}$$

$$\frac{\partial \mathbf{q}^{e}_{n+1}}{\partial \boldsymbol{\varphi}^{e}_{n+1}} = \frac{1}{\Delta t}\Big(\bar{\lambda}\, \left(\mathbf{I}\otimes\mathbf{I}\right) - \left(\bar{\mu} - \bar{\mu}_c\right)\, \left(\mathbb{I} - \bar{\mathbb{I}}\right)\Big)\mathbf{B}_{\varphi}. \quad \text{if} \quad \bar{\mu} < \bar{\mu}_c \tag{4.106}$$

where $\mathbb{O}$ is the fourth order zero tensor, $\mathbb{I}$, $\bar{\mathbb{I}}$ are the fourth order unit tensors and $\mathbf{I}$ is the second order identity tensor. The system of nonlinear equation in (4.88) are solved according to the procedure explained in Section 4.2.1.

5. Numerical results

This chapter deals with the presentation of computational results obtained from the numerical simulations of the developed Cosserat continuum models for granular materials. It is further divided into two sections where in the first section results from the elastic Cosserat continuum model are presented and in the second section the results from the rate-dependent inelastic Cosserat continuum model are presented. Finite element method has been used for the numerical implementation of both the elastic and rate-dependent inelastic Cosserat models.

5.1. Numerical results from the elastic Cosserat continuum model

The material model presented in Chapter 3 (see Section 3.4) is analyzed for the possible distribution of microstructure in four special cases. In the first case, a square plate with a central hole is used for the observation of microstructure in the material. In the second case, the distribution of microstructure in a Couette shear geometry is examined. In the third case, a tension-compression test is performed on a rectangular specimen for the investigation of the onset of localized behavior of the material leading to possible material failure. In the fourth case, the distribution of microstructure in a rectagnular specimen of granular particles is simulated under the impact of an indenter where the Prandtl slip line solution is evidented with the formation of microstructure in the region beneath the indenter.

5.1.1. Microstructure in a square plate with a central hole

In this first example, the behavior of the elastic Cosserat material model (presentd in Chapter 3, see Section 3.4.1) is analyzed on an infinitely long brick specimen with a circular hole at its center. The geometry and the loading conditions are shown in Figure 5.1(a). The geometry of the problem allows to use plane strain conditions for the implementation of the proposed model using finite element scheme. For this purpose a perforated square plate of unit thickness is chosen as a cross-section of the brick specimen as shown in Figure 5.1(b). Due to the symmetry of the problem in consideration only one fourth of the plate is analyzed subjected to tension test. The selected domain is then discretized into finite elements with a total of 800 elements. All the field variables in each element are approximated with eight nodes using bi-quadratic shape functions. The spatial integration is carried out with nine Gaussian quadrature points per element. The material parameters used in the numerical calculations are presented in Table 5.1. A Newton-Raphson iteration scheme is used for solving the system of nonlinear equilibrium equations resulting from the two-field variational formulation of the proposed model. A displacement controlled quasi-static loading is applied to the specimen in sixty five loading steps with a loading step size of 1.0×10^{-2} where

Table 5.1.: Material parameters for the analysis of a square plate with a central hole.

E	ν	μ_c	α	β	$\overline{\mu}$	$\overline{\lambda}$	$\overline{\mu}_c$
(MPa)	-	(MPa)	(N.mm^2)	(mm^{-1})	(N)	(N)	(N)
2.0×10^4	0.3	2.0×10^2	1.0×10^2	1.0×10^1	3.0×10^2	5.0×10^1	2.0×10^2

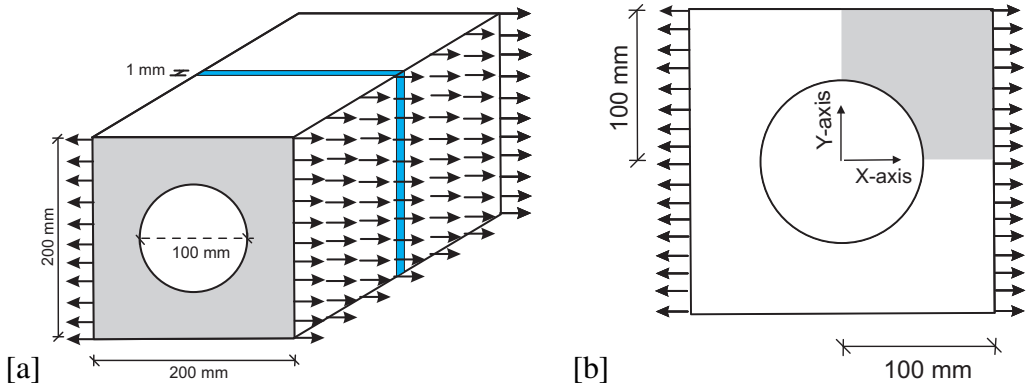

Figure 5.1.: (a) Geometry of the brick specimen with a central hole and loading conditions, (b) Reduced Geometry (shaded region) due to symmetrical loading conditions.

a maximum displacement of 17mm is prescribed. For the stopping criterion of Newton-Raphson iteration scheme a tolerance of 1.0×10^{-8} is used.

Results from the numerical simulations shows that the material exhibits a microstructure in translational motions of the continuum particles. The distribution of microstructural and non-microstructural regions in the material are demonstrated in the Figure 5.2. The red coloured (Phase 3) structural part is corresponding to the material with microstructure in translational motions of the particles and the purple coloured (Phase 2) is corresponding to the material where there is no microstructure. It is observed that the part of the material where there are maximum stresses transforms to the microstructural phase where it experience a microstructure in translational motions of continuum particles. The complete picture of the development of microstructure in the perforated square plate is shown in Figure 5.3(a).

In Figure 5.3(b) the distribution of the horizontal component of Cosserat strain tensor $\mathbf{e}$ is presented. Higher values of gradients of the field variables is seen in the zone of material where there is a microstructure. In Figure 5.4 the load displacement curves for different discretized meshes consisting of 200, 800, 1800 and 3200 elements are presented. It is shown that for each discretized mesh the load-displacement response of the material is the same regardless of the mesh, which implies that the solution obtained by using the proposed numerical model is mesh objective. In Figure 5.5 the load-displacement curves for varying values of the material parameters $\overline{\mu}_c$ are shown, whereas slopes to these curves with the prescribed displacement are seen in Figure 5.6. These Figures do not only demostrate on the development of microstructure in the material affected by the change in the values of $\overline{\mu}_c$ but also allow to observe that the Cosserat tangent modulus is nonlinear in the non-microstructural regime and is linear (having a constant value) in the microstructural regime of the material. The effect of different material parameters on the development of microstructure in translational motions of the continuum particles is demonstrated in Figures 5.7 and 5.8.

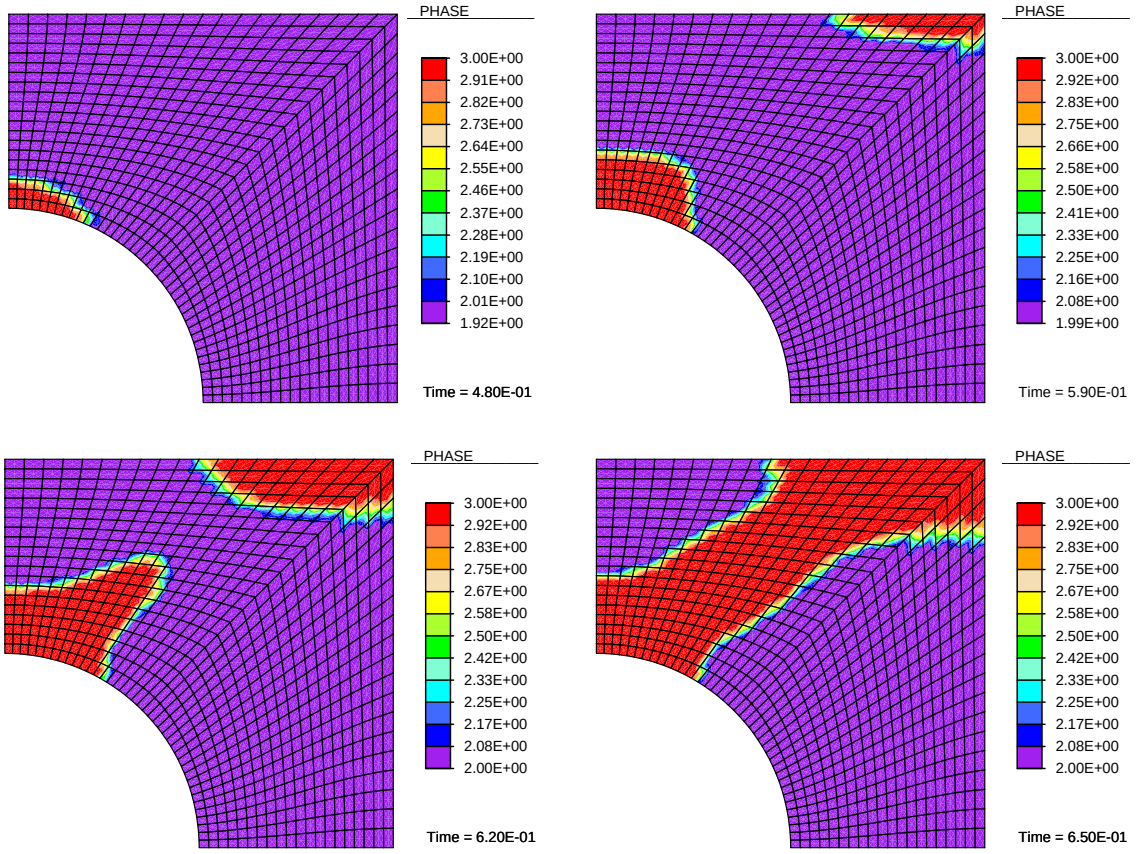

Figure 5.2.: Development of microstructure in the material and the distribution of phase fraction at different loading steps.

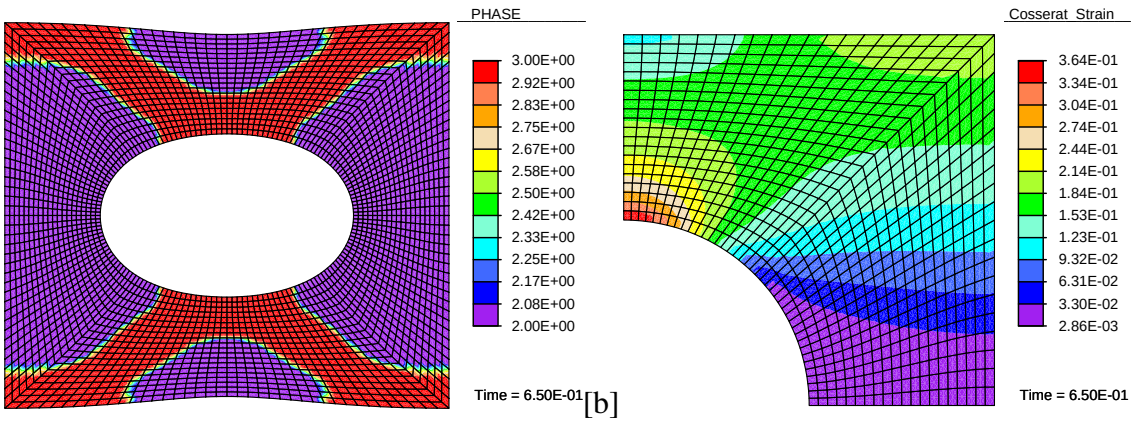

[a] [b]

Figure 5.3.: (a) Deformed configuration of the square plate with central hole, (b) Contour plot of Cosserat strain component in horizontal direction.

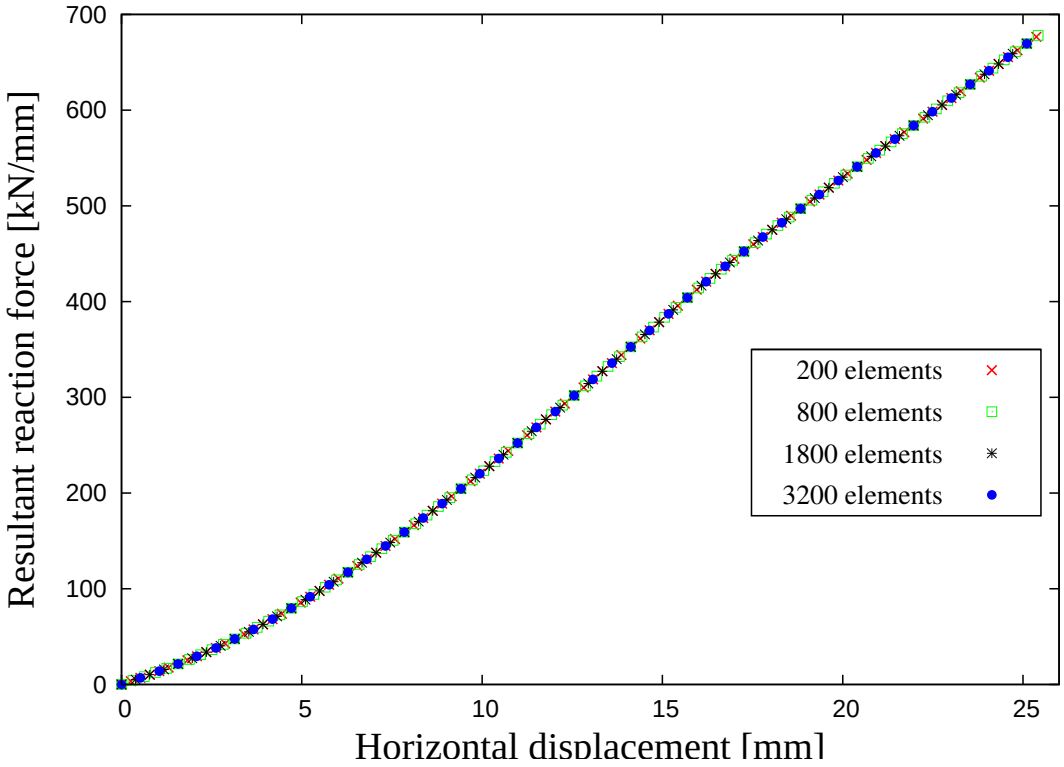

Figure 5.4.: Load-displacement curves obtained from different simulations performed on the meshes consisting of 200, 800, 1800 and 3200 elements.

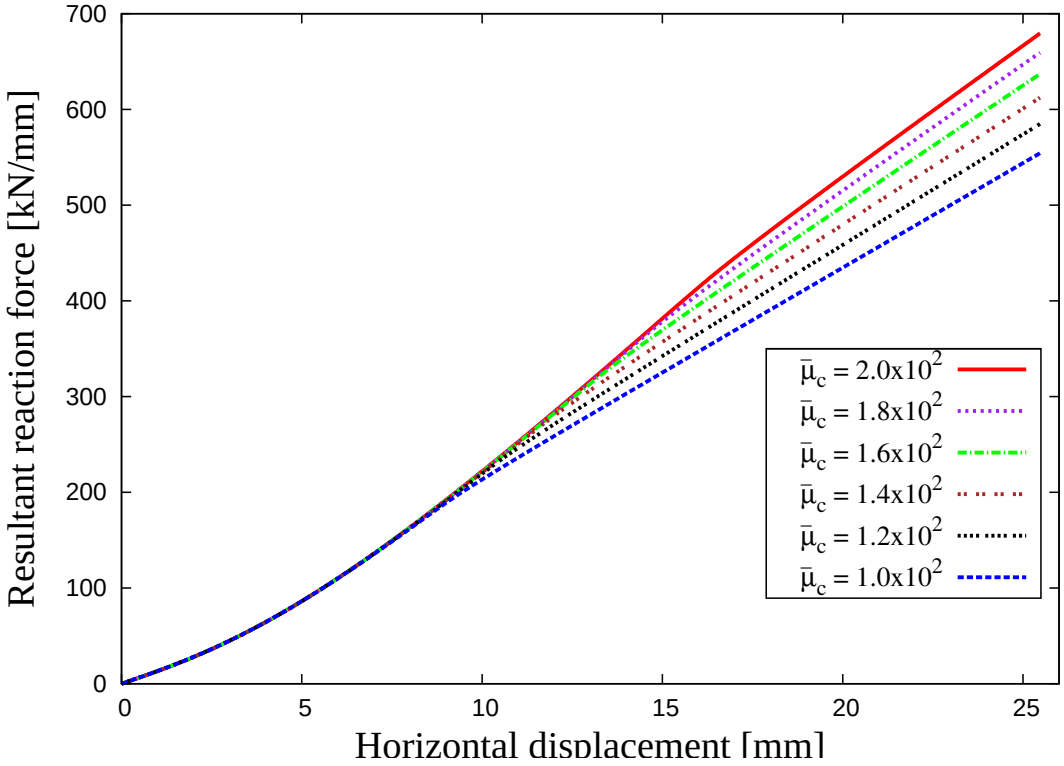

Figure 5.5.: Load-displacement curves obtained from different simulations performed with varying the values of the material parameter $\bar{\mu}_c$.

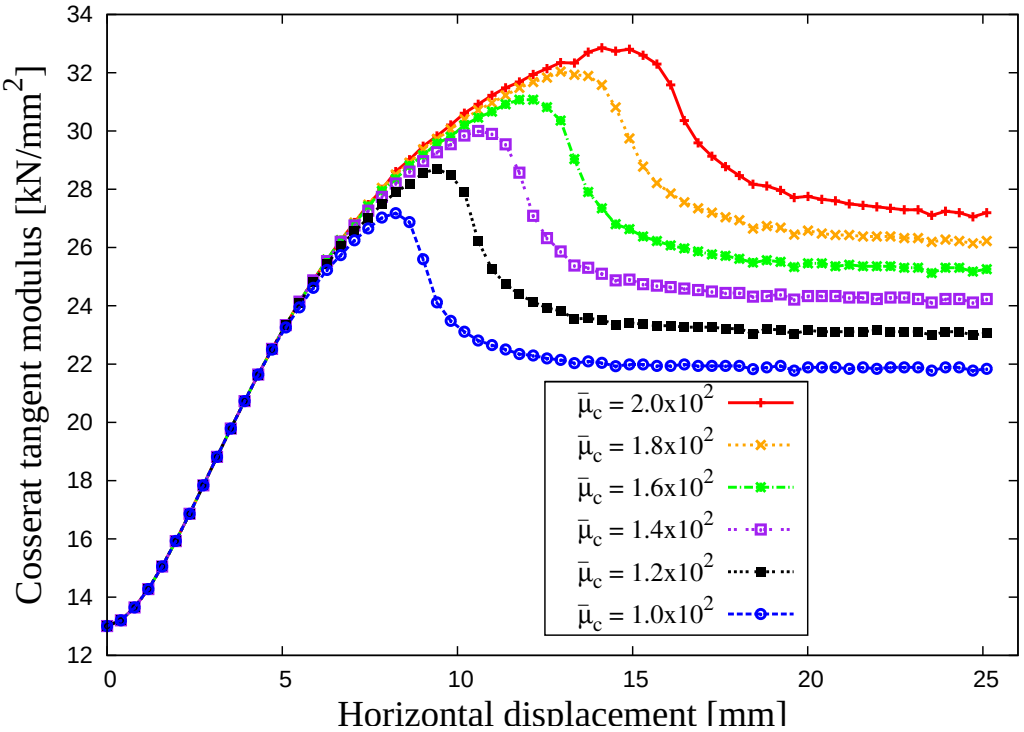

Figure 5.6.: The effect of Cosserat coupled shear modulus $\bar{\mu}_c$ in changing the tangent modulus of Cosserat elasticity.

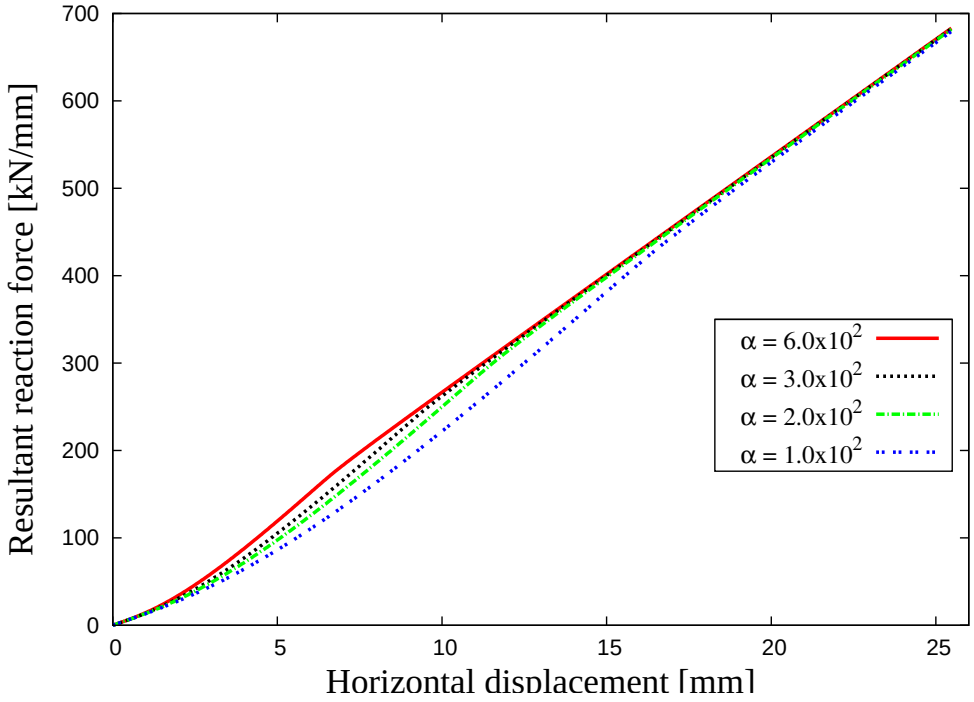

Figure 5.7.: Load-displacement curves obtained from different simulations performed with varying the values of the material parameter α.

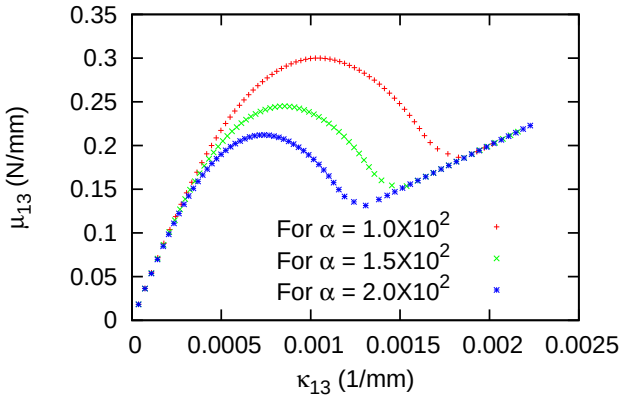

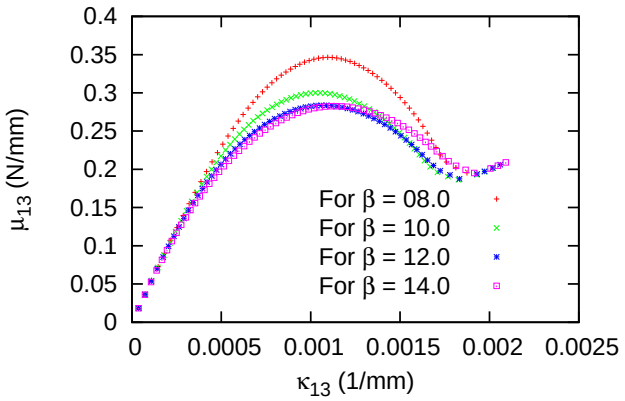

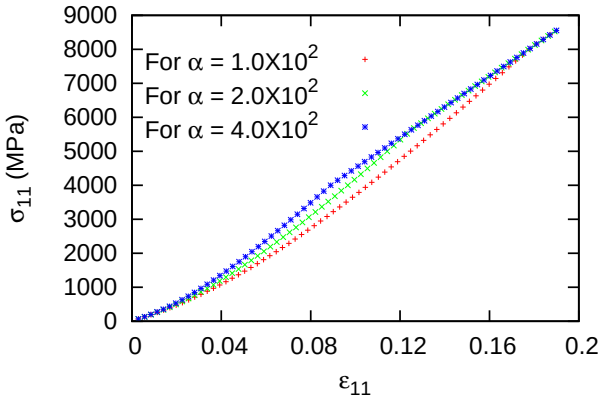

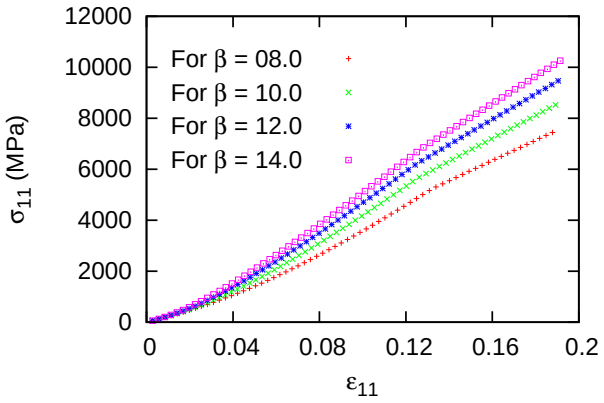

Figure 5.8.: Stress-strain curves obtained from different simulations performed with varying the values of material parameters α and β.

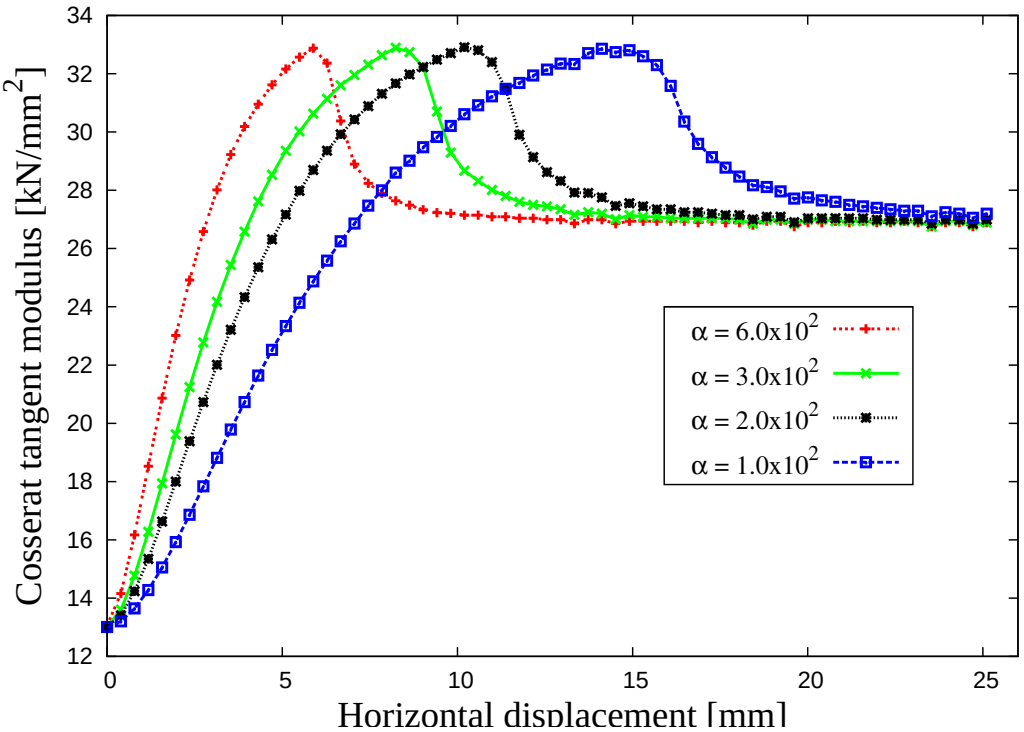

Figure 5.9.: Change in the tangent modulus of Cosserat elasticity is observed with varying values of the material parameter α.

The mechanical response of the material with some selected material parameters α and β is demonstrated in Figure 5.8. It is observed that for relatively large particle size and with large interaction modulus the material microstructure in translational motions is more pronounced. In Figure 5.9 the varying values of material parameter α are taken to observe the microstructure formation where it is observed that for large values the microstructure develops much earlier than the small value of α. Figure 5.10 depicts the behavior of the material in uni-axial tension-compression test with varying values of the material parameter β. The test is performed on the same geometry as discussed above. The interaction modulus is chosen as $\alpha = 1.0 \times 10^3$ N.mm^2, with fixed μ. The value of $\bar{\mu}_c$ varies according to $\bar{\mu}_c = 60, 80, 100, 120$ N. We observe that for a larger value of β the microstructure develops earlier than for a smaller value. For the relatively small value of $\beta = 8.0064$ mm^{-1}, the material still has not experienced any microstructure in translational motions until 3.5 percent strain. This shows that with smaller particle size the microstructure in translational motions is more pronounced. Same conclusion has been drawn before where analytical computations along some chosen strain paths were carried out. For the displacement controlled quasi-static loading a step size of 5.0×10^{-3} is used.

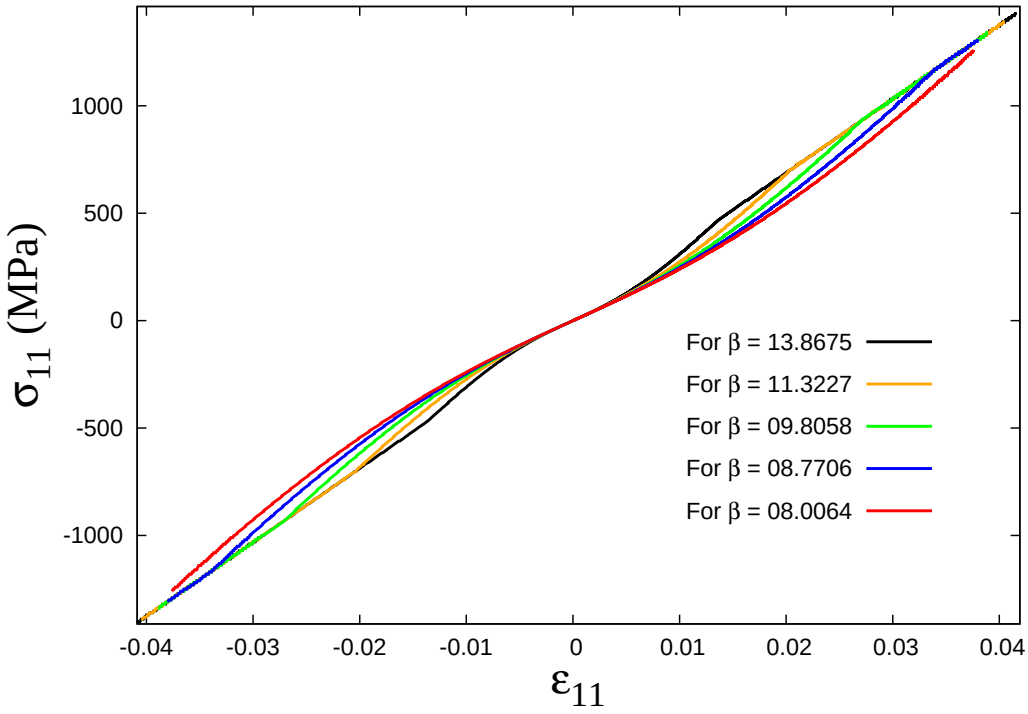

Figure 5.10.: Stress-strain response of the notched plate with a central hole subjected to tension with varying particle size.

5.1.2. Microstructure in an annular material domain

To observe all the non-microstructural and microstructural phases in the material it is required to develop a test where there are strong rotations among the material particles which can contribute an intense rotational effect to the material strain energy. The kinematics of particle rotations is shown in Figure 5.11 where two possible kind of particle rotations, namely, counter rotations and identical rotations are seen. The rotational effect of the counter rotating particles contribute strong rotational effect to the proposed interaction energy potential, whereas, in a situation of identical rotations of the particles it contributes much sliding effect to the interaction energy potential. Within a confined geometry and under certain boundary conditions the phenomenon of particle rotations is affected by particle size.

Couette annular geometry is taken for the observation on the formation of microstructure using the proposed model. Couette geometries has been used in experiments for the analysis of shear flows in granular materials. The evidence of the formation of shear localization near the inner rotating cylinder in a Couette annular geometry is provided in an experiment by Debrégeas et al. [Deformation and flow of a two-dimensional foam under continuous shear, *Phys. Rev. Lett.*, 87:178305, 2001]. Veje et al. [Kinematics of a two-dimensional granular Couette experiment at the transition to shearing, *Phys. Rev. E* 59, 739-745, 1999] used to shear the photoelastic polymer disks in a Couette flow. Another experiment on shearing the granular material inside the Couette geometry is performed by Savage and Sayed in [Stresses developed by dry cohesionless granular materials sheared in an annular shear cell, *Journal of Fluid Mechanics*, 142, 391-430, 1984]. Among other works related to the experimental observation of shearing effect in a Couette cell are found in the papers by Behringer et al. [Stress Fluctuations in a 2D Granular Couette Experiment: A Continuous Transition

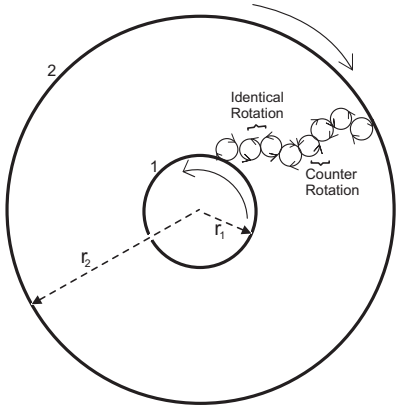

Figure 5.11.: Kinematics of particle rotations: Rotating particle chain exhibiting two different rotational phenomenon.

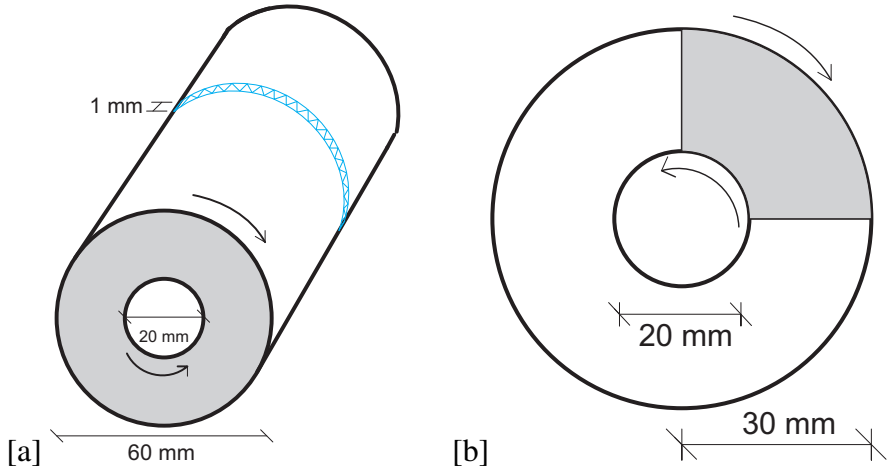

Figure 5.12.: (a) Geometry of the two circular rotating cylinders, (b) Reduced Couette geometry and boundary conditions.

Phy. Rev. Lett., 82(26), 5241-5244, 1999] , Utter and Behringer [Multiscale Motion in the Shear Band of Granular Couette Flow, *AIP Conf. Proc.* 1145, 339-342, 2009]. For a detailed overview on the comparison between numerical and experimental results obtained in a granular Couette shear the reader is referred to the paper by Lätzel et al. [Comparing simulation and experiment of a 2D granular Couette shear device. *Eur. Phys. J. E* 11, 325-333, 2003]. Consider the granular material confined between two concentric rigid circular cylinders as shown in Figure 5.12. The cylinders are subjected to rotations in opposite directions. Due to symmetry we take only first quadrant of an annular plate for the observation of microstructure formation inside it. The annular domain is subjected to an in-plane shear deformation with the application of rotational motions at the outer boundaries. The width of the annular is taken to be 20 mm. The inner circular boundary is at a radius of 10 mm from the origin of the annulus. The circular boundaries are supposed to rotate in opposite direction and as a consequence two type of rotations among the particles inside the annular domain can be observed. These identical and counter rotations of the granular particles within the annular domain can be viewed as in Figure 5.11. The boundary conditions for the numerical simulation using the proposed model uses fixed displacement along the circular boundaries whereas a micromotion of one radiant is prescribed at the boundaries.

Our intension with this study is to observe the development of microstructural phases within

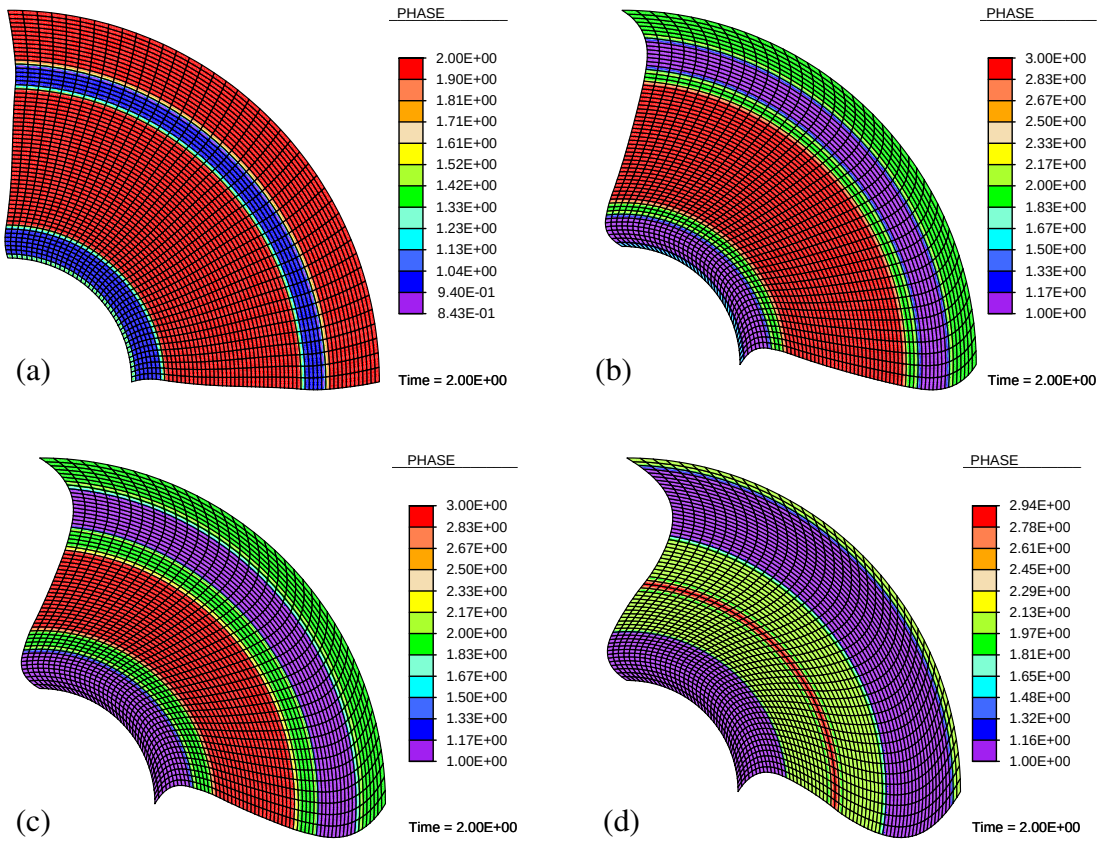

Figure 5.13.: (a) Phase with microstructure in micro-motions and no internal structure phase coexists, (b) All the three phases coexists, (c) Three phases coexists with more pronounced microstructure in micro-motions, (d) Coexistence of the three phases with almost vanishing microstructure in translational motions.

the annular domain subjected to rotational deformation. The development of microstructures in both the translational and micro-rotational motions of the particles are observed as can be seen in Figure 5.13. Where, in Figure 5.13(a) material exhibits a microstructure in micro-rotations of the continuum particles. In Figures 5.13(a), 5.13(b) and 5.13(c) it is shown that for a particular values as listed in Table 5.2 the material has microstructure in both the translational and micro-rotational motions of the particles. Thus allowing to observe that all the material phases can coexist. Moreover the deformed configurations with different values of β depicts that decreasing the value of β causes the material to behave softly. Also with the decrease in the particle size the microstructure in the micromotions of the particles is more pronounced.

Table 5.2.: Material parameters for the shear test in a Couette geometry.

-	E	ν	μ_c	α	β	$\overline{\mu}$	$\overline{\mu}_c$
-	(MPa)	-	(MPa)	(N.mm^2)	(mm^{-1})	(N)	(N)
Figure 5.13(a)	2.0×10^2	0.3	2.0	2.0×10^5	5.8×10^{-1}	8.0×10^1	5.0×10^1
Figure 5.13(b)	2.0×10^2	0.3	2.0×10^2	2.0×10^5	5.8×10^{-1}	8.0×10^1	5.0×10^1
Figure 5.13(c)	2.0×10^2	0.3	2.0×10^2	2.0×10^5	4.0×10^{-1}	8.0×10^1	5.0×10^1
Figure 5.13(d)	2.0×10^2	0.3	2.0×10^2	2.0×10^5	2.0×10^{-1}	8.0×10^1	5.0×10^1

5.1.3. Onset of localized deformations in a granular medium

The localization of deformations leads to possible material failure and such localized zones have been observed by Kaus and Podladchikov [Initiation of localized shear zones in viscoelastic rocks. *Journal of Geophysical Research*, 111, B04412(1-18), 2006]. Our emphasis with this study is not to show these localized deformations rather it is possible to observe this phenomenon with the exact relaxed potentials. The exact relaxed potentials are enable enough to predict on the formation of microstructures within these localized zones in the material. We emphasize on the formation of microstructure and thus provide a clue that how these localized deformations can form different possible bands. This may be important to know that under certain boundary conditions the material can form different localized deformation bands which afterwards possibly leads to material failure. To illustrate on the formation of these localized deformation bands a tension-compression test performed on a rectangular specimen is presented. The formation of microstructure clearly predicts the localized deformation mechanism observed by Kaus and Podladchikov (2006).

Example: Compression test on a rectangular specimen with a small imperfection

In this example, a rectangular specimen of granular material is considered with a small imperfection in the form of a weak element at the center of the specimen as shown in Figure 5.14. The material parameters used for the simulation are given in Table 5.3. The geometry and boundary conditions are shown in Figure 5.14, where the vertical displacements on both top and bottom of the specimen are constrained. The material points can move horizontally at both the top and bottom boundary of the specimen except the point at the left lower corner of the specimen which is fixed in both the horizontal and vertical direction. Additionally a frictional boundary condition is used where the micro-rotation of the continuum points is allowed at both the top and bottom boundary of the specimen. A maximum displacement of -34.8cm is applied on top boundary in vertical direction over a 1000 loading steps with a load step size of 4.35×10^{-3}.

The purpose of this analysis is to observe the development of microstructural zones in the specimen under compression. The analysis is performed on the specimen with two different mesh sizes where in the first analysis (see first column of Figure 5.15) the specimen is discretized into 765 finite elements whereas in the second analysis (see second column of Figure 5.15) 4214 elements are used. The formation of microstructure in the material is triggered with the introduced inhomogeneity in the form of a weak element in the specimen. It is observed that the microstructure in the material develops in the zones where possible material failure can occur. The developed microstructural zones in the material resembles to the results observed by Kaus and Podladchikov (2006). This development of the microstructure is gradually increasing with the increase in the loading. The two colors in Figure 5.15 depicts the microstructural and non-microstructural part of the material. The red color zones is corresponding to the material phase where there is a microstructure in the material. This microstructure is due to the translational motions of the continuum particles which give information on the possible localized zone formation within the material.

The onset of the localized zones are predicted by the formation of microstructure in the material as shown in Figure 5.15. The development of this microstructural zones leads to the information on the possible material failure. It is observed that the width of the microstruc-

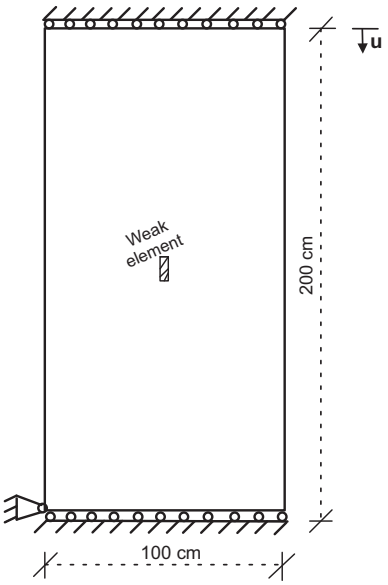

Figure 5.14.: Geometry and boundary conditions of the rectangular specimen with weak element.

tural band is not affected by the mesh size, this is highly due to the properties of the relaxed potentials. The microstructural bands are the regimes in the material where the dissipation occurs while deformation takes place after yielding of the material.

Figure 5.17 clearly shows an increased value of the microrotation inside the width of the microstructural zone. The microrotations are more concentrated towards the center of the microstructrual zones. This is why these microstructural zones can be seen as a patterns on which the material can lead to possible failure, since inside the localized zones of deformations the particle rotations are found to be large. Since the material model used for these observations do not accommodate plastic deformations therefore we cannot show but are able to predict on the possible material failure zones that are related to energy dissipation.

From Figures 5.18, 5.19 and 5.20 it can be seen that the micro-rotational field attains

Table 5.3.: Material parameters for the specimen with introduced imperfection in compression.

-	E	ν	μ_c	α	β	$\overline{\mu}$	$\overline{\mu}_c$
-	(MPa)	-	(MPa)	(N.mm^2)	(mm^{-1})	(N)	(N)
Mesh	2.0×10^5	0.3	2.0×10^1	5.0×10^1	1.5	7.0	2.0×10^1
Weak element	2.0×10^3	0.3	2.0×10^1	1.0×10^3	1.5	3.0×10^2	4.0

its highest value at the center across the width of the microstructural zones. The curvature strain and Cosserat strains are more concentrated towards the center of these microstructural zones. The couple stress and the Cosserat shear stress switch their direction at the center across the width of the microstructural zones. The physical significance of this phenomenon can be realized by considering the center line of the microstructural zones as a slip or shearing line where there is strong shearing effect which causes the flip of shear and couple stress direction. Our results are in accordance to the observation of Alshibli et. al. [KAV06] where they show the formation of strain localization in a rectangular specimen of granular material applying Cosserat continuum theory.

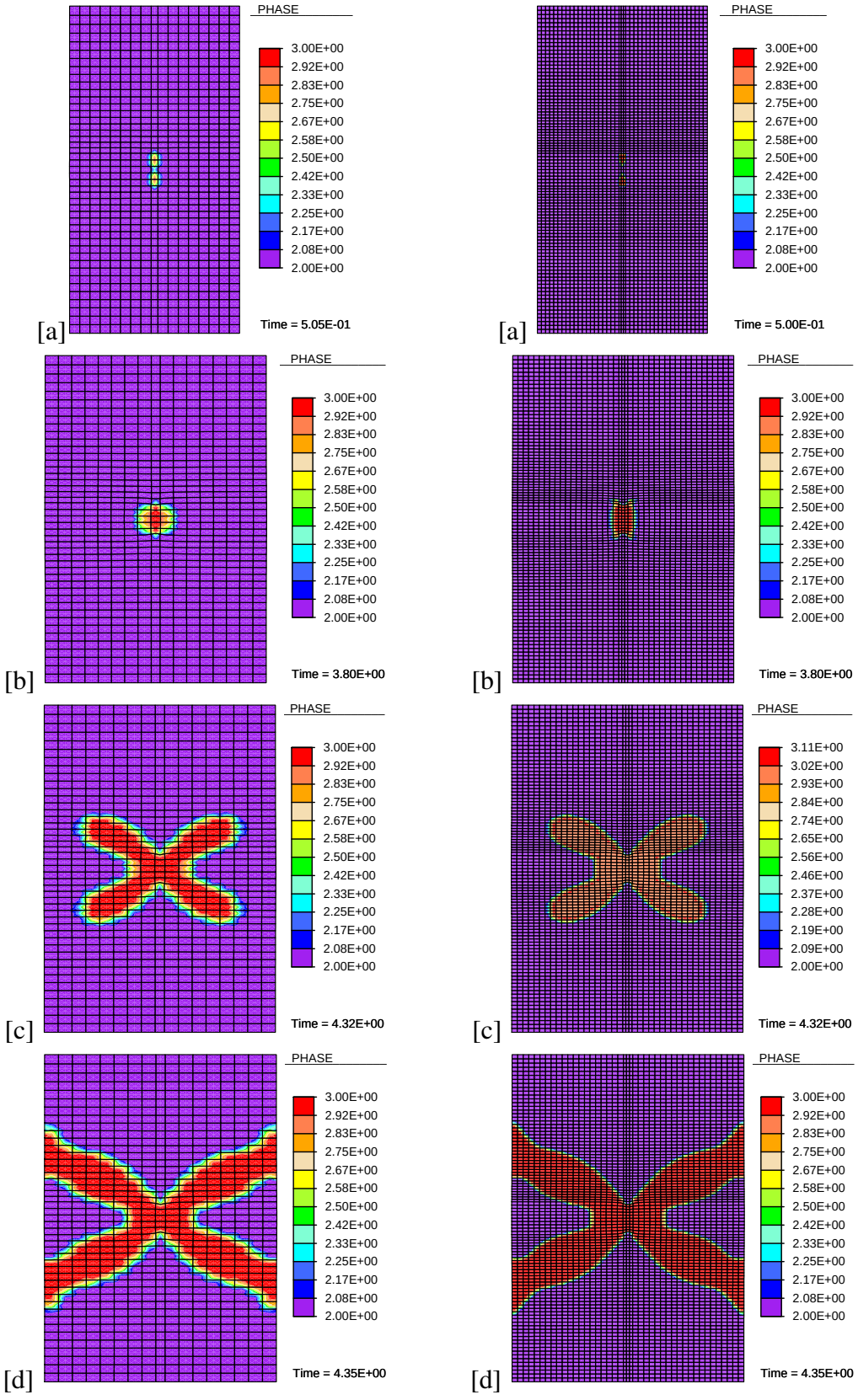

Figure 5.15.: Rectangular specimen in compression. In first column: The deformed configuration of the specimen under compression with coarse mesh consisting of 765 elements. In second column: The deformed configuration of the specimen under compression with fine mesh consisting of 4214 elements

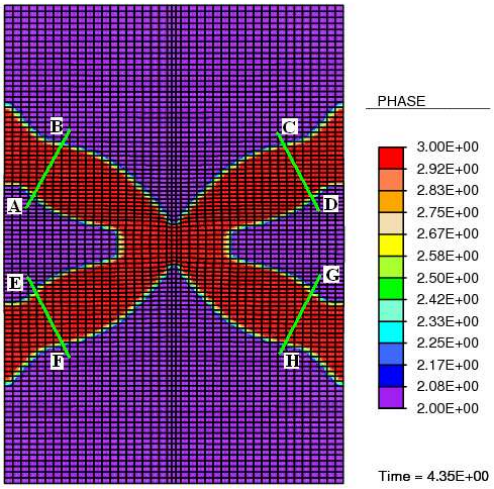

Figure 5.16.: Selected lines along the width of the microstructural zone.

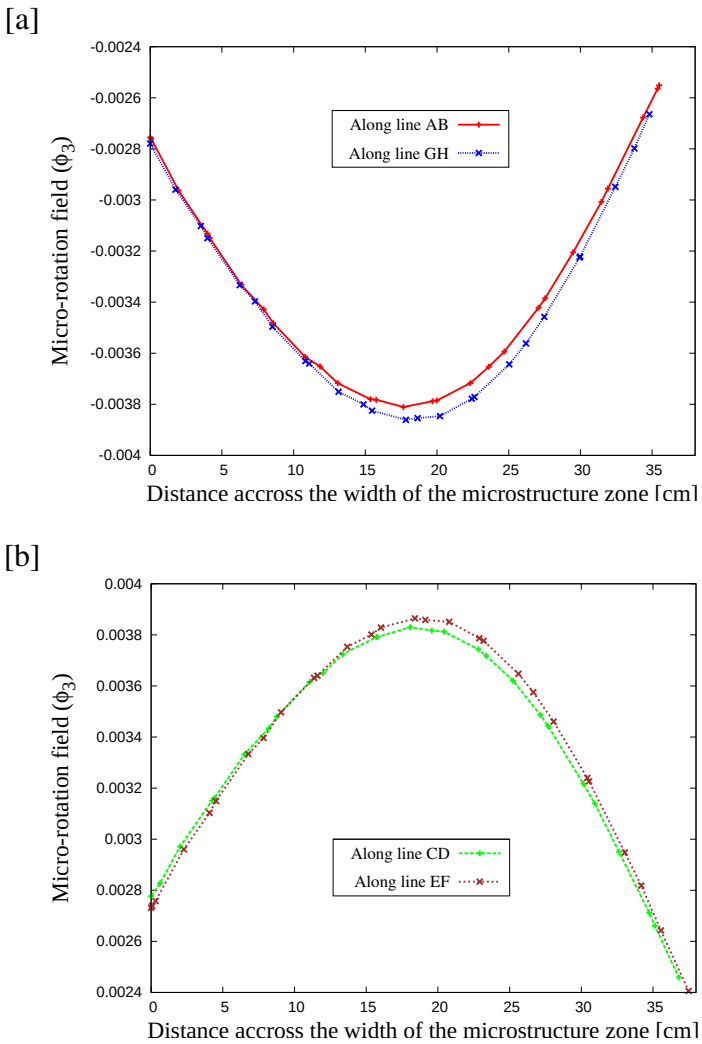

Figure 5.17.: Distribution of micro-rotation φ_3 along the width of the microstructural zone.

[a]

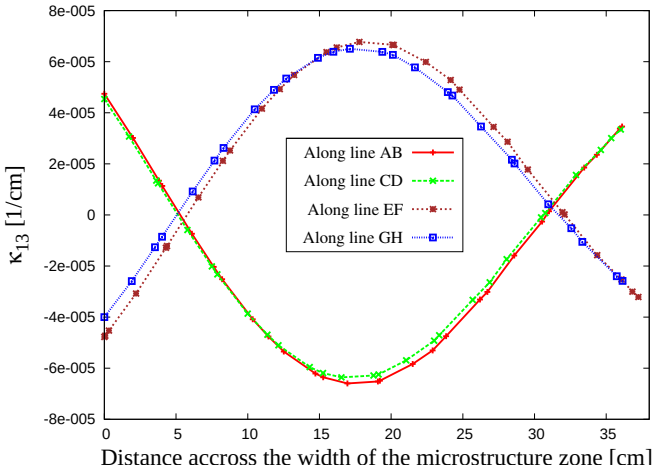

Figure 5.18.: Distribution of curvature strain along the width of the microstructural zone.

[a]

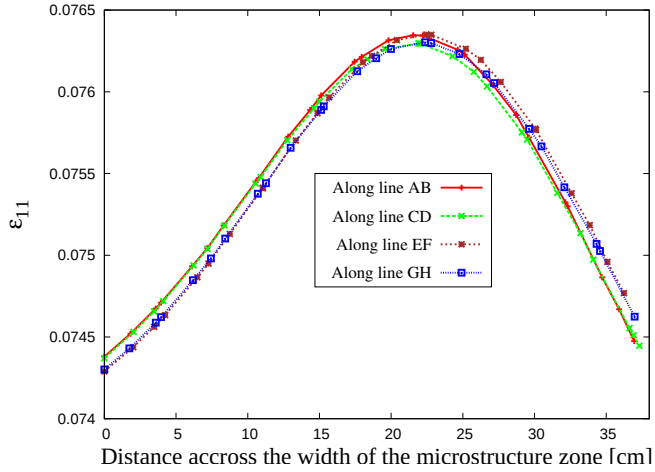

[b]

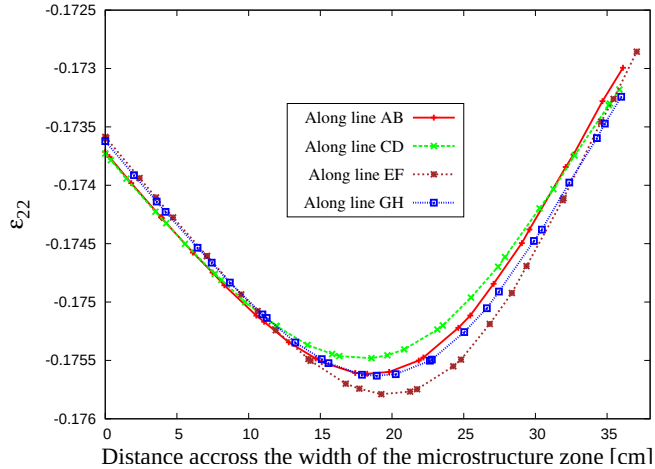

Figure 5.19.: Distribution of horizontal and vertical strain components along the width of the microstructural zone.

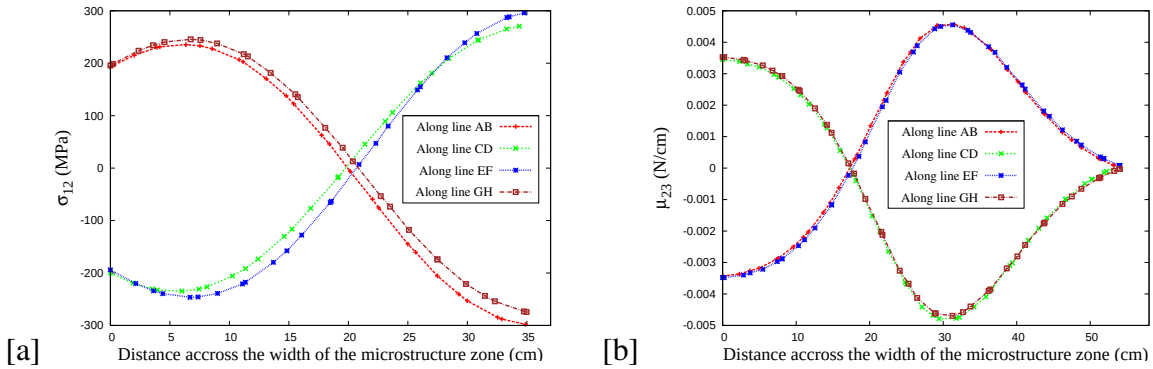

Figure 5.20.: Distribution of shear force-stress (a) and couple stress (b) components along the width of microstructural zone.

5.1.4. Indentation test and the elastic material microstructure

The significance of the observation of mechanical response of a granular medium to indentation is evident from the load bearing capacity problem in geotechnical engineering. In this example we study the indentation of a granular medium under plain strain assumptions. In plain strain conditions indentation of granular material has also been studied by Tordesillas and Shi [TS98, TS99], by Murthy et. al. [MGC12]. The role of particle rotations in a granular medium to indentation is studied by Tordesillas et. al. [TPM05] where they use discrete element method for the simulation and the observation of mechanical response of the material. Cosserat continuum constitutive theory has been applied by Walsh and Tordesillas [WT06] for the numerical simulation of granular medium subjected to indentation. Sulem and Derrolaza [SD02] also analyze the microstructure in an indentation test on rocks using the finite element method in a Cosserat continuum.

A granular medium of dimensions 200×100 cm^2 is subjected to indentation by a flat rigid indenter with a dimension of 50×5 cm^2 as shown in Figure 5.21. The geometry of the granular medium is discretized into 2560 finite elements whereas the geometry of the indenter is discretized into 250 finite elements. The indenter can only move in vertical direction and this constraint is applied by fixing the horizontal degrees of freedom of all the nodal points of indenter. Both the horizontal and vertical degrees of freedom on the right and left boundary of the granular medium are fixed. The continuum points can move only in the horizontal direction at the base of the granular medium which is ensured by fixing the vertical degrees of freedom at the base of the granular medium. The punching of the indenter is controlled by the applied vertical displacements, where a maximum displacement of 3.76 cm is applied at the top nodes of the indenter mesh in 1390 loading steps with a step size of 1.4×10^{-3}. The material parameters used for the indenter and the granular medium (granular medium 1) are shown in Table 5.4. A large number of experiments have been performed on the granular foundations subjected indentation revealing similar bands of localized deformations as shown in this investigation. Also numerical simulation using finite element scheme for the Cosserat continuum by Walsh and Tordesillas [WT06] has shown such kind of microstructure formation in a granular medium punched by rigid indenter. We show a numerical solution where the development of microstructure has been predicted in the localized zones around the indenter. The nucleation and the evolution of microstructural zone can be observed as the indenter moves downward. This microstructural zone is corresponding to the material where there are localized gradients. These are the regions where the dissipation in the mate-

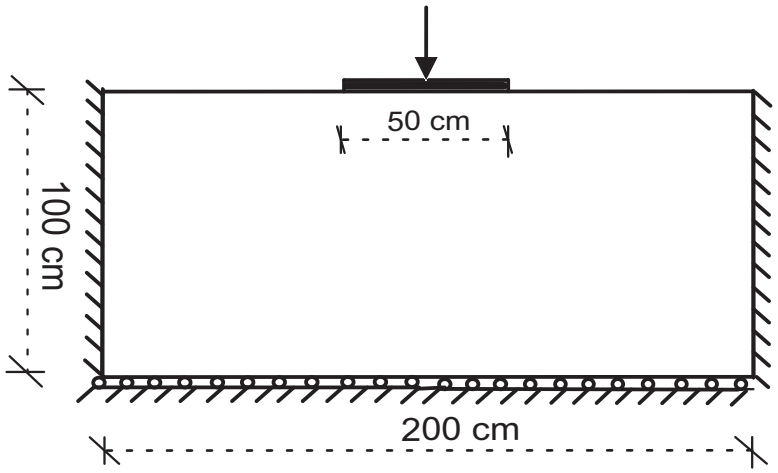

Figure 5.21.: Geometry of the granular medium under indentation along with the prescribed boundary conditions.

rial takes place upon yielding in plasticity analysis. Results from the numerical simulations in Figure 5.22 are in accordance to the generalized Prandtl's solution of a rigid flat punch problem, where the dead material (there is no microstructure in this region) underneath the rigid indenter has a triangular shape as seen in the second column of Figure 5.22 d. The red

Table 5.4.: Material parameters for the indentation test on a granular medium.

-	E	ν	μ_c	α	β	$\overline{\mu}$	$\overline{\mu}_c$
-	$(\frac{N}{cm^2})$	-	$(\frac{N}{cm^2})$	(N.cm^2)	(cm^{-1})	(N)	(N)
Granular medium 1	2.0×10^4	0.3	2.0	5.0×10^4	0.5	7.0×10^3	2.0×10^2
indenter	2.0×10^{12}	0.3	2.0	5.0×10^3	0.5	7.0×10^3	2.0×10^2

color zones of the material are corresponding to the phase where there is a microstructure due to translational motions of the particles, whereas the purple colored zones are the regimes where there is no internal structure in the material.

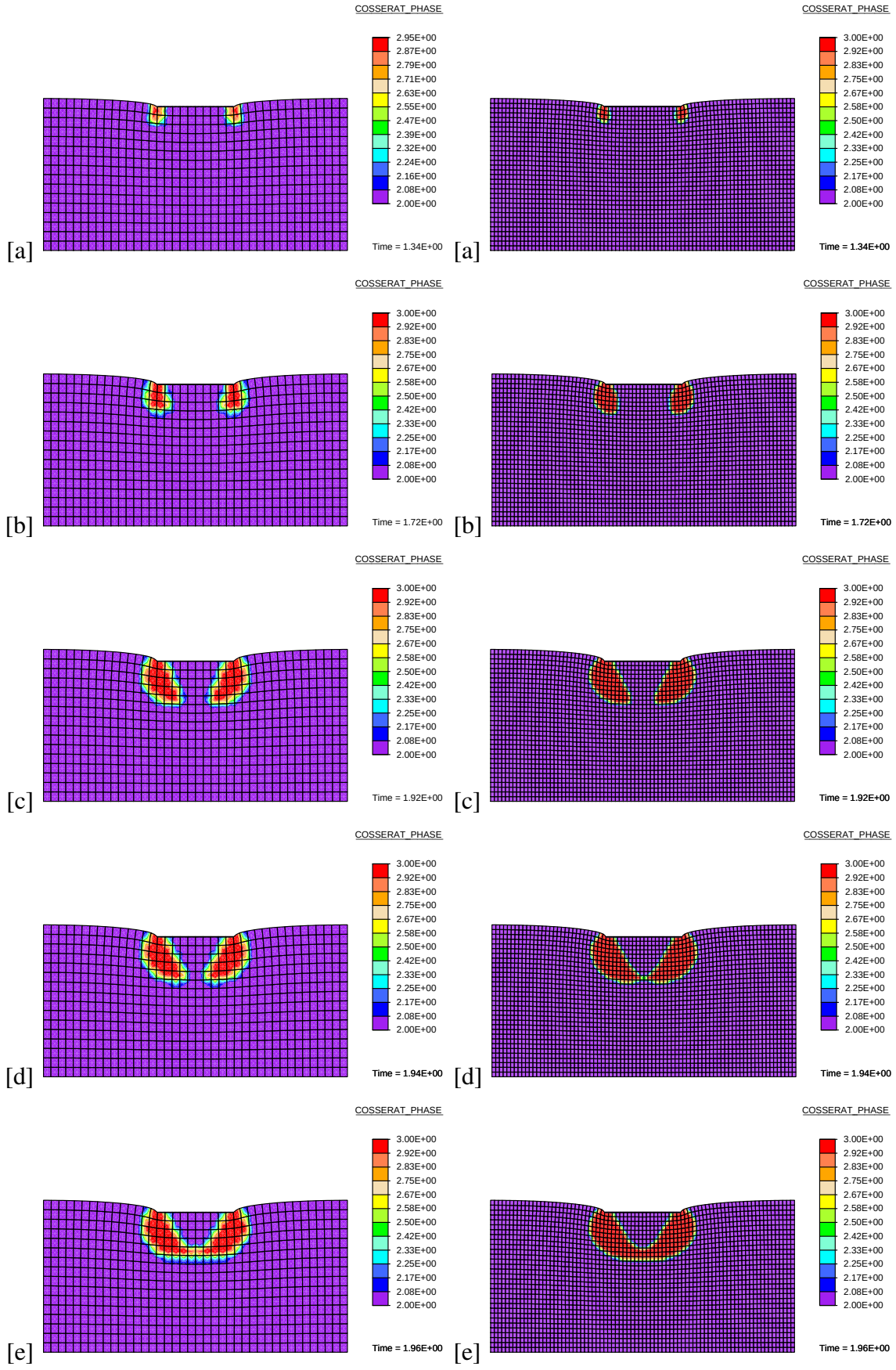

Figure 5.22.: Microstructure development beneath the indenter in a granular foundation.

5.2. Numerical results from the inelastic Cosserat material model

5.2.1. Indentation test and the inelastic material microstructure

The purpose of this test is to study the mechanical response of the material under indenter for different material parameters. The influence of these material parameters on the overall deformation mechanism and on the development of microstructures is investigated. The comparison with any empirical study would not be done.

A granular foundation with the geometry as shown in Figure 5.21 is taken for the numerical simulation. The foundation is discretized into 6400 finite elements whereas the indenter is discretized into 80 finite elements. The boundary conditions are chosen such that both the horizontal and vertical displacements are fixed at the right and left side of the foundation. Also the vertical displacements are fixed at the bottom of the foundation whereas the rotational degrees of freedom are free to move. Moreover, at the top of the foundation all degrees of freedom are allowed to move. The material parameters used in the numerical simulation are as given as in Table 5.5. The problem is force controlled where a vertical force of $0.814\,\mathrm{N}$ is applied at each nodal point at the top of the indenter. Upon loading the material microstructure develops beneath the indenter and its distribution within the granular foundation is shown in Figure 5.23. The material exhibits a rate-dependent response, which upon unloading continues to deform, this creep behavior can be observed from Figure 5.24. In Figure 5.25 the rate-dependent behavior of the granular foundation under indenter is analyzed. The nonlinear curve plotted between the rate of the displacement field ($\dot{\mathbf{u}}$) and the maximum resultant reaction force clearly shows that with the increase in the applied displacement rate the maximum resultant reaction force also increases. The simulation was carried out under the displacement controlled settings where varying displacement rates are used. The time step chosen for this analysis is 1.98×10^{-2} sec. The material parameters used in the simulation are shown in Table 5.6.

Table 5.5.: Material parameters for the indentation test on a granular medium using inelastic formulation.

-	E	ν	μ_c	α	β	$\overline{\mu}$	$\overline{\mu}_c$
-	$(\frac{N}{cm^2})$	-	$(\frac{N}{cm^2})$	(N.cm^2)	(cm^{-1})	(N)	(N)
Granular medium	2.0×10^4	0.3	2.0	5.0×10^4	1.0×10^2	0.5	2.0×10^2
indenter	2.0×10^{12}	0.3	2.0	5.0×10^4	1.0×10^2	0.5	2.0×10^2

Table 5.6.: Material parameters for the indentation test on a granular medium using inelastic formulation.

-	E	ν	μ_c	α	β	$\overline{\mu}$	$\overline{\mu}_c$
-	$(\frac{N}{cm^2})$	-	$(\frac{N}{cm^2})$	(N.cm^2)	(cm^{-1})	(N)	(N)
Granular medium	2.0×10^4	0.3	2.0	5.0×10^2	1.0×10^1	1.0×10^3	2.0×10^3
indenter	2.0×10^{12}	0.3	2.0	5.0×10^2	1.0×10^1	1.0×10^3	2.0×10^3

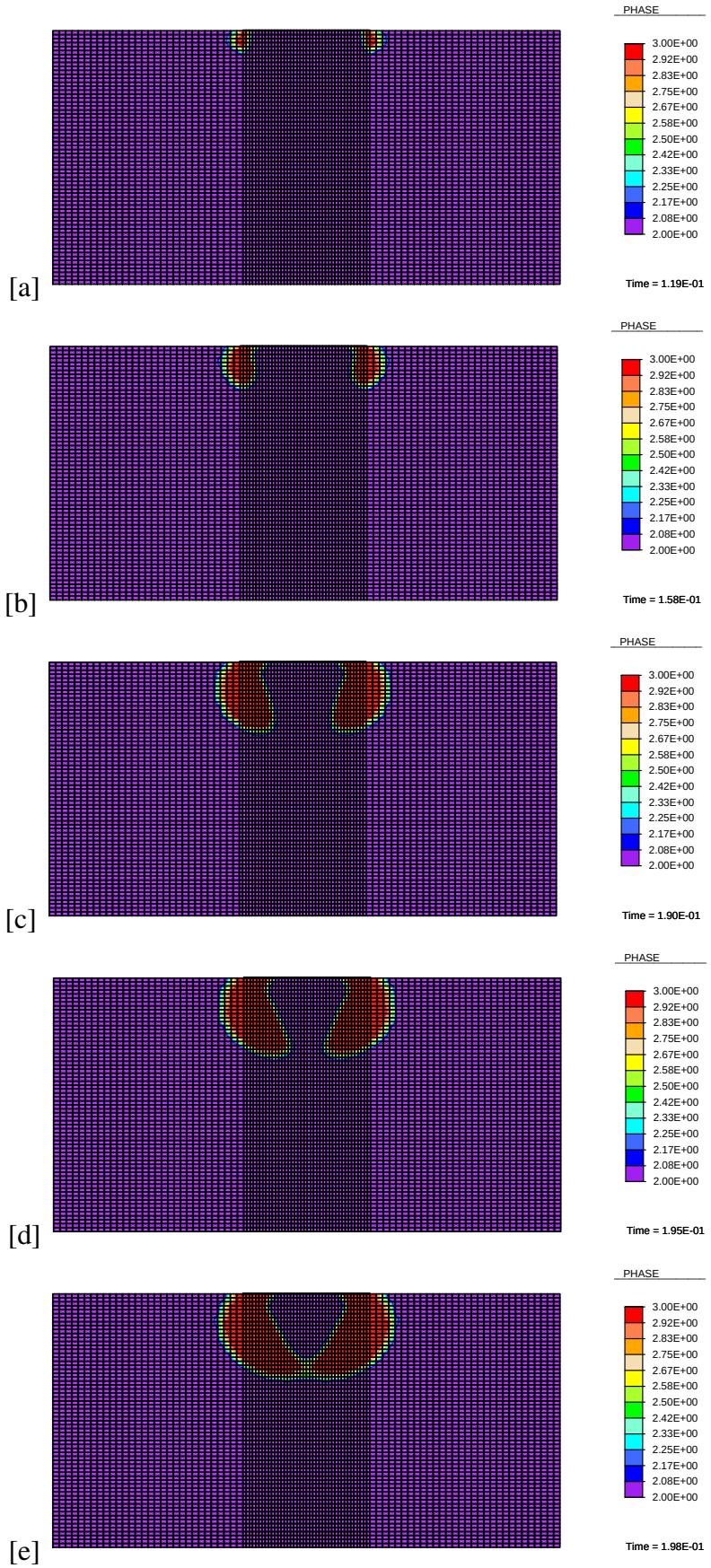

Figure 5.23.: Development of a microstructural zone beneath the indenter in a granular foundation.

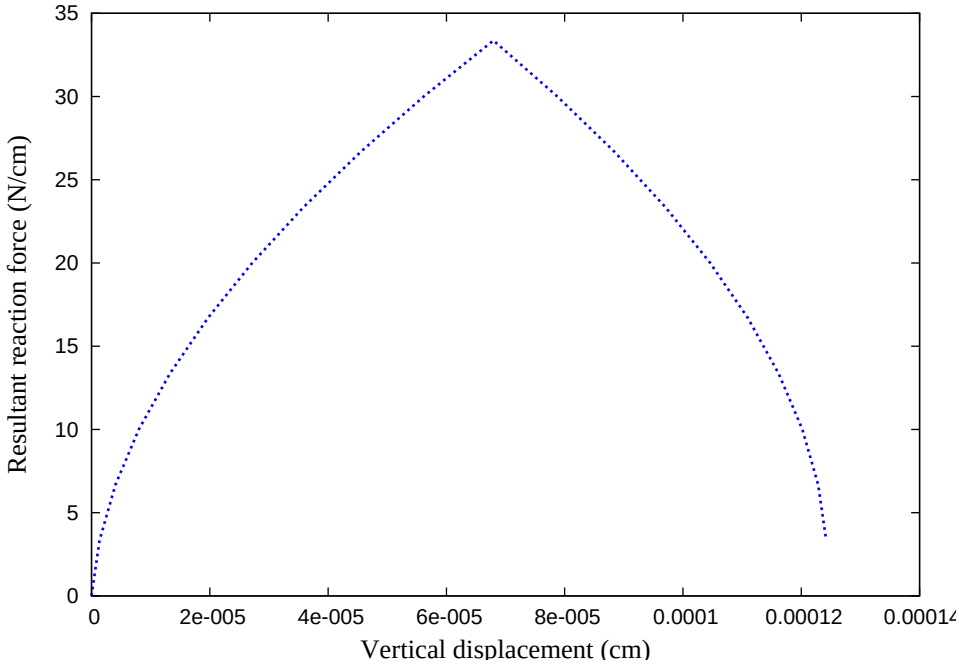

Figure 5.24.: Load-displacement curve exhibiting creep behavior.

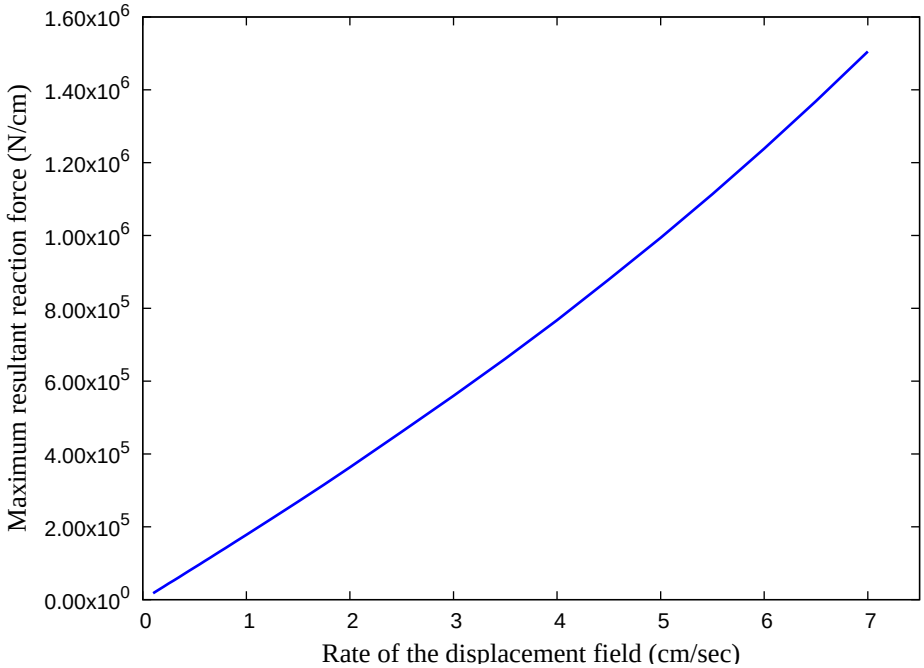

Figure 5.25.: Rate dependent response of the granular foundation under indentation.

Part II.

Variational modeling of detwinning in phase transforming inelastic solids using exact relaxed potential

6. Modeling detwinning of martensitic microstructures

6.1. Detwinning theory of martensitic microstructures

Detwinning (deformation twinning) is one of the important mechanism of inelastic deformation in crystalline solids, among other modes of plastic deformations e.g., plastic slip, dislocations and martensitic phase transformations. The formation of deformation twinns has been observed experimentally by many researchers in a large number of materials. In silicon the exhibition of deformation twinns has been reported in an experimental study by Franks et. al. [FGC95]. Later Churchman et. al. [CGW56] showed that similar to Silicon structure four other A4 (Diamond) crystal structure material namely, germanium, indium antimonide, gallium antimonide and zinc blende can produce deformation twins. Suzuki et. al. [SB58] observed experimentally that the deformation twinning appear in a silver-gold alloy single crystals. These modes of deformation are very common in hexagonal closed-pack (hcp) crystalline solids (for example Ti, Mg etc) and in body-centred cubic (bbc) crystalline solids (for instance Fe,). Although the formation of deformation twins in the face-centered cubic (fcc) crystalline materials (such as Cu, Ni and Al etc) has been reported in 1950s by Blewitt et al. [BCR57] and Suzuki and Barrett [SB58] and later by Venables [Ven61] but seminal experimental work was carried out recently by Christian and Mahajan in the book [CM95], Han et al. [HZWL08], Huang et al. [HWW$^+$06] and Zhu et al. [ZLW12]. The formation of deformation twins in coarse grained Cu metal with fcc crystallographic structure occurs in localized deformation bands and their interactions [HWW$^+$06]. The reason behind this is the presence of high stress field in these bands. Contrary to the observations and investigations of Reed-Hill et al. [RH64], Rohatgi et al. [RVG01] the formation of deformation twins at room temperature and low strain rate in coarse grained fcc metals is also possible [HWW$^+$06]. At low temperatures its observation Cu and Cu-Zn alloys have been reported by Thornton and Mitchell [TM62]. For a comprehensive and most recent review on the deformation twinning in crystalline materials of fcc, bcc and hcp crystallographic structures the reader is referred to the seminal work of Zhu et al. [ZLW12].

Formation of deformation twins (see Figure 6.1 for different types of twinns) is strongly influenced by some microstructural parameters for instance, grain size, stacking-fault energy and dislocation density [EDKD99, HZWL08]. Among other factors that can affect the occurrence of deformation twinns are the strain, strain rate, crystallographic orientation and temperature [BCR57, HZWL08]. For detailed discussion on the factors affecting the formation of deformation twinning in craystallographic materials the reader is referred to the paper [ZLW12]. The significance of studying detwinning can be realized from the fact that it strongly effects the mechanical properties of materials [CM95, ZLW12]. It can play a crucial role in the nucleation of fracture in materials [CM95]. The macroscopic stress-strain response of a crystalline material is significantly influenced with the formation of detwinning modes [ACB04, CM95, ZLW12].

Phase transforming inelastic materials exhibiting microstructures have been modeled using

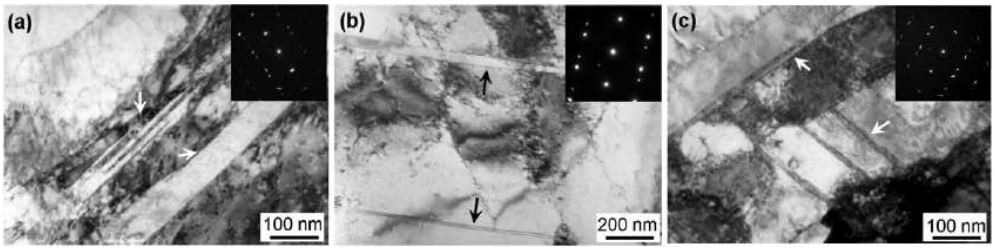

Figure 6.1.: Transmission electron microscopy micrographs of (a) Type I, (b) Type II, (c), Type III deformation twins formed in a Cu single crystal. Reprinted from [HZWL08] with permission of Zhang, Z. F.

energy formulations by many researchers. The energy potential resulting from the construction of these models comes out to be non-quasiconvex in general. Computation of corresponding relaxed energy is not always possible in every situation and therefore there is no general analytical expression for martensitic materials. In the case of an n-variant martensitic material an upper bound to the quasiconvex energy potential of the corresponding non-convex free energy is provided in the works of Govindjee, Hackl and Heinen [GHH07], Govindjee, Mielke and Hall [GMH02] and Hackl and Heinen [HH08]. In the case of two-variant mathematical modeling of martensitic materials has already been discussed in the early works of Ball and James [BJ87, BJ92], Carstensen and Plecháč [CP97] and Kohn [Koh91]. Corresponding to these two-variant martensitic material the two-well energy structure becomes non-convex of which an explicit formula for the relaxed energy was possible [BJ87, BJ92, Koh91]. Here, in a time incremental setting a mathematical model for detwinning microstructures is presented where initially a two phase twinned crystalline microstructure in the material is assumed. Corresponding to each twinned phase there exists an energy potential that can be used to describe the material behavior in deformation. Together, the energy function of the material becomes nonconvex thus allowing microstructures to appear. The analysis of detwinning microstructures is made possible with the derivation of an analytical expression for the partially relaxed energy. The modeling approach is based on energy principles in material modeling where a principle of minimum of dissipation potential is employed in order to compute the equilibrium state of the material.

6.2. Analysis of a simple model for martensitic detwinning

Consider an inelastic crystalline material with two phase martensitic microstructure. The material response can be characterized by assuming a two well energy potential in the energy minimization problem for the description of its equilibrium configuration. For a single well energy structure with continuous energy function on a given domain Ω there is no jump in the deformation gradient $\nabla \mathbf{u}(\mathbf{x})$ for a deformation $\mathbf{u}$. But in the case of two well energy structure there exists a jump in the deformation gradient where energy of the material is divided into two parts, one part is corresponding to the I^{th} martensitic variant and the other part is corresponding to the J^{th} martensitic variant. In such a situation the deformation gradient is written as

$$\nabla \mathbf{u} = \begin{cases} \nabla \mathbf{u}_1(\mathbf{x}) & \text{for } \mathbf{x} \in \Omega_1, \\ \nabla \mathbf{u}_2(\mathbf{x}) & \text{for } \mathbf{x} \in \Omega_2. \end{cases} \tag{6.1}$$

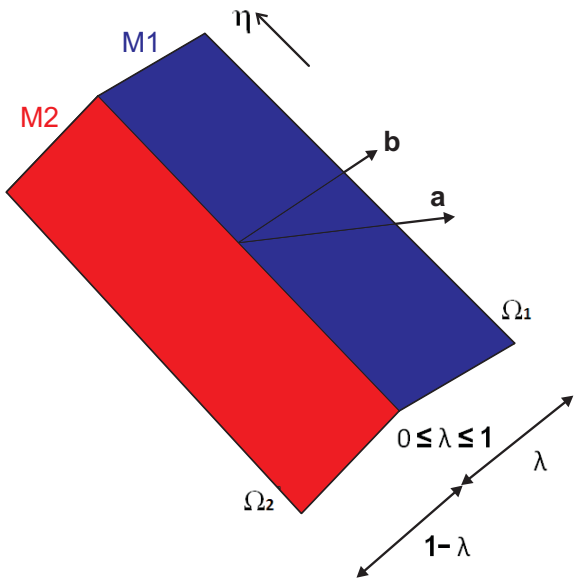

Figure 6.2.: Twinning Elements. The two martensitic variants M1 and M2 respectively having a volume fraction of λ and $1-\lambda$, are differentiated by a twinning plane (dark line) having a normal unit vector $\mathbf{b}$ and a geometric vector $\mathbf{a}$. The shearing direction is represented by η.

The deformation gradient further can be decomposed into rotation and transformation matrices in each of the material domain as follows

$$\nabla \mathbf{u}_1(\mathbf{x}) = \mathbf{Q}_1 \mathbf{U}_{\mathrm{I}}, \quad \nabla \mathbf{u}_2(\mathbf{x}) = \mathbf{Q}_2 \mathbf{U}_{\mathrm{J}}. \tag{6.2}$$

where $\mathbf{U}_{\mathrm{I}}$ is the transformation matrix (also called Bain matrix) corresponding to I^{th} martensitic variant, $\mathbf{U}_{\mathrm{J}}$ is the transformation matrix corresponding to J^{th} martensitic variant, $\mathbf{Q}_1$ and $\mathbf{Q}_2$ are some rotation matrices. Due to this discontinuity in the deformation gradient on the boundary between the domain Ω_1 and Ω_2 of the material body the deformation gradient need to satisfy a compatibility condition known as kinematic compatibility condition or the Hadamard jump condition [Bha01]

$$\nabla \mathbf{u}_1(\mathbf{x}) - \nabla \mathbf{u}_2(\mathbf{x}) = \mathbf{a} \otimes \mathbf{b}, \quad \text{for some vector} \quad \mathbf{a} \text{ and } \quad \mathbf{b} \tag{6.3}$$

where $\mathbf{b}$ must be a unit normal to the twinning plane (see Figure 6.2) which separates the two domains Ω_1 and Ω_2. The equation (6.3) that characterizes the two twins corresponding to the two energy wells is called the twinning equation. With known deformation matrices the solution procedure to the twinning equation can be traced in the lecture notes from Bhattacharya [Bha01]. We study a material which can undergo phase-transformation between two martensitic variants destinguished by transformation strains $\pm\boldsymbol{\varepsilon}_{\mathrm{T}}$. The transformation strains are assumed to be twin-compatible, hence we can write

$$\boldsymbol{\varepsilon}_{\mathrm{T}} = \mathbf{a} \otimes \mathbf{b} + \mathbf{b} \otimes \mathbf{a}, \tag{6.4}$$

where $\mathbf{a}$ and $\mathbf{b}$ are vectors, see [Bha03]. The two variants possess elastic energies of the form

$$\Psi_{\pm}(\boldsymbol{\varepsilon}) = \frac{1}{2}\left(\boldsymbol{\varepsilon} \mp \boldsymbol{\varepsilon}_{\mathrm{T}}\right) : \mathbb{C} : \left(\boldsymbol{\varepsilon} \mp \boldsymbol{\varepsilon}_{\mathrm{T}}\right), \tag{6.5}$$

where $\boldsymbol{\varepsilon}$ is the elastic strain tensor to be determined by

$$\boldsymbol{\varepsilon} = \frac{1}{2}\left(\nabla \mathbf{u} + \nabla \mathbf{u}^{\mathrm{T}}\right), \tag{6.6}$$

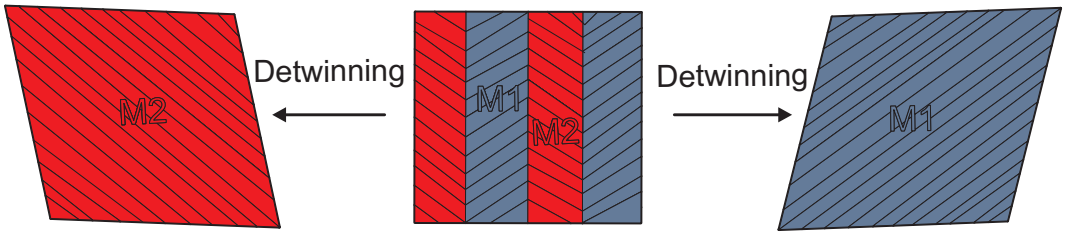

Figure 6.3.: Detwinning microstructure. Initially the material is assumed to have a twin structure with equal amount of volume fractions of each martensitic variant M1 and M2, which upon loading completely transform to a detwinned martensitic variant M1 and upon unloading and changing the loading direction it completely transforms into the detwinned martensitic variant M2.

$\mathbb{C}$ the fourth-order tensor of elastic constants, and ":" denotes contraction over all tensor components. Let us assume now, that the material is in a state characterized by a voulume fraction λ of variant one, and correspondingly by a volume fraction $1-\lambda$ of variant two, with $0 \leq \lambda \leq 1$. The material will adjust strains in a compatible way as to minimize its overall energy. This leads to the so-called relaxed energy

$$\Psi^{\mathrm{rel}}(\boldsymbol{\varepsilon}, \lambda) = \inf_{\substack{\mathbf{c},\mathbf{d};\\ |\mathbf{d}|=1}} \left\{ \lambda\, \Psi_+(\boldsymbol{\varepsilon} + (1-\lambda)\, \mathbf{c} \otimes \mathbf{d}) + (1-\lambda) \Psi_-(\boldsymbol{\varepsilon} - \lambda\, \mathbf{c} \otimes \mathbf{d}) \right\}. \tag{6.7}$$

The minimization can be carried out analytically, for instance consider

$$\Psi(\boldsymbol{\varepsilon}, \lambda, \mathbf{c}, \mathbf{d}) = \lambda\, \Psi_+(\boldsymbol{\varepsilon} + (1-\lambda)\, \mathbf{c} \otimes \mathbf{d}) + (1-\lambda) \Psi_-(\boldsymbol{\varepsilon} - \lambda\, \mathbf{c} \otimes \mathbf{d}). \tag{6.8}$$

After some simple calculations one arrives at

$$\begin{aligned} \Psi(\boldsymbol{\varepsilon}, \lambda, \mathbf{c}, \mathbf{d}) \;=\; & \left(\frac{\lambda}{2} - \frac{\lambda^2}{2}\right) (\mathbf{c} \otimes \mathbf{d}) : \mathbb{C} : (\mathbf{c} \otimes \mathbf{d}) + \frac{1}{2}\, \boldsymbol{\varepsilon} : \mathbb{C} : \boldsymbol{\varepsilon} + \left(\frac{1-2\lambda}{2}\right) \boldsymbol{\varepsilon} : \mathbb{C} : \boldsymbol{\varepsilon}_{\mathrm{T}} \\ & + \left(\frac{1-2\lambda}{2}\right) \boldsymbol{\varepsilon}_{\mathrm{T}} : \mathbb{C} : \boldsymbol{\varepsilon} + \left(\lambda^2 - \lambda\right) (\mathbf{c} \otimes \mathbf{d}) : \mathbb{C} : \boldsymbol{\varepsilon} + \frac{1}{2}\, \boldsymbol{\varepsilon}_{\mathrm{T}} : \mathbb{C} : \boldsymbol{\varepsilon}_{\mathrm{T}} \\ & + \left(\lambda^2 - \lambda\right) \boldsymbol{\varepsilon} : \mathbb{C} : (\mathbf{c} \otimes \mathbf{d}) \end{aligned} \tag{6.9}$$

Using this energy potential one may rewrite the aforementioned minimization problem as

$$\Psi^{\mathrm{rel}}(\boldsymbol{\varepsilon}, \lambda) = \inf_{\substack{\mathbf{c},\mathbf{d};\\ |\mathbf{d}|=1}} \left\{ \Psi(\boldsymbol{\varepsilon}, \lambda, \mathbf{c}, \mathbf{d}) \right\}. \tag{6.10}$$

The stationarity conditions to this problem thus implies $(\mathbf{c} \otimes \mathbf{d}) = 2\boldsymbol{\varepsilon}_{\mathrm{T}}$, and hence the relaxed energy Ψ^{rel} if obtained as

$$\Psi^{\mathrm{rel}}(\boldsymbol{\varepsilon}, \theta) = \frac{1}{2}\, (\boldsymbol{\varepsilon} - \theta \boldsymbol{\varepsilon}_{\mathrm{T}}) : \mathbb{C} : (\boldsymbol{\varepsilon} - \theta \boldsymbol{\varepsilon}_{\mathrm{T}}), \tag{6.11}$$

where for later convenience we introduced the parameter $\theta = 2\lambda - 1$, i.e. it holds $-1 \leq \theta \leq 1$. In a fully elastic regime, the material will also tend to minimize the volume rations for given strain. This leads to the fully relaxed energy

$$\Psi^{\mathrm{rel}}(\boldsymbol{\varepsilon}) = \inf_{\substack{\theta;\\ -1 \leq \theta \leq 1}} \left\{ \Psi^{\mathrm{rel}}(\boldsymbol{\varepsilon}, \theta) \right\}, \tag{6.12}$$

see [Koh91]. In this work, however, we will be interested in the evolution of θ. Thus we will work with the partially relaxed energy in (6.11).

The volume fraction θ being an internal variable accounting for material microstructures. Any change in the microstructure is thus being characterized by a change in θ, which leads to the dissipation of the material energy if this microstructural change is irreversible. This dissipation of the material energy, within the framework of rate-independent inelastic evolution of microstructures [HHK12], is quantified by a dissipation-potential

$$\Delta(\dot{\theta}) = r\,|\dot{\theta}|. \tag{6.13}$$

Here $r > 0$ denotes a material parameter. Since the dissipation potential defined above is homogeneous of degree one, it is therefore convenient to use the minimum-principle of dissipation potential for obtaining the evolution equations instead of deriving them using the principle of maximum dissipation (both the principles in this case are equivalent, see for example Hackl and Fischer [HF08]). Introducing the Lagrange functional

$$\mathcal{L}\left(\boldsymbol{\varepsilon}, \theta, \dot{\theta}\right) = \frac{\mathrm{d}}{\mathrm{d}t}\,\Psi^{\mathrm{rel}}(\boldsymbol{\varepsilon}, \theta) + \Delta(\dot{\theta}), \tag{6.14}$$

one can then determine the evolution of volume fraction θ from the minimum-principle of dissipation potential [HF08]

$$\dot{\theta} = \arg\left\{\min_{\dot{\theta}} \mathcal{L}\left(\boldsymbol{\varepsilon}, \theta, \dot{\theta}\right)\right\}. \tag{6.15}$$

The evolution of θ is thus obtained from the stationarity condition which implies

$$\boldsymbol{\varepsilon}_{\mathrm{T}} : \mathbb{C} : (\boldsymbol{\varepsilon} - \theta\boldsymbol{\varepsilon}_{\mathrm{T}}) \in \operatorname{sign} \dot{\theta}. \tag{6.16}$$

6.2.1. Time-incremental variational formulation

The choice of dissipation potential in (6.13) ensures to work within the framework of rate-independent inelasticiy. In this case it is now possible to consider the aforementioned minimization problem in its time-incremental formulation as introduced by Carstensen et al. [CHM02]. The new formulation reads, for a given set $\left\{\mathbf{u}_n, \theta_n\right\}$ at at time t_n the set of unknowns $\left\{\mathbf{u}_{n+1}, \theta_{n+1}\right\}$ at time t_{n+1} may be obtained via the minimization

$$\left\{\mathbf{u}_{n+1}, \theta_{n+1}\right\} = \arg\left\{\min_{\substack{\mathbf{u}_{n+1}, \theta_{n+1};\\ -1 \le \theta_{n+1} \le 1}} \left\{\int_\Omega \left(\Psi^{\mathrm{rel}}\left(\boldsymbol{\varepsilon}(\mathbf{u}_{n+1}), \theta_{n+1}\right) + r|\theta_{n+1} - \theta_n|\right) dV - \ell(\mathbf{u}_{n+1})\right\}\right\}, \tag{6.17}$$

where $\ell(\mathbf{u}_{n+1})$ is the potential of external forces. The rate-independent inelastic response of many materials is modeled using the concept of condensed energy. Minimization with respect to θ_{n+1} can be carried out directly giving rise to the so-called condensed energy

$$\Psi^{\mathrm{cond}}_{\theta_n}\left(\boldsymbol{\varepsilon}_{n+1}\right) = \inf_{\substack{\theta_{n+1};\\ -1 \le \theta_{n+1} \le 1}} \left\{\Psi^{\mathrm{rel}}\left(\boldsymbol{\varepsilon}_{n+1}, \theta_{n+1}\right) + r|\theta_{n+1} - \theta_n|\right\}. \tag{6.18}$$

In the case $-1 < \theta_{n+1} < 1$ we obtain the stationarity condition

$$\boldsymbol{\varepsilon}_{\mathrm{T}} : \mathbb{C} : (\boldsymbol{\varepsilon}_{n+1} - \theta_{n+1}\boldsymbol{\varepsilon}_{\mathrm{T}}) \in r \operatorname{sign}(\theta_{n+1} - \theta_n) \tag{6.19}$$

giving the update formula for the volume fraction θ_{n+1} as

$$\theta_{n+1} = \theta_n + \frac{1}{\|\boldsymbol{\varepsilon}_{\mathrm{T}}\|^2} \Big(|\boldsymbol{\varepsilon}_{\mathrm{T}} : \mathbb{C} : (\boldsymbol{\varepsilon}_{n+1} - \theta_n \boldsymbol{\varepsilon}_{\mathrm{T}})| - r \Big)_+ \operatorname{sign} \Big(\boldsymbol{\varepsilon}_{\mathrm{T}} : \mathbb{C} : (\boldsymbol{\varepsilon}_{n+1} - \theta_n \boldsymbol{\varepsilon}_{\mathrm{T}}) \Big), \tag{6.20}$$

where $(\bullet)_+$ is the Macaulay bracket and is defined as

$$(f)_+ = \begin{cases} 0 & \text{if } f < 0, \\ f & \text{if } f \geq 0. \end{cases} \tag{6.21}$$

This results into the final expression for the condensed energy in the form

$$\Psi^{\mathrm{cond}}_{\theta_n}(\boldsymbol{\varepsilon}_{n+1}) = \begin{cases} \dfrac{1}{2}(\boldsymbol{\varepsilon}_{n+1} + \boldsymbol{\varepsilon}_{\mathrm{T}}) : \mathbb{C} : (\boldsymbol{\varepsilon}_{n+1} + \boldsymbol{\varepsilon}_{\mathrm{T}}) & \text{for} \quad \theta_{n+1} = -1 \\ \begin{cases} \dfrac{1}{2}(\boldsymbol{\varepsilon}_{n+1} - \theta_n \boldsymbol{\varepsilon}_{\mathrm{T}}) : \mathbb{C} : (\boldsymbol{\varepsilon}_{n+1} - \theta_n \boldsymbol{\varepsilon}_{\mathrm{T}}) \\ \quad - \dfrac{1}{2\|\boldsymbol{\varepsilon}_{\mathrm{T}}\|^2} \left(|\boldsymbol{\varepsilon}_{\mathrm{T}} : \mathbb{C} : (\boldsymbol{\varepsilon}_{n+1} - \theta_n \boldsymbol{\varepsilon}_{\mathrm{T}})| - r \right)^2_+ \end{cases} & \text{for} \quad -1 < \theta_{n+1} < 1 \\ \dfrac{1}{2}(\boldsymbol{\varepsilon}_{n+1} - \boldsymbol{\varepsilon}_{\mathrm{T}}) : \mathbb{C} : (\boldsymbol{\varepsilon}_{n+1} - \boldsymbol{\varepsilon}_{\mathrm{T}}) & \text{for} \quad \theta_{n+1} = 1 \end{cases} . \tag{6.22}$$

Thereby spliting the original minimization problem into two steps. In the first step, a pure elastic problem

$$\{\mathbf{u}_{n+1}\} = \arg \left\{ \min_{\mathbf{u}_{n+1}} \left\{ \int_\Omega (\Psi^{\mathrm{cond}}_{\theta_n}(\boldsymbol{\varepsilon}(\mathbf{u}_{n+1}))\, \mathrm{d}V - \ell(\mathbf{u}_{n+1}) \right\} \right\}, \tag{6.23}$$

is addressed by carrying out the minimization with respect to the displacement field variable $\mathbf{u}_{n+1}$. In the second step, an update (6.20) of the inelastic variable θ_{n+1} is made. Such procedures for modeling the rate-independent inelastic evolution of microstructures has already been adopted by Bartels et al. [BCC$^+$06, BCHH04], Carstensen et al. [CCO08], Conti and Theil [CT05], Lambrecht et al. [LMD03], Mielke [Mie04] and Ortiz and Repetto [OR99].

6.2.2. Radially symmetric case

Consider from now on a radially symmetric case. Denoting the radial coordinate by x and introduce unit-vectors $\mathbf{e}_{\mathrm{n}}$ in radial and $\mathbf{e}_{\mathrm{t}}$ in tangential direction the displacement then takes the form

$$\mathbf{u} = u(x)\, \mathbf{e}_{\mathrm{n}}, \tag{6.24}$$

while the strain becomes

$$\boldsymbol{\varepsilon} = u'(x)\, \mathbf{e}_{\mathrm{n}} \otimes \mathbf{e}_{\mathrm{n}} + \frac{u(x)}{x}\, \mathbf{e}_{\mathrm{t}} \otimes \mathbf{e}_{\mathrm{t}}. \tag{6.25}$$

Thus our energy (6.11) acquire the form

$$\Psi^{\mathrm{rel}}(u, u', \theta) = \frac{\lambda + 2\mu}{2} \left[(u' - a\theta)^2 + \left(\frac{u}{x} + b\theta \right)^2 + c^2 \theta^2 \right], \tag{6.26}$$

where we introduced the abbreviations $a = 2a_1b_1$, $b = -2a_2b_2$ and $c = \sqrt{\frac{4\mu}{\lambda + 2\mu}}|a_1b_2 + a_2b_1|$. Here λ and μ denote the usual Lamé-parameters of isotropic elasticity. The material tensor $\mathbb{C}$ of elastic constants is given by $\mathbb{C} = \mathrm{diag}[C11, C22, C33]$ where $C11 = C22 = \lambda + 2\mu$ and $C33 = \mu$.

Assume that any change in the volume fraction θ will produce dissipation which is quantified by a dissipation-potential

$$\Delta(\dot{\theta}) = r\,|\dot{\theta}|. \tag{6.27}$$

Here $r > 0$ denotes a material parameter (e.g. yield stress) in MPa. Thus we are interested in the evolution of θ. For $-1 < \theta < 1$ the evolution of θ can then be determined from the minimum-principle

$$\dot{\theta} = \arg \left\{ \min_{\dot{\theta}} \left\{ \frac{\mathrm{d}}{\mathrm{d}t} \Psi^{\mathrm{rel}}(\boldsymbol{\varepsilon}, \theta) + \Delta(\dot{\theta}) \right\} \right\}, \tag{6.28}$$

Consider a time incremental formulation as introduced in [CHM02]. For given θ_n at time t_n the values of displacement $\mathbf{u}$ and θ at time t_{n+1} may be obtained via the minimization

$$\{\mathbf{u}, \theta\} = \arg \left\{ \min_{\substack{\mathbf{u}, \theta; \\ -1 \le \theta \le 1}} \left\{ \int_\Omega (\Psi^{\mathrm{rel}}(\boldsymbol{\varepsilon}(\mathbf{u}), \theta) + r|\theta - \theta_n|)\,\mathrm{d}\boldsymbol{x} - \ell(\mathbf{u}) \right\} \right\}. \tag{6.29}$$

Minimization with respect to θ can be carried out directly giving rise to the so-called condensed energy

$$\Psi^{\mathrm{cond}}_{\theta_n}(\boldsymbol{\varepsilon}) = \inf_{\substack{\theta; \\ -1 \le \theta \le 1}} \left\{ \Psi^{\mathrm{rel}}(\boldsymbol{\varepsilon}, \theta) \; + \; r|\theta - \theta_n| \right\}. \tag{6.30}$$

In the case $-1 < \theta < 1$ we obtain the stationarity condition

$$(\lambda + 2\mu)\Big(au' - \frac{b}{x}u - K\theta \Big) \in r\,\mathrm{sign}\,(\theta - \theta_n), \tag{6.31}$$

where $K = a^2 + b^2 + c^2$, it can be solved by implicit or explicit schemes. Implicit solution is obtained by

$$\theta = \theta_n - \frac{2\mathrm{sign}\,(k)}{C11 * K} \Big(|C11(au' - \frac{b}{x}u - K\theta)|\mathrm{sign}\,(k) - r \Big)_+ \mathrm{sign}\,\Big(C11(au' - \frac{b}{x}u - K\theta) \Big), \tag{6.32}$$

where k is given by

$$k = r - \frac{C11 * K}{2}|\theta - \theta_n|. \tag{6.33}$$

whereas explicit solution is given by

$$\theta = \theta_n + \frac{1}{C11 * K} \Big(|C11(au' - \frac{b}{x}u - K\theta_n)| - r \Big)_+ \mathrm{sign}\,\Big(C11(au' - \frac{b}{x}u - K\theta_n) \Big). \tag{6.34}$$

Finally using explicit solution for θ we arrive at the condensed energy

$$\Psi^{\mathrm{cond}}_{\theta_n}(u,u') = \begin{cases} \dfrac{C11}{2}\left[(u'+a)^2+(\dfrac{u}{x}-b)^2+c^2\right] & \text{for} \quad \theta=-1 \\ \dfrac{C11}{2}\left[(u'-a\theta_n)^2+(\dfrac{u}{x}+b\theta_n)^2+c^2\,\theta_n^2\right]- & \\ \dfrac{1}{2C11*K}\left(|C11(au'-\dfrac{b}{x}u-K\theta_n)|-r\right)_+^2 & \text{for} \quad -1<\theta<1 \\ \dfrac{C11}{2}\left[(u'-a)^2+(\dfrac{u}{x}+b)^2+c^2\right] & \text{for} \quad \theta=1 \end{cases} \tag{6.35}$$

Taking explicit solution (6.34) of (6.31) into account and having condensed energy (6.35) at hand we can split our elastoplastic problem into two steps. The displacements $\mathbf{u}$ at time t_{n+1} are computed first for given θ_n by

$$\{\mathbf{u}\} = \arg\left\{\min_{\substack{\mathbf{u};\\ -1\le\theta\le1}}\left\{\int_\Omega \Psi^{\mathrm{cond}}_{\theta_n}\left(\boldsymbol{\varepsilon}\left(\mathbf{u}\right),\theta_n\right)\,\mathrm{d}\boldsymbol{x}-\ell\left(\mathbf{u}\right)\right\}\right\}. \tag{6.36}$$

then an update of internal variable (volume fraction θ) is calculated using equation (6.34). Without affecting the stability of the algorithm presented above we use θ_n in place of θ in (6.36).

Stationarity conditions and regimes

In order to study various properties of solutions of the variational problem introduced let us also establish the stationarity condition for variation with respect to $\mathbf{u}$. If we assume $\ell(\mathbf{u})$ to be dependent on $\mathbf{u}$ only through its values at the boundary we obtain

$$u''-\frac{1}{x^2}\,u = a\theta'+\frac{b}{x}\,\theta. \tag{6.37}$$

Let now (u,θ) denote a minimizer of the incremental problem for given θ_0 and boundary-data. Then we say:

(u,θ) is in **regime 1** at the point x, if $\theta=\theta_0$ holds in an environment of x.

(u,θ) is in **regime 2** at the point x, if $\theta=-1$ holds in an environment of x or $\theta=1$ holds in an environment of x.

(u,θ) is in **regime 3** at the point x, if $\theta\neq\theta_0$ and $\theta\neq\pm1$ holds in an environment of x.

In physical terms, phase/transformations occur in regime 3 only. Regime 2 corresponds to homogeneous material, while in regime 1 the driving forces are too small to overcome dissipation.

7. Numerical results

This chapter deals with the presentation of numerical results obtained from the numerical simulations of the rate-independent inelastic detwinning material model by using finite element method.

7.1. Numerical results from the detwinning material model

7.1.1. Computational results for a radially symmetric case

Consider a material consisting of an annular domain, initially with equally distributed martensitic variants in it. The inner radius r_0 is assumed to be 20mm and the outer radius r_1 of the annular domain is taken to be 160mm. The boundary conditions are assumed such that the problem becomes axially symmetric. This reduces the two dimensional boundary value problem into one dimensional boundary value problem. In this case, only a radial line is modeled and the distribution of the martensitic variants is analyzed. For numerical computations the geometry is implemented using finite element method, where the radial line is discretized into one hundred finite elements. Each element is using two quadrature points for the approximation of the unknown displacement field within the element. The boundary conditions states

$$u'(r_0) = 0, \qquad u(r_1) = u_p, \tag{7.1}$$

where u_p is the prescribed displacement at each time step. The time step size is taken to be $\delta t = 1.0 \times 10^{-3}$sec. The transformation strain vector is computed using the vectors

$$a = (0.37335238, 0.241830519) \quad \text{and} \quad b = \frac{1}{\sqrt{2}}(1.0, 1.0), \tag{7.2}$$

according to formula in equation (6.4). Initially the material is twinned with an equal volume fraction each of the two phases, i.e. initially $\theta_0 = 0.0$. The other material parameters are E $= 2.0 \times 10^3$ MPa, $\nu = 0.3$, r $= 1.0 \times 10^2$ MPa.

In Figure 7.1 column 1 shows the change in volume fraction θ over the radial line in tension test during loading (top figure) and unloading (bottom figure) while column 2 shows the change in volume fraction θ in compression test during loading (top figure) and unloading (bottom figure). From the first column (top figure) it is seen that the initially equally distributed twinns are completely detwinned at $t = 5$sec where the detwinned martensitic phase with $\theta = 1$ is stable. From the second column (top figure) it can be observed that during compression the material changes its phase and at $t = 15$sec it completely transformed into a second detwinned martensitic variant where the material is stable in the case of $\theta = -1$.

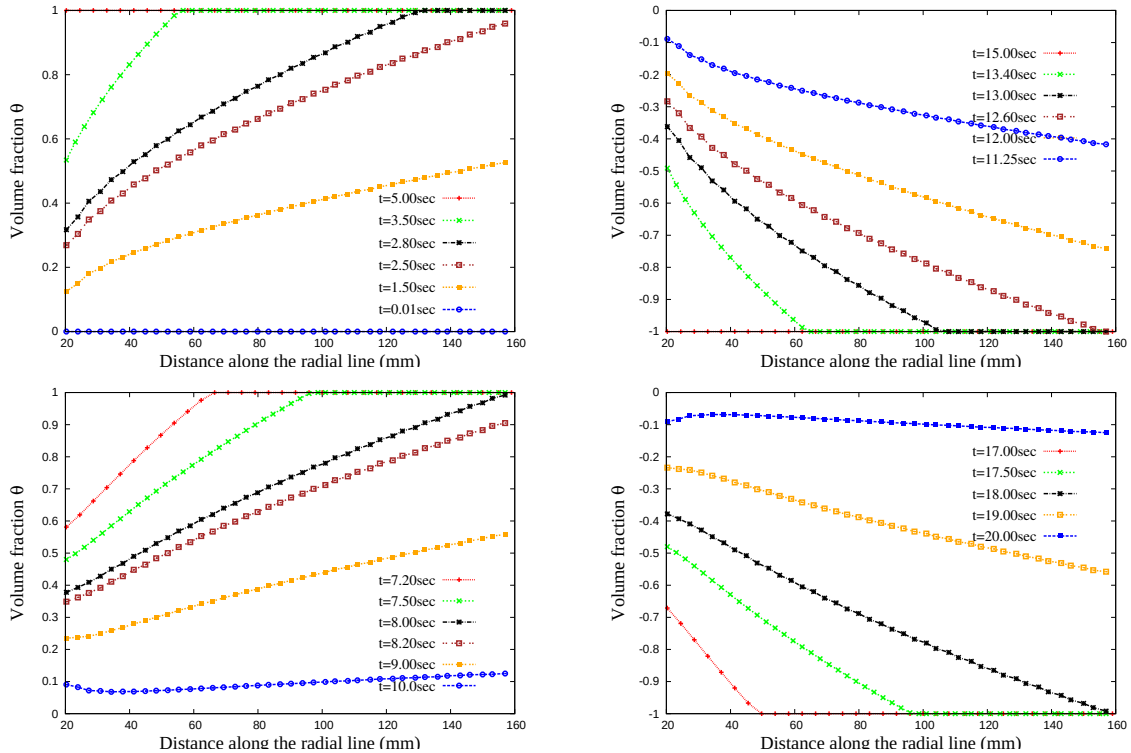

Figure 7.1.: Distribution of volume fraction over the radial line during loading and unloading cycle in tension-compression test.

7.1.2. Two-dimensional numerical simulations of detwinning

A single crystal $\Omega = [0,1]^2$ of Nickel-Titanium (NiTi) alloy in two dimension is used for a cubic to monoclinic-I transformation test with two martensitic variants initially equally distributed over the domain Ω. We consider a two well energy formulation where the transformation strain characterizes the two martensitic detwinned phases. Transformation strain is further depending on the transformation matrices which transform the austenite lattice to the martensite lattice. The material is undergoing cubic to monoclinic transformation where the axis of the monoclinic symmetry corresponds to a $\langle 110 \rangle_{\text{cubic}}$ direction. To compute the matrix of transformation strain for the numerical simulation of the model on the selected domain the values of vectors $\mathbf{a}$ and $\mathbf{b}$ are required. These values are calculated according the procedure mentioned in the book by Bhatacharya [Bha03]. Here an example is presented for the demonstration on the computation of these values. Consider two martensitic variants $\mathbf{U}_I$ and $\mathbf{U}_J$ in a material undergoing cubic to monoclinic-I transformation. Then according to [Bha03] (see Table 4.3) for $I = 1$ and $J = 5$ these bain matrices are given by

$$U_1 = \begin{pmatrix} \gamma & \epsilon & \epsilon \\ \epsilon & \alpha & \delta \\ \epsilon & \delta & \alpha \end{pmatrix}, \quad U_5 = \begin{pmatrix} \alpha & \epsilon & \delta \\ \epsilon & \gamma & \epsilon \\ \delta & \epsilon & \alpha \end{pmatrix}. \tag{7.3}$$

where the values of α, γ, δ and ϵ for the Ni-49.75at.%Ti shape memory alloy are given (see in [Bha03]) as 1.0243, 0.9563, 0.058 and -0.0427 respectively. These two martensitic variants form twinn. To calculate the twinning elements we proceed as follows, take $\mathbf{U}_1$ and choose $\mathbf{R}$ to be a 180° rotation matrix (In the point group (see Table 3.1 in [Bha03]) of a simple cubic lattice) about a vector $\hat{\mathbf{e}} = \frac{1}{\sqrt{2}}(1,-1,0)^T$ (which is a plane of symmetry in the

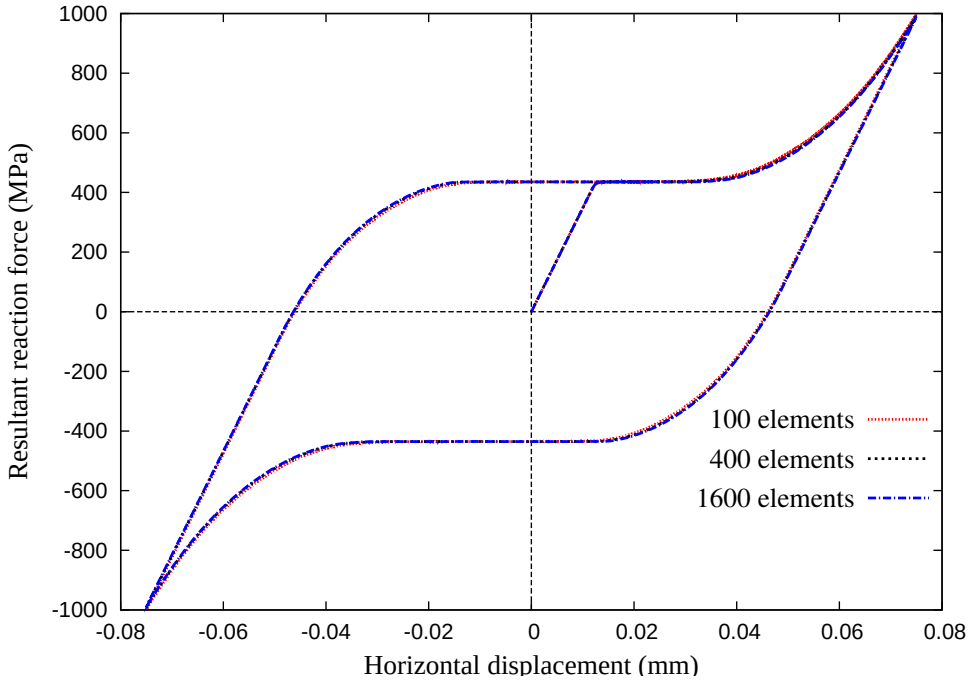

Figure 7.2.: Load-displacement curves with different mesh size.

austenite lattice) then with

$$\mathbf{R} = -\mathbf{I} + 2\,\hat{\mathbf{e}}_1 \otimes \hat{\mathbf{e}}_1 \quad \text{where} \quad \hat{\mathbf{e}}_1 = (1,0,0)^T \tag{7.4}$$

it is now easy to verify that

$$\mathbf{R}^T\mathbf{U}_1\mathbf{R} = \mathbf{U}_5. \tag{7.5}$$

Hence, both $\mathbf{U}_1$ and $\mathbf{U}_5$ form twinn and the solution of the twinning equation

$$\mathbf{Q}\mathbf{U}_5 - \mathbf{U}_1 = \mathbf{a} \otimes \mathbf{b}, \tag{7.6}$$

is given by [Bha03]

$$\mathbf{b} = \hat{\mathbf{e}}, \quad \mathbf{a} = 2\left(\frac{\mathbf{U}_1^{-T}\hat{\mathbf{e}}}{\left|\mathbf{U}_1^{-T}\hat{\mathbf{e}}\right|^2} - \mathbf{U}_1\hat{\mathbf{e}}\right), \tag{7.7}$$

which after simple calculations are obtained as

$$\mathbf{b} = \frac{1}{\sqrt{2}}(1,-1,0)^T, \quad \mathbf{a} = (0.0814, 0.1161, 0.2835)^T. \tag{7.8}$$

Other twinning modes (see Table 5.1 in [Bha03]) can also be computed in a similar fashion. The transformation strain (6.4) thus becomes

$$\boldsymbol{\varepsilon}_{\mathrm{T}} = \frac{1}{2}\left(\mathbf{a} \otimes \mathbf{b} + \mathbf{b} \otimes \mathbf{a}\right). \tag{7.9}$$

The load-displacement curves from Figure 7.2 shows a quasiplastic (also called pseudo-plastic) material response. The analysis is performed with three different meshes where the corresponding material domain is discretized into a 100, 400 and 1600 elements. It can be

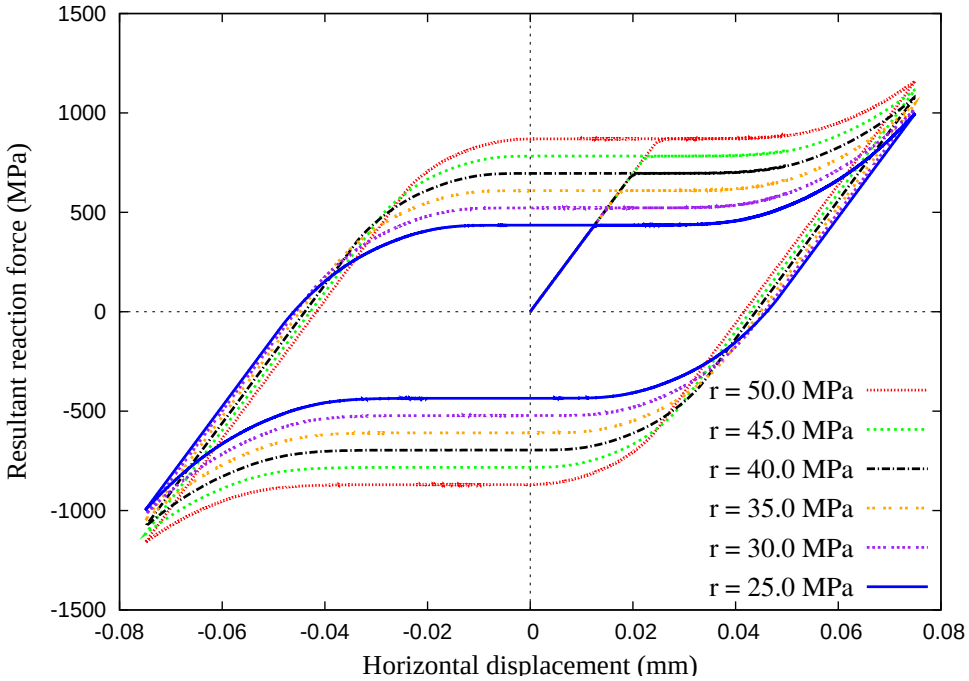

Figure 7.3.: Load-displacement curves in tension-compression test for varying values of the material parameter r.

seen from the Figure 7.2 that the solution is not depending on the discretization of the domain and hence the proposed detwinning model exhibit mesh independent results. The red colored part of the material in Figure 7.4 (First column) is corresponding to the completely detwinned first martensitic variant, obtained during the tensile test. The part of the material which is shaded with the purple color code is corresponding to the homogeneously transformed material which is assumed initially having twinn phases with equal volume ratios. The remaining part of the material/mesh with other than the purple and red colored code is corresponding to the phase where the transformation is taking place. In second column, part of the mesh shaded with the purple color code is corresponding to the second detwinned martensitic variant. The part of the material shaded with the red color code is corresponding to the homogeneously transforming phase with initially assumed equally distributed twinn martensitic phases. The remaining part of the mesh is experiencing a phase transition from martensitic twinn phase to martensitic detwinned second variant. Inhomogeneous boundary conditions are used where at the left boundary of the material both the displacement components in horizontal and vertical directions are fixed whereas all the nodes at the other parts are free. A fixed displacement of 0.075mm is applied at the right side boundary of the material. The material parameters used in the simulations are mentioned in the table 7.1. The

Table 7.1.: Material parameters for the analysis of detwinning in a NiTi alloy.

E	ν	r
(MPa)	-	(MPa)
3.0×10^4	0.33	2.5×10^1

solution vectors $\mathbf{a}$ and $\mathbf{b}$ of the twinning equation (7.6) are taken from equation (7.8). The time step size is chose to be $\delta t = 1.0 \times 10^{-3}$ sec. Initially the material is assumed to be in

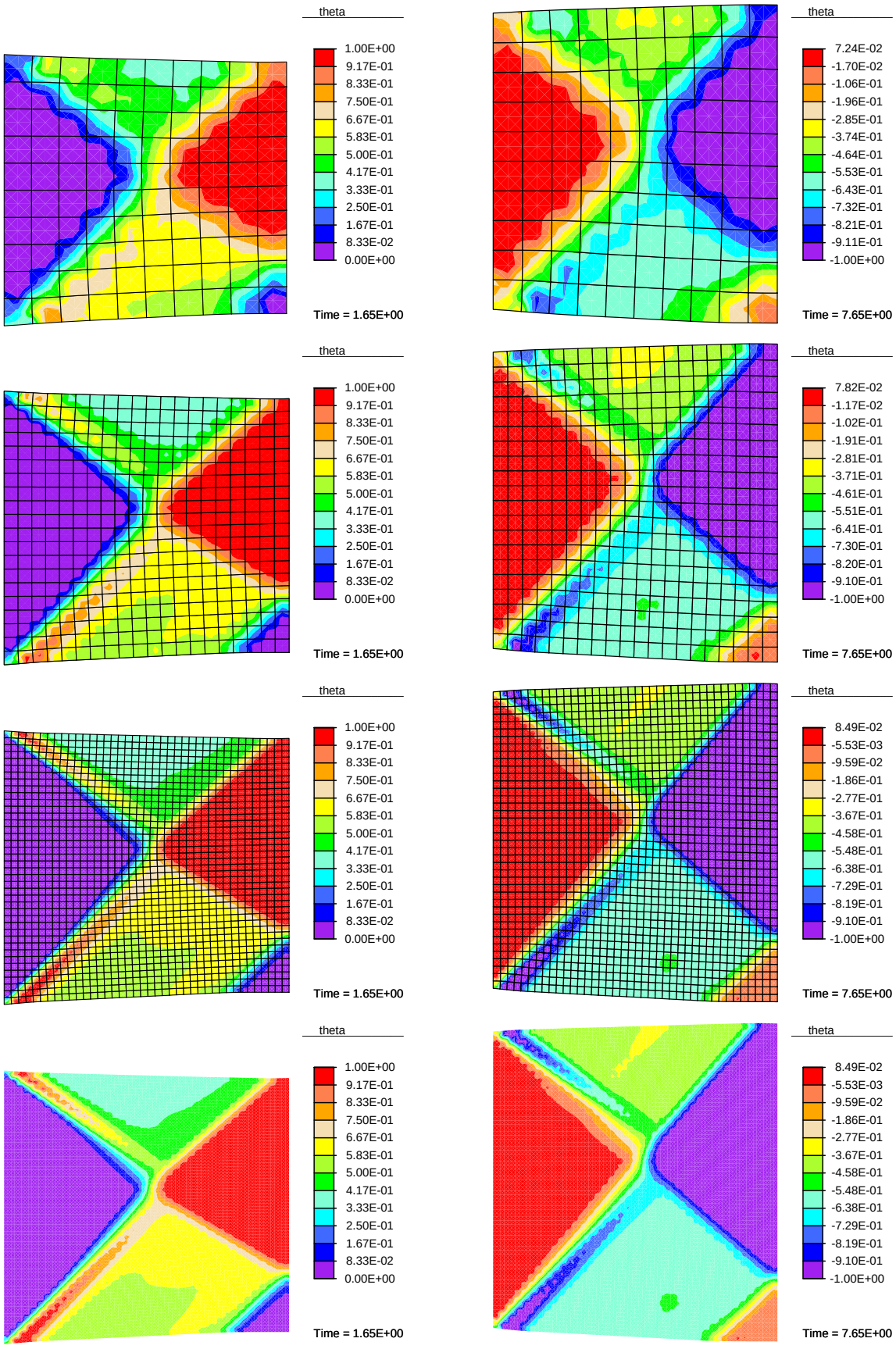

Figure 7.4.: Distribution of the volume fraction θ over the material domain in tension (first column) and in compression (second column).

a state where each of the martensitic variant is equally distributed over the material domain, this is assured with the assumption that $\theta_\circ = 0.0$ at the beginning of the load step.

8. Conclusion and Outlook

8.1. Conclusion

In this thesis, an investigation of two complementary cases of material microstructures is presented. In the first case, we studied the formation of rotational microstructures in granular media, whereas, in the second case, detwinning of martensitic microstructure is analyzed. In both the cases, we are interested in finding the minimizers of the corresponding non-quasiconvex energy minimization problems.

In nature granular materials exhibit distinct patterns under deformation. The formation of these patterns is strongly influenced by counter-rotations of the interacting particle at the microscale. These counter-rotations of the particles influence the macroscopic shear and hence the overall material behavior. Therefore an energy potential taking into consideration the interparticle interactions can be devised.

We formulate an interaction energy potential accounting for this microstructural phenomenon at the continuum scale. The proposed interaction energy potential does not only bridges the gap between microstructural features and the macroscopic behavior of granular materials but also enabled us to characterize the different microstructural regimes in the material. The rotational microstructures in granular materials are modeled by employing the calculus of variations, specifically the concept of energy relaxation. Within the framework of Cosserat continuum and in the case of elastic isotropic material the free energy is enriched with the proposed interaction energy potential. The resulting total energy potential came out to be non-quasiconvex, when enters in the energy minimization problem does not guarantee all possible field fluctuations as minimizers. Hence as a result the microstructure occurs in both the displacement and micro-rotation field.

By employing the direct methods in the calculus of variations it turns out to be possible to derive an exact quasiconvex envelope of the energy potential. It is worth mentioning that there are no further assumptions necessary to derive this quasiconvex envelope. The computed relaxed potential yields all the possible displacement and micro-rotation field fluctuations as minimizers. We conclude with the result that the granular material behavior can be divided into three different regimes. Two of the material regimes are exhibiting microstructures in rotational and translational motions of the particles, respectively, and the third one is corresponding to the case where there is no internal structure of the deformation field. The principle of minimum of potential energy is followed to model the elastic response of granular materials with microstructures within the framework of Cosserat continuum. Whereas, by following the principle of minimum of dissipation potential the rate-dependent response of the granular materials with microstructures is modeled within the framework of Cosserat viscoplasticity.

The proposed models are analyzed with different numerical tests where the numerical com-

putations are based on the finite element method. Distribution of microstructure in a high stress regime of the material, onset of localized deformations, microstructure development in a granular foundation beneath the indenter has been successfully predicted using the proposed theory. Moreover, It has been shown that all the material phases can coexist in a material under shear in a Couette shear cell. The numerical analysis performed do not only demonstrate on the possible use of the proposed theory and material models but also draw attention towards its different possible applications. Further, it has been shown that the exact relaxed potential obtained in this case is enable enough to demonstrate on both the extended and localized microstructures in granular materials. Also the mesh independence of the minimizing deformations has been shown.

In the second case, a simple model for the detwinning of martensitic microstructure in phase transforming inelastic crystalline materials is presented. The material can undergo a phase transition between two martensitic variants, Corresponding to these martensitic variants and their related martensitic material phases there is a two-well energy potential for the characterization of material behavior and the description of its equilibrium configuration. Due to the non-convex nature of the two-well energy potential relaxation methods are employed to compute an analytical expression for the partially relaxed energy. To quantify for the inelastic response a rate-independent dissipation function is introduced. The modeling approach is based on the energy principles (principle of minimum of potential energy and principle of minimum of dissipation potential) where an incremental variational formulation of the proposed model is presented for the simulation and investigation of detwinning microstructure. Numerical computations are performed using finite element method to demonstrate on the distribution of detwinning microstructure in a single crystal. Moreover, it has been shown that the minimizers of the corresponding energy minimization problem are mesh independent.

8.2. Outlook

There are many possible directions to be investigated and open issues to be addressed in the future. Among them some are outlined here in this Section.

The theory presented in the first part of the thesis is based on small-strain formulation where linearized strain measures are considered. Not in every physical situation this approach is applicable, therefore to model the more realistic behavior of granular materials one can think of nonlinear strain measures and to account for finite rotations of the granular particles its possible extension to the case of finite strains. The proposed models are based on the framework of pure elasticity and pure vicsoplasticity within the context of Cosserat continuum. These models can be extended using an elasto-plastic or elasto-vicsoplastic framework with the specification of a suitable dissipation potential for these materials.

It is difficult to compare the results of the proposed theory with the experimental observations, since the Cosserat elastic constants are not known for most of the granular materials. The complexity arises in this situation as the two additionally introduced material parameters in the interaction energy potential are also unidentified constants. One possible direction for future work can be to identify these material constants for the better description of the material behavior and possible comparison with the observed experimental results. Especially in the case of geomaterials some additional material parameters (for instance, frictional angle,

dilatancy angle and void ratio) needed to be incorporated in the theory for better prediction on the response of these materials.

One possible investigation can be on the interaction potential energy itself. Since the material parameters related to the particle size and frictional modulus are constant, in which the frictional modulus can be considered as variable in order to comply a more realistic situation with the deforming granular medium. This changing parameter will then play a role of internal variable and therefore an evolution equation will be required to compute it. This can be achieved by choosing a suitable dissipation potential and using the principle of minimum of dissipation potential. Then, in this case the more realistic dissipative nature of granular materials is possible to predict.

In the second part of the thesis, it is difficult to compute an exact relaxed potential for n-martensitic variant case, however within the present context the proposed model can be extended to account for rate-dependent response of the phase transforming inelastic solids with the introduction of a suitable rate-dependent dissipation function.

Bibliography

[AAE10] J. Altenbach, H. Altenbach, and V. A. Eremeyev. On generalized cosserat-type theories of plates and shells: a short review and bibliography. *Arch. Appl. Mech.*, 80:73–92, 2010.

[ACB04] K. E. Allain, J. P. Chateau, and O. Bouaziz. A physical model of the twinning-induced plasticity effect in a high manganese austenitic steel. *Mater. Sci. Eng. A*, 387:143–147, 2004.

[ACL94] W.B. Anderson, C.P. Chen, and R.S. Lakes. Experimental study of size effects and surface damage of polymethacrylimide closed-cell foam. *Cellular Polymers*, 13:01–15, 1994.

[AF84] E. Aacerbi and N. Fusco. Semicontinuity problems in the calculus of variations. *Arch. Rational Mech. Anal.*, 86:125–145, 1984.

[AK60] E. L. Aero and E. V. Kuvshinski. Fundamental equations of the theory of elastic media with rotationally interacting particles. *Fizika Tverdogo Tela*, 2:1399–, 1960.

[AL94] W.B. Anderson and R.S. Lakes. Size effects due to cosserat elasticity and surface damage in closed-cell polymethacrylimide foam. *Journal of Materials Science*, 29:6413–6419, 1994.

[AMVH+06] F. Alonso-Marroquín, I. Vardoulakis, H.J. Herrmann, D. Weatherley, and P. Mora. Effect of rolling on dissipation in fault gouges. *Phys. Rev. E*, 74(3):301–306, 2006.

[AP01] E. Aranda and P. Pedregal. Numerical approximation of non-homogeneous, non-convex vector variational problems. *Numer. Math.*, 89:425–444, 2001.

[AS06] H. Arslan and S. Sture. The importance of length scale in computational modelin go granular materials. *Proceedings of GeoCongress*, pages 1–6, 2006.

[AT02] S.D.C. Walsh A. Tordesillas. Incorporating rolling resistance and contact anisotropy in micromechanical models of granular media. *Powder Technology*, 124:106–111, 2002.

[AT09] I. Aranson and L. Tsimring. *Granular Patterns*. Oxford University Press, 2009.

[AVA06] M. I. Alsaleh, G. Z. Voyiadjis, and K. A. Alshibli. Modeling strain localization in granular materials using micropolar theory: Mathematical formulations. *Int. J. Numer. Anal. Meth. Goemech.*, 30:1501–1524, 2006.

[Bag41] R. A. Bagnold. The physics of blown sand and desert dunes. *London: Methuen*, 1941.

[Bal76] J. M. Ball. Convexity conditions and existence theorems in nonlinear elasticity. *Arch. Rational Mech. Anal.*, 63(4):337–403, 1976.

[Bal88] J. M. Ball. *A version of the fundamental theorem for Young measures, In: Partial Differential Equations and Continuum Models of Phase Transitions*. Springer, d. serre, ed. edition, May 1988.

[Bar94] J.P. Bardet. Observation on the effects of particle rotations on the failure of idealized granular materials. *Mech. Mater.*, 18(2):159–182, 1994. Special Issue on Microstructure and Strain Localization in Geomaterials.

[Bar01] S Bartels. *Numerical Analysis of Some Non-Convex Variational Problems*. 2001. PhD thesis.

[BC94] B. Brighi and M. Chipot. Approximated convex envelope of a function. *SIAM J. Numer. Anal.*, 31:128–148, 1994.

[BCC+06] S. Bartels, C. Carstensen, S. Conti, K. Hackl, U. Hoppe, and A. Orlando. *Relaxation and the computation of effective energies and microstructures in solid mechanics, In Analysis, modeling and simulation of multiscale problems*, pages 197–224. Springer, 2006.

[BCHH04] S. Bartels, C. Carstensen, K. Hackl, and U. Hoppe. Effective relaxation for microstructure simulations: algorithms and applications. *Comp. Meth. Appl. Mech. Eng.*, 193:5143–5175, 2004.

[BCR57] T. H. Blewitt, R. R. Coltman, and J. K. Redman. Low-temperature deformation of copper single crystals. *J. Appl. Phys.*, 28(6):651–660, 1957.

[BD88] D. Besdo and H.-U. Dorau. Zur modellierung von verbundmaterialien als homogenes cosserat-kontinuum. *ZAAM*, 68:T153–T155, 1988.

[BH99] E. Bauer and W. Huang. *Numerical study of polar effects in shear zones. In: Pande and Pietruszczak and Schweiger (eds.), Numerical Models in Geomechanics-NUMOG VII. Rotterdam: A.A. Balkema*, pages 133–138. 1999.

[BH01] E. Bauer and W. Huang. *Numerical investigation of strain localization in a hypoplastic Cosserat material under shearing. In 10th International Conference on Computer Methods and Advances in Geomechanis, IACMAG, Desai (ed.). Balkema Press: Tucson, Arizona*, pages 525–528. 2001.

[Bha01] K. Bhattacharya. *Theory of martensitic microstructure and the shape-memory effect*, 2001.

[Bha03] K. Bhattacharya. *Microstructure of Martensite*. Oxford University Press, Oxford, 2003.

[BJ87] J. M. Ball and R. D. James. Fine phase mixtures as minimizers of energy. *Arch. Rational Mech. Anal.*, 100:13–52, 1987.

[BJ92] J. M. Ball and R. D. James. Proposed experimental test of a theory of fine microstructure and the two well problem. *Philos. Trans. Roy. Soc. London Ser. A*, 338:389–450, 1992.

[BJS97] K. Bhattacharya, R. D. James, and P. J. Swart. Relaxation in shape memory alloys, part i: Mechanical model, ; part ii: Thermo-mechanical model and proposed experiments. *Acta Materialia*, 45(11):4547–4560; 4561–4568, 1997.

[BL03] P.M. Buechner and R.S. Lakes. Size effects in elasticity and viscoelasticity of bone. *Biomechanics and Modeling in Mechanobiology*, 1(4):295–301, 2003.

[BMD87] C.S. Breed, J.F. McCauley, and P.A. Davis. Sand sheets of the eastern sahara and ripple blankets on mars. *Geological Society, London*, 35:337–359, 1987.

[BP04] S. Bartels and A. Prohl. Multiscale resolution in the computation of crystalline microstructure. *Numer. Math.*, 96:641–660, 2004.

[BS89] J. Badur and H. Stumpf. On the influence of e. and f. cosserat on modern continuum mechanics and field theory. *Mitteilungen aus dem institut für mechanik*, (72), December 1989.

[CC09] E. Cosserat and F. Cosserat. Théorie des corps déformables (theory of deformable bodies). 1909.

[CC92] M. Chipot and C. Collins. Numerical approximation in variational problems with potential wells. *SIAM J. Numer. Anal.*, 29(4):1002–1019, 1992.

[CCM01] R. Chambon, D. Caillerie, and T. Matsuchima. Plastic continuum with microstructure, local second gradient theories for geomaterials: localization studies. *Int. J. of Solids Struct.*, 38:8503–8527, 2001.

[CCO08] C. Carstensen, S. Conti, and A. Orlando. Mixed analytical-numerical relaxation in finite single-slip crystal plastictiy. *Continuum Mech. Therm.*, 20(5):275–301, 2008.

[CDK09] S. Conti, G. Dolzmann, and C. Klust. Relaxation of a class of variational models in crystal plasticity. *Proc. R. Soc. A*, 465:1735–1742, 2009.

[CGW56] A. T. Churchman, G. A. Geach, and J. Winton. Deformation twining in materials of the a4 (diamond) crystal structure. *Proc. R. Soc. Lond. A*, 238:194–203, 1956.

[CH05] C.S. Chang and P.-Y. Hicher. An elasto-plastic model for grnaular materials with microstructural consideration. *Int. J. Solids Struct.*, 42:4258–4277, 2005.

[Chi99] M. Chipot. The appearance of microstructures in problems with incompatible wells and their numerical approach. *Numer. Math.*, 83:325–352, 1999.

[CHM02] C. Carstensen, K. Hackl, and A. Mielke. Nonconvex potentials and microstructures in finite-strain plasticity. *Proc. R. Soc. Lond. A*, 458:299–317, 2002.

[CHO07] S. Conti, P. Hauret, and M. Ortiz. Conurrent multiscale computing of deformation microstructure by relaxation and local enrichment with application to single-crystal plasticity. *Multiscale Model. Simul.*, 6(1):135–157, 2007.

[Cia88] P.G. Ciarlet. *Mathematical Elasticity Three-Dimensional Elasticity*. Elsevier Science Publishers B.V, Amsterdam, 1988.

[CKL91] C. Collins, D. Kinderlehrer, and M. Luskin. Numerical approximation of the solution of a variational problem with a double well potential. *SIAM J. Numer. Anal.*, 28(2):321–332, 1991.

[CL95] M. Chipot and V. Lécuyer. *Analysis and computations on the four well problem, In Nonlinear Analysis and Applications*, volume 7 of *GAKUTO International Series*. 1995.

[CLR93] C. Collins, M. Luskin, and J. Riordan. *Microstructure and Phase Transition*, volume 54, pages 51–57. Berlin Hiedelberg New York: Springer, 1993.

[CM91] C.S. Chang and L. Ma. A micromechanical-based micro-polar theory for deformation of grnaular solids. *Int. J. Solids Structures*, 28(1):67–86, 1991.

[CM92] C.S. Chang and L. Ma. Elastic material constants for isotropic granular solids with particle rotation. *Int. J. Solids Structures*, 29(8):1001–1018, 1992.

[CM95] J. W. Christian and S. Mahajan. *Deformation twinning*, volume 39. Elsevier, 1995.

[CO05] S. Conti and M. Ortiz. Dislocation microstructures and the effective behavior of single crystals. *Arch. Rational Mech. Anal.*, 176:103–147, 2005.

[Col90] C. Collins. *Computation and analysis of twinning in crystalline solids*. PhD thesis, University of Minnesota, 1990.

[Cou76] C. A. Coulomb. Essai sur une application des regles des maximas et minmas a quelques problemes de statique relatifs a l'architecture. *Mem. Acad. Roy. Pres.*, 7:343–382, 1776.

[CP97] C. Carstensen and P. Plecháč. Numerical solution of the scalar double-well problem allowing microstructure. *Math. Comp.*, 66(219):997–1026, 1997.

[CR97] C. Carstensen and T. Roubíček. *Numerical approximation of young measures in non-convex variational problems, Tech. Rep.* Universität Kiel, 1997.

[CR00] C. Carstensen and T. Roubíček. Numerical approximation of young measures in non-convex variational problems. *Numer. Math.*, 84:395–415, 2000.

[CT05] S. Conti and F. Theil. Single-slip elastoplastic microstructures. *Arch. Rational Mech. Anal.*, 178(1):125–148, 2005.

[Dac82] B. Dacorogna. Quasiconvexity and relaxation of nonconvex problems in the calculus of variations*. *Journal of Funct. Anal.*, 46:102–118, 1982.

[Dac89] B Dacorogna. *Direct Methods in the Calculus of Variations*. Springer-Verlag Berlin Heidelberg New York, 1989.

[Dac01] B. Dacorogna. Necessary and sufficient conditions for strong ellipticity of isotropic functions in any dimension. *Discret. Contin. Dyn. S.-Series B*, 1(2):257–263, 2001.

[dB91] R. de Borst. Simulation of strain localization: a reappraisal of the cosserat-continuum. *Engng. comp.*, 8:301–332, 1991.

[dBS91] R. de Borst and L.J. Sluys. Localisation in a cosserat continuum under static and dynamic loading conditions. *Comput. Methods Appl. Mech. Engrg.*, 90:805–827, 1991.

[DD02] A. DeSimone and G. Dolzmann. Macroscopic response of nematic elastomers via relaxation of a class of so(3)-invariant energies. *Arch. Rational mech. Anal.*, 161:181–204, 2002.

[DeS04] A. DeSimone. Coarse-grained models of materials with non-convex free-energy: two case studies. *Comput. Methods Appl. Mech. Engrg.*, 193:5129–5141, 2004.

[DFC98] R. Dendievel, S. Forest, and G. Canova. An estimation of overall properties of heterogeneous cosserat materials. *journal de Physique IV*, 8:111–118, 1998.

[Dol99] G. Dolzmann. Numerical computation of rank-one convex evelopes*. *Siam J. Numer. Anal.*, 36(5):1621–1635, 1999.

[dPI96] C. di Prisco and S. Imposimato. Time dependent mechanical behaviour of loose sands. *Mech. Cohes.-Frict. Mat.*, 1:45–73, 1996.

[dPIA02] C. di Prisco, S. Imposimato, and E. C. Aifantis. A visco-plastic constitutive model for granular soils modified according to non-local gradient approaches. *Int. J. Numer. Anal. Meth. Geomech.*, 26(2):121–138, 2002.

[DR95] H. Le Dret and A. Raoult. The quasiconvex envelope of the saint venant-kirchhoff stored energy function. *Proc. Roy. Soc. Edinburgh*, 125A:1179–1192, 1995.

[DSW93] A. Dietsche, P. Steinmann, and K.J. Willam. Micropolar elasto-plasticity and its role in localization analysis. *Int. J. Plast.*, 9:831–831, 1993.

[DW00] G. Dolzmann and N. J. Walkington. Estimates for numerical approximations of rank one convex envelopes. *Numer. Math.*, 85:647–663, 2000.

[EDKD99] E. El-Danaf, S. R. Kalidindi, and R. D. Doherty. Influence of grain size and stacking-fault energy on deformation twinning in fcc metals. *Metall. Mater. Trans. A*, 30(5):1223–1233, 1999.

[EGGS00] S. A. Elaskar, L. A. Godoy, D. D. Gray, and J. M. Stiles. A viscoplastic approach to model the flow of granular solids. *Int. J. Solids Struct.*, 37:2185–2214, 2000.

[Eri68] A. C. Eringen. Theory of micro-polar elasticity. in: Fracture - an advance treatise. 2:621–693, 1968. Liebo-witz, H., ed.

[Eri02] A. C. Eringen. *Nonlocal Continuum Field Theories*. Springer-Verlag New York Berlin Heidelberg, 2002.

[ES64] A. C. Eringen and E. S. Suhubi. Nonlinear theroy of simple micro-elastic solids-i. *Int. J. Eng. Sci.*, 2:189–203, 1964.

[ET58] J. L. Ericksen and C. Truesdell. Exact theory of stress and strain in rods and shells. *Arch. Rat. Mech. Anal.*, 1:295–323, 1958.

[EV97] W. Ehlers and W. Volk. On shear band localization phenomena of liquid-saturated granular elastoplastic porous solid materials accounting for fluid viscosity and micropolar solid rotations. *Mech. Cohes.-Frict. Mat.*, 2:301–320, 1997.

[EV98] W. Ehlers and W. Volk. On theoretical and numerical methods in the theory of porous media based on polar and non-polar solid materials. *Int. J. Solids and Struct.*, 35:4597–4616, 1998.

[FG06] G. A. Francfort and A. Garroni. A variational view of partial brittle damage evolution. *Arch. for Rat. Mech. and Anal.*, 182:125–152, 2006.

[FGC95] J. Franks, G. A. Geach, and A. T. Churchman. Lamellar defects in single crystals of silicon. *Proc. Phys. Soc. B*, 68:111–, 1995.

[FM93] G. A. Francfort and J.J. Marigo. Stable damage evolution in a brittle continuous medium. *European Journal of Mechanics, A/Solids*, 12:149–189, 1993.

[FS06] S. Forest and R. Sievert. Nonlinear microstrain theories. *Int. J. Solids Struct.*, 43:7224–7245, 2006.

[G8] W. Günther. Zur statik und kinematic des cosseratscen kontinuums, in: Abhandlungen der braunscheigschen wissenschaftlichen gesellschaft. *Verlag E. Goltze, Göttingen*, 10:195–213, 1958.

[GHH07] S. Govindjee, K. Hackl, and R. Heinen. An upper bound to the free energy of mixing by twin-compatible lamination for n-variant martensitic phase transformations. *Continuum Mech. Therm.*, 18:443–453, 2007.

[GM11] E. Gürses and C. Miehe. On evolving deformation microstructures in non-convex partially damaged solids. *J. Mech. Phys. Solids*, 59:1268–1290, 2011.

[GMH02] S. Govindjee, A. Mielke, and G. J. Hall. The free energy of mixing for n-variant martensitic phase transformations using quasi-convex analysis. *J. Mech. Phys. Solids*, 50:1897–1922, 2002.

[GN04] G. Gudehus and K. Nübel. Evolution of shear bands in sand. *Géotechnique*, 54:187–201, 2004.

[God86] J. D. Goddard. Dissipative materials as constitutive models for granular media. *Acta Mechanica*, 63:3–13, 1986.

[GP98a] M. K. Gobbert and A. Prohl. A discontinuous fininte element method for solving a multi-well problem. 1998.

[GP98b] M. K. Gobbert and A. Prohl. A survey of classical and new finite element methods for the computation of crystalline microstructure. 1998.

[Gri60] G. Grioli. Elasticità asimmetrica. *Ann. di Mat. pura ed appl.*, 50:389–417, 1960.

[Gur03] M. E. Gurtin. On a framework for small-deformation viscoplasticity: free energy, microforces, strain gradients. *Int. J. Plasticity*, 19:47–90, 2003.

[Hac97] K. Hackl. Generalized standard media and variational principle in classical and finite strain elastoplasticity. *J. Mech. Phys. Solids*, 45:667–688, 1997.

[HB03] W. Huang and E. Bauer. Numerical investigations of shear localization in a micro-polar hypoplastic material. *Int. J. Numer. Anal. Meth. Geomech.*, 5:124–148, 2003.

[HC07] P.-Y. Hicher and C.S. Chang. A microstructural elastoplastic model for unsaturated granular materials. *Int. J. Solids Structures*, 44:2304–2323, 2007.

[HF08] K. Hackl and F. D. Fischer. On the relation between the principle of maximum dissipation and inelastic evolution given by dissipation potentials. *Proc. R. Soc., A*, 464:117–132, 2008.

[HH01] K. Hackl and U. Hoppe. *On the calculation of microstructures for inelastic materials using relaxed energies, IUTAM Symposium on Computational Mechanics of Solid Materials at Large Strains*, pages 20–24. August 2001.

[HH08] K. Hackl and R. Heinen. An upper bound to the free energy of n-variant polycrystalline shape memory alloys. *J. Mech. Phys. Solids*, 56:2832–2843, 2008.

[HHK12] K. Hackl, U. Hoppe, and D. M. Kochmann. Generation and evolution of inelastic microstructures - an overview. *GAMM-Mitt.*, 35(1):91–106, 2012.

[HN75] B. Halphen and Q. S. Nguyen. Sur les matériaux standards généralisés. *J. de Mécanique*, 14:39–63, 1975.

[HNB02] W. Huang, K. Nübel, and E. Bauer. Polar extension of a hypoplastic model for granular materials with shear localization. *Mechanics of Materials*, 34:563–576, 2002.

[HWW+06] C. X. Huang, K. Wang, S. D. Wu, Z. F. Zhang, G. Y. Li, and S. X. Li. Deformation twinning in polycrystalline copper at room temperature and low strain rate. *Acta Materialia*, 54:655–665, 2006.

[HZWL08] W. Z. Han, Z. F. Zhang, S. D. Wu, and S. X. Li. Combined effects of crystallographic orientation, stacking fault energy and grain size on deformation twinning in fcc crystals. *Philosophical Magazine*, 88(24):3011–3029, 2008.

[JK89] R.D. James and D. Kinderlehrer. *Theory of diffusionless phase transitions, PDE's and Continuum Models of Phase Transitions, Lecture Notes in Physics*, volume 344. Springer, 1989.

[KAV06] K.A.Alshibli, M.I. Alsaleh, and G.Z. Voyiadjis. Modelling strain localization in granular materials using micropolar theory: Numerical implementation and verification. *Int. J. Numer. Anal. Meth. Goemech.*, 30:1525–1544, 2006.

[KE71] C. B. Kafadar and A. C. Eringen. Micropolar media–i. the classical theory. *Int. J. Eng. Sci.*, 9:271–305, 1971.

[KE76] C. B. Kafadar and A. C. Eringen. *Polar field theories*, volume 4. Academic Press, New York, eringen, a.c. (ed.) continuum physics edition, 1976.

[Koh91] R.V. Kohn. The relaxation of a double-well energy. *Continuum Mech. Therm.*, 3(3):193–236, 1991.

[KP94] D. Kinderlehrer and P. Pedrega. Weak convergence of integrands and the young measure representation. *J. Geom. Anal.*, 4(1):59–90, 1994.

[KS82] R.V. Kohn and G. Strang. Structural design optimization, homogenization, and relaxation of variational problems. In *Macroscopic Properties of Disorderd Media, Lecture Notes in Physics*, volume 154. Springer-Verlag, 1982.

[KS83] R.V. Kohn and G. Strang. Explicit relaxation of a variational problem in optimal design. *Bull. A.M.S. Vol.*, 9:211–214, 1983.

[KS86a] R.V. Kohn and G. Strang. Optimal design and relaxation of variational problems i. *Cont. Mech. Thermodynam.*, 39:113–137, 1986.

[KS86b] R.V. Kohn and G. Strang. Optimal design and relaxation of variational problems ii, iii. *Comm. Pure Appl. Math.*, 39:139–182, 353–377, 1986.

[KV87] R.V. Kohn and M. Vogelius. Relaxation of a variational method for impedance computed tomography. *Comm. Pure Appl. Math.*, 40:745–777, 1987.

[Lad94] P. V. Lade. Creep effects on static and dyclic instability of granular soils. *J. Geotech. Eng.*, 120:404–419, 1994.

[Lak83] R.S. Lakes. Size effects and micromechanics of a porous solid. *J. Materials Science*, 18:2572–2581, 1983.

[Lak86] R.S. Lakes. Experimental microelasticity of two porous solids. *Int. J. Solids Struct.*, 22(1):55–63, 1986.

[Lak95] R.S. Lakes. Experimental methods for study of cosserat elastic solids and other generalized elastic continua. In *In Continuum models for materials with micro-structure*, pages 1–22. J. Wiley, N. Y., 1995.

[LGM] M. Lambrecht, E. Gürses, and C. Miehe. Relaxation analysis of material instabilities in damage mechanics based on incremental convexification techniques. In *Proceedings of the VII International Conference on Computational Plasticity (COMPLAS), Barcelona*, —-.

[LL96] B. Li and M. Luskin. *Nonconforming finite element approximation of crystalline microstructure*, 1996. Tech. Rep. 1420, IMA.

[LL98] B. Li and M. Luskin. Finite element analysis of microstructure for cubic to tetragonal transformation. *SIAM J. Numer. Anal.*, 35:376–392, 1998.

[LMD03] M. Lambrecht, C. Miehe, and J. Dettmar. Energy relaxation of non-convex incremental stress potentials in a strain-softening elastic-plastic bar. *Internaltional Journal of Soids and Structures*, 40(6):1369–1391, 2003.

[Lus96a] M. Luskin. Approximation of a laminated microstructure for a rotationally invariant, double well energy density. *Numer. Math.*, 75:205–221, 1996.

[Lus96b] M. Luskin. On the computation of crystalline microstructure. *Acta Numerica*, 5:191–257, 1996.

[M9a] H. B. Mühlhaus. Application of cosserat theory in numerical solution of limit load problems. *Ing. Archiv*, 59:124–137, 1989.

[M9b] H. B. Mühlhaus. Shear band analysis for granular materials within the framework of cosserat theory. *Ing. Archiv*, 56:389–399, 1989.

[M6] H. B. Mühlhaus. 5th int. symp. on plasticity and its current applications. pages 427–430, July 1996.

[M9] S. Müller. *Variational models for microstructure and phase transitions*. Number 1713. Springer, Berlin, hildebrandt, s., struwe, m. (eds) edition, 1999.

[MA91] H. B. Mühlhaus and E.C. Aifantis. The influence of microstructure-induced gradients on the localization of deformation in viscoplastic materials. *Acta Mechanica*, 89:217–231, 1991.

[Mai69] G. Maier. Some theorems for plastic strain rates and plastic strains. *J. Mch.*, 8:5–19, 1969.

[Mau92] G. A. Maugin. *The thermomechanics of plastictiy and fracture*. Cambridge University Press, 1992.

[MGC12] T. G. Murthy, E. Gnanamanickam, and S. Chandrasekar. Deformation field in indentation of granular ensemble. *Phys. Rev. E*, 85(6):061306(1–11), 2012.

[Mie04] A. Mielke. Deriving new evolution equations for microstructures via relaxation of variational incremental problems. *Comp. Meth. Appl. Mech. Eng.*, 193(48-51):5095–5127, 2004.

[Min64] R. D. Mindlin. Microstructure in linear elasticity. *Arch. Rat. Mech. Anal.*, 16:51–78, 1964.

[ML03] C. Miehe and M. Lambrecht. A two-scale finite element relaxation analysis of shear bands in non-convex inelastic solids: small-strain theory for standard dissipative materials. *Comput. Methods Appl. Mech. Engrg.*, 192:473–508, 2003.

[MLG04] C. Miehe, M. Lambrecht, and E. Gürses. Analysis of material instabilities in inelastic solids by incremental energy minimization and relxation methods: evolving deformation microstructures in finite plasticity. *J. Mech. Phys. Solids*, 52:2725–2769, 2004.

[MNR99] L. S. Mohan, P. R. Nott, and K. K. Rao. A frictional cosserat model for the flow of granular materials through a vertical channel. ——-, 138(1-2):75–96, 1999.

[Mor52] C. B. Morrey. Quasi-convextiy and the lower seimicontinuity of multiple integrals. *Pacific J. Math.*, 2:25–53, 1952.

[MP66] J. B. Martin and A. R. S. Ponter. A note on a work inequality in linear viscoelasticity. *Q. Appl. Math.*, 24:161–165, 1966.

[MR06] A. Mielke and T. Roubíček. Rate-independent damage processes in nonlinear elasticity. *Mathematical Models and Methods in Applied Sciences*, 16:177–209, 2006.

[MS84] J. K. Mitchell and Z. V. Solymar. Time-dependent strength gain in freshly deposited or ensified sand. *J. Geotech. Eng.*, 110:1559–1576, 1984.

[MSL02] C. Miehe, J. Schotte, and M. Lambrecht. Homogeneization of inelastic solid materials at finite strains based on incremental minimization principles. application to the texture analysis of polycrystals. *J. Mech. Phys. Solids*, 50:2123–2167, 2002.

[MT85] F. Murat and L. Tartar. *Calcul des variations et homogénéisation*, pages 319–370. 1985.

[MV87] H. B. Mühlhaus and I. Vardoulakis. The thickness of shear bands in granular material. *Geotechnique*, 37:271–283, 1987.

[Nef06] P. Neff. Existence of minimizers for a finite-strain micromorphic elastic solid. *Proc. Roy. Soc. Edinb. A*, 136(5):997–1012, 2006.

[NO93] H. Nishimori and N. Ouchi. Formation of ripple patterns and dunes by windblown sand. *Phys. Rev. Lett.*, 71:197–200, 1993.

[Now68] W. Nowacki. Couple-stresses in the theory of thermo-elasticity, in proc. of the iutam symposia, vienna, june 22-28. pages 259–278. Springer Verlag, Wien, 1968.

[Now69] W. Nowacki. Formulae for overall thermoelastic deformation in a micropolar body. *Bull. Acad. Pol. Sc., Sr. Sc. Techn.*, 17(4):257–262, 1969.

[Now70] W. Nowacki. *Theory of micropolar elasticity*. Springer Verlag, Wien, 1970.

[NW92a] R. A. Nicolaides and N.J. Walkington. *Computation of microsturcture utilizing Young measures representations*, pages 131–141. Technomic Publ., Lancaster, c.a.rogers, r.a.rogers (eds.) edition, 1992.

[NW92b] R. A. Nicolaides and N.J. Walkington. Strong convergence of numerical solutions to degenrate variational problems. *Math. Comp.*, 64:117–127, 1992.

[OK98] M. Oda and H. Kazama. Microstructure of shear bands and its relation to the mechanisms of dilatancy and failure of dense granular soils. *Gotechnique*, 48(4):465–481, 1998.

[OKNN82] M. Oda, J. Konishi, and S. Nemat-Nasser. Experimental micromechanical evaluation of strength of granular materials: effects of particle roling. *Mech. Mater*, 1(4):269–283, 1982.

[OR99] M. Ortiz and E. A. Repetto. Nonconvex energy minimzation and dislocation structures in ductile single crystals. *J. Mech. Phys. Solids*, 47(2):397–462, 1999.

[Pal64] N. A. Palmov. Fundamental equations of the theory of asymmetric elasticity. *prikl. Mat. Mekh.*, 28:401–, 1964.

[Ped95] P. Pedregal. Numerical computation of parametrized measures. *Numer. Funct. Anal. Optim.*, 16:1049–1066, 1995.

[Ped96] P. Pedregal. On numerical analysis of non-convex variational problems. *Numer. Math.*, 74:325–336, 1996.

[Ped97] P. Pedregal. *Parametrized Measures and Variational Principles*, 1997.

[PL86] H.C. Park and R.S. Lakes. Cosserat micromechanics of human bone: strain redistribution by a hydration sensitive constituent. *J. Biomechanics*, 19(5):385–397, 1986.

[PM01] E. Pasternak and H.-B. Mühlhaus. *Cosserat continuum modelling of granulate materials*, pages 1189–1194. Elsevier Science, s. valliappan and n. khalili, eds. edition, 2001.

[PV11] S.-A. Papanicolopulos and E. Veveakis. Sliding and rolling dissipation in cosserat plasticity. *Granular Matter*, 13:197–204, 2011.

[Rao86] A. Raoult. Non-polyconvexity of the stored energy function of a saint venant-kirchhoff material. *Apliace Matematiky*, 31:417–419, 1986.

[Rao10] A. Raoult. *Quasiconvex Envelopes in Nonlinear Elasticity*, pages 17–51. J. schröder, p. neff (ed.) edition, 2010.

[Rei73] E. Reissner. On kinematics and statics of finite-strain force and moment stress elasticity. *Stud. Appl. Math.*, 52:93–101, 1973.

[Rei87] E. Reissner. A further note on the equations of finite-strain force and moment stress elasticity. *ZAMP*, 38:665–673, 1987.

[RH64] R. E. Reed-Hill. *Deformation twinning*. New York: Gordon and Breach, 1964. In Poly-,Quasi- and Rank-one Convexity in Applied Mechanics, R. E. Reed-Hill, J. P. Hirth and H. C. Rogers (eds.).

[Rou94] T. Roubíček. Finite element approximation of a microstructure evolution. *Math. Methods in the Applied Sciences*, 17:377–393, 1994.

[Rou96] T. Roubíček. Numerical approximation of relaxed variational problems. *J. Convex Anal.*, 3:329–347, 1996.

[Rou97] T. Roubíček. *Relaxation in Optimization Theory and Variational Calculus*. W. de Gruyter, Berlin, New York, 1997.

[RVG01] A. Rohatgi, S. K. Vecchio, and T. G. Gray. The influence of stacking fault energy on the mechanical behavior of cu and cu-al alloys: deformation twinning, work hardening, and dynamic recovery. *Metall. Mater. Trans. A*, 32(1):135–145, 2001.

[San09] O. Sano. Solid-fluid transition and the formation of ripples in vertically oscillated granular layers. In *AIP Conf. Proc.*, number 1227, pages 100–114, 2009.

[SB58] H. Suzuki and C.S. Barrett. Deformation twinning in silver-gold alloys. *Acta Metallurgica*, 6(3):156–165, 1958.

[SBH03] M. Schmidt-Baldassari and K. Hackl. Incremental variational principles in damage mechanics. *Proc. Appl. Math. Mech.*, 2:216–217, 2003.

[Sch62] H. Schaefer. *Versuch einer Elastizitätstheorie des zweidimensionalen ebenen Cosserat-Kontinuums*. Festschrift W. Tollmien, Berlin: Akademie-Verlag, 1962.

[Sch67] H. Schaefer. Das cosserat-kontinuum. *ZAMM*, 47(8):485–498, 1967.

[SD02] J. Sulem and M. Derrolaza. Finite element analysis of the indentation test on rocks with microstructure. *Computers and Geotechnics*, 29:95–117, 2002.

[SdBC01a] A. S. J. Suiker, R. de Borst, and C. S. Chang. Micro-mechanical modelling of granular material. part 1: Derivation of a second-gradient micro-polar constitutive theory. *Acta Mechanica*, 149:161–180, 2001.

[SdBC01b] A. S. J. Suiker, R. de Borst, and C. S. Chang. Micro-mechanical modelling of granular material. part 2: Plane wave propagation in infinite media. *Acta Mechanica*, 149:181–200, 2001.

[SE64] E. S. Suhubi and A. C. Eringen. Nonlinear theroy of micro-elastic solids-ii. *Int. J. Eng. Sci.*, 2(4):389–404, 1964.

[Sev92] V. Sevrak. Rank-one convexity does not imply quasiconvexity. *Proc. Roy. Soc. Edinburgh Sect. A*, 120:185–189, 1992.

[sKMS84] S. Murayama snf K. Michihiro and T. Sakagami. Creep characteristics of sands. *Soils and Foundations*, 24(2):1–15, 1984.

[Ste94] P. Steinmann. A micropolar theory of finite deformation and finite rotations multiplicative elasto-plasticity. *Int. J. Solids Struct.*, 31:1063–1084, 1994.

[Sto69] R. Stojanović. *Mechanics of Polar Continua, Theory and Applications*. Springer, Wien, r. stojanović (ed.) edition, 1969.

[Sto72] R. Stojanović. *Nonlinear micropolar elasticity*, pages 73–103. Springer, Wien, nowacki, w., olszak, w. (eds.) edition, 1972.

[SZY06] K. Sawada, F. Zhang, and A. Yashima. Rotation of granular material in laboratory tests and its numerical simulation using tij-cosserat continuum theory. *Computational Methods*, –:1701–1706, 2006.

[TB96] J. Tejchman and E. Bauer. Numerical simulation of shear band formation with a polar hypoplastic model. *Comp. Geotech.*, 19(3):221–244, 1996.

[Tej97] J. Tejchman. *Modelling of shear localisation and autogeneous dynamic effects in granular bodies*, volume 140. Veröffnet-lichungen des Institutes für Bodenmechanik und Felsmechanik der Universität Fridericiana in Karlsruhe, 1997.

[TG93] J. Tejchman and G. Gudehus. Silo-music and sio-quake experiments and a numrical cosserat approach. *Powder Technology*, 76:201–212, 1993.

[TM62] P. R. Thornton and T. E. Mitchell. Deformation twinning in alloys at low temperatures. *Philosophical Magazine*, 7:361–375, 1962.

[TN06] J. Tejchman and A. Niemunis. Fe-studies on shear localization in an anisotropic micro-polar hypoplastic granular material. *Granular Matter*, 8:205–220, 2006.

[Tou62] R. A. Toupin. Elastic materials with couple stresses. *Arch. Rat. Mech. Anal.*, 11(1):385–414, 1962.

[Tou64] R. A. Toupin. Theory of elasticity with couple-stress. *Arch. Rat. Mech. Anal.*, 11:85–112, 1964.

[Tp01] J. Tejchman and G. poland. Patterns of shear zones in granular bodies within a polar hypoplastic continuum. *Acta Mechanica*, 155:71–94, 2001.

[TPG04] A. Tordesillas, J.F. Peters, and B. Gardiner. Shear band evolution and accumulated microstructural development in cosserat media. *Int. J. Numer. Anal. Methods Geotech. Eng.*, 29:981–1010, 2004.

[TPM05] A. Tordesillas, J. Peters, and M. Muthuswamy. Role of particle rotations and rolling resistance in a semi-infinite particulate solid indented by a rigid flat punch. *ANZIAM Journal*, 46(E):C260–275, 2005.

[TS98] A. Tordesillas and J. Shi. Indentation of a double shearing dilatant granular material by a smooth rigid wedge. *Q. J. Mechanics Appl. Math.*, 51(4):633–646, 1998.

[TS99] A. Tordesillas and J. Shi. Frictional indentation of dilatant granular materials. *Proc. R. Soc. Lond. A*, 455:261–283, 1999.

[TT60] C. Truesdell and R. A. Toupin. *The classical field theories*, volume 3. Berlin-Göttingen-Hiedelberg: Springer, 1960.

[TW93] J. Tejchman and W. Wu. Numerical study of patterning of shear bands in a cosserat continuum. *Acta Mechanica*, 99:61–74, 1993.

[TW94] J. Tejchman and W. Wu. Numerical study on sand and stell interfaces. *Mech. Res. Comm.*, 21:109–119, 1994.

[TW05] A. Tordesillas and S.D.C. Walsh. Analysis of deformation and localization in thermomicromechanical cosserat models of granular media. In *Proceedings of the Fifth International Conference on the Micromechanics of Granular Media Powders and Grains*, volume 1, pages 419–424. A.A. Balkema, Rotterdam, 2005.

[TW12] J. Tejchman and W. Wu. Dynamic patterning of shear bands in cosserat continuum. *Journal of Enginnering Mechanics*, 123(2):123–133, 2012.

[TWG04] A. Tordesillas, S.D.C. Walsh, and B. Gardiner. Bridging the length scales: Micromechanics of granular media. *BIT Numer. Maths.*, 44:539–556, 2004.

[TZ05] P.J. Thomas and F. Zoueshtiagh. Granular ripples under rotating flow: a new experimental technique for studying ripples in non-rotating, geophysical application? *Phil. Trans. R. Soc. A*, 363:1663–1676, 2005.

[Var96] *Proceedings of the 8th Int. Symp. on Continuum Models and Discrete Systems*, pages 342–349. ed. k. y. markov edition, June 11-16 1996.

[Var09] I. Vardoulakis. *Lecture notes on Cosserat continuum mechanics with application to the mechanics of granular media*, 2009. 3rd National Meeting on "Generalized Continuum Theories and Applications".

[Ven61] J. A. Venables. Deformation twinning in face-centred cubic metals. *Philosophical Magazine*, 6(63):379–396, 1961.

[Voi87] W. Voigt. *Theoretische studien über die elasticitätsverhältnisse der krystalle (In English: Theoretical studies of the elastic behavior of crystals)*, 1987.

[VS95] I. Vardoulakis and J. Sulem. *Bifurcation Analysis in Geomechanis*, 1995.

[WADS95] K. Willam, M-M Iordache A. Dietsche, and P. Steinmann. *Localization in micropolar continua*, pages 297–339. Wiley: New York, mühlhaus h (ed.) edition, 1995.

[Wil13] E. B. Wilson. An advance in theoretical mechanics. *Bull. Amer. Math. Soc.*, 19(5):242–246, 1913.

[Wil81] J.R. Willis. Variational and related methods for the overall properties of composites. *Advances in Applied Mech.*, 21:2–78, 1981.

[WL07] X. Wang and Y. Li. A numerical iterative scheme for computing finite order rank-one convex envelopes. *Appl. Math. Comput.*, 185(1):19–30, 2007.

[WT06] S.D.C. Walsh and A. Tordesillas. Finite element methods for micropolar models of granular materials. *Applied Mathematical Modeling*, 30:1043–1055, 2006.

[WTP07] S.D.C. Walsh, A. Tordesillas, and J.F. Peters. Development of micromechanical models for granular media: The projection problem. *Granular Matter*, 9:337–352, 2007.

[You37] L. C. Young. Generalized curves and the existence of an attained absolute minimum in the calculus of variations. *C. R. Soc. Sci. Lett.*, 3:212–234, 1937.

[Zei90] E. Zeidler. *Nonlinear Functional Analysis and its Applications, Vol. II 1A: Linear Monotone Operators (1990), Vol. II 1B: Nonlinear Monotone Operators (1990), Vol. III: Variational Methods and Optimization*. Springer-Verlag New York Berlin Heidelberg London Paris Tokyo, 1990.

[ZHL75] O. C. Zienkiewicz, C. Humpheson, and R. W. Lewis. Associated and non-associated visco-plasticity in soil mechanics. *Géotechnique*, 25(4):671–689, 1975.

[ZJM06] X. Zhang, R. G. Jeffrey, and Y-W. Mai. A micromechanics-based cosserat-type model for dense particulate solids. *Z. angew. Math. Phys.*, 57:682–707, 2006.

[ZLW12] Y. T. Zhu, X. Z. Liao, and X. L. Wu. Deformation twinning in nanocrystalline materials. *Progress in Materials Science*, 57:1–62, 2012.

[ZT00] O. C. Zienkiewicz and R. Taylor. *The Finite Element method - Solid mechanics*, volume 2. Woburn: Butter-Heinemann, fifth edition, 2000.

Curriculum Vitae

Personal Data

Name	Muhammad Sabeel Khan
Date of Birth	23.07.1982
Place of Birth	Mansehra, Pakistan
Marital Status	Married, two children

School Education

1988-1993	Federal Government Primary School, G-9/2, Islamabad
1994-1997	Federal Government Higher Secondary School, G-9/1, Islamabad
1997-2000	Islamabad Model College For Boys, G-10/4, Islamabad
2000-2002	Islamabad Model College For Boys, F-8/4, Islamabad

University Education

2002-2006	BS(Hons.) Mathematics, COMSATS Institute of Information Technology, Islamabad, Pakistan
2007-2009	M.Sc. (Computational Engineering), Ruhr-Universität Bochum, Germany
2009-2013	PhD student, Institute of Mechanics-Material theory, Ruhr-Universität Bochum, Germany

Professional Occupation

2006-2007	Teaching assistant, COMSATS Institute of Information Technology, Islamabad, Pakistan
since 2013	wissenschaftliche Mitarbeiter, Lehrstuhl für Energieanlagen und Energieprozesstechnik, Ruhr-Universität Bochum, Germany

Mitteilungen aus dem Institut für Mechanik
RUHR-UNIVERSITÄT BOCHUM
Nr. 156

ISBN 978-3-935892-34-6